THE UNIVERSITY
of EDINBURGH

Multidentate Ligands for Aluminium Hydrides and Halides

Abigail Levy

A Thesis Submitted for the Degree of Doctor of Philosophy

School of Chemistry

College of Science and Engineering

University of Edinburgh

2022

Declaration

I hereby certify:

a) That the thesis has been composed by me under the supervision of Dr Michael J. Cowley.

b) Either that the work is my own, or, where I have been a member of a research group, that I have made a substantial contribution to the work, such contribution being clearly indicated.

c) That the work has not been submitted for any other degree or professional qualification.

Abigail Levy

Lay Summary

Aluminium is the third most abundant element in the Earth's crust (8.1 %). The low cost and attractive mechanical properties of aluminium metal have resulted in its widespread use, ranging from window frames and solar shading to aeroplanes and power lines. Its low toxicity has also led to the use of aluminium cans and foil in the preservation of food. You have probably used an aluminium containing appliance or device within the last day.

On the other hand, molecules containing aluminium do not have as many applications, despite showing promise in a wide range of emerging technologies. For example, molecules that contain aluminium (Al) bonded to hydrogen (H) have potential as hydrogen storage materials. Another application where aluminium-based molecules have shown promise is in catalysis, speeding up reactions that are important for industrial processes (e.g. in the production of plastics).

This thesis focuses on the formation of molecules containing aluminium-hydrogen bonds to contribute to our fundamental understanding of these interactions. Modification of the elements that surround aluminium allows us to control the properties of the aluminium-hydrogen bond. This work investigates how we can gain access to new aluminium molecules in which the aluminium is encapsulated by carbon, nitrogen and phosphorus atoms. The properties of these molecules will be discussed.

Abstract

Low-oxidation state organoaluminium compounds, in which aluminium is in the oxidation state +1, are highly reactive yet isolable species. The desire to synthesise and study aluminium(I) compounds stems from their potential reactivity, in particular oxidative addition, and the prospect of offering an alternate to rare and expensive transition metals. To access stable aluminium(I) species, suitable ligands and precursors are required. This thesis discusses the synthesis, properties and reactivity of multidentate ligand-supported aluminium halide and hydride complexes, which are explored as potential precursors to aluminium(I) complexes.

Chapter 1 presents an overview of the synthesis and properties of reported aluminium hydride compounds including alane, $(AlH_3)_n$, and its adducts, as well as organoaluminium hydrides which are supported by group 14- and group 15-based ligands. The use of aluminium halides as precursors to low-oxidation state aluminium species is also discussed, along with a brief overview of aluminium(I) chemistry. In addition, the properties of bi- and tri-dentate ligands and the affects they may have on metal centres are also highlighted.

Chapter 2 discusses the synthesis, reactivity and potential reduction chemistry of PNP-pincer ligand-supported aluminium hydrides and halides. The nitrogen and phosphorus-containing pincer ligand has a rigid carbazole backbone bearing two phosphine donors which allows for tridentate coordination to the aluminium centre. Varying the P-substituents from phenyl groups to *tert*-butyl groups, offers insight into how the steric and electronic properties of the ligand can affect the preparation and reactivity of the aluminium hydride and halide compounds, and whether PNP-type ligands are able to support neutral aluminium(I) centres. The reactivity of a PNP-aluminium dihydride towards anilines and isonitriles, along with magnesium and palladium complexes was explored. The reduction of PNP-aluminium halide complexes was also attempted.

Chapter 3 discusses the use of carbon- and nitrogen-containing pincer ligands to support aluminium centres. The NCN-pincer ligand consists of a phenyl backbone with two dimethylamine donors. The small NCN-ligand offers different donating and steric properties compared to the ligand discussed in chapter 2. This work shows the synthesis of the aluminium dibromide, $(^{Me}NCN)AlBr_2$, which is then studied as a potential precursor to NCN-

supported aluminium(I). The NCN-aluminium dibromide complex was reacted with a range of group 1 metal reducing agents, including potassium naphthalenide and sodium-potassium alloy. The magnesium(I) dimer [(^{Mes}NacNac)Mg]$_2$ was also explored as a reducing agent.

Chapter 4 explores the potential for diphosphide ligands to support an anionic aluminium(I) centre. Many reported aluminyl anions use nitrogen-based ligands, but phosphorus-containing aluminyl anions are yet to be reported. Two novel diphosphines, with a silicon-containing alkyl linker, are used as the ligand precursors. The preparation of the diphosphide-supported aluminium bromide, {^{Tipp}SiP}AlBr(THF), is discussed. Reduction of the aluminium bromide complex is attempted with the aim to synthesise the aluminium(I) anion or the aluminium(II) dimer. Moreover, the contrast in properties of the diphosphine ligands compared to the diamine analogue is revealed in the synthesis of phosphine-aluminium adducts, in which P→Al dative bonds are formed.

Acknowledgements

First and foremost, thank you to Dr Michael Cowley for giving me the opportunity to be a part of his research group and for all his guidance and support during my PhD.

I would also like to thank all the past and present members of the Cowley group for the guidance and support they have given me and for all the memories made over the past four years. Thank you to Dr Martin Stanford for all your support and everything you have taught me, showing me around the lab when I started my PhD and exploring Edinburgh with me. Thank you to Ella Rice for all the support you have given me over the last few years and for all the good times, both in and out of the lab. Thank you to Alex Beaton-Garcia for all your help with the organic side of chemistry and the lunchtime chats, mostly about Spain. Thank you to Dr Peter Cleaves for all that you taught me and for keeping me calm during the stressful times. Thank you to Dr Ryan Schwamm for all your help, guidance, and support during the final months of my PhD and for everything you have taught me.

I would also like to thank Cora Wang for your friendship and support over the last four years. For all the good times we had in the gym, at the pub, and out on our weekend walks.

Most of all, thank you to my family, Toni, Neal, and Charlotte, for all the love and support you have given, for always believing in me and being there for me.

Abbreviations

(^{Ph}PNP)	3,6-di-*tert*-butyl-1,8-bis(diphenylphosphinomethyl)carbazolide
(^{tBu}PNP)	3,6-di-*tert*-butyl-1,8-bis(di-*tert*-butylphosphinomethyl)carbazolide
(^{Me}NCN)	2,6-bis(diemthylaminomethyl)phenyl
{SiP^{Tipp}}	1,2-bis(2,4,6-tri*iso*propylphenylphosphidodimethylsilyl)ethane
{SiP^{Mes*}}	1,2-bis(2,4,6-tri-*tert*-butylphenylphosphidodimethylsilyl)ethane
Cp*	Pentamethylcyclopentadienyl
Cy	Cyclohexyl
Dipp	2,6-di*iso*propylphenyl
DMAP	4-Dimethylaminopyridine
IR	Infrared
Mes	2,4,6-trimethylphenyl, mesityl
Mes*	2,4,6-tri-*tert*-butylphenyl
Me	Methyl
NacNac	(ArNC{CH_3})$_2$CH
NHC	*N*-Heterocyclic carbene
NMR	Nuclear magnetic resonance
Ph	Phenyl
*t*Bu	*tert*-Butyl
THF	Tetrahydrofuran
Tipp	2,4,6-tri*iso*propylphenyl
Xyl	2,6-dimethylphenyl, 2,6-Xylyl

Table of Contents

Chapter 1

Introduction

1. Introduction

This thesis details the synthesis, characterisation and reactivity of aluminium hydride and halide compounds supported by multidentate ligands. The objective of the work presented here is to explore the ligating properties of bi- and tri-dentate ligand systems at aluminium centres and demonstrate the effectiveness of these ligand systems for the stabilisation of reactive aluminium species.

1.1 Aluminium

Aluminium is the most abundant metal in the Earth's crust.[1] Naturally found in minerals such as bauxite, pure aluminium metal is extracted through the Hall-Héroult process, from which most commercially available aluminium is produced.[2] Metallic aluminium plays a vital role in range of applications, likewise, many molecular aluminium species play a vital role in the chemical sciences.

Aluminium is found in the second row of group 13 in the periodic table and has an atomic radius of 1.43 Å. With an electronic configuration of $[Ne]3s^2 3p^1$, aluminium typically uses its three valence electrons to form three bonding interactions. The high electropositivity of aluminium results in often highly polarised bonds in which aluminium carries a partial positive charge, Al(δ+)–E(δ−). Thus, in compounds, aluminium is usually found in its highly stable +3-oxidation state. Aluminium centres can also be found in the considerably less stable +1 oxidation state, possessing a lone pair of electrons. In contrast, heavier group 13 metal centres favour the +1 oxidation state. Upon descending group 13, the effective nuclear charge increases, due to poor shielding from the d-type orbitals, resulting in stabilisation of the valence s-type orbital, in which the lone pair of electrons are located, relative to valence p-type orbitals. This influences the trends in ionisation energies and atomic radii of group 13 elements. This observation is known as the inert pair effect.[3] Furthermore, formation of strong covalent bonds is an energetic driving force for metal centres to be in higher oxidation states. Aluminium is able to form strong bonding interactions and, with relatively low ionisation energies compared to heavier group 13 elements, causes aluminium(III) species to be inherently more stable than aluminium(I) species.

In a simple derivative of three-coordinate aluminium, AlX_3, the three Al–X bonds are arranged in a trigonal planar geometry. Orthogonal to the AlX_3 plane, is a vacant p-type orbital, which gives rise to the Lewis acidic nature of the aluminium centre. As such, aluminium(III) compounds have been exploited for their Lewis acid properties, for example, in frustrated Lewis pair (FLP) chemistry and as Lewis acid catalysts for various organic transformations.[4–7] In contrast, aluminium(I) species, in which there is a lone pair of electrons at aluminium, can also display Lewis base character, allowing for more diverse reactivity which cannot be achieved using aluminium(III) species.[8–10] The synthesis and characteristics of aluminium(III) hydrides and halides, and aluminium(I) species, will be discussed in further detail in this chapter.

1.2 Aluminium Hydrides

1.2.1 Hydrides as Ligands

Hydride ligands (H^-) are the simplest possible ligand in both steric and electronic terms and have been used to support metal centres across the periodic table.[11–14] Despite the relatively simple electronic profile of hydride ligands, with no significant potential to form π-type interactions, the bonding between hydrogen (H) and metal centres (M) can offer a wide variety of structural and chemical properties. Acting as a medium σ-donor to medium-strong σ-acceptor to one or more metal centres,[15,16] M–H bonds typically feature superior bond dissociation energies than their M–CH_3 counterparts.[17] However, the strength of the M–H bond is often undermined by the strength of H–H bond and M–O bonds, and so are often unstable with respect to thermal decomposition and oxidation.[18] M–H bonds exhibit a high degree of polarizability, demonstrated by the wide variation in polarity ranging from extremes of $M^{n+}\cdots H^-$ to $M^{\delta-}–H^{\delta+}$ depending on the character of the metal and other ligands. Group 13 metal-hydrogen bonds exhibiting primarily hydridic character ($M^{\delta+}–H^{\delta-}$) will be the focus of the work in this thesis.

Hydride ligands offer the smallest steric contribution to the coordination sphere of a metal centre. This often results in a coordinatively unsaturated metal centre which readily

undergo aggregation to form higher oligomers through bridging ligand interactions. As such, a variety of bridging bonding modes have been observed for hydride ligands involving two or more metal centres (figure 1.1, **B** and **C**). The tendency for bridging is increased in the group 13 elements due to their high Lewis acidity and the presence of a vacant p-type orbital. For example, diborane $(BH_3)_2$ and digallane $(GaH_3)_2$ both exist as a dimers linked through two 3-centre-2-electron B–H and Ga–H bonding interactions (**B**, figure 1.1).[19] In contrast, terminal M–H bonds (**A**) typically require either the incorporation of a strong Lewis base to displace the bridging hydride, or sterically demanding ancillary ligands to disfavour bridging interactions.

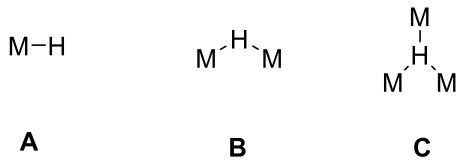

Figure 1.1 The various bonding modes of a hydride ligand: **A** terminal hydride ligand, **B** μ^2 hydride ligand, **C** μ^3 hydride ligand.

1.2.2 Spectroscopic and Crystallographic Features

Understanding the properties and nature of metal hydride species can typically be achieved using a combination of techniques:

1) **Infra-red (IR) spectroscopy**: In many instances, M–H bonds can be identified using Infra-red (IR) spectroscopy, with characteristic frequencies for M–H stretching modes. In terms of Al–H bonds, these may occupy a wide range, with differentiation between bridging (930 – 1790 cm^{-1}) and terminal (1700 – 1970 cm^{-1}) bonding modes possible.[20–22] The combination of this technique with matrix-isolation strategies has aided in the identification of fundamental hydride species which are unstable under ambient conditions.[22]

2) **Nuclear Magnetic Resonance (NMR) spectroscopy**: ^1H NMR spectroscopy is a powerful tool for understanding M–H interactions, allowing the determination of the number of

hydride ligands present in the molecule through relative integrals, and a relative measure for the hydridic character of the M–H bond through comparison of chemical shifts to related metal hydrides. Heteronuclear NMR spectroscopy can also prove useful in determining the presence of hydride ligands at a metal centre through observable heteronuclear coupling. In the case of aluminium hydrides, the Al*H* resonances are typically broad in appearance which is attributed to the influence of the quadrupolar nucleus of aluminium.[20,23]

3) **X-ray and neutron diffraction**: The determination of the metric parameters of M–H interactions can aid in understanding the role that hydride ligands play in the structural and chemical aspects of a molecular metal hydride species in the solid-state. X-ray crystallography is the most accessible of these techniques, but limitations in the accuracy of the measurements of M–H bonds result in a reduced capacity for comparison of bond lengths and angles.[24,25] Neutron crystallography provides the only definitive measure of the metric parameters relating to hydride ligands in the solid-state.[26] However, the poor availability of neutron sources precludes the widespread use of this technique. Therefore, most experiments involving main group metal hydrides rely solely on X-ray crystallography to determine their solid-state structures. Despite the poor accuracy of X-ray crystallography and the relatively large errors associated with measuring M–H bonds using this technique, the bond lengths and angles will be discussed with significant differences highlighted where appropriate.

1.2.3 Lithium Aluminium Hydride

Lithium aluminium hydride ($LiAlH_4$) (**1.1**) is one of the most widely used and accessible aluminium hydride compounds. A colourless solid at room temperature, **1.1** consists of lithium cation (Li^+) and aluminium tetrahydride anion (AlH_4^-) fragments. In the solid state, each Li^+ has five neighbouring AlH_4^- tetrahedra, interacting through Li–H–Al bridges which have substantial covalent character.[27] Since its discovery in 1947, various routes to **1.1** have been reported.[28–30] For example, the Schlesinger process involves refluxing a mixture of lithium hydride (LiH) and aluminium trichloride ($AlCl_3$) in diethyl ether (Et_2O) to give **1.1** and lithium chloride.[30] Alternatively, a more direct route involving the reaction LiH and Al metal,

under a high-pressure atmosphere of H_2 (5000 psi), also affords **1.1** (scheme 1.1).[29] **1.1** is now commercially available at low cost, often sold as a grey solid due to contamination, but simple purification by recrystallisation from Et_2O is possible. Though **1.1** is relatively stable as a solid at room temperature, over time decomposition to LiH and Al metal can occur. Furthermore, storage of **1.1** requires dry atmospheres due to its high moisture sensitivity.

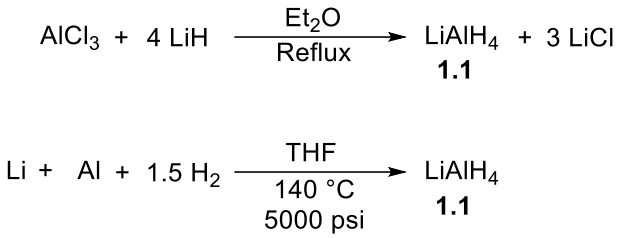

Scheme 1.1 The reported syntheses of $LiAlH_4$ (**1.1**) through the Schlesinger process and direct route.

Within synthetic chemistry, **1.1** has been used for a number of transformations, most commonly as a strong reducing agent for organic functional groups. For example, $LiAlH_4$ can be used in stoichiometric quantities as an unselective source of H^- in the conversion of carbonyl groups to alcohols.[31] Extension of catalytic reduction chemistry has also been achieved using $LiAlH_4$ in conjunction with a suitable hydride source (e.g. Si–H, B–H or H_2). For example, Cowley and coworkers highlighted the potential to use $LiAlH_4$ as a catalyst for the hydroboration and hydrosilylation of alkenes and alkynes,[32,33] while the catalytic hydrogenation of imines using H_2 has also been reported.[34] However, the role of the lithium cation in these processes is not yet fully understood, with on-going efforts seeking to explore this further.[34] Moreover, **1.1** may be used to access the neutral aluminium hydride species alane (AlH_3), discussed in section 1.2.4, and chloroalanes (H_2AlCl and $HAlCl_2$).[30,35]

1.2.4 Alane

Alane, AlH_3 (**1.2**), is the simplest aluminium(III) hydride. In the solid-state, **1.2** exists as a metastable crystalline polymer $(AlH_3)_n$, with seven different polymorphs**,** contrasting to the simple dimeric hydrides of boron and gallium.[19] For example, α-AlH_3 has a hexagonal

structure, consisting of six-coordinate aluminium centres, linked through bridging hydride ligands, with Al–H distances of 1.715 Å and Al–H–Al angles of 141.2˚, determined by X-ray and neutron diffraction.[36] Aggregation of AlH_3 fragments is proposed to aid in the decomposition process, which is initiated by Al–H cleavage and is thought to proceed through an associative mechanism, leading to the loss of H_2.[29] To overcome this, coordinative saturation or greater steric bulk around aluminium is required to disfavour the formation of Al–H–Al bridges, without which the associative decomposition pathway would diminish. One strategy that has been used to limit association at aluminium through the use of coordinating Lewis bases to form base-stabilised adducts of **1.2**.[37]

Alane adducts (AlH_3•nL, L = neutral donor/Lewis base, n = 1 to 2) consist of AlH_3 fragments coordinated by a Lewis base through donation of a lone pair of electrons into the p-type orbital at aluminium. Coordination of one or more donor ligands is sufficient to break the polymeric structure of $(AlH_3)_n$, allowing isolation of base-stabilised monomers. Thus, adducts of AlH_3 exhibit increased stability and are easier to handle compared to polyalane. In 1942, Stecher and Wiberg reported the first alane adducts, AlH_3•NMe_3 (**1.3**) and AlH_3•$(NMe_3)_2$ (**1.4**), supported by trimethylamine donor ligands.[37] Following this, solvated alane AlH_3•nEt_2O (**1.5**) (n = 1 to 2) was reported and is prepared by reacting lithium hydride (LiH) with aluminium trichloride ($AlCl_3$) in diethyl ether (Et_2O) (scheme 1.2). Alternatively, reacting $LiAlH_4$ with $AlCl_3$ also gives adduct **1.5** and lithium chloride (LiCl).[30] Removal of the coordinated solvent molecules was achieved by exposing a pentane solution of adduct **1.5** to reduced pressure for 12 hours to afford γ-AlH_3, a thermodynamically unstable polymorph of polyalane, allowing for facile access to **1.2**.[38,39]

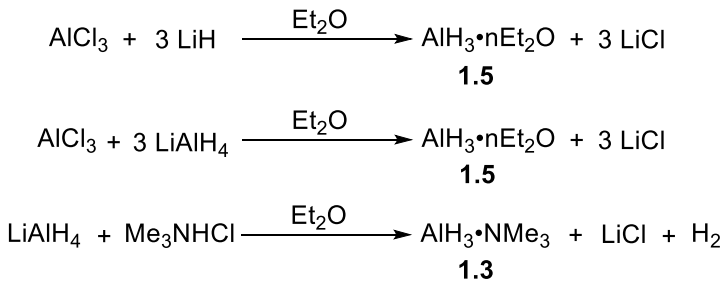

Scheme 1.2 The reported syntheses of AlH_3•nEt_2O (**1.5**) and AlH_3•NMe_3 (**1.3**).[28,30,37]

Although adduct **1.5** can be easily prepared, control over the number of donors that coordinate to the aluminium centre is lacking. In 1960, Ruff and Hawthorne demonstrated that it is possible to limit coordination to a single donor through the reaction of $LiAlH_4$ with trimethylammonium chloride ($[Me_3NH][Cl]$) to give amine adduct **1.3**, which can be isolated from by-products LiCl and H_2 (scheme 1.2).[28] Other trialkyl amines have been used to support AlH_3 fragments such as triethylamine (Et_3N) and tripropylamine (Pr_3N), as well as mixed alkyl amine diethylmethylamine (Et_2MeN).[28] Dialkyl amines R_2HN (R = Me or Et) are also able to datively bond to AlH_3 at –40 ˚C. However, an increase in temperature to –10 ˚C results in the formation of aluminium amide H_2AlNR_2, with an an Al–N covalent bond, formed through the elimination of H_2.[28] Thus, amine-alane adducts which are stable at ambient temperature are limited to tertiary amines only. Base-stabilised alane monomers have now been reported using phosphorus- or oxygen-based Lewis base donors, and more recently, N-heterocyclic carbene ligands have been shown to be effective stabilising ligands.[30,40,41]

1.2.5 Organoaluminium Dihydrides

The replacement of a hydride ligand with another larger ligand can be used to tune the electronic and steric properties of an aluminium species.[42] Substitution of a hydride for a methyl or ethyl ligand afford the simplest organoaluminium dihydrides, which were isolated as amine adducts, $MeAlH_2{\bullet}NMe_3$ (**1.6**) and $EtAlH_2{\bullet}NMe_3$ (**1.7**).[43] Synthesised by reacting $LiAlH_4$ (**1.1**) with R_2AlX (X = Cl, Br), forming R_2AlH and AlH_3 *in situ* which undergo ligand redistribution to afford $RAlH_2$. The addition of gaseous NMe_3 allowed aluminium dihydrides **1.6** and **1.7** to be isolated as adducts (scheme 1.3), identified using IR spectroscopy. When the aluminium bears a methyl ligand, synthesis is selective towards the organoaluminium dihydride product **1.6**. However, the presence of an ethyl ligand results in a mixture of **1.7** and diethyl aluminium hydride adduct $Et_2AlH{\bullet}NMe_3$, separated through fractional distillation. Moreover, methyl lithium (MeLi) can be reacted with chloroalane adduct $H_2AlCl{\bullet}NMe_3$ to generate **1.6** *via* salt elimination (scheme 1.3).[44]

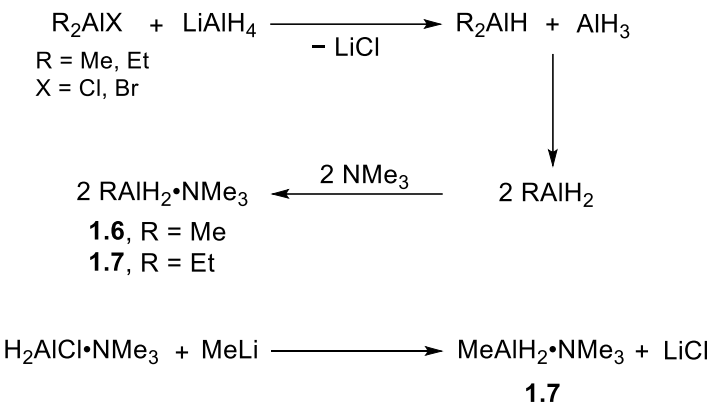

Scheme 1.3 The syntheses of alkyl aluminium dihydride adducts $MeAlH_2•NMe_3$ (**1.6**) and $EtAlH_2•NMe_3$ (**1.7**).

Substitution of a hydride ligand with an aryl group provided greater insight into the Al–H association. Extending the family of aluminium dihdyrides to include phenyl (Ph) and Mes* (Mes* = 2,4,6-tri-*tert*-butylphenyl) groups results in contrasting solid-state species. The synthesis of $PhAlH_2•NR_3$ (R = Me, **1.8**, or Et, **1.9**) proceeds through salt elimination upon reacting $H_2AlCl•NR_3$ with phenyl lithium (PhLi) (scheme 1.4).[44] Despite the increase steric encumbrance of Ph compared to Me and Et substituents, the inclusion of a Lewis base was still deemed necessary for isolation of the alane. Increasing the bulk about the aluminium through incorporation of a bulky Mes* substituent precludes the need for a Lewis base, instead forming aluminium dihydride $[Mes*AlH_2]_2$ (**1.11**), which does not contain a coordinating base. The preparation of **1.11** proceeds by $[Mes*AlH_3Li(THF)_2]_2$ (**1.10**) reacting with methyliodide (MeI) to give **1.11**, and methane, LiI and THF as by-products (scheme 1.4).[45] The absence of a Lewis base allows aluminium dihydride **1.11** to form a dimer, linked through bridging hydride ligands with an aluminium-aluminium separation of 2.652(2) Å, as shown in the solid-state structure. The Al–(μ)H (bridging) bonds have lengths measured at 1.69(4) and 1.70(4) Å, and the Al–H (terminal) bond length measured at 1.50(4) Å. The aluminium centre has a distorted tetrahedral geometry with angles ranging from 77.0(2)˚ ((μ)H–Al–(μ)H) to 135.5(1.3)˚ (H–Al–C). The X-ray diffraction data indicates that a single Mes* ligand is not sterically sufficient to overcome dimerization.[45]

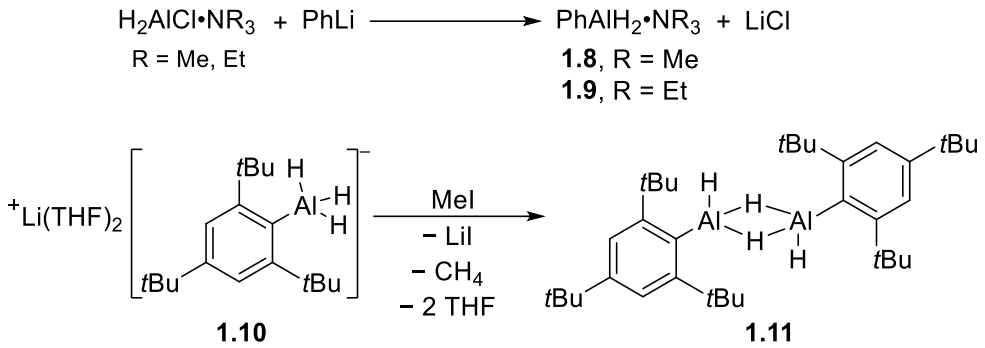

Scheme 1.4 The reported preparations of phenylaluminium dihydride adduct $PhAlH_2•NR_3$ (**1.8**, **1.9**) and aluminium dihydride dimer $[Mes*AlH_2]_2$ (**1.11**).

Power and co-workers sought to further increase the steric hinderance of the ligand to favour formation of monomeric aluminium dihydrides. 2,6-Diarylphenyl ligands were used to decrease aggregation of aluminium dihydrides.[46] $[(2,6\text{-}Mes_2C_6H_3)AlH_2]_2$ (**1.15**) (Mes = 2,4,6-trimethylphenyl) is synthesised by the reaction of $[2,6\text{-}Mes_2C_6H_3Li]_2$ (**1.12**) with $AlH_3•NMe_3$ to give the aluminium hydride salt $[(2,6\text{-}Mes_2C_6H_3)AlH_3Li(Et_2O)_{1.5}]$ (**1.13**). However, difficulties in the separation of **1.13** from LiH led them to explore an alternate route. Reacting aryl lithium **1.12** with $AlH_3•NMe_3$ also affords **1.13**, which is subsequently reacted with trimethylsilyl chloride (Me_3SiCl) to give aluminium dihydride adduct $(2,6\text{-}Mes_2C_6H_3)AlH_2•Et_2O$ (**1.14**). Dissociation of Et_2O is achieved by heating **1.14** to 90 – 120 ˚C, or can occur spontaneously when **1.14** is dissolved in benzene, to afford aluminium dihydride $[(2,6\text{-}Mes_2C_6H_3)AlH_2]_2$ (**1.15**) (scheme 1.5).[46]

The solid-state structure reveals **1.15** to be a dimer consisting of two $(2,6\text{-}Mes_2C_6H_3)AlH_2$ fragments, bonded through two bridged H-ligands. The X-ray diffraction determined Al–H and Al–(μ)H bond lengths of 1.44(4) and 1.65(5) Å, respectively, and the Al···Al separation of 2.630(2) Å, are similar to the respective distances of aluminium dihydride **1.11**. The distance between the two aluminium centres is 2.630(2) Å. The four-coordinate aluminium centre has a distorted tetrahedral geometry.

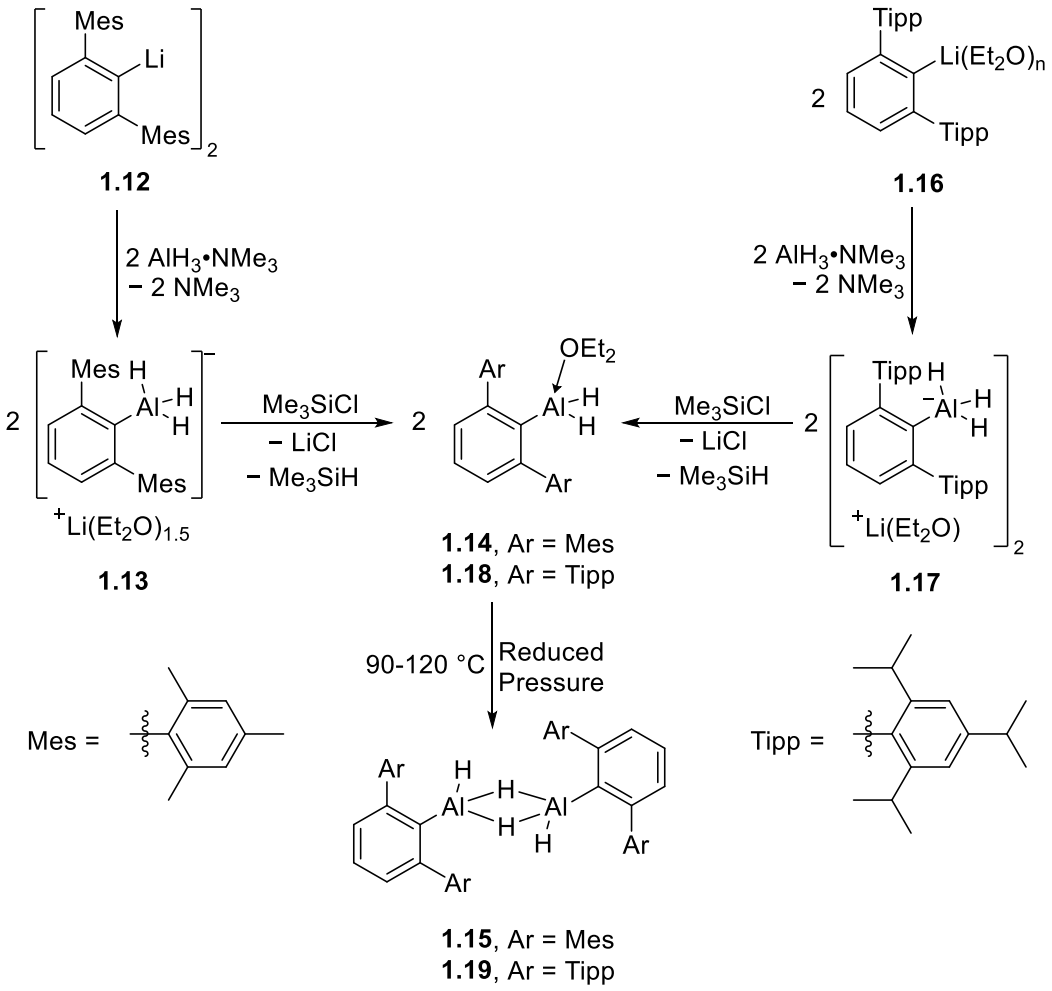

Scheme 1.5 The synthesis of $[(2,6\text{-}Mes_2C_6H_3)AlH_2]_2$ (**1.15**) and $[(2,6\text{-}Tipp_2C_6H_3)AlH_2]_2$ (**1.19**).

The larger analogue of **1.15**, $[(2,6\text{-}Tipp_2C_6H_3)AlH_2]_2$ (**1.19**) (Tipp = 2,4,6-tri*iso*propylphenyl) was also reported.[46] Analogous to **1.15**, the synthetic route to **1.19** begins with the reaction of $(2,6\text{-}Tipp)_2C_6H_3Li(Et_2O)_n$ (**1.16**) with AlH_3•NMe_3 (**1.3**) to give $[(2,6\text{-}Tipp_2C_6H_3)AlH_3Li(Et_2O)]_2$ (**1.17**). This is followed by reacting **1.17** with Me_3SiCl to form $(2,6\text{-}Tipp_2C_6H_3)AlH_2$•$Et_2O$ (**1.18**), which is heated to 95 ˚C, under reduced pressure, to afford aluminium dihydride $[(2,6\text{-}Tipp_2C_6H_3)AlH_2]_2$ (**1.19**) (scheme 1.5). The solid-state structure, which is similar to that of **1.15**, shows **1.19** to also have a dimeric structure, indicating that the $2,6\text{-}Tipp_2C_6H_3$ ligand is not able to prevent dimerization. However, a larger separation of the aluminium centres, a distance of 2.7042(13) Å, suggests the larger Tipp groups do indeed have an effect on the structure of **1.19**.

Aluminium dihydride species featuring covalent aluminium-group 15 element bonds have also been investigated. Amide ligands, bearing an anionic nitrogen centre, are commonly

used within aluminium chemistry, due in part to their attractive π-stabilising properties. The reaction of a primary or secondary amine with an aluminium hydride is a simple route to aluminium amides. The protic NH of the amine, combined with the hydridic nature of AlH, allows for facile formation of an Al–N covalent bond, through elimination of H_2. For example, aluminium amide $[H_2AlNMe_2]_3$ (**1.20**, figure 1.2) is synthesised from $LiAlH_4$ and dimethyl ammonium chloride (Me_2NH_2Cl), eliminating H_2 and LiCl.[47] Trimer **1.20** is comprised of a six-membered metallacycle, $[AlN]_3$, in a chair conformation, confirmed by X-ray diffraction studies. Despite the bridging bonding mode, the average Al–N bond length is 1.9355 Å, shorter than the Al–N bond of adduct AlH_3•NMe_3 (**1.3**) (2.063(8) Å).[48] The X-ray crystallographically determined Al–H bond lengths occupy a large range (1.45 to 1.71 Å) and are comparable to the Al–H distance reported for aryl aluminium dihydrides **1.11** and **1.15**. Increasing the size of the N-substituents gives rise to dimeric structures as seen for aluminium amide species $[H_2AlNMeEt]_2$ (**1.21**), $[H_2AlNEt_2]_2$ (**1.22**), and $[H_2AlN$*i*$Pr_2]_2$ (**1.23**) (figure 1.2).[49,50]

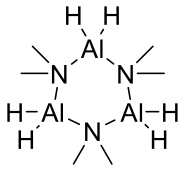

1.20

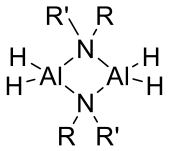

1.21, R = Me, R' = Et
1.22, R = R' = Et
1.23, R = R' = *i*Pr

Figure 1.2 Trimeric and dimeric aluminium amide compounds **1.20** to **1.23**.

Aluminium phosphide compounds are scarce compared to their amide counterparts, especially for substituted aluminium dihydride species. Well-defined phosphidoalane species of the general form R_2PAlH_2•$(NMe_3)_n$ were first reported over 20 years ago. The first example, where R = Mes (**1.24**, figure 1.3), involves coordination of a single trimethylamine base to the aluminium to give a monomeric alane species.[51] In contrast, when R = $SiMe_3$ (**1.25**, figure 1.3) the complex was isolated as a trimer linked through bridging phosphide ligands to form a Al_3P_3 metallacycle in an analogous manner to **1.20**, with tetrahedral aluminium and phosphorus centres, and terminal Al–H bonds.[52] Lithium and sodium aluminates containing two $P(SiMe_3)_2$ phosphide ligands have also been reported (figure 1.3, **1.26** and **1.27**). These species feature

a formally anionic aluminium centres with terminal Al–H bonds and two bridging Al–P–M interactions (where M = Li or Na).[53]

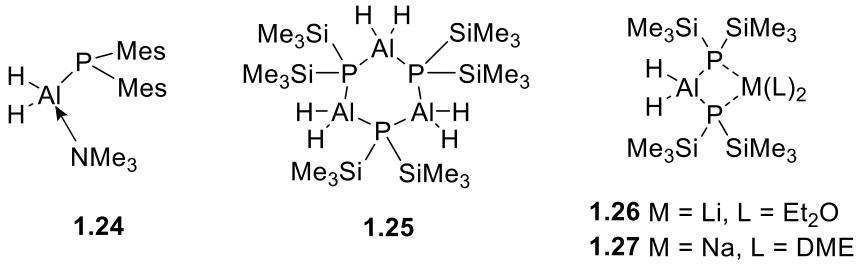

Figure 1.3 Phosphide-supported aluminium dihydrides **1.24** to **1.27**.

As revealed by the previous examples, monodentate ligand-supported aluminium dihydrides typically form aggregates linked through bridging interactions. Multidentate ligands can offer enhanced steric and electronic stabilisation which can allow the isolation of monomeric aluminium dihydrides. Bidentate β-diketiminate ligands, $(CH_2\{CMeNAr\}_2$, Ar = aryl group), referred to as ^{Ar}NacNac henceforth, coordinate to AlH_2 using both nitrogen centres to give monomer (^{Ar}NacNac)AlH_2 (Ar = Mes (**1.28**), 2,6-Xylyl (**1.29**), Dipp (**1.30**)) (2,6-Xylyl = 2,6-dimethylphenyl).[54,55] The addition of $LiAlH_4$ to (^{Ar}NacNac)H (Ar = Mes (**1.31**), 2,6-Xylyl (**1.32**)) affords **1.28** and **1.29** by elimination of H_2 and LiH (scheme 1.6). Alternatively, the oxidative addition of H_2 by aluminium(I) species (^{Dipp}NacNac)Al (**1.33**) yields **1.30** (scheme 1.6). The bidentate binding of ^{Ar}NacNac gives rise to a four-coordinate aluminium centre reducing the tendency for coordination of a Lewis base. The steric protection provided by the N-substituents allows for the formation of stable monomeric aluminium dihydride species.

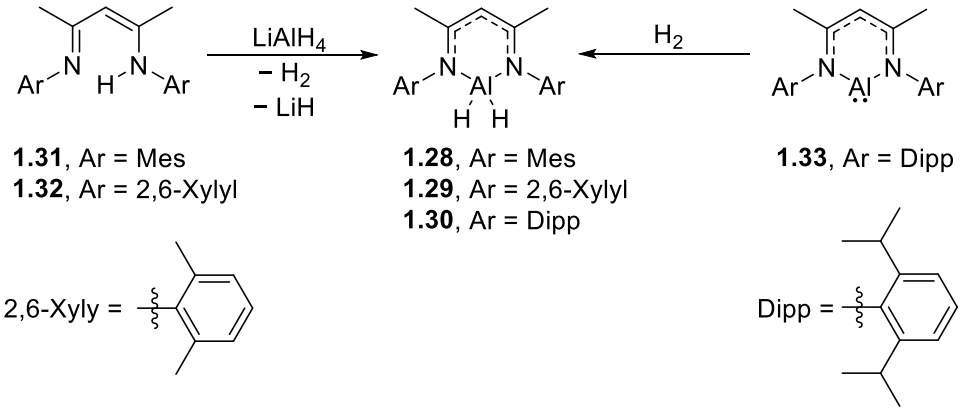

Scheme 1.6 Syntheses of (^{Ar}NacNac)AlH_2 (Ar = Mes **1.28**, 2,6-Xylyl **1.29**, Dipp **1.30**).

Bidentate amidophosphine ligands enable different ligand-metal interactions, compared to ^{Ar}NacNac, featuring a covalent Al-N bond and an intramolecular P→Al dative bond. Previous work within our group has highlighted the variable binding modes of these ligands in amidophosphine-stabilised aluminium dihydride **1.34** (scheme 1.7).[20] Deprotonation of the aminophosphine preligand, followed by the addition of two equivalents of AlH_3•NMe_3, generates aluminium dihydride **1.34**, and by-product $LiAlH_4$. In the solid state, the ligand of **1.34** binds exclusively through N,P-coordination. However, the lability of the phosphorus donor is observed in the solution phase, by NMR spectroscopy, where P-dissociation makes way for the coordination of the adjacent nitrogen centre to aluminium, forming an N,N'-donor-stabilised aluminium dihydride (**1.35**), existing in equilibrium (scheme 1.7).

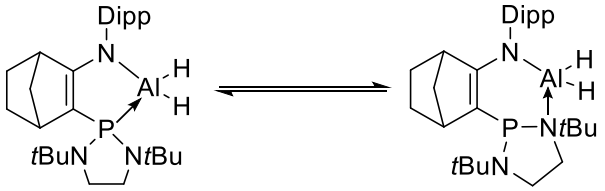

1.34 **1.35**

Scheme 1.7 The flexible coordination of N,P-donor stabilised aluminium dihydride **1.34** allowing form the formation of N,N'-donor stabilised aluminium dihydride **1.35**.

Tridentate ligands which have a central anionic coordination centre and two neutral pendant donors, have also been shown to stabilise AlH_2 fragments. Most examples contain central Al–C or Al–N covalent bonds with two pendant amine donors. For example, amidoamine (NNN) ligands featuring three nitrogen coordination centres are the most common type of tridentate ligand used to support aluminium dihydrides. Coordination of ethylene bridged amidoamine $(Me_2NCH_2CH_2)_2N^-$ ($N^{Et}NN$) to AlH_2 occurs when AlH_3•$(Et_2O)_n$ reacts with ($N^{Et}NN$)H , eliminating H_2 to give aluminium dihydride ($N^{Et}NN$)AlH_2 (**1.36**, figure 1.4).[18] Incorporation of a pyrrole group in the backbone introduces greater rigidity into amidoamine ligand $(Me_2NCH_2)_2C_4H_2N^-$ ($N^{Pyr}NN$). Synthesis of ($N^{Pyr}NN$)AlH_2 (**1.37**, figure 1.4) proceeds by reacting aluminium dichloride ($N^{Pyr}NN$)$AlCl_2$ with $LiAlH_4$ to give a dimeric tetra-aluminium hydride species which then reacts with two equivalents of water to afford monomeric aluminium dihydride **1.37**.[56] Both of these systems utilise a symmetric

coordination mode to chelate the aluminium centre. In contrast, systems derived from the bidentate β-diketiminate ligand systems have been developed which feature a pendant NMe_2 substituent capable of coordinating to the aluminium centre, as in aluminium dihydride **1.38** (figure 1.4).[57,58] While pendant amine groups are the most common side-arm functional groups, there is only a single example of an aluminium dihydride where phosphines donors are incorporated into the ligand system, featuring a central secondary amide with pendant di-*iso*-propylphosphine donors (**1.39**, figure 1.4).[23,59]

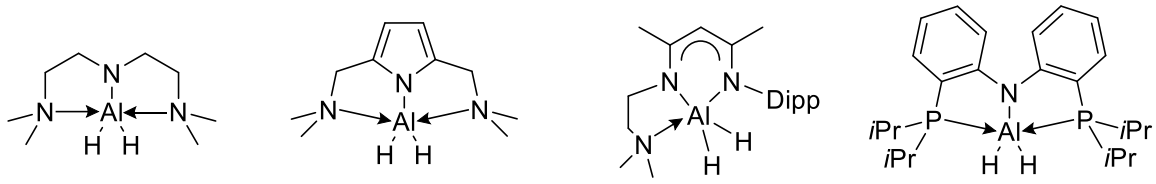

1.36 **1.37** **1.38** **1.39**

Figure 1.4 A selection aluminium dihydride species supported by tridentate amidoamine (NNN) and amidophosphine (PNP) ligands.

1.2.6 Diorganoaluminium Hydrides

Disubstituted aluminium monohydride compounds (R_2AlH), in which aluminium is supported by two organo or amido ligands and a single hydride ligand, are scarce. Peters and co-workers revealed two possible synthetic routes to dialkyl aluminium hydride species $Me_2AlH{\bullet}NMe_3$ (**1.40**) and $Et_2AlH{\bullet}NMe_3$ (**1.41**).[43] Firstly, reacting $AlH_3{\bullet}NMe_3$ with two equivalents of $AlR_3{\bullet}NMe_3$ (R = Me or Et) results in ligand redistribution to give dialkyl aluminium hydrides **1.40** and **1.41** (scheme 1.8). The second method involves the reaction of $AlH_3{\bullet}NMe_3$ and dialkyl mercury (R_2Hg, R = Me or Et), proceeding by elimination of H_2 and deposition of Hg, to afford **1.40** and **1.41** (scheme 1.8). A third pathway to diethyl aluminium hydride **1.41**, in which $Et_2AlCl{\bullet}NMe_3$ reacts with LiH *via* salt elimination, was also reported (scheme 1.8). However, attempts to synthesise dimethyl aluminium hydride **1.40** through the same reaction were unsuccessful as $Me_2AlCl{\bullet}NMe_3$ appeared unreactive towards LiH. Cryoscopy analysis reveals that in solution, the degree of association is 1.34 for **1.40** and 1.18

for **1.41**. This indicates that increasing the size of the alkyl ligand reduces the propensity to form intermolecular associations.

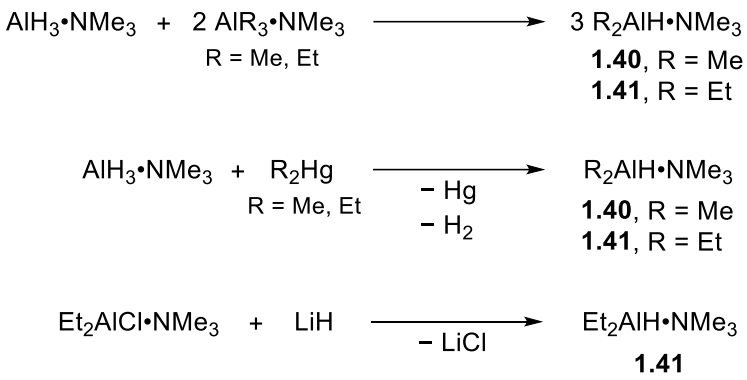

Scheme 1.8 The synthetic routes for $Me_2AlH{\bullet}NMe_3$ (**1.40**) and $Et_2AlH{\bullet}NMe_3$ (**1.41**).

The presence of the amine donors in **1.40** and **1.41** also influences the degree of association experienced by the dialkyl aluminium hydride adducts. Without a Lewis base, dialkyl aluminum hydride species aggregate, even with larger alkyl ligands such as tertiary butyl (*t*Bu) groups. Aluminium hydride $[t\text{Bu}_2\text{AlH}]_3$ (**1.42**), synthesised from aluminium bromide ($AlBr_3$) and alkyl lithium *t*BuLi (scheme 1.9) involving *in-situ* β-hydride elimination, possesses a trimeric solid-state structure consisting of a six-membered heterocycle linked through H-bridges.[60] The four-coordinate aluminium centre has a distorted tetrahedral geometry. The H–Al–H angle is 89.2(8)˚, while the C–Al–C angle is 119.0(1)˚, which can be ascribed to the steric effects of the large *t*Bu groups and the constraints of the $[AlH]_3$ ring.

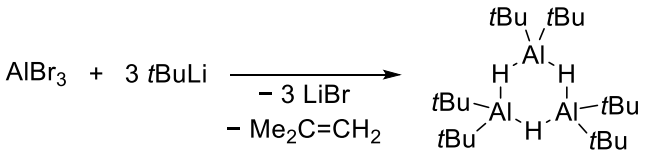

Scheme 1.9 The synthesis of $[t\text{Bu}_2\text{AlH}]_3$ (**1.42**).

Diaryl aluminium hydride species present structural difference in comparison to dialkyl aluminium hydrides. Diphenyl aluminium hydride adduct $Ph_2AlH{\bullet}NEt_3$ (**1.43**) is synthesised by reacting $Cl_2AlH{\bullet}NEt_3$ with phenyl lithium (PhLi).[44] Molecular weight studies determined that in solution the degree of association of **1.43** is 1.31.

Increasing the steric bulk of the aryl ligands at aluminium can have a drastic affect on the structure. The increased steric encumbrance given by Mes* ligands, owed to the ortho-*t*Bu groups, facilitates the partial protection the AlH moiety, impeding the formation of H-ligand bridges. Aluminium hydride Mes*$_2$AlH (**1.46**) was the first base-free monomeric di-substituted aluminium hydride to be reported.[61] The formation of **1.46** occurs through transmetallation by the reaction of group 13 metal chloride species Mes*$_2$MCl (M = Ga (**1.44**), In (**1.45**)) and $LiAlH_4$ (scheme 1.10). The solid-state structure of **1.46** shows aluminium to be three-coordinate with a trigonal planar geometry. The C–Al–H angles are slightly narrow at 113.1(14)˚ and 114.3(14)˚. The C–Al–C angle, 131.7(3)˚, is much wider, showing strain within **1.46** due to steric repulsion between the Mes* ligands.

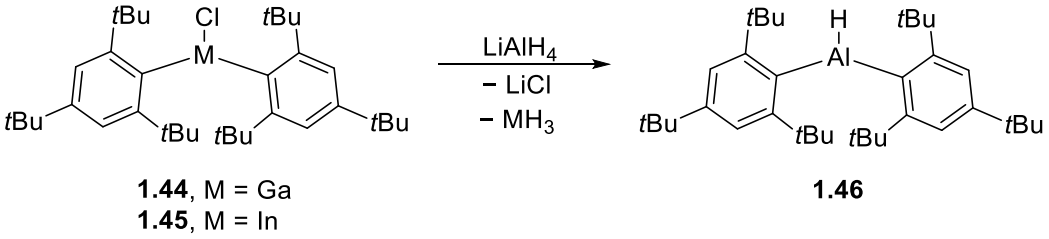

1.44, M = Ga
1.45, M = In

1.46

Scheme 1.10 The synthesis and solid-state structure of Mes*$_2$AlH (**1.46**).

The use of amide ligands also demonstrates how steric properties of the N-substituents impact the structures of aluminium hydrides. The small dimethyl amido ligands of $[HAl(NMe_2)_2]_2$ (**1.47**, figure 1.5) allow for dimerization to occur by forming amido-bridges, giving rise to a planar 4-membered N-heterocycle.[42] The average Al–(μ)N bond length of **1.47** is 1.966(2) Å, which is longer in comparison to trimer $[H_2AlNMe_2]_3$ (**1.20**) (1.936(3) Å). Varying the amide ligands to tetramethylpiperidine (tmp), causes aluminium hydride $[HAl(tmp)_2]_2$ (**1.48**, figure 1.5) to dimerise through formation of hydrido-bridges.[62] The average Al–(μ)H bond length is 1.68(2) Å, comparable to other reported bridging Al–H distances, but longer than terminal Al–H bonds. The average Al–N bond length of **1.48** is 1.835(3) Å, which, although shorter than Al–(μ)N of **1.47**, is longer than other terminal Al–N bond lengths, such as in $Al(N\{SiMe_3\}_2)_3$ (Al–N = 1.78(2) Å).[42] The lengthening of Al–N bonds in **1.48** is also a consequence of the greater steric bulk of the tmp ligands.

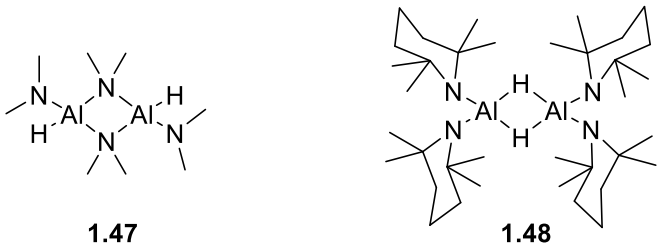

1.47 **1.48**

Figure 1.5 The dimeric structures of $[HAl(NMe_2)_2]_2$ (**1.47**) and $[HAl(tmp)_2]_2$ (**1.48**).

Oxidative addition pathways have also been used to access asymmetric aluminium hydride species of the type HAlRR' (where R ≠ R'). For example, the low oxidation state aluminium complex (^{Dipp}NacNac)Al (**1.33**) has been shown to activate H–X bonds to give (^{Dipp}NacNac)AlHX (X = SiHMePh (**1.49**), Bpin (**1.50**), Cp* (**1.51**), NH*t*Bu (**1.52**), NHPh (**1.53**), PPh_2 (**1.54**), O*i*Pr (**1.55**)) (Bpin = pinacol boryl, $B(OMe_2)_2$; Cp* = pentamethylcyclopentadienyl, C_5Me_5).[54] The solid-state structures of **1.49** to **1.55** show all products to be monomeric and the four-coordinate aluminium to have a distorted tetrahedral geometry. Distortion around the aluminium centre increases upon increasing the steric bulk of X, observed by the decrease in N–Al–N angle. The greatest distortion occurs in (^{Dipp}NacNac)AlHCp* (**1.51**), which has the smallest N–Al–N angle of 93.64(7)˚, as a result of the sterically hindered Cp* ligand, bonded to aluminium in an η^1 fashion.

1.3 Aluminium Halides

1.3.1 Aluminium Trihalides

Aluminium trihalides, AlX_3 (X = F, Cl, Br, I), feature an aluminium(III) centre bonded to three highly electronegative halide ligands through highly polarised largely ionic bonding interactions. In the solid state, aluminium trihalides exist as dimers containing halide-ligand bridges and four-coordinate aluminium centres. Synthesis of AlX_3 can proceed directly from aluminium metal and dihalogen, X_2 (X = Cl, Br, I). Alternatively, these species can also be synthesised by reacting aluminium with the respective acids, HX (X = Cl, Br).[63] Aluminium trihalides are strong Lewis acids due to the electron withdrawing properties of the halide substituents. As such, aluminium trichloride ($AlCl_3$) is commonly used within synthetic chemistry as a Lewis acid catalyst. For example, $AlCl_3$ can be used to affect the Friedel Crafts

alkylation of benzene to generate alkylbenzene derivatives.[64] As the halogens are descended, the relative Lewis acidity of the aluminium centre increases due to decreased ability for π-donation from the halide ligand to aluminium, while the Al–X bond enthalpy decreases.

1.3.2 Organoaluminium Halides

Simple organoaluminium halides [R_nAlX_{3-n}] (n = 1 or 2) are common reagents in organic synthesis and are commercially available. Featuring a reduction in the Lewis acidity compared to the corresponding aluminium trihalides, the incorporation of a highly polarised Al–C bond into the molecule also introduces a Brønsted basic and nucleophilic functionality. Organoaluminium halides are typically accessed through three different pathways: 1) Oxidative addition of alkyl halides to aluminium metal, 2) Redistribution reactions between trialkylaluminium and aluminium trihalides, and 3) Protonation of trialkylaluminium with a hydrogen halide. Pathway 2 has also been demonstrated for the synthesis of arylaluminium halide species $PhAlX_2$ and Ph_2AlX. Alternatively, salt elimination reactions employing metallated aryl systems and AlX_3 have been used to access more encumbered arylaluminium halide species. For example, Mes*$AlCl_2$ (**1.58**) is prepared by reacting Mes*Li$(THF)_2$ (**1.56**) with $AlCl_3$ to give THF-adduct Mes*$AlCl_2$•THF (**1.57**). Purification by sublimation not only separates the product from impurities, but also results in the removal of THF from **1.57** to give base-free aluminium dichloride **1.58** (scheme 1.11). This route can also be used to access aluminium bromide analogue **1.59**, by reacting **1.56** with $AlBr_3$.[65] An alternate pathway to **1.58** is through substitution of hydride ligands, reacting lithium-alane salt **1.10** with three equivalents of trimethylchlorosilane, eliminating LiCl and trimethylsilane (scheme 1.11). The solid-state structure reveals **1.58** to be monomeric, in contrast to the hydride analogue **1.11**, which is a dimer.

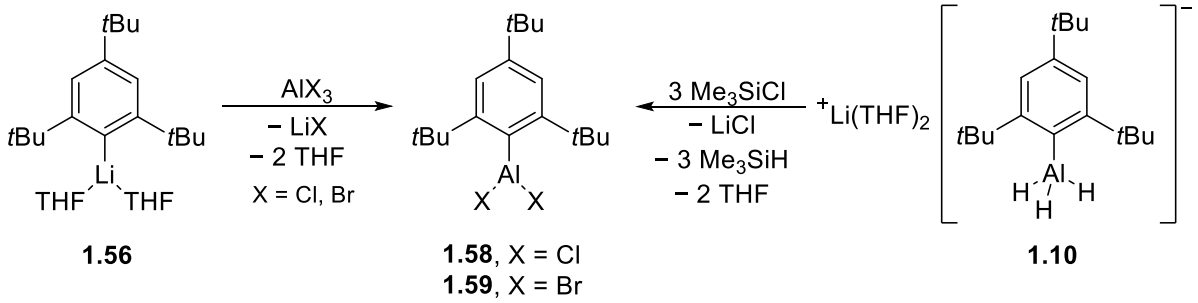

Scheme 1.11 Reported syntheses of Mes*AlX_2 (X = Cl **1.58**, Br **1.59**).

The salt elimination pathway can also be applied to amide-supported aluminium halides.[66] The reaction of two equivalents of tmpLi (**1.60**) with the corresponding aluminium trihalide AlX_3 affords aluminium halides $(tmp)_2AlX$ (X = Cl **1.61**, Br **1.62**, I **1.63**, scheme 1.12). In contrast to the dimeric aluminium hydride analogue **1.48**, aluminium halides **1.61** to **1.63** are monomeric.

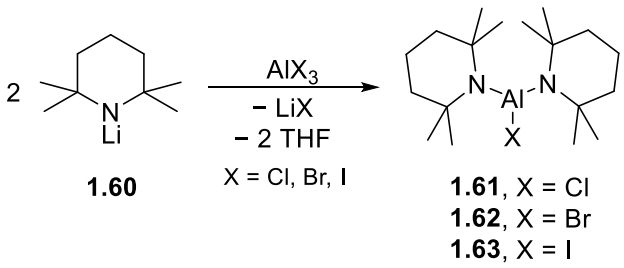

Scheme 1.12 The synthesis of $(tmp)_2AlX$ (X = Cl **1.61**, Br **1.62**, I **1.63**) through a salt elimination reaction.

Using the Brønsted basic properties of the Al–C bond in organoaluminium halides, deprotonation of a proligand with a suitably acidic hydrogen (e.g. NH or OH) can be used to coordinate the desired ligand system.[67–69] For example, aryl-substituted 1,3,5-triazapenta-1,3-diene (**1.64**) reacts with $MeAlCl_2$, evolving methane, to afford the aluminium dichloride product, **1.65** (scheme 1.13).[69] However, this pathway is limited to aluminium dichloride species and is scarcely reported compared to the salt elimination and ligand reproportionation routes due to the equilibria with dialkyl and trialkylaluminium species *in-situ* resulting in uncontrolled reactivity.

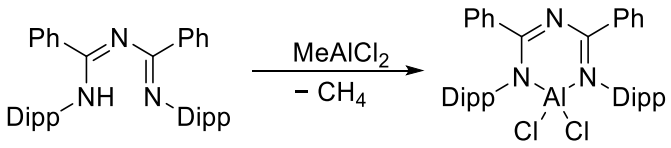

1.64 **1.65**

Scheme 1.13 The methane elimination reaction of aryl-substituted 1,3,5-triazapenta-1,3-diene (**1.64**) with $MeAlCl_2$ to give aluminium dichloride (**1.65**).

1.3.3 Precursors to Aluminium(I)

Low-oxidation state aluminium chemistry has seen significant new developments in recent years, due to the strong reducing power of aluminium(I) species allowing access to unprecedented reactivity. Access to aluminium(I) species has typically been achieved by the reduction of a corresponding aluminium(III) halide species. From a practical viewpoint, the aluminium halide reacts with the reducing agent, which in most cases is a group 1 metal (M), to give the aluminium(I) species and the MX salt by-product. Selection of the appropriate halide ligand is believed to facilitate reduction of the aluminium centre. The Al–X bond enthalpies decrease upon descending group 17: Al–Cl 494(13) kJ/mol, Al–Br 439(8) kJ/mol, and Al–I 368(4) kJ/mol.[70] Combined with a weakened bonding interaction, an Al–I bond results in a more accessible association between reductant and the iodide. Therefore, aluminium iodide species are generally used as precursors to aluminium(I) compounds. For example, (^{Dipp}NacNac)AlI_2 (**1.67**), synthesised by reacting (^{Dipp}NacNac)$AlMe_2$ (**1.66**) with iodine (I_2), is reduced using potassium metal (K) to give aluminium(I) species (^{Dipp}NacNac)Al (**1.33**) (scheme 1.14).[71]

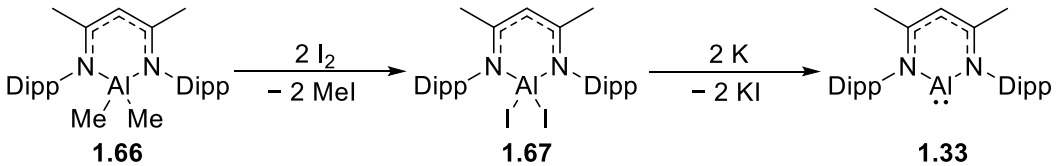

1.66 **1.67** **1.33**

Scheme 1.14 The synthesis and subsequent reduction of (^{Dipp}NacNac)AlI_2 (**1.67**) to afford (^{Dipp}NacNac)Al (**1.33**).

1.4 Low-Oxidation State Aluminium

Molecular complexes of aluminium typically prefer the +3 oxidation state, formed through use of the 3 valence electrons. Low-oxidation state aluminium complexes, in which the aluminium centre is in either the +1, +2, or 0 oxidation state, have received considerable interest in recent years. In comparison to aluminium(III), aluminium centres which are in formal +1 or +2 oxidation states are inherently less stable with respect to disproportionation, requiring extreme conditions or stabilisation from ligands.

The first reported example is monovalent aluminium chloride, AlCl (**1.68**), which is synthesised at high temperature and low pressures. Aluminium metal is reacted with hydrogen chloride at over 900 ˚C and a pressure of 0.2 mbar to give **1.68** which is isolated by deposition at low temperatures of −196 ˚C, affording a red solid.[72] However, an increase in temperature results in the decomposition of **1.68** and, at approximately −93 ˚C, **1.68** undergoes disproportionation to aluminium trichloride and aluminium metal, demonstrating the instability of aluminium(I). Therefore, isolation of aluminium(I) under ambient conditions requires greater stabilisation of the metal centre, which can be attained through the use of ligand systems which can impart favourable steric and electronic contributions to the low-oxidation state metal centre. For example, the hydride analogue of **1.68**, cyclic alkyl amino carbene-stabilised AlH•$(cAAC^{Dipp})_2$ (**1.69**, $cAAC^{Dipp}$ = {NDippCMe$_2$CH$_2$CMe$_2$}C), can be isolated under ambient conditions, demonstrating the stabilising effects of the Lewis donors on an aluminium(I) centre.[73]

1.4.1 Neutral Aluminium(I)

The metal centre of a neutral aluminium(I) compound is supported by a single monoanionic ligand. In 1991, Schnöckel and co-workers reported the first room temperature-stable neutral aluminium(I) species, supported by a pentamethylcyclopentadienyl (Cp*) ligand.[74] The reaction of AlCl•$(Et_2O)_n$ and $MgCp^*_2$ gives tetrameric aluminium(I) $[Cp^*Al]_4$ (**1.70**). The solid-state structure of **1.70** reveals an Al_4 tetrahedron with average Al–Al distance of 2.769 Å and Al–Al–Al angle of 60.0˚. The Cp* ligands adopt η^5-coordination with an average Al–C_{ring} distance of 2.334 Å. Dissociation of tetramer **1.70** occurs at high

temperatures, or in the gas phase, forming monomeric Cp*Al (**1.70a**). Although **1.70** is stable under ambient conditions, the synthesis of aluminium chloride adduct $AlCl•(Et_2O)_n$ still requires harsh reaction conditions. However, **1.70** can also be prepared through a reductive elimination pathway.[75] Dichloroaluminium hydride ($HAlCl_2$) is reacted with potassium salt Cp*K to give Cp^*_2AlH (**1.71**), in which the Cp*-ligands bond to aluminium by η^2- and η^3-coordination. Upon heating to 110 ˚C, **1.71** is in equilibrium with the reductive elimination products, aluminium(I) tetramer **1.70** and Cp*H. Removal of Cp*H is achieved under reduced pressure or by filtration to afford **1.70** as a yellow crystalline solid (scheme 1.15).

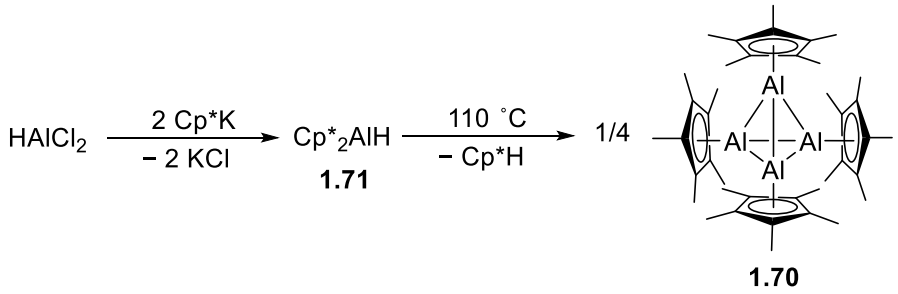

Scheme 1.15 The reductive elimination pathway to $[Cp^*Al]_4$ (**1.70**).

The effects that the steric properties of the ligand have on the structure of the compound can be demonstrated by increasing the size of the alkyl groups of the Cp-ligand. Modifying the Cp-ring to include bulky tertiary-butyl groups to give the 1,3,5-tri-*tert*-butylcyclopentadienyl (Cp^{3tBu}) ligand, which enhances the steric hindrance around aluminium that formation of a monomeric species is more favoured.[76] Aluminium tribromide ($AlBr_3$) is reacted with $Mg(Cp^{3tBu})_2$ (**1.72**) to give aluminium dibromide $(Cp^{3tBu})AlBr_2$ (**1.73**). This is followed by the reaction of **1.73** with aluminium(I) tetramer **1.70**, affording aluminium adduct $Cp^*AlBr_2•Al(Cp^{3tBu})$ (**1.74**), in which aluminium(I) species is acting as a Lewis base forming a dative Al–Al bond. Displacement of the aluminium donor with a cyclic alkyl amino carbene ($cAAC^{Me}$, $\{NMeCMe_2CH_2CMe_2\}C$) allows for isolation of monomeric aluminium (I), $(Cp^{3tBu})Al$ (**1.75**) (scheme 1.16).

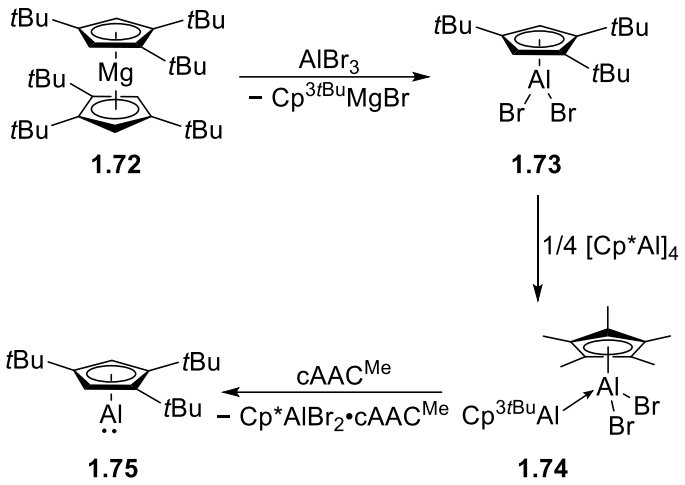

Scheme 1.16 The synthesis of monomeric aluminium(I) (Cp^{3tBu})Al (**1.75**).

(^{Dipp}NacNac)Al (**1.33**), for which the synthesis is discussed in section 1.3.3, is another example of a monomeric aluminium(I) compound.[71] Formation of the monomer is aided by the steric protection from the N-substituents of the ligand. The bidentate NacNac-ligand is bonded to the metal through two Al–N bonds to form a six-membered planar heterocycle incorporating the two-coordinate aluminium centre. The Al–N distance is 1.957(2) Å which is longer than in (^{Dipp}NacNac)$AlMe_2$ (**1.66**), consistent with coordination to a larger Al(I) centre.[77,78] The aluminium has a lone pair of electrons in a p-type orbital, with an orthogonal vacant p-type orbital and calculations suggest amphoteric behaviour is possible. Reported reactivity of **1.33** has been dominated by the oxidative addition of small molecules and activation of H–X bonds (discussed in sections 1.2.5 and 1.2.6). However, acting as a Lewis base, **1.33** is able to coordinate to the transition metal centres.[79,80] For example, the coordination of aluminium to copper in (^{Mes}NacNac)CuAl(^{Dipp}NacNac) (**1.77**), synthesised from [{(^{Dipp}NacNac)Cu}$_2$(μ-C_6H_6)] (**1.76**) and **1.33**, (scheme 1.17), which has a Cu–Al distance of 2.3010(6) Å, and is the first example of an unsupported Al–Cu bond.[81]

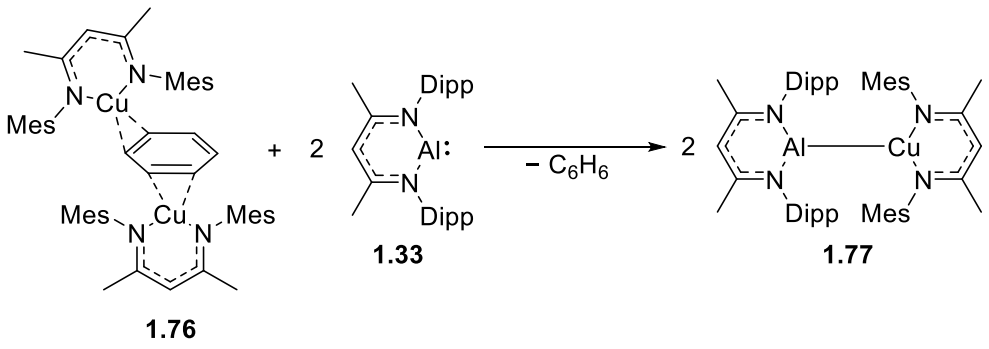

Scheme 1.17 The synthesis of of aluminium-copper complex (^{Mes}NacNac)CuAl(^{Dipp}NacNac) (**1.77**).

The use of sterically hindered ligands has now been established for the formation of monomeric aluminium(I) species. More recently, this class of compounds was extended further by the reports of terphenyl- and carbazole-supported aluminium(I) monomers. Power and co-workers showed that aluminium(I) centres can also be supported by a bulky terphenyl-ligand to give monomer (2,6-Tipp$_2$-3,5-*i*Pr$_2$-C$_6$H)Al (**1.78**, figure 1.6), which is synthesised through the reduction of its corresponding aluminium diiodide with sodium on sodium chloride (Na/NaCl, 5% w/w).[82] The solid-state structure of **1.78** reveals the aluminium centre to be one-coordinate, bonded solely to the ipso carbon at a distance of 1.9883(36) Å (Al–C), and resides symmetrically between the two neighbouring Tipp groups. The Al···H and Al···C separations for centres in the closest methyl groups (>2.9 Å), flanking aryl groups (>3.0 Å), and benzene molecule (>4.8 Å) (co-crystallised with **1.78**) suggests that no secondary bonding interactions are present in the solid-state.

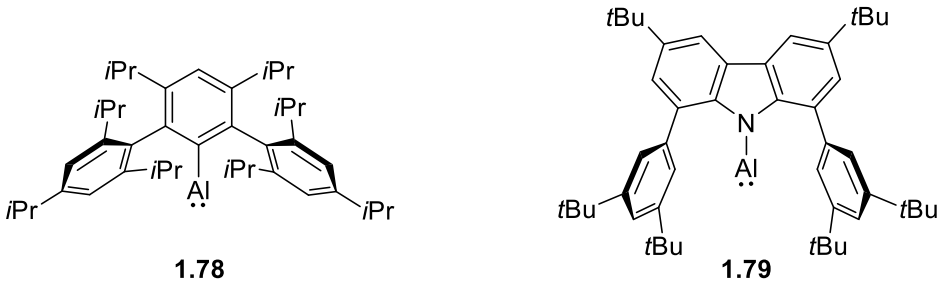

Figure 1.6 Monomeric aluminium(I) species (2,6-Tipp$_2$-3,5-*i*Pr$_2$-C$_6$H)Al (**1.78**) and (^{tBu}Ph$_2$CbzI)Al (**1.79**).

Aryl-substituted carbazolyl-supported aluminium(I) compound ($^{t\text{Bu}}$Ph$_2$Crbzl)Al (**1.79**, figure 1.6) ($^{t\text{Bu}}$Ph$_2$Cbzl = 1,8-bis(3,5-di-*tert*-butylphenyl)-3,6-di-*tert*-butylcarbazolide) displays similarities to terphenyl-derived aluminium(I) **1.78**.[83] The synthesis of **1.79** also proceeds through the reduction of the corresponding aluminium diiodide, but instead uses K/KI (5% w/w) or potassium graphite (KC_8) as the reducing agent.[84] The solid-state structure of **1.79** confirms the aluminium centre to be one-coordinate, residing almost symmetrically between the flanking aryl groups, with no evidence of secondary bonding interactions, as seen for **1.78**. The Al–N bond length is 1.913(9) Å which is marginally shorter than the Pyykkö standard value for an Al–N single bond, suggesting weak π-donation from nitrogen to aluminium.[85] The vacant p-type orbitals and the lone pair of electrons at aluminium give rise to both Lewis acid and Lewis base character. Demonstrating the ambiphilic nature of the aluminium centre, **1.78** was reacted with tungsten hexacarbonyl (W{CO}$_6$) to give aluminium-tungsten adduct (CO)$_5$WAl($^{t\text{Bu}}$PhCbzl), where aluminium is acting as a Lewis base. The addition of N-donor DMAP (DMAP = 4-dimethylaminopyridine), which acts as a Lewis base, results in coordination to the aluminium centre through N→Al donation, to afford (CO)$_5$WAl($^{t\text{Bu}}$PhCbzl)•(DMAP)$_2$.

Within the class of neutral aluminium(I) species, dimeric compounds containing Al=Al double bonds, known as dialumenes, have also been established. The first reported dialumene consists of two aluminium(I) centres, each supported by a trialkylsilyl ligand and an N-heterocyclic carbene (NHC).[86] Dialumene [(*t*Bu$_2$MeSi)Al(I*i*Pr$_2$Me$_2$)]$_2$ (**1.83**) (I*i*Pr$_2$Me$_2$ = 1,3-di-*iso*-propyl-4,5-dimethylimidazol-2-ylidene) is synthesised by the reaction of NHC-alane adduct AlH$_3$• I*i*Pr$_2$Me$_2$ (**1.80**) and BX$_3$•dms (X = Br, I; dms = dimethylsulfide) and *t*Bu$_2$MeSiNa to give silyl aluminium dihalide (*t*Bu$_2$MeSi)AlX$_2$• I*i*Pr$_2$Me$_2$ (X = Br **1.81**, I **1.82**), which is then reduced over KC_8 to give dialumene **1.83** (scheme 1.18). The isolated yields of **1.83** suggest the reduction of aluminium diiodide **1.82** is more successful compared to the aluminium dibromide precursor **1.81**, giving yields of 53% and 34%, respectively. The solid-state structure of **1.83** reveals an overall trans-planar geometry, with each aluminium centre in a trigonal planar geometry and the dihedral angles between the ligands are approximately 180˚. The Al–Al distance is 2.3943(16) Å, which is shorter than calculated Al–Al single bond lengths of dichloro- and dihydroalanes (X$_2$AlAlX$_2$, X = Cl, H), 2.494 and 2.444 Å, respectively, and shorter than that predicted for HAl=AlH, calculated to be 2.613 Å[86] Furthermore, calculations show

the natural bond orders (NBO) of the Al–Al σ-bond and π-bond to be 1.91 and 1.78, respectively, and the Wiberg bond index (WBI) to be 1.70, suggesting significant multiple bond character in **1.83**.

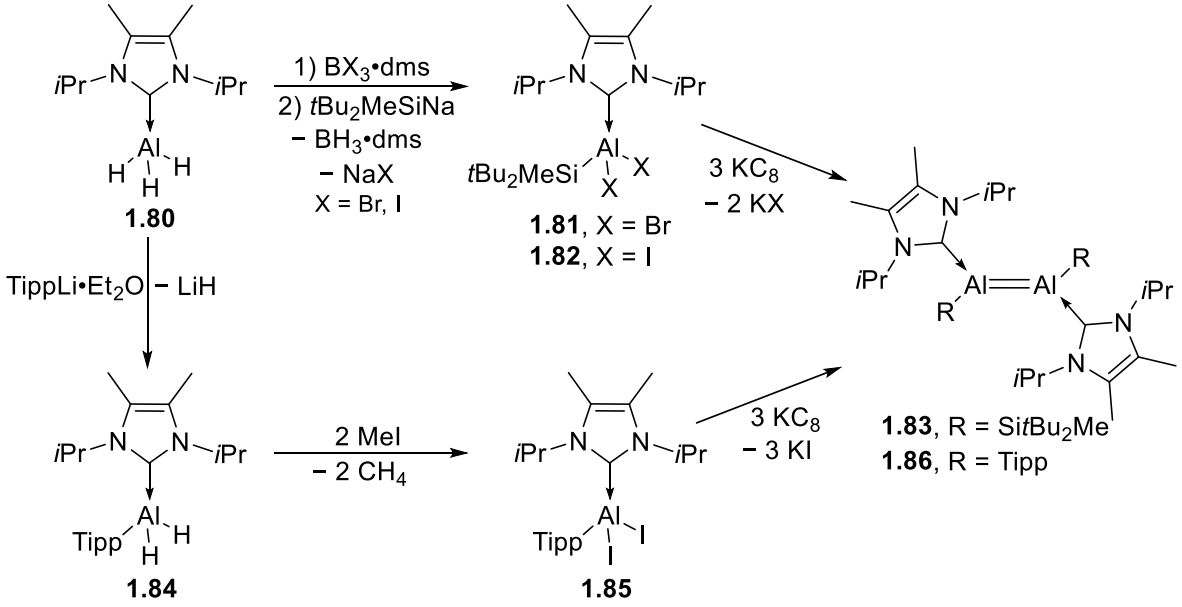

Scheme 1.18 The synthesis of dialumenes [(*t*Bu$_2$MeSi)Al(I*i*Pr$_2$Me$_2$)]$_2$ (**1.83**) and [(Tipp)Al(I*i*Pr$_2$Me$_2$)]$_2$ (**1.86**).

Modifying the silyl ligands in **1.83** to Tipp ligands in [(Tipp)Al(I*i*Pr$_2$Me$_2$)]$_2$ (**1.86**, Tipp = 2,4,6-tri*iso*propylphenyl) demonstrates the influence the ligands have on the properties of dialumenes.[87] Firstly, differences in synthesis arise in the ligand coordination steps in which AlH$_3$•I*i*Pr$_2$Me$_2$ (**1.80**) is reacted with TippLi•Et$_2$O, giving TippAlH$_2$•I*i*Pr$_2$Me$_2$ (**1.84**), followed by the addition of methyliodide (MeI) to give TippAlI$_2$•I*i*Pr$_2$Me$_2$ (**1.85**). The reduction of **1.85**, similar to that described for **1.83**, occurs over KC$_8$ to afford dialumene **1.86** (scheme 1.18). The solid-state structure of **1.86** shows a trans-bent and twisted geometry, in contrast to trans-planar dialumene **1.83**, with the NHC fragments almost perpendicular (85˚). The Al–Al distance is 2.4039(8) Å, marginally longer than **1.83**, whereas the Al–C$_{NHC}$ bond lengths, 2.059(16) and 2.0422(17) Å, are shorter than in **1.83**, suggesting a weaker Al=Al double bond and higher covalent character in the Al–C$_{NHC}$ bonds. The calculated WBI values for **1.86**, Al=Al: 1.53 and Al–C$_{NHC}$: 0.55 (**1.83** Al–C$_{NHC}$: 0.49), are in concordance with experimental

observations and, although slightly diminished compared to **1.83**, shows dialumene **1.86** has significant Al=Al double bond character.

In addition to the base-supported dialumenes **1.83** and **1.86**, an example of an amidophosphine-supported dialumene, **1.88** (scheme 1.19) has also been reported.[88] Dialumene **1.88** is prepared by the reduction of the corresponding aluminium(II) iodide dimer (**1.87**) with sodium-potassium alloy (NaK) (scheme 1.19). The solid-state structure shows **1.88** to have a highly trans-bent structure, but with no twisting of the ligands. The Al–Al bond length is 2.5190(14) Å, which is considerably longer than in **1.83** and **1.86**,[86,87] suggesting a much weaker interaction between the two metal centres. The narrow N–Al–P angles (83-84˚), a result of ligand constraints, and the electronegative NR_2, allowing for a polar Al–N bond (1.909(2) Å), are responsible for the trans-bending observed. Calculations suggest a reduced multiple bond character for Al=Al with a WBI of 1.31 which is significantly lower than that of **1.83** and **1.86**.[86,87] Dialumene **1.88** is predominantly dimeric in solution, but exists in equilibrium with the corresponding monomeric aluminium(I) species through homolysis of the Al=Al bond. In addition to solution-state interconversion between stereoisomers, the reactivity of **1.88** towards bis(trimethylsilyl)acetylene to give monomeric product **1.89** (scheme 1.19), was used to indicate that dissociation of the dimer occurs.

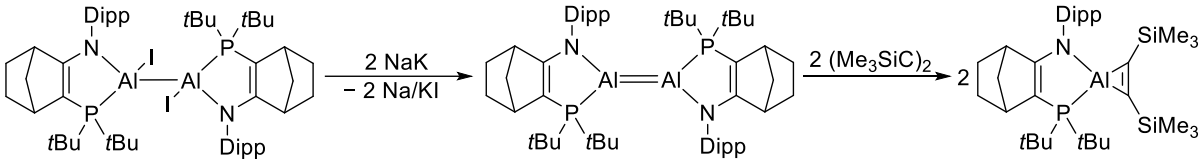

1.87 **1.88** **1.89**

Scheme 1.19 The synthesis of amidophosphine-supported dialumene **1.88** and subsequent reaction with bis(trimethylsilyl)acetylene.

1.4.2 Anionic Aluminium(I) Complexes

In the last few years, a series of anionic aluminuim(I) nucleophiles, known as aluminyl anions have been reported, broadening our understanding of aluminium(I) chemistry. An aluminyl anion is a formal anionic $[AlR_2]^-$ fragment and accompanied by a positively charged

counter ion forms a contact ion pair.[10] Interactions between the anionic fragment and the cation vary depending on the ligand properties and identity of the cation, and can result in the formation of contacted dimeric pairs, in which two aluminyl anions are linked through two bridging cations, or monomeric ion pairs, where there is a direct contact between the aluminium centre and the cation.[89]

The first reported aluminyl anion, $[K\{(NON)Al\}]_2$ (**1.92**), was a dimethylxanthene-supported aluminium(I) complex (NON = 4,5-bis(2,6-di-*iso*-propylanilido)-2,7-di-*tert*-butyl-9,9-dimethylxanthene).[90] The dianionic tridentate NON-ligand can coordinate to aluminium through two Al–N covalent bonds and an O→Al dative bond and uses sterically demanding Dipp-substituents to stabilise the reactive species. Aluminyl **1.92** is synthesised by deprotonation of the diamine ligand $(NON)H_2$ (**1.90**) and subsequent reaction with aluminium triiodide (AlI_3) to give aluminium iodide (NON)AlI (**1.91**), which is then reduced using an excess of KC_8 to afford **1.92** (scheme 1.20).

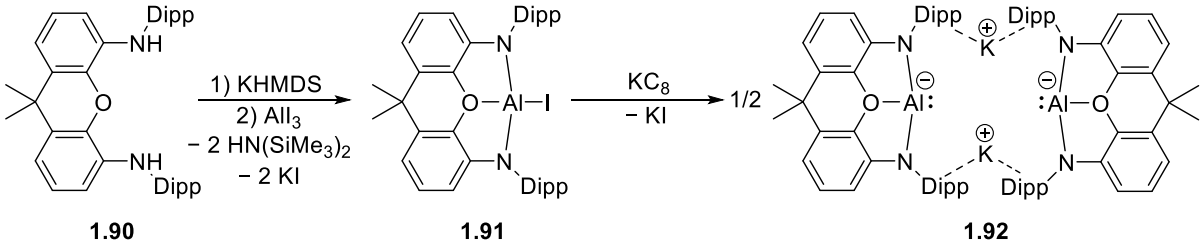

1.90 **1.91** **1.92**

Scheme 1.20 The synthetic route to aluminyl anion $[K\{(NON)Al\}]_2$ (**1.92**).

The solid-state structure of **1.92** reveals a centrosymmetric contacted dimeric pair consisting of two $[(NON)Al]^-$ fragments linked through π-donor interactions between the Dipp groups and the potassium cations which are bonded in an η^6 fashion. The aluminium centre has a large N–Al–N angle of 128.1(1)˚ owing to the rigid nature of the xanthene backbone. However, the N–Al–O angles of 72.9(1)˚ and 72.5(1)˚ and slight puckering of the NON-ligand suggest that there is some flexibility in the coordination of the ligand system. The Al···Al separation is 6.627(7) Å, indicating no interaction between the two metal centres, and the Al···K distances are 4.070(1) and 3.844(1) Å, which are comparable to other group 13 metal anion complexes.[91] The Al–N bond lengths are 1.963(2) and 1.956(2) Å, similar to those in neutral aluminium(I) (^{Dipp}NacNac)Al (**1.33**) (Al–N: 1.957(2) Å), but considerably longer than in

aluminium iodide **1.91** (Al–N: 1.846(2) Å).[71,90] The Al–O distance in aluminyl **1.92** is 2.279(2) Å is significantly longer than in **1.91**, 1.967(2) Å, consistent with the decreased Lewis acidity of an aluminium(I) centre, but is still contributing to coordination of the ligand system.

The reactivity of aluminyl **1.92** has been explored extensively.[10] Oxidative addition reactions of **1.92** with H_2, benzene (C_6H_6), and di-*iso*-propylaniline ($DippNH_2$) proceed by activation of H–X bonds (X = H, C, N). The resulting aluminium(III) products, $[K\{(NON)AlHR\}]_2$ (R = H, C_6H_5, NHDipp), retain their dimeric structure and formal negative charges at the five-coordinate aluminium centres.[10] Moreover, nucleophilic substitution reactions of **1.92** with magnesium iodide (^{Mes}NacNac)MgI(Et_2O) and gold iodide tBu$_3$PAuI give aluminium-metal products (NON)AlMg(^{Mes}NacNac), containing an Al(δ−)–Mg(δ+) bond, and (NON)AlAuPtBu$_3$, which, due to the higher electronegativity of gold (2.54), displays reactivity suggestive of a Al(δ+)–Au(δ−) bond.[10,92]

Treatment of **1.92** with 2.2.2-cryptand (crypt-222) affords charge-separated complex [K(crypt-222)][Al(NON)] (**1.3**) (scheme 1.21).[93] The solid-state structure showed a monomeric structure comprised of the anionic $[(NON)Al]^-$ and cationic $[K(crypt\text{-}222)]^+$ fragments. The Al–N bond lengths, 2.022(1) and 2.049(1) Å, are longer than those in dimer **1.92**, conversely the Al–O bond length, 2.175(1) Å, is shorter than in **1.92**, but remain consistent with a formal +1 oxidation state at aluminium. The angles around aluminium (N–Al–N: 126.7(1)˚, N–Al–O: 72.5(1)˚, 72.7(1)˚) are close to those found in **1.92**, showing that sequestration of the potassium ion has little impact of the geometry of the metal centre. However, formation of a 'naked' aluminyl centre severely alters the reactivity observed of monomer **1.93** compared to dimer **1.92**. In contrast to dimer **1.92**, which reacts with benzene by C–H activation, monomer **1.93** is able to oxidatively add benzene through C–C activation at room temperature to form the seven-membered metallacycle [K(crypt-222)][(NON)Al(C_6H_6)] (**1.94**) (scheme 1.21). The activation of benzene by **1.93** is reversible at elevated temperatures, where the C_6H_6 fragment exchanges with C_6D_6 giving deuterio analogue [K(crypt-222)][(NON)Al(C_6D_6)].

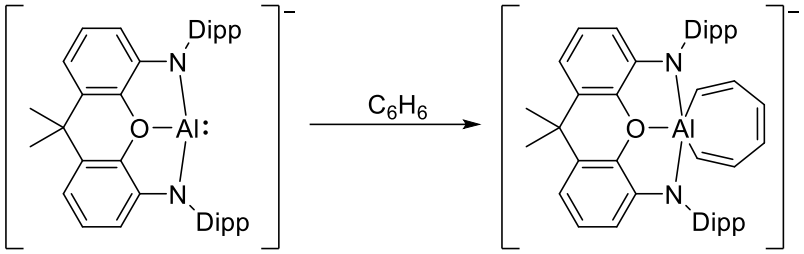

Scheme 1.21 The C–C activation of benzene by [K(crypt-222)][Al(NON)] (**1.93**).

In addition to **1.92**, three further diamido-stabilised aluminyl anions, $[K\{(OSiN)Al\}]_2$ (**1.95**), $[K\{(SiN^{Dipp})Al\}]_2$ (**1.96**), and $[K\{N(C)_3N\}Al]_2$ (**1.97**) have been reported (OSiN = $O(SiMe_2NDipp)_2$, SiN^{Dipp} = $(CH_2SiMe_2NDipp)_2$, $N(C)_3N$ = NDippC(Me)C(H)C(CH_2)NDipp) (figure 1.7).[94–96] Aluminyls **1.95**-**1.97** demonstrate that isolable anionic aluminium(I) species can be stabilised by bidentate diamide ligands, giving rise to two-coordinate aluminium centres. The solid-state structures confirm that **1.95**-**1.97** are dimers with two potassium cations linking the anionic aluminium-containing fragments, as seen for aluminyl **1.92**.

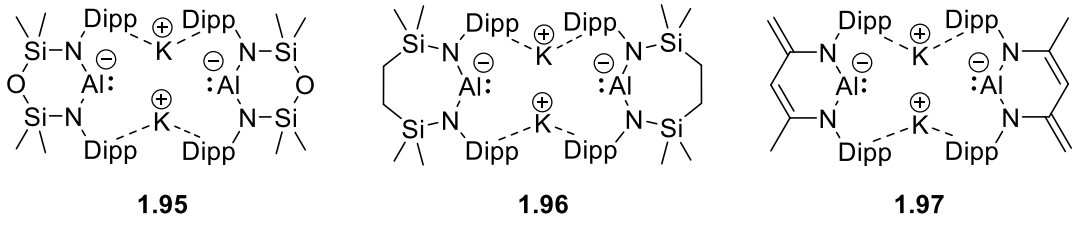

Figure 1.7 Diamido-supported aluminyl anions $[K\{(OSiN)Al\}]_2$ (**1.95**), $[K\{(SiN^{Dipp})Al\}]_2$ (**1.96**), and $[K\{N(C)_3N\}Al]_2$ (**1.97**).

Further investigations into the reducing agents used to access anionic aluminium(I) resulted in a complete series of groups 1 metal incorporated aluminyl anions, $[M\{(OSiN)Al\}]_2$ (M = Li **1.99**, Na **1.100**, Rb **1.101**, Cs **1.102**). The reduction of the aluminium iodide precursor, (OSiN)AlI (**1.98**), using heavier group 1 metal reducing agents RbC_8 or CsC_8 affords dimeric aluminyl anions **1.101** and **1.102** (scheme 1.22), whose structures are akin to potassium aluminyl **1.95**.[89] However, reducing aluminium iodide **1.98** with an excess of lithium or sodium resulted in **1.99** and **1.100** having 'slipped' dimeric structures, in which each metal cation

interacts with one arene group (π(arene)···M) and with one aluminium centre (Al···M), causing asymmetry within the dimers (scheme 1.22).[97]

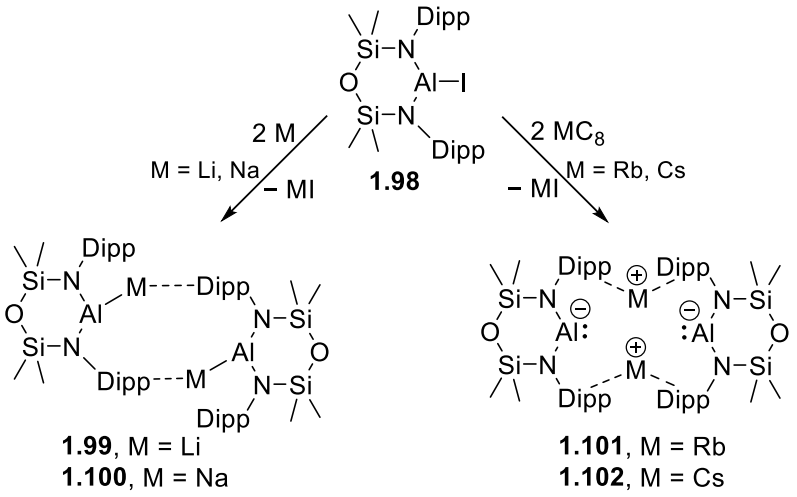

Scheme 1.22 The reduction of (OSiN)AlI (**1.98**) using various group 1 metal reducing agents, showcasing the effect the cation has on the structure of dimeric aluminyl anions $[M\{(OSiN)Al\}]_2$ (M = Li **1.99**, Na **1.100**, Rb **1.101**, Cs **1.102**).

Chelating bidentate dialkyl ligands have also been used to support aluminium(I) anions. Aluminyl anion $(\{CH_2C(SiMe_3)_2\}_2)AlK\bullet(toluene)_2$ (**1.105**) illuminates the effects of stabilising anionic aluminium(I) with an alkyl-support system, from which π-interactions between the ligand and cation are not possible, thus forming a monomeric ion pair.[98] In contrast to the diamido-aluminyls (**1.92**, **1.95**-**1.97**), the synthesis of alkyl-aluminyl **1.105** occurs through reduction of the corresponding aluminium(II) dimer $[\{(SiMe_3)_4C_4H_4\}Al]_2$ (**1.104**), which is prepared from reacting aluminium iodide $\{(Me_3Si)_4C_4H_4\}AlI$ (**1.103**) with excess lithium. Aluminium(II) dimer **1.104** is then reduced using NaK alloy to give aluminyl anion **1.105** (scheme 1.23). The solid-state structure of **1.105** shows a monomeric ion pair comprised of a five-membered metallacycle and a two-centre-two-electron Al–K interaction (3.4549(5) Å). The aluminium centre has a trigonal planar geometry with a narrow C–Al–C angle (90.40(5)˚) and long Al–C bonds (2.0846(9) Å), compared to bond lengths in alkyl-aluminium(III) compounds.[45,61,65]

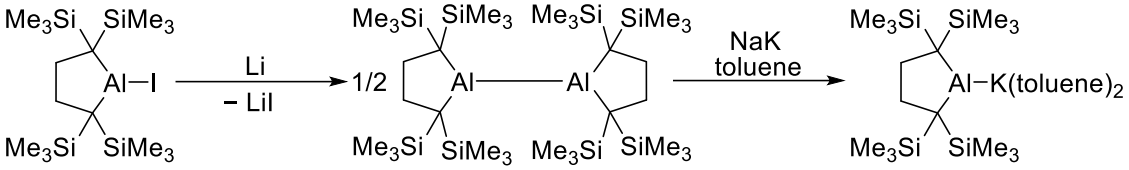

1.103 **1.104** **1.105**

Scheme 1.23 The preparation and reduction of $[\{(SiMe_3)_4C_4H_4\}Al]_2$ (**1.104**) to give alkyl-substituted aluminyl anion $[\{(SiMe_3)_4C_4H_4\}AlK]$ (**1.105**).

Bridging the gap between alkyl- and diamido-aluminyl anions is the alkyl-amido aluminyl [K(12-c-4)][Al(CN^{Ad})] (**1.108**) (CN^{Ad} = N(Ad)CHCHC($SiMe_3$)$_2$, Ad = adamantyl, 12-c-4 = 12-crown-4 ether [$\{C_2H_4O\}_4$]).[99] The synthetic route to **1.108** proceeds through the reduction of aluminium bromide (CN^{Ad})AlBr(Et_2O) (**1.106**) to give aluminium(II) dimer [(CN^{Ad})Al]$_2$ (**1.107**), followed by a second reduction with KC_8 and the addition of a crown ether (12-c-4) to give **1.108** (scheme 1.24). The solid-state structure of **1.108** reveals a separated ion pair structure. The anionic fragment is comprised of a five-membered heterocycle containing a two-coordinate aluminium centre. The Al–N bond length is 1.895(2) Å which is considerably shorter than the charge-separated diamido-aluminyl **1.93** (Al–N: 2.022(1), 2.049(1) Å).[90] The Al–C bond length is 2.095(3) Å which is marginally longer than in alkyl-aluminyl **1.105** (Al–C: 2.0846(9) Å). The N–Al–C angle is very narrow at 86.8(1)˚, smaller than the C–Al–C angle of **1.105** (90.40(5)˚).[98] The Al···K distance is 6.660 Å which is greater than the sum of the van der Waals radii for aluminium and potassium (4.59 Å), indicating no interaction between the two metal centres.

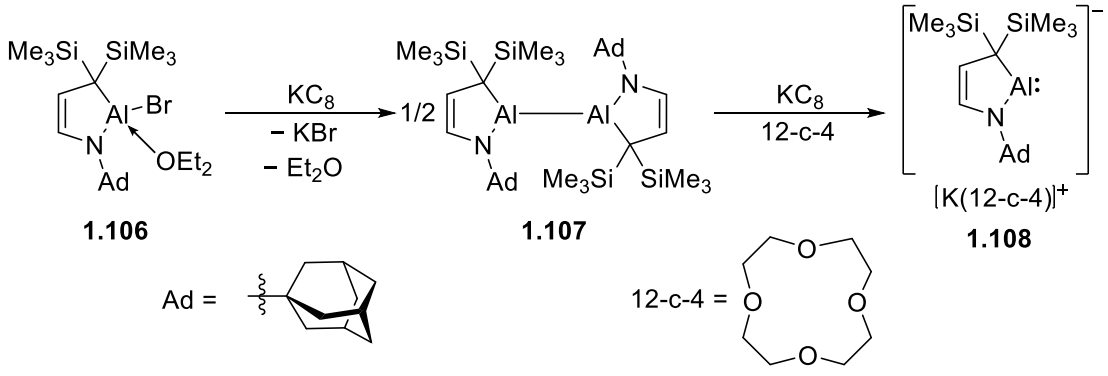

1.106 **1.107** **1.108**

Scheme 1.24 The synthesis of [K(12-c-4)][Al(CN^{Ad})] (**1.108**).

1.5 Multidentate Ligand Systems

Multidentate ligands are support systems which are able to coordinate to a metal centre through two or more bonds. The donors, or binding sites, are appropriately spaced within the ligand scaffold to allow for the formation of a stable metal-containing heterocycle. Several advantages are gained through using multidentate ligands in comparison to monodentate ligands, which possess a single coordination site:

1) **Enthalpic and Entropic Stabilisation**: Multiple ligand-metal interactions allow for greater stability of the metal complex. Enthalpic stabilisation arises due to the increased energy requirements for loss of the ligand from the coordination sphere of the metal as cleavage of more than one bond is required. Chelation of a metal by a ligand is also entropically favoured over an equivalent number of monodentate ligands. These driving forces can be used to enforce unusual and weak bonding interactions.

2) **Geometry**: Multidentate ligands give the potential for greater control over the coordination sphere and, in systems with a rigid backbone, a more predictable arrangement of donors around the metal centre. Control of the geometry of a metal centre has been demonstrated to introduced subsequent control over the energetics of the frontier orbitals of the metal. Using a simplified hybridisation model, we can understand how constrained geometries may affect the frontier orbital energies and shapes. The idealised geometry for frontier orbitals of pure p-character is pyramidal with three orthogonal orbitals at 90° with respect to each other. Increasing the amount of s-character in the frontier orbitals results in an increase in the bond angles about the metal centre, with pure sp^3-orbitals having idealised angles of 109°. In the context of this thesis, the energy of the lone pair of electrons in an aluminium(I) species may be modulated through control of the angles about the aluminium centre, with larger angles resulting in more p-character in the lone pair, corresponding to increased directionality, nucleophilicity and a higher energy lone pair.

3) **Coordination centres**: The identity of the coordinated donor atom and the surrounding substituents can have a large effect on the energetics of the frontier orbitals of the metal centre. Coordinated atoms can have differing σ- and π-donor/acceptor properties which influence the reactivity of the metal centre. One of the benefits of a multidentate system

is the ability to use donating groups which would be too unstable as monodentate ligands, allowing access to a greater variety of donor-acceptor properties.[100]

4) **Hemilability**: The ability to fluxionally dissociate and re-associate from the coordination sphere is a powerful tool employed commonly in transition metal catalysis.[101,102] Multidentate ligands can allow for this type of binding behaviour in a more controlled fashion through the combination of strong coordinating centres and weakly donating centres. This allows retention of a coordination site during reactivity with an entropic driving force for re-association.

The scope of multidentate ligands extends to systems which boast a high number of coordination sites, forming 'pre-organised' macrocycles, such as crown ethers. For the purposes of brevity, this section will focus on chelating bidentate and tridentate ligands, and the effects their properties have on an aluminium centre. Chelating systems which can introduce control over a single aluminium centre will be the focus of this thesis, and as such, ligands which display predominantly bridging interactions will not be discussed here.

1.5.1 Bidentate Ligands at Aluminium

Bidentate ligands are two-coordinate systems which can undergo cyclisation upon chelating to a metal centre. In many cases, the metallacycles are five- to seven-membered, although stable four-membered cycles are known.[103] Bidentate ligands can be neutral (**I**), anionic (**II**), or dianionic (**III**) (figure 1.8). Two types of donors are used within bidentate ligands, neutral donors (L) and anionic donors (X). A neutral donor forms a dative bond with the metal centre through donation of a lone pair of electrons to the metal, thus neutral LL-type ligands (**I**) do not affect the oxidation state of the metal. Anionic XL-type ligands (**II**) contain one anionic donor, which forms a covalent ligand-metal bond, and one neutral donor and, upon coordination, cause a change of +1 to the oxidation state of the metal centre. Dianionic XX-type ligands (**III**) consist of two anionic donors which form covalent bonds with the metal centre, giving rise to a change in metal oxidation state of +2.

Examples of each type of bidentate ligand (**I**-**III**) have been reported to support aluminium centres, the majority of which use either anionic or dianionic bidentate ligands. A

selection of aluminium(III) complexes which incorporate neutral (**1.109**), anionic (**1.110**), and dianionic (**1.111**) bidentate ligands are shown in figure 1.8.[104–106]

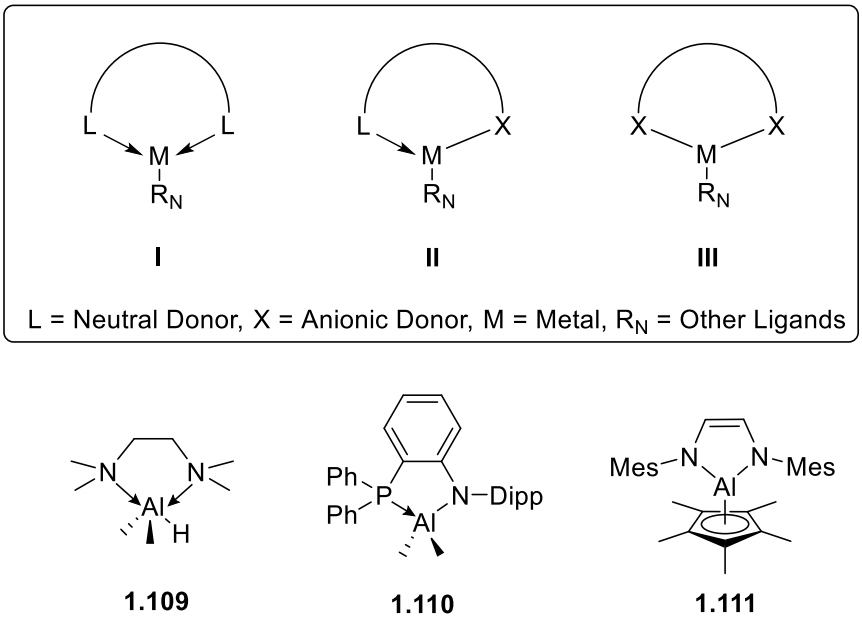

Figure 1.8 Types of bidentate ligand: neutral (**I**), anionic (**II**), and dianionic (**III**), and bidentate ligand-supported aluminium compounds **1.109**-**1.111.**

Modifications of a bidentate ligand alter the electronic and steric properties and, in turn, affect the stabilisation of the metal centre. Typically, this is achieved through two different strategies:

1) **Modification of the coordinating centres (L and X)**: Bidentate ligands using the σ-donating and π-accepting properties of nitrogen are now commonplace in the coordination chemistry of aluminium. The relatively strong bond enthalpy compared to Al–C bonds (Al–N, 297 kJ mol^{-1}, Al–C, 255 kJ mol^{-1}),[70] comparatively low Brønsted basicity, and potential for favourable π-donation have allowed the development of a variety of novel support systems for aluminium. For example, stable aluminyl anion species (**1.95 – 1.97**), utilising dianionic nitrogen-based ligand systems of the type **III**, have received considerable interest in recent years (section 1.4.2, figure 1.7). These systems utilise the high electronegativity of the α-nitrogen to stabilise the lone pair, while N to Al π-donation affects an increase the energy of the p-type orbital. The net effect is a large singlet-triplet energy gap and stabilisation of the monomeric singlet state. Changing one or both of the

substituents to the less electronegative carbon increases the relative energy of the aluminium-centred lone pair and the lack of π-donor properties decreases the energy of the empty p-type orbital resulting in a smaller singlet-triplet gap.[88] This effect is also observed in calculations performed on neutral aluminium(I) species which feature an anionic ligand and a neutral σ-donor.[88] Table 1.1 shows that the calculated singlet-triplet gap for monomeric aluminium(I) species is heavily dependent on both the covalently bonded ligand and the donor ligand, with a more electropositive covalently bonded ligand and a stronger σ-donating ligand resulting in a decreased singlet-triplet gap. In practicality, this effect is illustrated in bidentate ligand systems by the increased tendency for multiple-bond formation on going from (^{Dipp}NacNac)Al(I) (**1.33**) to the amidophosphine supported dialumene **1.88**.[71,88]

Table 1.1 The calculated singlet-triplet energy gaps of neutral aluminium(I) species with varying anionic ligands and σ-donors.

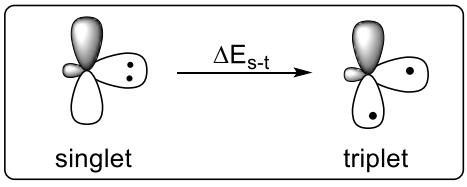

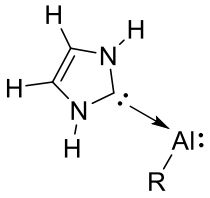

R =	ΔE_{s-t}
H	19.2
Ph	20.6
$SiMe_3$	12.3
NMe_2	25.5

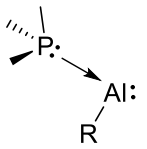

R =	ΔE_{s-t}
H	22.2
Ph	25.4
$SiMe_3$	16.4
NMe_2	32.4

2) **Changing the size of the metallacycle formed on chelation**: The size of the metallacycle formed upon chelation of a bidentate ligand can be used to constrain the angles of bonds about the metal centre. Most notably are the ligand bite angle (figure 1.9, θ) and the M–N–R angle (ϕ), which have a large influence on the electronic and steric properties imposed by the ligand system. The ideal internal angles for perfectly symmetrical and planar 4-, 5- and 6-membered rings increase with ring size such that θ = 90°, 108° and 120°, respectively, while the ideal external angle are ϕ = 135°, 126° and 120°, respectively. For example, comparison of the related 4-membered metallacyclic amidinatoaluminium species **1.112**, the 5-membered metalacyclic species **1.113** and 6-membered metallacyclic (^{Dipp}NacNac)AlMe$_2$ (**1.66**) show increasing bite angles due to relaxation of the constrained angles in the ring system.[71,107,108] As discussed previously, smaller bite angles correlate with an increase in p-character for the bonding orbitals, and in the case of singlet aluminium(I) species, results in greater s-character for the lone pair of electrons. The M-N-R angle can be used to control the steric influence of the ligand, through positioning of the often bulky nitrogen substituents. This is observed through a decreasing M-N-R angle resulting in forward projection of the nitrogen substituents as the size of the metallacycle increases. In the cases of **1.112**, **1.113** and **1.66**, there is a large decrease from ϕ = 145.65° to ϕ = 123.28° on going from 4-membered metallacycle to the 6-membered metallacycle. In all of these cases, the metallacycle remains planar. However, the introduction of a flexible backbone can be used to allow greater variation in the angles of interest and provide a more variable electronic and steric effect.

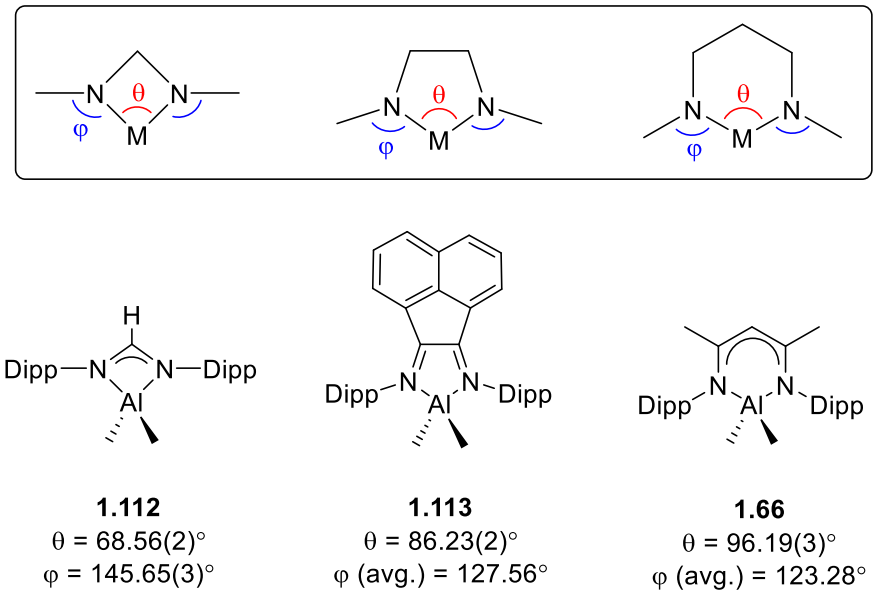

1.112
θ = 68.56(2)°
φ = 145.65(3)°

1.113
θ = 86.23(2)°
φ (avg.) = 127.56°

1.66
θ = 96.19(3)°
φ (avg.) = 123.28°

Figure 1.9 The bite angles (θ) and M–N–R angles (ϕ) of 4-, 5-, and 6-membered metallacycles of bidentate ligand-stabilised aluminium dimethyl species **1.112**, **1.113**, and **1.66**.

1.5.2 Tridentate Ligands at Aluminium

Tridentate ligands, or pincer ligands, are scaffolds that have three coordination sites. These support systems are well established in transition metal chemistry and are becoming more prevalent in the main group chemistry.[109] The various types of pincer ligands differ drastically in their electronic properties, ranging from neutral to trianionic, and can be selected based on the needs of the metal centre (figure 1.10).

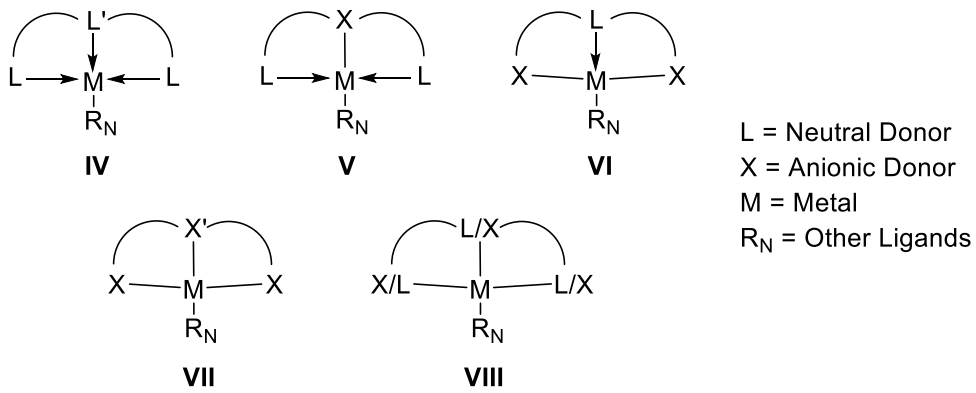

Figure 1.10 The various types of tridentate ligands: neutral (**IV**), anionic (**V**), dianionic (**VI**), trianionic (**VII**), and asymmetric (**VIII**).

The neutral ligand, **IV** (LL'L), consists of three L-type donors which coordinate to the metal centre through donation of a lone pair of electrons to form three dative bonds. As each donor is neutral, the oxidation state of the metal is not affected by coordination of the LL'L-type pincer ligand and so are useful for maintaining electron density at the metal. Next, anionic ligand **V** (LXL) is comprised of one negatively charged centre, which forms a covalent bond with the metal centre, and two flanking neutral donor groups, and can support a metal centre with an oxidation state of n+1 (n = oxidation state of metal in MR_N fragment). Anionic pincer ligands are the most common tridentate ligands. In contrast, dianionic pincer ligands, **VI** (XLX), are far scarcer. The central donor of **VI** is neutral, while the two flanking donors are anionic, and so can stabilise a metal centre with an n+2 oxidation state. In trianionic pincer ligands, **VII** (XX'X), all donors are anionic, forming three covalent bonds to the metal centre, which will have an n+3 oxidation state. Thus, trivalent ligands are capable of stabilising high valent metal centres. Lastly, ligand types **IV**-**VII** are all palindromic, where the donor arms are identical, but non-palindromic pincer ligands, **VIII**, are also known, in which the donor centres are unique from one another. Each of the three donor centres can be either neutral or anionic allowing for a wide range of possible bonding modes.[100]

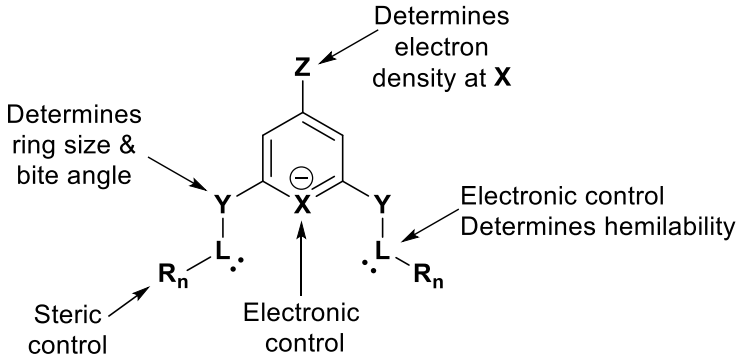

Figure 1.11 The properties of an anionic (type **V**) pincer ligand.

The properties of the different fragments of an anionic (**V**) ligand reveal the extent to which the ligand can stabilise the metal centre (figure 1.11). The central donor, **X**, allows for electronic control, determining the polarity of the **X**–M bond, and can also have an effect on the other ligands bonded to the metal. Neutral donors, **L**, also give electronic control and, depending on the strength of donation, fluxional coordination of the flanking donors may

occur. Thus, **L** determines the hemilability of the ligand. The **L**-substituents, $\mathbf{R_n}$, provide steric hindrance to protect the metal centre. The donor arms, **Y**, allows for control over ring size, by varying the number of centres within the metallocycle, which influences the bite angle. Furthermore, the rigidity of the linkers can also determine the coordination geometries.[110] Incorporation of electron-donating or electron-withdrawing groups at **Z** can affect the electron density at the central donor (**X**), hence allows for greater electronic control, but has little influence on the steric properties of the ligand. Modifications to each fragment of a pincer ligand enable fine tuning which allows for optimal stabilisation of the metal centre through steric and electronic effects.[100]

Within main group chemistry, tridentate ligands have already been reported to stabilise aluminium centres. Complexes **1.114**-**1.118** show that each type of tridentate ligand (**IV**-**VIII**) is able to coordinate an aluminium metal centre (figure 1.12).[111–115] The aluminium centres of **1.114**-**1.118** are all in the +3 oxidation state and have a coordination number of five, with the exception of **1.114**, in which the ligand is tridentate with respect to the aluminium, which is six-coordinate. However, the use of tridentate ligands to stabilise low-oxidation state aluminium remains underexplored. To date, only one example of a tridentate ligand-supported aluminium(I) complex has been reported, aluminyl anion $[K\{(NON)Al\}]_2$ (**1.92**) (discussed in section 1.4.2).

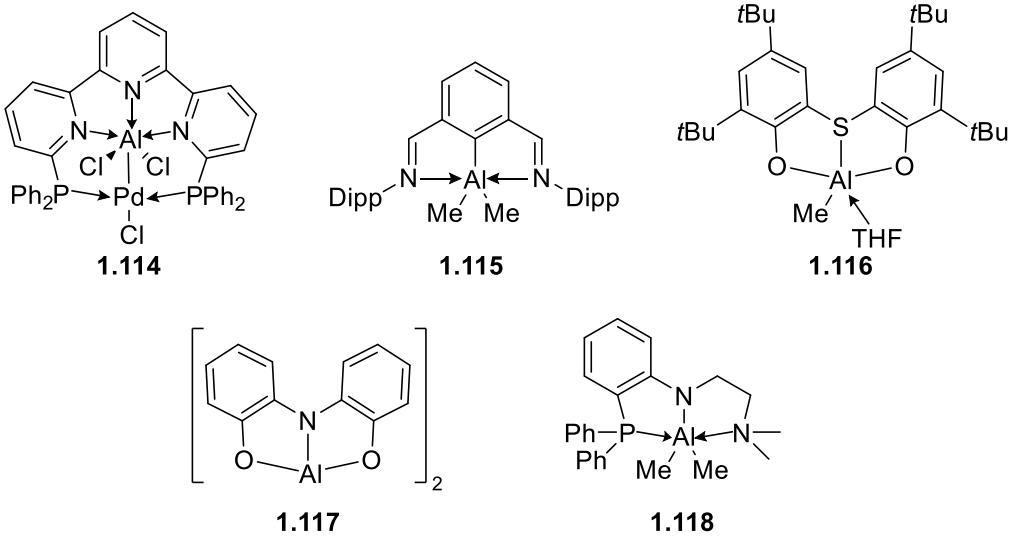

Figure 1.12 Tridentate ligand-supported aluminium(III) complexes **1.114**-**1.118**.

1.6 Outlook and Aims

The previous work discussed in this chapter shows the characteristics of aluminium compounds in which the metal centre is in either the +3 or +1 oxidations states. Investigations into aluminium(III) dihydrides revealed the use of monodentate ligands generally results in formation of dimeric or trimeric aluminium hydride species. However, it was shown the aggregation diminished upon coordination of a bi- or tri-dentate ligand or a Lewis base to the aluminium centre. More recently, research in to aluminium(III) halides demonstrate their reactivity towards reducing agents, as focus shifts to aluminium(I) chemistry. A range of isolable aluminium(I) species have been reported from neutral monomeric compounds to dialumenes, consisting of Al=Al double bonds, and most recently, aluminyl anions, the newest class of aluminium(I) compounds.

This thesis aims to explore the synthesis and reactivity of novel aluminium hydride and halide species, supported by bi- and tri-dentate ligands. The reduction of some compounds will also be investigated with the aim of accessing low-oxidation state aluminium. The first two chapters focuses on the use of anionic tridentate ligands to support the aluminium centre. The final chapter explores the synthesis of novel diphosphine ligands and coordination to aluminium centres.

1.7 References

(1) Haynes, W. M., *CRC Handbook of Chemistry and Physics*, 97th Edition, CRC Press, **2016**, pp 4-3 – 4-4.

(2) Brough, D.; Jouhara, H., *Int. J. Thermofluids*, **2020**, *1–2*, 100007.

(3) Drago, R. S., *J. Phys. Chem.*, **1958**, *62*, 353–357.

(4) Yous, S.; Poupaert, J. H.; Lesieur, I.; Depreux, P.; Lesieur, D., *J. Org. Chem.* **1994**, *59*, 1574–1576.

(5) Sunke, R.; Nallapati, S. B.; Kumar, J. S.; Kumar, K. S.; Pal, M., *Org. Biomol. Chem.* **2017**, *15*, 4042–4057.

(6) Uhl, W.; Appelt, C.; Backs, J.; Westenberg, H.; Wollschläger, A.; Tannert, J., *Organometallics* **2014**, *33* (5), 1212–1217. https://doi.org/10.1021/om4012246.

(7) Stennett, T. E.; Pahl, J.; Zijlstra, H. S.; Seidel, F. W.; Harder, S., *Organometallics* **2016**, *35*, 207–217.

(8) Nikonov, G.; Dmitrienko, A.; Pilkington, M.; Britten, J. F.; Gabidullin, B. M.; van der Est, A., *Angew. Chem. Int. Ed.*, **2020**, *59*, 16147 -16153.

(9) Roesky, H. W., *Inorg. Chem.* **2004**, *43*, 7284–7293.

(10) Hicks, J.; Vasko, P.; Goicoechea, J. M.; Aldridge, S., *Angew. Chem. Int. Ed.*, **2021**, *60*, 1702–1713.

(11) Stasch, A., *Angew. Chem. Int. Ed.*, **2012**, *51*, 1930–1933.

(12) Polukeev, A. V.; Marcos, R.; Ahlquist, M. S. G.; Wendt, O. F., *Organometallics* **2016**, *35*, 2600–2608.

(13) Etezadi, S.; Koppaka, A.; Gamage, M. M.; Captain, B., *J. Organomet. Chem.*, **2017**, *848*, 122–132.

(14) Takenaka, Y.; Hou, Z., *Organometallics*, **2009**, *28*, 5196–5203.

(15) J. Butler, M. R. Crimmin, M., *Chem. Commun.*, **2017**, *53*, 1348–1365.

(16) Ozimiński, W. P.; Dobrowolski, J. C., *J. Phys. Org. Chem.*, **2009**, *22*, 769–778.

(17) Armentrout, P. B.; Halle, L. F.; Beauchamp, J. L., *J. Am. Chem. Soc.* **1981**, *103*, 6501–6502.

(18) Luo, B.; Kucera, B. E.; Gladfelter, W. L., *Dalton Trans.*, **2006**, 37, 4491.

(19) Downs, A. J.; Pulham, C. R., *Chem. Soc. Rev.*, **1994**, *23*, 175–184.

(20) Falconer, R. L.; Nichol, G. S.; Cowley, M. J., *Inorg. Chem.*, **2019**, *58*, 11439–11448.

(21) Falconer, R. L.; Nichol, G. S.; Smolyar, I. V.; Cockroft, S. L.; Cowley, M. J., *Angew. Chem. Int. Ed.*, **2021**, *60*, 2047–2052.

(22) Wang, X.; Andrews, L.; Tam, S.; DeRose, M. E.; Fajardo, M. E., *J. Am. Chem. Soc.*, **2003**, *125*, 9218–9228.

(23) Contreras, L.; Cowley, A. H.; Gabbaï, F. P.; Jones, R. A.; Carrano, C. J.; Bond, M. R., *J. Organomet. Chem.*, **1995**, *489*, C1–C3.

(24) Woińska, M.; Grabowsky, S.; Dominiak, P. M.; Woźniak, K.; Jayatilaka, D., *Sci. Adv.*, *2*, e1600192.

(25) A. Malaspina, L.; A. Hoser, A.; J. Edwards, A.; Woińska, M.; J. Turner, M.; R. Price, J.; Sugimoto, K.; Nishibori, E.; Bürgi, H.-B.; Jayatilaka, D.; Grabowsky, S., *Cryst. Eng. Comm.*, **2020**, *22*, 4778–4789.

(26) Chidambaram, R.; Sikka, S. K., *Curr. Sci.*, **2003**, *85*, 871–877.

(27) Løvvik, O. M.; Opalka, S. M.; Brinks, H. W.; Hauback, B. C., *Phys. Rev. B*, **2004**, *69*, 134117.

(28) Ruff, J. K.; Hawthorne, M. F., *J. Am. Chem. Soc.*, **1960**, *82*, 2141–2144.

(29) Ashby, E. C., in *Advances in Inorganic Chemistry and Radiochemistry* (Ed.: Emeléus, H. J., Sharpe, A. G.); Academic Press, **1966**, Vol. 8, pp 283–335.

(30) Finholt, A. E.; Bond, A. C.; Schlesinger, H. I., *J. Am. Chem. Soc.*, **1947**, *69*, 1199–1203.

(31) Ashby, E. C.; Boone, J. R., *J. Am. Chem. Soc.*, **1976**, *98*, 5524–5531.

(32) Bismuto, A.; Thomas, S. P.; Cowley, M. J., *Angew. Chem. Int. Ed.*, **2016**, *55*, 15356–15359.

(33) Kobayashi, M.; Itoh, M., *Chem. Lett.* **1996**, *25* , 1013–1014.

(34) Elsen, H.; Langer, J.; Ballmann, G.; Wiesinger, M.; Harder, S., *Chem. Eur. J.*, **2021**, *27*, 401–411.

(35) Yoshio, M.; Ishibashi, N.; Waki, H.; Seiyama, T., *J. Inorg. Nucl.*, **1972**, *34*, 2439–2448.

(36) Turley, J. W.; Rinn, H. W., *Inorg. Chem.* **1969**, *8*, 18–22.

(37) Stecher, O.; Wiberg, E., *Ber. Dtsch. Chem. Ges.*, **1942**, *75* , 2003–2012.

(38) Wang, Y.; Yan, J.-A.; Chou, M. Y. *Phys. Rev. B*, **2008**, *77*, 014101.

(39) Chizinsky, G.; Evans, G. G.; Gibb, T. R. P.; Rice, M. J., *J. Am. Chem. Soc.* **1955**, *77*, 3164–3165.

(40) Janik, J. F.; Duesler, E. N.; McNamara, W. F.; Westerhausen, M.; Paine, R. T., *Organometallics*, **1989**, *8*, 506–514.

(41) Schneider, H.; Hock, A.; Bertermann, R.; Radius, U., *Chem. Eur. J.*, **2017**, *23*, 12387–12398.

(42) Aldridge, S.; Downs, A. J., *Chem. Rev.*, **2001**, *101*, 3305–3366.

(43) Peters, F. M.; Bartocha, B.; Bilbo, A. J., *Can. J. Chem.*, **1963**, *41*, 1051–1058.

(44) Ehrlich, R.; Parisek, C. B.; Rice, G., *Inorg. Chem.*, **1965**, *4*, 1075–1076.

(45) Wehmschulte, R. J.; Power, P. P., *Inorg. Chem.*, **1994**, *33*, 5611–5612.

(46) Wehmschulte, R. J.; Grigsby, W. J.; Schiemenz, B.; Bartlett, R. A.; Power, P. P., *Inorg. Chem.*, **1996**, *35*, 6694–6702.

(47) Downs, A. J.; Duckworth, D.; Machell, J. C.; Pulham, C. R., *Polyhedron*, **1992**, *11*, 1295–1304.

(48) Atwood, J. L.; Bennett, F. R.; Elms, F. M.; Jones, C.; Raston, C. L.; Robinson, K. D., *J. Am. Chem. Soc.*, **1991**, *113*, 8183–8185.

(49) Bernert, T.; Ley, M. B.; Ruiz-Fuertes, J.; Fischer, M.; Felderhoff, M.; Weidenthaler, C., *Acta Crystallogr. Sect. B*, **2016**, *72*, 232–240.

(50) Dümichen, U.; Gelbrich, T.; Sieler, J., *Z. Anorg. Allg. Chem.*, **1999**, *625*, 262–268.

(51) Atwood, D. A.; Contreras, L.; Cowley, A. H.; Jones, R. A.; Mardones, M. A., *Organometallics* **1993**, *12*, 17–18.

(52) Janik, J. F.; Wells, R. L.; White, P. S., *Inorg. Chem.*, **1998**, *37*, 3561–3566.

(53) von Hänisch, C.; Rolli, B., *Z. Anorg. Allg. Chem.*, **2004**, *630*, 1987–1990.

(54) Chu, T.; Korobkov, I.; Nikonov, G. I., *J. Am. Chem. Soc.*, **2014**, *136*, 9195–9202.

(55) Yow, S.; Gates, S. J.; White, A. J. P.; Crimmin, M. R., *Angew. Chem. Int. Ed.*, **2012**, *51*, 12559–12563.

(56) Chang, J.-C.; Hung, C.-H.; Huang, J.-H., *Organometallics*, **2001**, *20*, 4445–4447.

(57) Nako, A. E.; Gates, S. J.; White, A. J. P.; Crimmin, M. R., *Dalton Trans.*, **2013**, *42*, 15199–15206.

(58) Nako, A. E.; Gates, S. J.; Schädel, N.; White, A. J. P.; Crimmin, M. R., *Chem. Commun.*, **2014**, *50*, 9536–9538.

(59) Lee, P.-Y.; Liang, L.-C., *Inorg. Chem.*, **2009**, *48*, 5480–5487.

(60) Uhl, W., *Z. Anorg. Allg. Chem.*, **1989**, *570*, 37–53.

(61) Cowley, A. H.; Isom, H. S.; Decken, A., *Organometallics*, **1995**, *14*, 2589–2592.

(62) Klein, C.; Nöth, H.; Tacke, M.; Thomann, M., *Angew. Chem.*, **1993**, *105*, 923–926.

(63) Greenwood, N. N.; Earnshaw, A.; Earnshaw, E.; A, E. *Chemistry of the Elements*; Butterworth-Heinemann, **1984**.

(64) Olah, G. A.; Lee, C. S.; Prakash, G. K. S.; Moriarty, R. M.; Rao, M. S. C., *J. Am. Chem. Soc.*, **1993**, *115*, 10728–10732.

(65) Wehmschulte, R. J.; Power, P. P., *Inorg. Chem.*, **1996**, *35*, 3262–3267.

(66) Krossing, I.; Nöth, H.; Tacke, C.; Schmidt, M.; Schwenk, H., *Chem. Ber.*, **1997**, *130*, 1047–1052.

(67) Vidovic, D.; Moore, J. A.; Jones, J. N.; Cowley, A. H., *J. Am. Chem. Soc.*, **2005**, *127*, 4566–4567.

(68) Lewiński, J.; Pasynkiewicz, S.; Lipkowski, J., *Inorg. Chim. Acta*, **1990**, *178*, 113–123.

(69) Bakthavachalam, K.; Reddy, N. D., *Organometallics*, **2013**, *32*, 3174–3184.

(70) Darwent, B. deB., Bond Dissociation Energies in Simple Molecules, *U.S National Bureau of Standards*, **1970**, 60.

(71) Cui, C.; Roesky, H. W.; Schmidt, H.-G.; Noltemeyer, M.; Hao, H.; Cimpoesu, F., *Angew. Chem. Int. Ed.*, **2000**, *39*, 4274–4276.

(72) Tacke, M.; Schnoeckel, H., *Inorg. Chem.*, **1989**, *28*, 2895–2896.

(73) Mellerup, S. K.; Cui, Y.; Fantuzzi, F.; Schmid, P.; Goettel, J. T.; Bélanger-Chabot, G.; Arrowsmith, M.; Krummenacher, I.; Ye, Q.; Engel, V.; Engels, B.; Braunschweig, H., *J. Am. Chem. Soc.*, **2019**, *141*, 16954–16960.

(74) Dohmeier, C.; Robl, C.; Tacke, M.; Schnöckel, H., *Angew. Chem. Int. Ed.*, **1991**, *30*, 564–565.

(75) Ganesamoorthy, C.; Loerke, S.; Gemel, C.; Jerabek, P.; Winter, M.; Frenking, G.; Fischer, R. A., *Chem. Commun.*, **2013**, *49*, 2858–2860.

(76) Hofmann, A.; Tröster, T.; Kupfer, T.; Braunschweig, H., *Chem. Sci.*, **2019**, *10*, 3421–3428.

(77) Knabel, K.; Krossing, I.; Nöth, H.; Schwenk-Kircher, H.; Schmidt-Amelunxen, M.; Seifert, T., *Eur. J. Inorg. Chem.*, **1998**, 1095–1114.

(78) Qian, B.; Ward, D. L.; Smith, M. R., *Organometallics*, **1998**, *17*, 3070–3076.

(79) Kempter, A.; Gemel, C.; Fischer, R. A., *Chem. Eur. J.*, **2007**, *13*, 2990–3000.

(80) Kong, R. Y.; Crimmin, M. R., *Dalton Trans.*, **2021**, *50*, 7810–7817.

(81) Mears, K. L.; Stennett, C. R.; Taskinen, E. K.; Knapp, C. E.; Carmalt, C. J.; Tuononen, H. M.; Power, P. P., *J. Am. Chem. Soc.*, **2020**, *142*, 19874–19878.

(82) Queen, J. D.; Lehmann, A.; Fettinger, J. C.; Tuononen, H. M.; Power, P. P., *J. Am. Chem. Soc.* **2020**, *142*, 20554–20559.

(83) Zhang, X.; Liu, L. L., *Angew. Chem. Int. Ed.*, **2021**, *60*, 27062–27069.

(84) Hinz, A.; Müller, M. P., *Chem. Commun.*, **2021**, *57*, 12532–12535.

(85) Pyykkö, P.; Atsumi, M., *Chem. Eur. J.*, **2009**, *15*, 186–197.

(86) Bag, P.; Porzelt, A.; Altmann, P. J.; Inoue, S., *J. Am. Chem. Soc.*, **2017**, *139*, 14384–14387.

(87) Weetman, C.; Porzelt, A.; Bag, P.; Hanusch, F.; Inoue, S., *Chem. Sci.*, **2020**, *11*, 4817–4827.

(88) Falconer, R. L.; Byrne, K. M.; Nichol, G. S.; Krämer, T.; Cowley, M. J., *Angew. Chem. Int. Ed.*, **2021**, *60*, 24702–24708.

(89) Gentner, T. X.; Evans, M. J.; Kennedy, A. R.; Neale, S. E.; McMullin, C. L.; Coles, M. P.; Mulvey, R. E., *Chem. Commun.*, **2022**, *58*, 1390–1393.

(90) Hicks, J.; Vasko, P.; Goicoechea, J. M.; Aldridge, S., *Nature*, **2018**, *557*, 92–95.

(91) Twamley, B.; Power, P. P., *Angew. Chem. Int. Ed.*, **2000**, *39*, 3500–3503.

(92) Hicks, J.; Mansikkamäki, A.; Vasko, P.; Goicoechea, J. M.; Aldridge, S., *Nat. Chem.*, **2019**, *11*, 237–241.

(93) Hicks, J.; Vasko, P.; Goicoechea, J. M.; Aldridge, S., *J. Am. Chem. Soc.*, **2019**, *141*, 11000–11003.

(94) Schwamm, R. J.; Anker, M. D.; Lein, M.; Coles, M. P., *Angew. Chem. Int. Ed.*, **2019**, *58*, 1489–1493.

(95) Schwamm, R. J.; Coles, M. P.; Hill, M. S.; Mahon, M. F.; McMullin, C. L.; Rajabi, N. A.; Wilson, A. S. S., *Angew. Chem. Int. Ed.*, **2020**, *59*, 3928–3932.

(96) Harder, S.; Grams, S.; Eyselein, J.; Langer, J.; Färber, C., *Angew. Chem. Int. Ed.,* **2020**, *59*, 15982–15986.

(97) Evans, M. J.; Anker, M. D.; McMullin, C. L.; Neale, S. E.; Coles, M. P., *Angew. Chem. Int. Ed.*, **2021**, *60*, 22289–22292.

(98) Kurumada, S.; Takamori, S.; Yamashita, M., *Nat. Chem.*, **2020**, *12*, 36–39.

(99) Koshino, K.; Kinjo, R., *J. Am. Chem. Soc.*, **2020**, *142*, 9057–9062.

(100) Peris, E.; Crabtree, R. H., *Chem. Soc. Rev.* **2018**, *47*, 1959–1968.

(101) Lindner, R.; van den Bosch, B.; Lutz, M.; Reek, J. N. H.; van der Vlugt, J. I., *Organometallics*, **2011**, *30*, 499–510.

(102) Slone, C. S.; Weinberger, D. A.; Mirkin, C. A., in *Progress in Inorganic Chemistry*; John Wiley & Sons, Ltd, **1999**; pp 233–350.

(103) A. Kitos, A.; Mavragani, N.; Murugesu, M.; L. Brusso, J., *Mater. Adv.*, **2020**, *1*, 2688–2706.

(104) Pörschke, K.-R.; Kleimann, W.; Tsay, Y.-H.; Krüger, C.; Wilke, G., *Chem. Ber.*, **1990**, *123*, 1267–1273.

(105) Liang, L.-C., *Coord. Chem. Rev.*, **2006**, *250*, 1152–1177.

(106) Cowley, A. H.; Gorden, J. D.; Abernethy, C. D.; Clyburne, J. A. C.; McBurnett, B. G., *Dalton Trans.*, **1998**, 12, 1937–1938.

(107) Hamidi, S.; Dietrich, H. M.; Werner, D.; Jende, L. N.; Maichle-Mössmer, C.; Törnroos, K. W.; Deacon, G. B.; Junk, P. C.; Anwander, R., *Eur. J. Inorg. Chem.*, **2013**, 13, 2460–2466.

(108) Schumann, H.; Hummert, M.; Lukoyanov, A. N.; Fedushkin, I. L., *Organometallics*, **2005**, *24*, 3891–3896.

(109) Dostál, L.; Jambor, R., in *Pincer Compounds*; (Ed: Morales-Morales, D.); Elsevier, **2018**; pp 47–65.

(110) Robinson, T. P.; De Rosa, D.; Aldridge, S.; Goicoechea, J. M., *Chem. Eur. J.*, **2017**, *23*, 15455–15465.

(111) Takaya, J.; Iwasawa, N., *J. Am. Chem. Soc.*, **2017**, *139*, 6074–6077.

(112) Liu, Z.; Ganguly, R.; Vidović, D., *Dalton Trans.*, **2017**, *46*, 753–759.

(113) Tiempos-Flores, N.; Metta-Magaña, A.-J.; Montiel-Palma, V.; Cortés-Llamas, S.-A.; Muñoz-Hernández, M.-Á., *Dalton Trans.*, **2010**, *39*, 4312–4320.

(114) Wang, P.; Zhang, M.; Zhu, C., *Organometallics*, **2020**, *39*, 2732–2738.

(115) Lee, W.-Y.; Liang, L.-C., *Dalton Trans.*, **2005**, 11, 1952–1956.

Chapter 2

PNP-Pincer Ligands for Aluminium Hydrides and Halides

2.1 Introduction

Pincer ligands are chelating support systems which coordinate to a metal centre through bonding to three adjacent sites, usually in a meridional arrangement, as discussed in section 1.5.2. The use of pincer ligands is well-established in transition metal chemistry and, over more recent years, such ligands have become more popular in main group chemistry.[1–4] The multidentate nature of pincer ligands provides support for a metal centre through both electronic and steric effects. The charge of the ligand, for example neutral, monoanionic, or dianionic, allows for support of a metal in various oxidations states, while the choice of hard or soft donors allows for electronic tuning of the ligand.

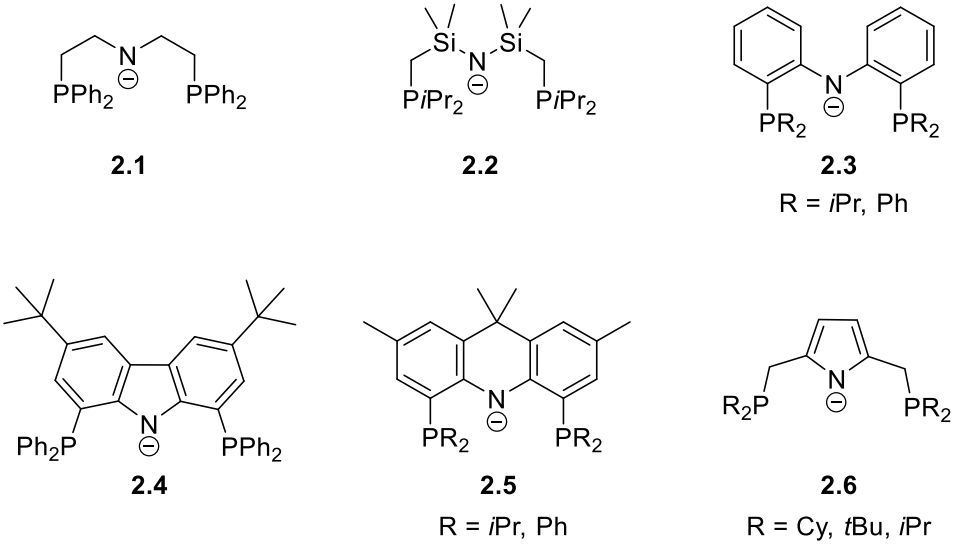

Figure 2.1 A selection of monoanionic PNP-type pincer ligands.[5–12]

Monoanionic PNP-type pincer ligands, or amidophosphines, are support systems comprised of a hard anionic nitrogen donor, combined with two soft neutral phosphorus donors. The first example of an amidophosphine ligand was reported by Sacconi in the 1960's, which saw two phosphine fragments linked to nitrogen through ethylene bridges (**2.1**).[6] Over time, the class of PNP-pincer ligands has expanded through modifications of the backbone, ranging from aliphatic and aromatic linkers to nitrogen-containing heterocycles, altering the flexibility of the ligand. Ligands **2.1** – **2.6** (figure 2.1) showcase the diversity within the class

of PNP-pincer ligands. Moreover, variations of the phosphine substituents affect the donating and steric properties of the ligands.[13–15]

Monomeric organoaluminium dihydride and dihalide compounds are notoriously unstable and usually require bulky, electron donating ligands for stabilisation of the electron deficient aluminium centre.[16,17] Therefore, it is unsurprising that pincer ligands have proven to be effective support systems for stabilising aluminium hydride and halide species. [18,19] The majority of the ligands reported to date feature nitrogen and carbon donors, yet phosphine-supported aluminium dihydrides and dihalides are still rare.

2.1.1 PNP-Supported Aluminium Complexes

While phosphine-supported aluminium species are scarcer than their nitrogen counterparts, a handful have been reported to date. Fryzuk and co-workers disclosed the synthesis of the first PNP-supported organoaluminium alkyl and halide compounds in 1996 (Scheme 2.1).[7] $[N(SiMe_2CH_2P\textit{i}Pr_2)_2]^-$ (**2.2**), an XL_2-type ligand with a flexible aliphatic backbone, consists of an anionic binding site at nitrogen and two neutral phosphine donor, giving rise to potential tridentate coordination to the metal centre. The lithium salt of the ligand precursor, **2.7**, was reported to react with $AlCl_3$ to generate monomeric aluminium dichloride complex **2.8**.

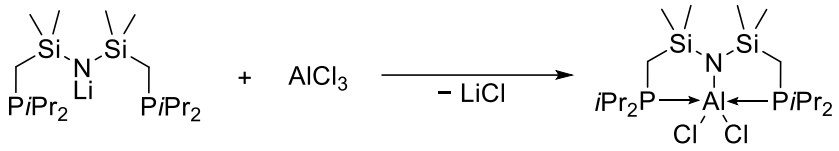

2.7 **2.8**

Scheme 2.1 Reported preparation of aliphatic PNP-supported aluminium dichloride **2.8** through salt metathesis.

The $^{31}P\{^1H\}$ NMR spectrum of aluminium dichloride **2.8** consists of a broad signal at −10.5 ppm. Moreover, the solid-state structure, determined by X-ray crystallography, reveals

the aluminium centre to be five-coordinate with a trigonal bipyramidal geometry as a result of ligand constraints. The N–Al bond has a typical length of 1.89(1) Å,[17,20,21] whilst the two phosphorus centres donate into a p-type orbital at aluminium, with distances of 2.542(7) Å and 2.509(7) Å for P1–Al1 and P2–Al1 respectively. The P1–Al1–P2 bond angle of 171.8(3)˚ reveals the extent of distortion from the ideal trigonal bipyramidal geometry (180˚).

The hydrocarbyl aluminium counterparts to aluminium dichloride **2.8** were synthesised by the reaction of **2.8** with alkyl lithium or magnesium reagents, shown in scheme 2.2. For example, dimethyl aluminium **2.9** was generated by the metathesis reaction of aluminium dichloride **2.8** with either methyl lithium or dimethyl magnesium dioxane. In contrast to aluminium dichloride **2.8**, the $^{31}P\{^{1}H\}$ NMR spectra for hydrocarbyl aluminium compounds **2.9** - **2.11** consist of sharp singlet resonances between −3.6 ppm and −4.9 ppm which is thought to be due to weak or fluxional coordination of the phosphorus donors.

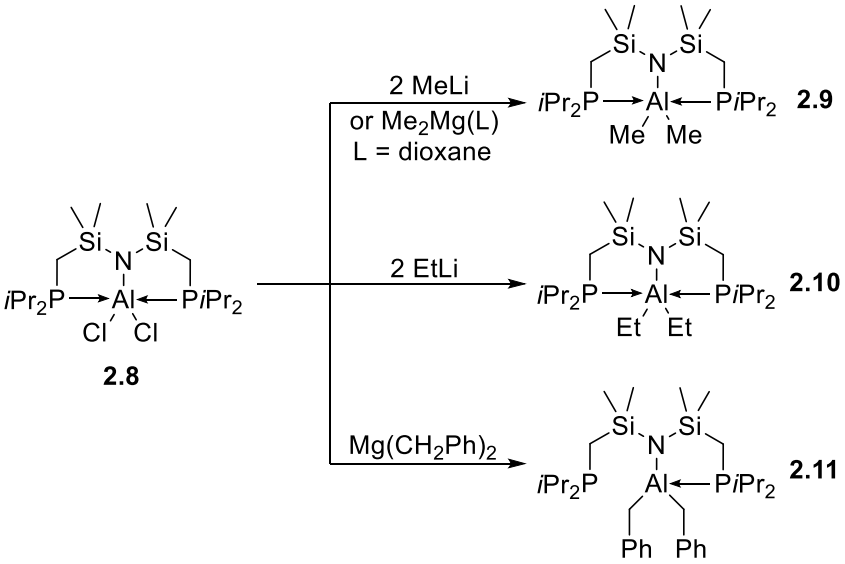

Scheme 2.2 Reported synthesis of hydrocarbyl aluminium compounds **2.9**, **2.10**, and **2.11** from the reaction of aluminium dichloride **2.8** with alkyl lithium and magnesium reagents.

The solid-state structure of dibenzyl aluminium **2.11** was determined by X-ray crystallography and shows aluminium to be four-coordinate with only one phosphorus coordinating to aluminium. The larger size of the benzyl substituents, compared to the chloride centres of **2.8**, results in greater steric repulsions between benzyl and *iso*-propyl

groups, causing dissociation of a phosphine arm, demonstrating the lability of the neutral donors. The aluminium centre has a distorted tetrahedral geometry, attributed to steric constraints of the ligand, with bond angles ranging from 92.1(2)˚ to 117.5(3)˚. The Al–P bond length of 2.453(3) Å in **2.11** is marginally shorter than in aluminium dichloride **2.8**, suggesting slightly stronger P→Al donation in **2.11**. Likewise, the aluminium-nitrogen distance of 1.853(5) Å is shorter compared to that of **2.8**, which may be due to a higher degree of π-donation from the nitrogen lone pair to aluminium.

Further to the work of Fryzuk and co-workers, only one other PNP-pincer ligand, diaryl amidophosphine **2.3** (figure 2.1), has been used to coordinate aluminium.[12] The backbone of ligand **2.3** is significantly more rigid than that of aliphatic ligand **2.2**, which led to differences in geometry, coordination numbers and potential reactivity of the aluminium centre. Furthermore, the phosphorus-substituents were varied from symmetric diphenyl- (**2.3a**) and *iso*-propyl-phosphine fragments (**2.3b**) to asymmetric phenyl/*iso*-propyl phosphine arms (**2.3c**) (scheme 2.2).

The reported syntheses of aluminium dichlorides **2.13a** – **2.13c** proceed by the reaction of lithium amide precursors **2.12a** – **2.12c** (lithium salts of ligand **2.3**) with aluminium trichloride ($AlCl_3$). Alternatively, aminophosphines **2.14a** – **2.14c** react with methyl aluminium dichloride ($MeAlCl_2$) to give **2.13a** – **2.13c** by methane elimination (scheme 2.3). However, aluminium dichlorides **2.13a** – **2.13c** were not isolated but prepared *in situ* before reacting with lithium aluminium hydride ($LiAlH_4$) to generate aluminium dihydrides **2.15a** – **2.15c**. In addition, dialkyl aluminium compounds **2.16a-c**, **2.17a-c**, and **2.18a-c** were also prepared through alkane elimination by the reaction of the protio ligands, **2.14a** – **2.14c**, with AlR_3 (R = Me, Et or *i*Bu) (scheme 2.3).

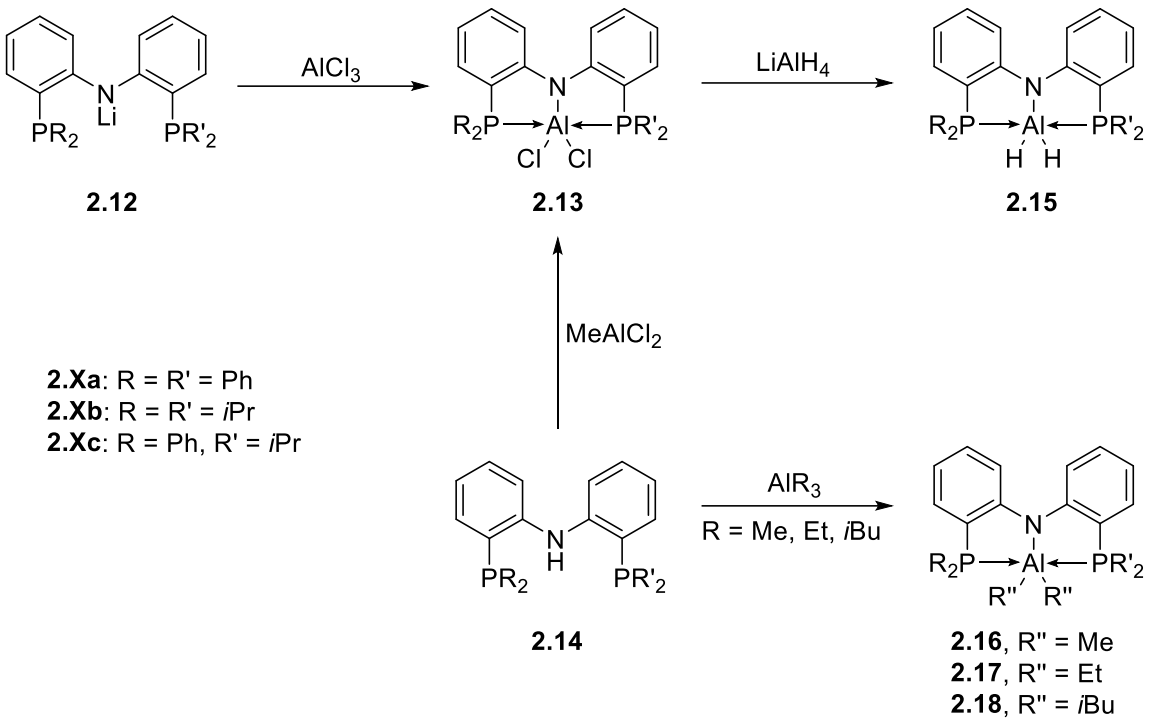

Scheme 2.3 Reported preparations of diaryl amido phosphine supported aluminium halides (**2.13a-c**), hydrides (**2.15a-c**) and hydrocarbyls (**2.16a-c**, **2.17a-c**, **2.18a-c**).

The $^{31}P\{^{1}H\}$ NMR spectra of each alkyl aluminium complex shows a singlet resonance with an upfield shift, such as aluminium methyls **2.16a** (−19.6 ppm) and **2.16b** (−17.6 ppm), in comparison to aminophosphines **2.14a** (−18.6 ppm) and **2.14b** (−13.3 ppm). The α-C centres of alkyl aluminium complexes **2.16a,b**, **2.17a,b** and **2.18a,b** correlate to triplet resonances in the $^{13}C\{^{1}H\}$ NMR spectra due to the coupling to two phosphorus centres indicating both phosphine groups are donating into the p-type orbital at aluminium. Increasing the bulk of the Al-substituents (Et and *i*Bu) and P-substituent (*i*Pr) led to desymmetrisation of the α-protons and the observation of two multiplet resonances in the ^{1}H NMR. In contrast, the presence of less sterically hindered P-substituents (Ph) (**2.17a** and **2.18a**) or smaller Al-substituents (Me) (**2.16a** and **2.16b**) allowed for more rapid rotation about the Al–C_α bonds causing the α-H atoms to become magnetically equivalent.

X-ray crystallography studies of the solid-state structures of methyl aluminium complexes **2.16a-c** allowed for comparison of the effect of varying the phosphine fragments. For the symmetrically substituted **2.16a** (PPh_2) and **2.16b** ($PiPr_2$), Al–P distances for **2.16a** (2.6202(13) Å, 2.202(13) Å) are marginally shorter than for those in **2.16b** (2.6343(10) Å,

2.6246(10) Å), which may be a result of *iso*-propyl groups being more sterically demanding than phenyl groups. However, when compared within the same molecule, the *i*Pr_2P–Al bond length (2.5499(18) Å) is much shorter compared to Ph_2P–Al (2.7902(17) Å) in asymmetric aluminium dimethyl **2.16c**. This is due to the greater electron donating properties of the di*iso*propyl phosphine fragments.

The solid-state structures, determined by X-ray crystallography, of aluminium dichloride **2.13b**, dihydride **2.15b**, and alkyl complexes **2.16b** ($AlMe_2$) and **2.17b** ($AlEt_2$) showcase the effects that the anionic monodentate ligands have on the coordination of aluminium(III) centres. Minimal change is observed upon increasing the alkyl ligand size from methyl (**2.16b**) to ethyl (**2.17b**) with only slight lengthening of P–Al bonds (2.6514(9) Å, 2.6578(9) Å) and marginal widening of P–Al–P angle (155.62(3)˚). In contrast, aluminium hydride **2.15b** has shorter ligand−Al bonds (N–Al: 1.899(6) Å, P–Al: 2.570(2) Å, 2.590(2) Å), which is compensated for by a wider P–Al–P angle (155.11(11)˚). However, aluminium chloride **2.13b** boasts the shortest P–Al bond lengths (2.481(2) Å, 2.481(2) Å), and the widest P–Al–P angle (160.36(18)˚) of all (*i*Pr-PNP)AlX_2 compounds (**2.15b** – **2.18b**).

2.1.2 Carbazolide-Based PNP-Pincer Ligands

Carbazolide-based PNP-ligands are rigid support systems containing a secondary diaryl amide centre and two neutral flanking phosphine donors (figure 2.2). Substitution of carbazole is favoured at the 3- and 6-positions, thus alkyl groups, such as methyl and *tert*-butyl groups, are commonly used to block these sites to direct derivatisation reactions to the 1- and 8-positions. Variations in the size of substituents and donating ability of the phosphine fragments allow PNP-pincer ligands to be used to stabilise transition metal centres.[22–26] Within main group chemistry, a diaryl-substituted carbazolide ligand has been used to support an aluminium(I) centre (**1.79**, discussed in section 1.4.1).[27] However, aluminium species supported by carbazolide-based pincer ligands are yet to be explored.

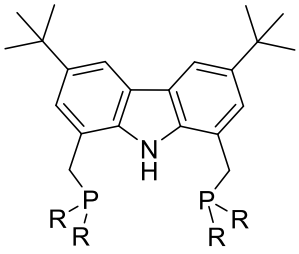

2.19, R = Ph
2.20, R = *t*Bu

Figure 2.2 Carbazole-based amido phosphine ligands **2.19** and **2.20**.

In comparison amidophosphines **2.2** and **2.3** (figure 2.1), carbazole-based aminophosphine ligands (**2.19** and **2.20**, figure 2.3) possess a more robust and rigid backbone. Methylene linkers can be installed between the carbazole and phosphine donors to introduce some flexibility into the ligand scaffold, which will influence the bite angle, chelation ring size, and the orientation of the phosphorus centres. Amidophosphine ligands **2.19** and **2.20** will be used to synthesise a series of aluminium halide and hydride compounds to investigate the influence carbazole-based PNP-pincer ligands have on the properties and reactivity of the aluminium centre.

2.2 Aims and Outlooks

The aims of the project were:

- To synthesise, isolate and characterise carbazolide-based PNP-supported aluminium dihydride and dihalide complexes.
- To probe the reactivity of the PNP-aluminium dihydrides with various organic substrates and other metal-containing complexes.
- To investigate possible reduction reactions of PNP-aluminium dihydrides and dihalides to access the aluminium(I) derivatives.

2.3 Synthesis of (^{Ph}PNP)AlH$_2$ (2.22)

Initial attempts to synthesise (^{Ph}PNP)AlH$_2$ (**2.22**) (^{Ph}PNP = 3,6-di-*tert*-butyl-1,8-bis(diphenylphosphinomethyl)carbazolide) aimed to proceed through the deprotonation of amino-phosphine (^{Ph}PNP)H (**2.19**) followed by metathesis reaction with chloroalane. NMR scale lithiation of aminophosphine **2.19** proceeded using 1.2 equivalents of n-butyllithium (nBuLi) to generate (^{Ph}PNP)Li (**2.21**) *in situ*, to afford an orange solution. The ^{31}P NMR spectrum contained a new singlet resonance at −10.5 ppm suggesting complete deprotonation of aminophosphine **2.19**, which resonates at −18.1 ppm. The ^{1}H NMR spectrum confirmed complete deprotonation by the absence of an N*H* resonance (8.36 ppm, **2.19**). The reaction was repeated on a larger scale, and lithium amide **2.21** was subsequently reacted with ClAlH$_2$•(NMe$_3$)$_2$ (scheme 2.1). Upon reacting **2.21** with ClAlH$_2$•(NMe$_3$)$_2$, a colour change from orange to yellow was observed.

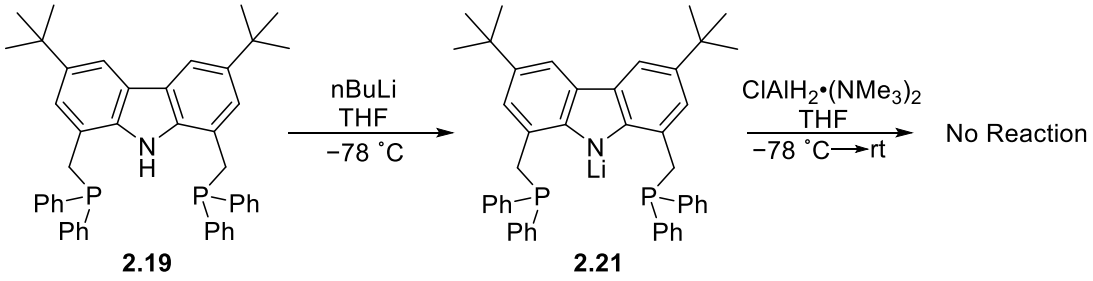

Scheme 2.4 Initial preparation of lithium amide **2.21** and subsequent addition of ClAlH$_2$•(NMe$_3$)$_2$.

Upon reacting lithium amide **2.21** with ClAlH$_2$•(NMe$_3$)$_2$, ^{31}P NMR spectroscopy of an aliquot showed the presence of a mixture of products with the major products resonating as singlets at −6.3, −12.3, and −16.9 ppm. Extraction with toluene allowed isolation of colourless crystals. Using single crystal X-ray diffraction analysis, the crystallised product was identified as a 1:1 mixture of amino-phosphine **2.19** and lithium amide **2.21**. The solid-state structure of lithium amide **2.21** shows the lithium atom to be bonded to nitrogen with a N–Li distance of 1.939(11) Å (figure 2.3). Interactions between lithium and the phosphorus centres are observed with Li–P distances of 2.476(11) and 2.463(11) Å. The NMR spectroscopic and X-ray

crystallographic observations suggest that **2.21** is unstable under the reaction conditions and had undergone protonolysis, generating amino phosphine **2.19**. Furthermore, as there was no evidence for the formation of an aluminium hydride species, alternate pathways to (^{Ph}PNP)AlH$_2$ (**2.22**) were explored.

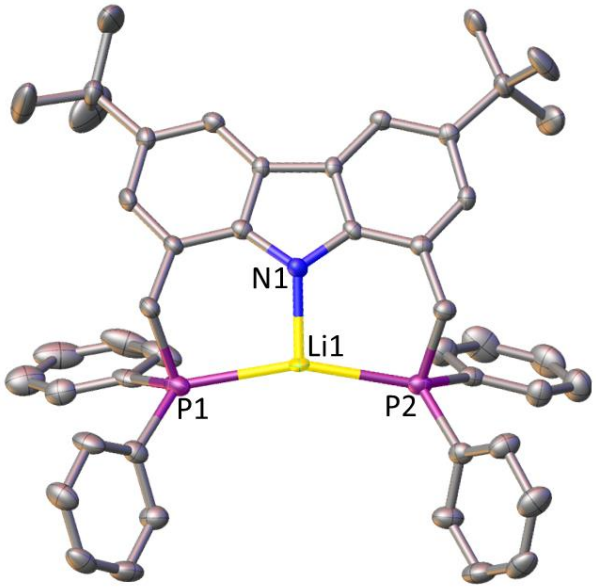

Figure 2.3 Solid-state structure of (^{Ph}PNP)Li (**2.21**). Hydrogen atoms omitted for clarity. Thermal ellipsoids set to 50% probability. Selected bond lengths (Å) and angles (˚) N1–Li1 1.939(11), P1–Li1 2.476(11), P2–Li1 2.463(11), N1–Li1–P1 99.1(4), N1–Li1–P2 101.3(4), P1–Li1–P2 158.2(5).

An alternate synthetic route to (^{Ph}PNP)AlH$_2$ (**2.22**) was considered. Reported alkyl organoaluminium complexes, stabilised by amino-phosphine ligands, are synthesised through reacting AlR$_3$ (R = Me, Et, *i*Bu) with amino-phosphines, resulting in alkane elimination, whilst synthesis the aluminium dihydride analogues required production of the aluminium dichloride which was then reacted with LiAlH$_4$ or LiH.[12,28] However, Lou and co-workers showed AlH$_3$•(OEt$_2$)$_n$, afforded by the reaction of AlCl$_3$ with three equivalents of LiAlH$_4$, could be used in a similar manner to AlR$_3$ in order to generate aluminium dihydride (NNN)AlH$_2$ (NNN

= N{$CH_2CH_2NMe_2$}$_2$) *via* hydrogen elimination.[29] The combined efficiency and ease of isolation of (NNN)AlH_2, makes this a very attractive route to aluminium dihydride complexes.

Amine-stabilised alane AlH_3.NMe_3 was used in place of AlH_3•$(OEt_2)_n$ to synthesise (^{Ph}PNP)AlH_2 (**2.22**). The acidity of the nitrogen-bound hydrogen atom of amino-phosphine **2.19**, along with the hydridic nature of the hydrogen atoms bound to the electropositive aluminium centre, allowed for successful production of aluminium dihydride **2.22**, through elimination of dihydrogen. Amino phosphine **2.19** was reacted with AlH_3•NMe_3 in toluene at ambient temperature in a one-step synthesis. The volatiles were removed, and residue washed with pentane to afford aluminium dihydride **2.22** as a colourless solid in yields of up to 91% (scheme 2.5).

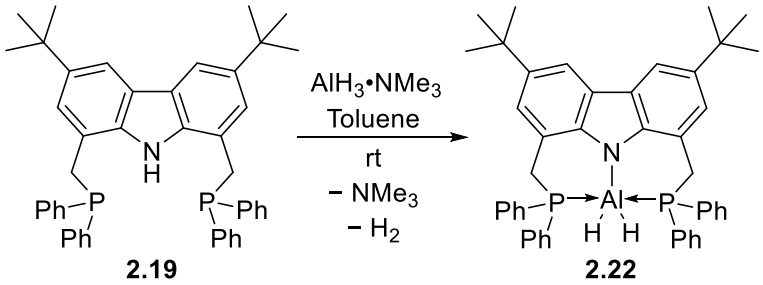

2.19 **2.22**

Scheme 2.5 The preparation of (PNP)AlH_2 (**2.22**) starting from amino-phosphine **2.19** and AlH_3•NMe_3.

The ^{1}H NMR spectrum of aluminium dihydride **2.22** (figure 2.4) reveals a singlet resonance for the protons of the methylene linkers (C*H*$_2$PPh_2, 4.11 ppm) showing them to be chemically equivalent, which is also the case for the *tert*-butyl groups of the carbazole backbone (1.40 ppm). A broad triplet at 5.84 ppm, with a coupling constant ($^2J_{H-P}$) of 56 Hz, corresponds to the aluminium hydrides. The splitting is due to coupling of the aluminium-bound hydrogen atoms to two ligand-based phosphorus atoms. This suggests that both phosphorus atoms are donating into the p-type orbital at aluminium. In contrast to aluminium dihydride **2.22**, resonances corresponding to Al*H* of previously reported amidophosphine-supported aluminium dihydrides are seen as broad singlet peaks with no observable splitting as a result of coupling to the donating phosphorus centres.[12,17] The hydrogen atoms being

bonded to aluminium, which possesses a quadrupolar nucleus (^{27}Al, I = 5/2, 100% abundant), causes broadening of the resonance as a result of rapid quadrupolar relaxation.

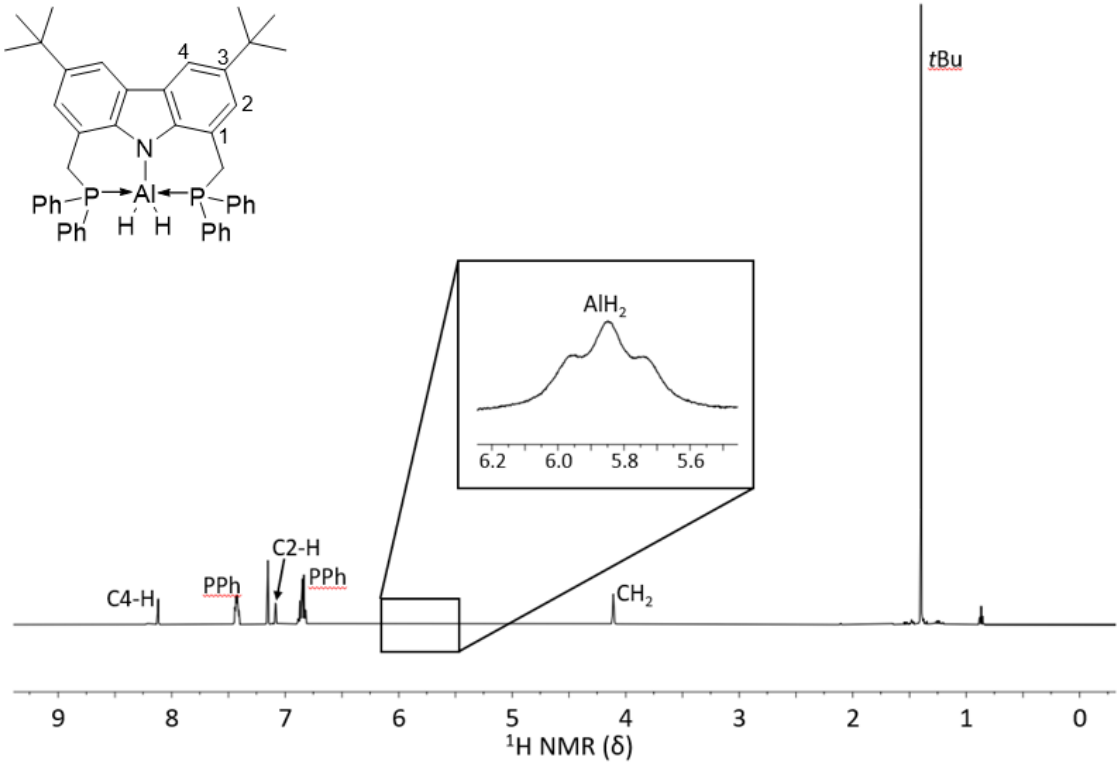

Figure 2.4 ^{1}H NMR spectrum of (^{Ph}PNP)AlH$_2$ (**2.22**) with a magnification of the aluminium hydride resonance at 5.84 ppm.

In the ^{31}P{^{1}H} NMR spectrum of (PNP)AlH$_2$ (**2.22**), a single resonance at −33.5 ppm is observed, indicating equivalent phosphorus centres. Furthermore, the ^{31}P NMR spectrum consists of a triplet ($^{2}J_{H\text{-}P}$ = 58 Hz) at −33.5 ppm (figure 2.5). The coupling constant is close in magnitude to that of Al–H signal in the ^{1}H NMR spectrum, which further supports that both phosphorus atoms are bonded to aluminium. Previous reports of aluminium(III) complexes containing two phosphorus-donating groups have shown a degree of hemilability of the P-donors.[7] The NMR spectroscopy data obtained implies that dissociation of P-donors is not occurring in aluminium dihydride **2.22** at room temperature, which may be attributed to the limited flexibility of the ligand.[12]

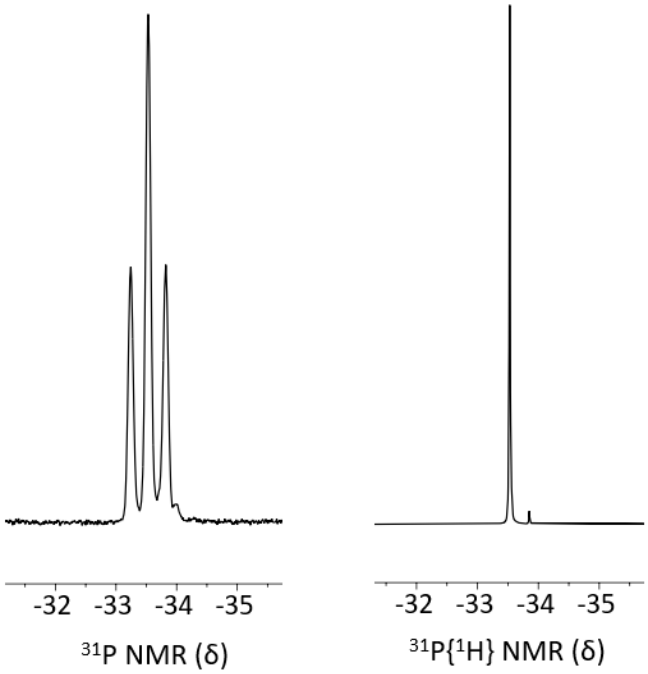

Figure 2.5 ^{31}P NMR spectrum (left) and $^{31}P\{^{1}H\}$ NMR spectrum (right) of $(PNP)AlH_2$.

The structure of (^{Ph}PNP)AlH_2 (**2.22**) was confirmed using single crystal X-ray diffraction (figure 2.6). The five-coordinate aluminium centre is best described as having a slightly distorted trigonal bipyramidal geometry with two Al–P bonds located axially. The wide P1–Al1–P2 angle of 177.88(2)˚ shows a lesser degree of distortion in comparison to diarylamido-phosphine aluminium dihydride **2.15b**, which has a P–Al–P angle of 159.11(11)˚.[12] It is worth noting that aluminium dihydride **2.15b** contains *iso*-propyl P-substituents, which may influence the bond angles due to electronic and steric differences of branched alkyl groups compared to aryl groups. The Al–P bond lengths of dihydride **2.22**, 2.5823(5) Å and 2.6217(5) Å for Al1–P1 and Al1–P2 respectively, are similar to reported Al–P distances of organoaluminium dihydride compounds containing aryl-substituted P-donor.[30] However, the Al–P distances of **2.22** are slightly longer than those of amidophosphine-supported aluminium compounds where phosphorus bears alkyl substituents such as *tert*-butyl groups.[17,30] The difference in Al–P bond lengths could arise from the greater donating ability of alkyl-bearing P-donors which lead to stronger Al–P bonds being formed.

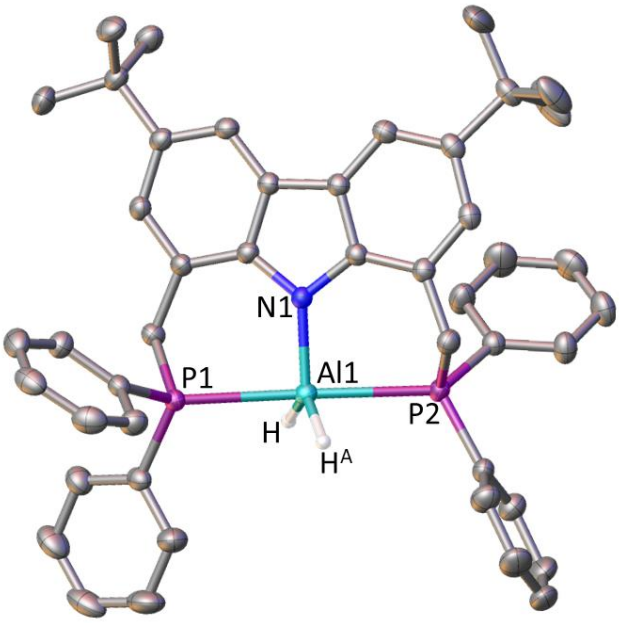

Figure 2.6 Solid-state structure of (PNP)AlH_2 (**2.22**). H atoms, except Al-bound H and HA, omitted for clarity. Thermal ellipsoids set to 50% probability. Select bond lengths (Å) and angles (˚): N1–Al1 1.9038(12), P1–Al1 2.5823(5), P2–Al1 2.6217(5), N1–Al1–P1 89.16(4), N1–Al1–P2 91.72(4), P1–Al1–P2 177.88(2).

In addition to P-donation, the ligand also coordinates to the metal centre through a covalent aluminium-nitrogen bond with an Al–N distance of 1.9038(12) Å, typical of Al-N single bonds.[20,21] The N1–Al1–P1 and N1–Al1–P2 angles, 89.16(4)˚ and 91.72(4)˚, respectively, which is a consequence of the formation of two six-membered metallocycles and rigidity of the carbazole backbone. The location of two hydride ligands could not be determined by X-ray crystallography, thus will not be commented on.

Infrared spectroscopy was used to measure Al−H stretching frequency of (^{Ph}PNP)AlH_2 (**2.22**) found at 1751 cm^{-1}, which is comparable to the terminal Al–H stretching frequencies reported monomeric aluminium hydride compounds.[17]

2.4 Reactivity of (^{Ph}PNP)AlH$_2$ (2.22)

Through exploiting the polarity of the Al$^{\delta+}$–H$^{\delta-}$ bond, (^{Ph}PNP)AlH$_2$ (**2.22**) was reacted with a variety of organic molecules such as anilines and isonitriles, as well as main group and transition metal complexes.

2.4.1 Reactivity with Anilines

Primary aryl amines, known as anilines, are commonly used in ligand synthesis and as substrates in various organic transformations.[31,32] The electronegativity of nitrogen and the presence of an aryl N-substituent, which is slightly electron-withdrawing, allows for the protic hydrogens to react with aluminium hydrides. Thermal dehydrocoupling is a well-known route to Al–N bonds, but is often subject to slow reaction rates.[33] Aluminium dihydride **2.22** was reacted with a variety of anilines to investigate the formation of Al–N$_{aniline}$ bonds and potential selectivity towards reacting with one or two equivalents of an aniline to give the products (^{Ph}PNP)AlH(NHAr) or (^{Ph}PNP)Al(NHAr)$_2$, respectively, which may be influenced by altering the steric and electronic properties of the aniline. In addition, if selectivity towards the single dehydrocoupled product, (^{Ph}PNP)AlH(NHAr), could be achieved, then there may be potential for the evolution of a second equivalent of H_2 to give (^{Ph}PNP)Al(NAr), forming an Al=N double bond.

Firstly, aluminium dihydride **2.22** was reacted with one equivalent of H_2NPh, which proceeded *via* hydrogen elimination at ambient temperature (scheme 2.6). The ^{31}P NMR spectrum reveals the major product to be aminophosphine ligand **2.19**, shown by a singlet at −18.1 ppm (55% by integration), and is considered the decomposition product of either aluminium dihydride **2.22** or the products of the dehydrocoupling reaction, which may be due contamination of aniline with trace amounts of water. Moreover, a doublet resonance was present at −31.0 ppm (19% by integration, $^2J_{H-P}$ = 55 Hz), a slight downfield shift compared to −33.5 ppm for aluminium dihydride **2.22**. The phosphorus-hydrogen coupling indicates that one hydrogen remained bonded to aluminium to give (^{Ph}PNP)AlH(NHPh) (**2.23**). In addition, a minor singlet resonance at −26.8 ppm (7% by integration) suggests that a second dehydrocoupling reaction had occurred to give a small amount of (^{Ph}PNP)Al(NHPh)$_2$ (**2.24**).

Furthermore, a modest amount of unreacted aluminium dihydride **2.22** was also present in solution. The observed signals in the ^{31}P NMR spectrum suggest that in both **2.23** and **2.24** the phosphorus donors are equivalent. Crimmin and co-workers reported that upon reacting a five-coordinate aluminium dihydride with two equivalents para-fluoroaniline to give the double dehydrocoupled product, dissociation of a pendant amine donor was observed.[34] Thus, as the phosphine donors are equivalent in **2.24**, it is assumed that both phosphine fragments remain coordinated to the aluminium centre.

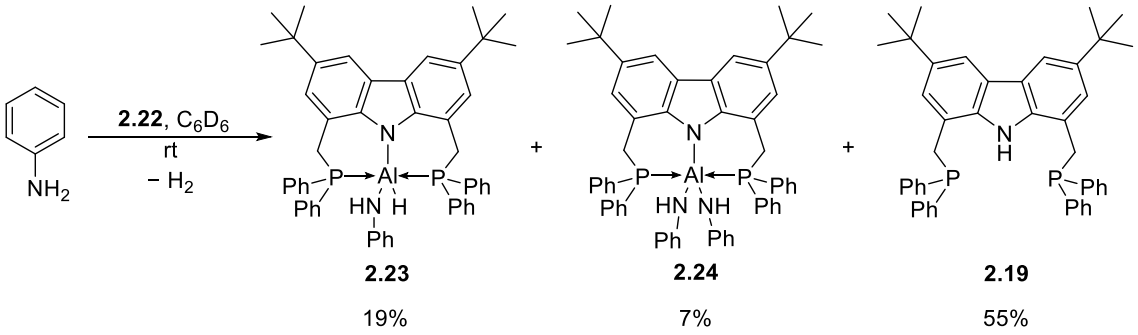

Scheme 2.6 Reaction of (^{Ph}PNP)AlH$_2$ (**2.22**) with aniline H$_2$NPh and the ratios (% by integration) of products.

Next, aluminium dihydride **2.22** was reacted with larger anilines in an effort to favour the single substituted product. A small excess of H$_2$NMes was added to a C$_6$D$_6$ solution of aluminium dihydride **2.22** at room temperature (scheme 2.7). After 24 hours, the ^{1}H NMR spectrum shows the Al*H* resonance for (^{Ph}PNP)AlH(NHMes) (**2.25**) is seen at 5.92 ppm, a downfield shift, with much less defined splitting, compared AlH$_2$ of aluminium dihydride **2.22**. The ^{31}P NMR spectrum shows a doublet resonance at -30.0 ppm (64% by integration, $^2J_{H-P}$ = 51.2 Hz) corresponding to the major product, **2.25**. Small quantities of aminophosphine **2.19** and unreacted **2.22** were present (14% and 18% by integration respectively). An additional singlet resonance at −28.0 ppm (4% by integration) suggested a trace amount of (^{Ph}PNP)Al(NHMes)$_2$ (**2.26**) had formed, a much lower quantity than that of phenyl analogue **2.24**, demonstrating that increasing the steric bulk of aniline improves selectivity in favour of (^{Ph}PNP)AlH(NHAr). In concordance with phenyl analogues **2.23** and **2.24**, dissociation of P-donors was not observed.

The reaction mixture was then heated to 60 ˚C in an attempt to induce the formation a second equivalent of H_2 from aluminium amide **2.25** in an attempt to generate (^{Ph}PNP)Al=NMes.[33] After 72 hours of heating, the ^{31}P NMR spectrum shows slightly more **2.26** had formed (22% by integration) but remains in much lower quantities than aluminium amide **2.25** (49% by integration). Minor singlet resonances at −19.5 and −26.9 ppm suggest formation of a new products at elevated temperatures occurring at very slow rates. However, the amount of aminophosphine **2.19** also increased, suggesting products **2.25** and **2.26** are potentially thermally unstable. The unsaturated product (^{Ph}PNP)Al=NMes was not observed.

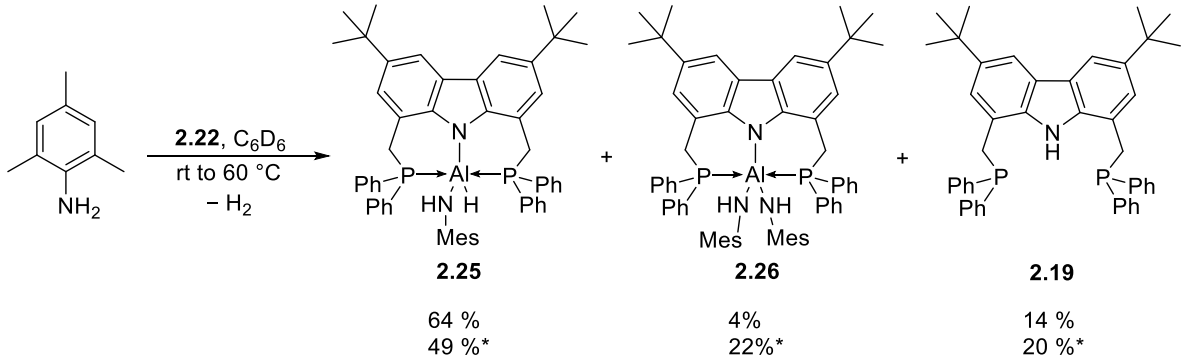

Scheme 2.7 Reaction of (^{Ph}PNP)AlH$_2$ (**2.22**) with H$_2$NMes and the ratios (% by integration) of products before and after (*) heating to 60 ˚C.

The steric hindrance of aniline was further increased, and aluminium dihydride **2.22** was reacted with H$_2$NDipp at room temperature (scheme 2.8). After 24 hours, ^{31}P NMR spectroscopy reveals the formation of (^{Ph}PNP)AlH(NHDipp) (**2.27**), evidenced by the doublet resonance at −27.8 ppm (72% by integration, $^2J_{H-P}$ = 41.3 Hz). The ^{1}H NMR spectrum supported the formation of **2.27**, revealing a broad singlet at 5.83 ppm (Al*H*) indicating only one hydride ligand is present, as judged by integration. The formation of (^{Ph}PNP)Al(NHDipp)$_2$ was not observed indicating selectivity towards the formation of aluminium amide **2.7**. To push the reaction to completion and allow for potential further reactivity, the mixture was heated to 70 ˚C for three hours. Almost complete depletion of all starting materials was observed and aluminium amide **2.35** remained the major product (80% by integration, ^{31}P NMR spectrum). The singlet resonances at −26.9 and −19.5 ppm are present, similar to those

observed upon heating the reaction of **2.22** and H_2NMes, and correspond to minor species (2% and 1% by integration, respectively) which could not be identified.

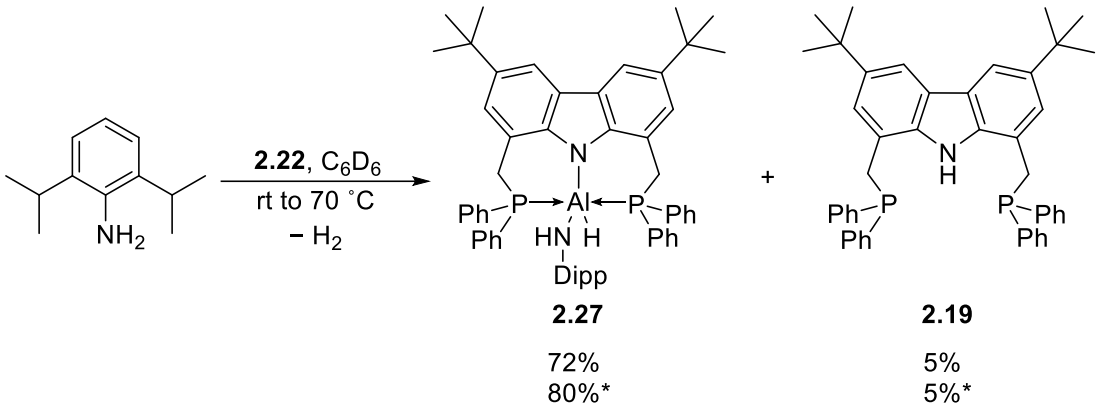

Scheme 2.9 Reaction of (^{Ph}PNP)AlH_2 (**2.22**) with H_2NDipp and the ratios (% by integration) of products before and after (*) heating to 70 ˚C.

In comparison to smaller anilines, the reaction of aluminium dihydride **2.22** and H_2NDipp required longer reaction times or heating to 70 ˚C to reach complete consumption of starting materials. However, formation of aluminium amide **2.35** occurs under milder conditions in comparison to reported analogue (^{Dipp}NacNac)AlH(NHDipp), which is synthesised from (^{Dipp}NacNac)AlH_2 and H_2NDipp at 150 ˚C.[34,35] Furthermore, the conversion to **2.27** (80% by integration) is much greater than that of (^{Dipp}NacNac)AlH(NHDipp) in deuterated toluene (1% conversion by NMR). The difference in reactivity may be due to greater steric congestion around aluminium in (^{Dipp}NacNac)AlH_2 resulting a smaller void in which the aniline can reside, thus disfavouring the reaction with H_2NDipp.

So far, the reactions of aluminium dihydride **2.22** with different anilines are clearly affected by the size of the aniline. Through increasing the steric bulk, single substitution of **2.22** is favoured. Furthermore, varying the ortho-groups of the aniline also influences the aluminium-ligand interactions, particularly the strength of P–Al interactions, signified by the $^2J_{H-P}$ coupling constants in the ^{31}P NMR spectra. It was observed that upon increasing the size of aniline, the coupling constants decreased: (^{Ph}PNP)AlH_2 (**2.22**, $^2J_{H-P}$ = 58.4 Hz) > (^{Ph}PNP)AlH(NHPh) (**2.23**, $^2J_{H-P}$ = 55.2 Hz) > (^{Ph}PNP)AlH(NHMes) (**2.25**, $^2J_{H-P}$ = 51.2 Hz) >

(^{Ph}PNP)AlH(NHDipp) (**2.27**, $^{2}J_{H-P}$ = 41.3 Hz). To accommodate larger aryl groups and minimise steric repulsions, the Al–P bonds likely lengthen, which reduces the magnitude of the $^{2}J_{H-P}$ coupling constant. Although weakening of the Al–P bonds is suggested, phosphine dissociation was not observed in the reactions conducted.

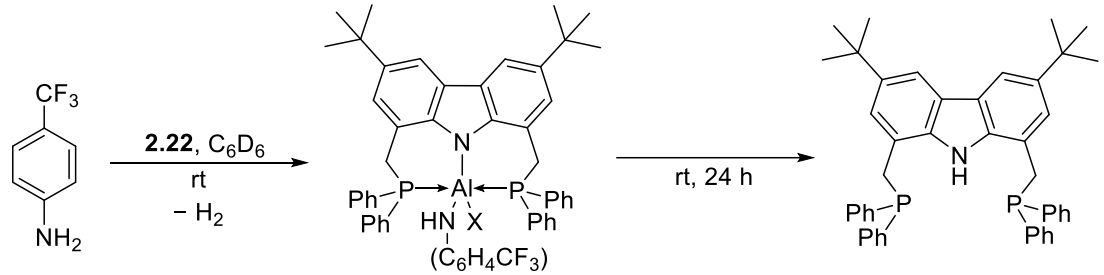

2.28, X = H, 51%
2.29, X = NH($C_6H_4CF_3$), 28%

2.19

Scheme 2.9 Reaction of (^{Ph}PNP)AlH_2 (**2.22**) with one equivalent of $H_2N(C_6H_4CF_3)$ and the ratios (% by integration) of the dehydrocoupled products before decomposition to (^{Ph}PNP)H (**2.19**).

The reactivity of (^{Ph}PNP)AlH_2 (**2.22**) towards anilines containing a wider variety of functionalised aryl groups was explored. The presence of strongly electron-withdrawing group $–CF_3$ at the para position increases the acidity of the amine, thus allowing for heightened reactivity with aluminium hydrides. Upon addition of $H_2N(C_6H_4CF_3)$ to aluminium dihydride **2.22** at room temperature (scheme 2.9), evolution of dihydrogen was observed and the formation of (^{Ph}PNP)AlH(NH{$C_6H_4CF_3$}) (**2.28**) was indicated by a new doublet resonance at −32.1 ppm (51% by integration, $^{2}J_{H-P}$ = 59.3 Hz) in the ^{31}P NMR spectrum. The $^{2}J_{H-P}$ coupling constant of **2.28** is greater than those measured for aluminium amides **2.23**, **2.25**, and **2.27** and even greater than aluminium dihydride **2.22**, suggesting a stronger aluminium-phosphorus interaction. A singlet resonance at −27.8 ppm was also present, suggesting the formation of (^{Ph}PNP)Al(N{$C_6H_4CF_3$})$_2$ (**2.29**) (28% by integration). Signals for aminophosphine **2.19** and unreacted aluminium dihydride **2.22** were also observed. The ^{19}F NMR spectrum consists of singlet resonances at −60.2 ppm and −60.5 ppm, assigned to aluminium amide **2.28** and aluminium diamide **2.29**, respectively. After 24 hours, the products began to

decompose, and after three days, the ^{31}P NMR consisted of only a singlet at −18.1 ppm for amino-phosphine **2.19**. Other decomposition products could not be identified as the ^{19}F NMR spectrum shows an intractable mixture of products. It appears that although reactivity towards N–H bonds is favoured over C–F bonds, the presence of fluoroalkyl groups causes issues with regards to the stability of the aluminium-amide compounds.

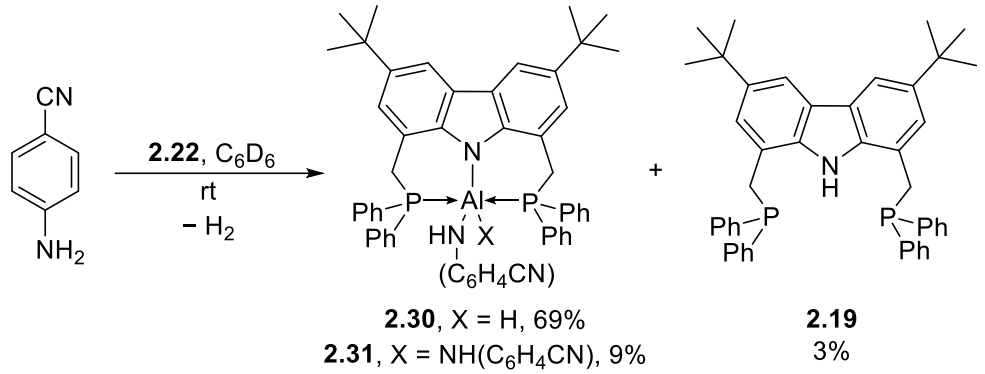

Scheme 2.10 The reaction of (^{Ph}PNP)AlH$_2$ (**2.22**) and H$_2$N(C$_6$H$_4$CN) and the ratios (% by integration) of the products.

To reduce further reactivity and decomposition of products, an alternate electron-withdrawing group, a nitrile group (–C≡N), was considered. The reaction of H$_2$N(C$_6$H$_4$CN) with aluminium hydride **2.22** proceeded at room temperature (scheme 2.11). The ^{31}P NMR spectrum shows (^{Ph}PNP)AlH(NH{C$_6$H$_4$CN}) (**2.30**) as the major product, presented as a doublet resonance at −32.4 ppm (69% by integration, $^2J_{H-P}$ = 62.4 Hz). A very small amount of (^{Ph}PNP)Al(N{C$_6$H$_4$CN}$)_2$ (**2.31**) had also been produced seen by the singlet resonance at −28.2 ppm (9% by integration). However, soon after NMR analysis had been performed, solid began to precipitate out of solution. The reaction was repeated in THF-d$_8$, but this resulted in decomposition to amino phosphine **2.19** and other products which could not be identified.

To improve solubility of the products, *ortho*-methyl groups were introduced to the nitrile-containing aniline, H$_2$N(XylCN) (XylCN = 4-cyano-2,6-dimethylphenyl). Upon reacting the more sterically hindered aniline with aluminium dihydride **2.22** at room temperature (scheme 2.11), a doublet resonance at −30.8 ppm (48% by integration, $^2J_{H-P}$ = 57.5 Hz), corresponding to (^{Ph}PNP)AlH(NH{XylCN}) **2.32**, was observed by ^{31}P NMR spectroscopy. The

reduction in magnitude of the $^{2}J_{H-P}$ coupling constant for **2.32**, compared to **2.30**, can be ascribed to the increase in steric bulk of the aniline, leading to a weakening of the Al–P bonds. Formation of the corresponding aluminium diamide products was not observed. The reaction mixture was then heated to 60 ˚C for 15 hours, after which complete consumption of **2.22** was observed, and the ^{31}P NMR spectrum reveals aminophosphine **2.19**, though in considerable amounts (66% by integration), was the only other phosphorus containing compound present in solution, along with aluminium amide **2.32** (34% by integration). However, as the reaction mixture cooled to room temperature, a precipitate formed, thus the ratio of products observed are only representative of products in solution.

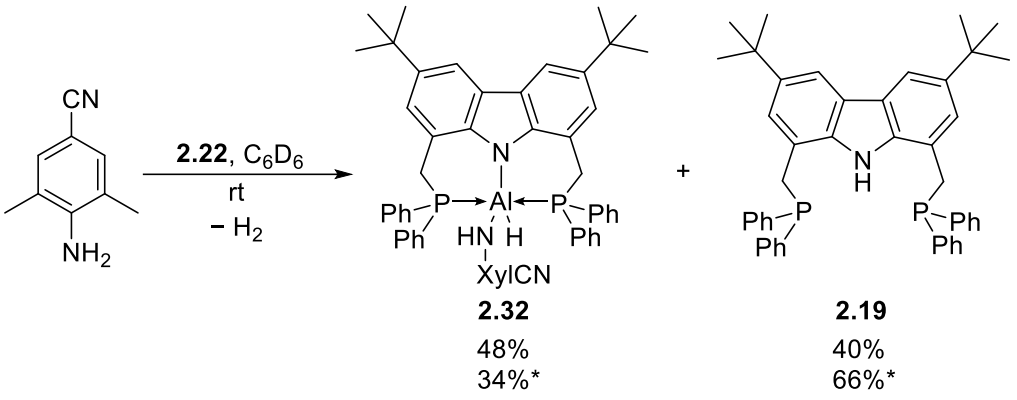

Scheme 2.11 The reaction of (^{Ph}PNP)AlH$_2$ (**2.22**) and H$_2$N(XylCN) and the ratios (% by integration) of the products before and after (*) heating to 60 ˚C.

2.4.2 Reactivity with Isonitriles

Aluminium hydrides have been reported to react with isonitriles to afford cyclic heteroatom-containing organoaluminium compounds.[36,37] Power and co-workers presented the reactivity of [Mes*AlH$_2$]$_2$ (Mes* = 2,4,6-tri-*tert*-butylphenyl) (**1.11**), a dimeric aluminium dihydride, towards *tert*-butylisonitrile (*t*BuNC). The reaction proceeded at 0 ˚C, and through transfer of both hydride centres to carbon, resulted in the formation of [Mes*AlN(*t*Bu)CH$_2$]$_2$ (**2.33**), a dimer consisting of a six-membered ring. Upon heating dimer **2.33**, ortho-methylation occurs to give product **2.34** (scheme 2.12). However, **2.34** was also reported to be observed at temperatures as low as 10 ˚C, showing the instability of dimer **2.33**.[37]

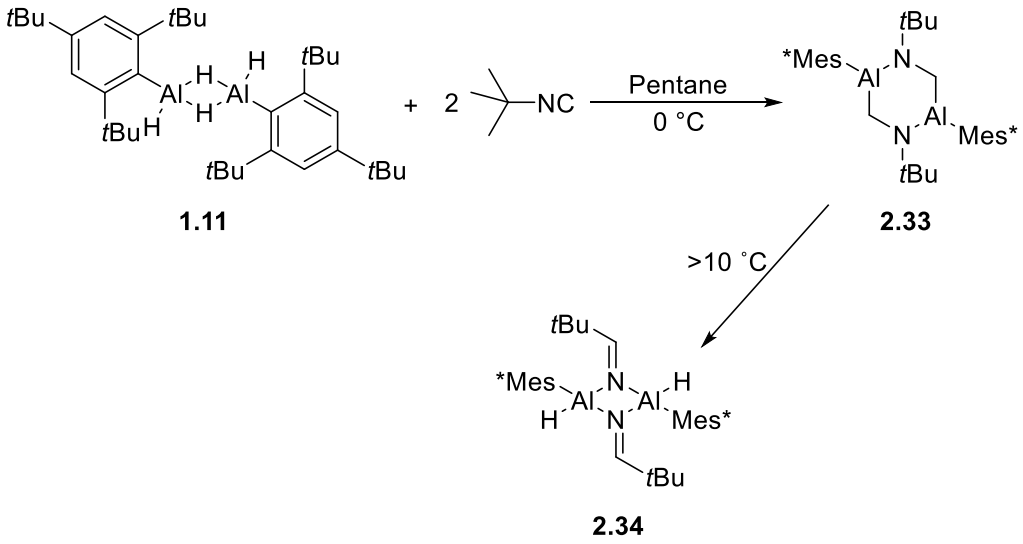

1.11 **2.33** **2.34**

Scheme 2.12 The reaction of $[Mes^*AlH_2]_2$ (**1.11**) and *tert*-butylisonitrile.

Considering the formation of **2.33** arose from a dimeric aluminium dihydride (**1.11**), the use of monomeric aluminium dihydride **2.22** may lead to different products or varying levels of reactivity towards isonitriles. The addition of a benzene solution of aluminium dihydride **2.22** to 2,6-xylylisonitrile (XylNC) at room temperature resulted in no reaction. The reaction mixture was then heated to 80 ˚C for one hour, after which a colour change from colourless to orange was observed, indicating a reaction between aluminium dihydride **2.22** and XylNC had occurred (scheme 2.13).

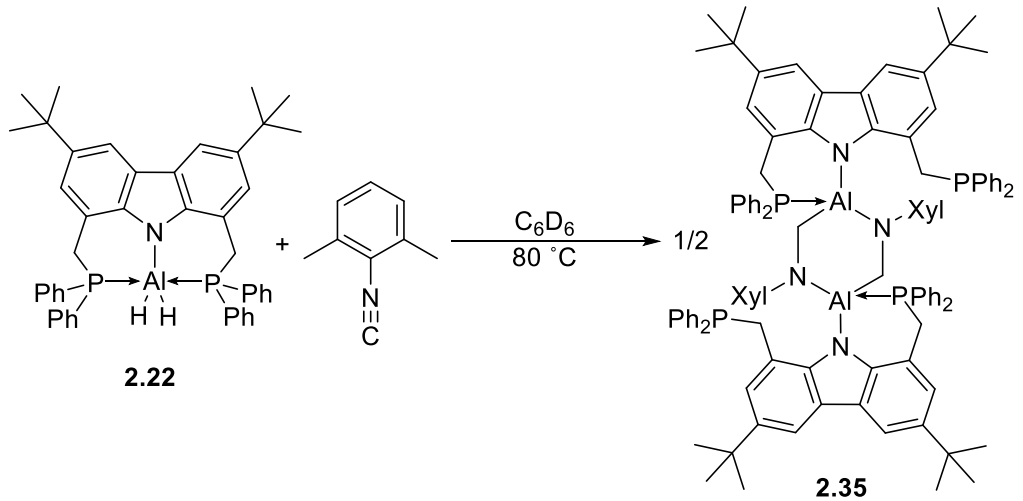

2.22 **2.35**

Scheme 2.13 Reaction of (^{Ph}PNP)AlH_2 (**2.22**) with 2,6-dimethylphenyl isonitrile.

The ^{31}P NMR spectrum of the reaction mixture shows the presence of several species, with the major signals resonating as singlets at −12.7 ppm and −17.7 ppm which integrated to a ratio of 1:1 which are assigned to the two phosphorus environments (free and coordinated) of the donating groups of dimer **2.35**. The ^{1}H NMR spectrum shows a similarly complex mixture of products and broad signals, and so could not be fully assigned. However, the absence of AlH_2 resonance at 5.84 ppm is clear, indicating complete consumption of **2.22**. The resonance for the PNP-based *t*Bu group at 1.45 ppm is shifted slightly downfield compared to aluminium dihydride **2.22**. The asymmetry of **2.35** would give rise to a second resonance for *t*Bu, which has been assigned as the broad signal at 1.43 ppm. The resonance of xylyl-based methyl groups of **2.35** at 1.96 ppm is shifted upfield compared to (Xyl)NC (2.02 ppm). Unfortunately, the Al–C*H*$_2$ resonance could not be identified.

Through slow evaporation colourless crystals were obtained and identified by X-ray crystallography as dimeric product **2.35** (figure 2.7). The solid-state structure of **2.35** shows the formation of a six-membered heterocycle in a chair conformation, comprising of two {(^{Ph}PNP)AlN(Xyl)CH_2} fragments. The Al1–C47 and Al1–N2 distances of 1.993(4) Å and 1.798(3) Å respectively, along with a C47–N2 distance of 1.490(4) Å, are comparable to reported distances of such bonds.[21,38,39] The aluminium centre is revealed to be four-coordinate and is κ^2-coordinated to the PNP-ligand, with only one phosphorus centre bonded to aluminium. The dissociation of a phosphine donating group is likely a result of increased steric bulk around the aluminium centre. The Al1–P1 distance of 2.5138(14) Å of **2.35** is marginally shorter than the Al–P distances (2.5823(5) Å and 2.6217(5) Å) of aluminium dihydride **2.22**, suggesting a slight increase in strength of the Al–P interaction of **2.35**. The bond angles around the aluminium centre range from 88.30(9)˚ to 122.98(14)˚, indicating aluminium to have a distorted tetrahedral geometry.

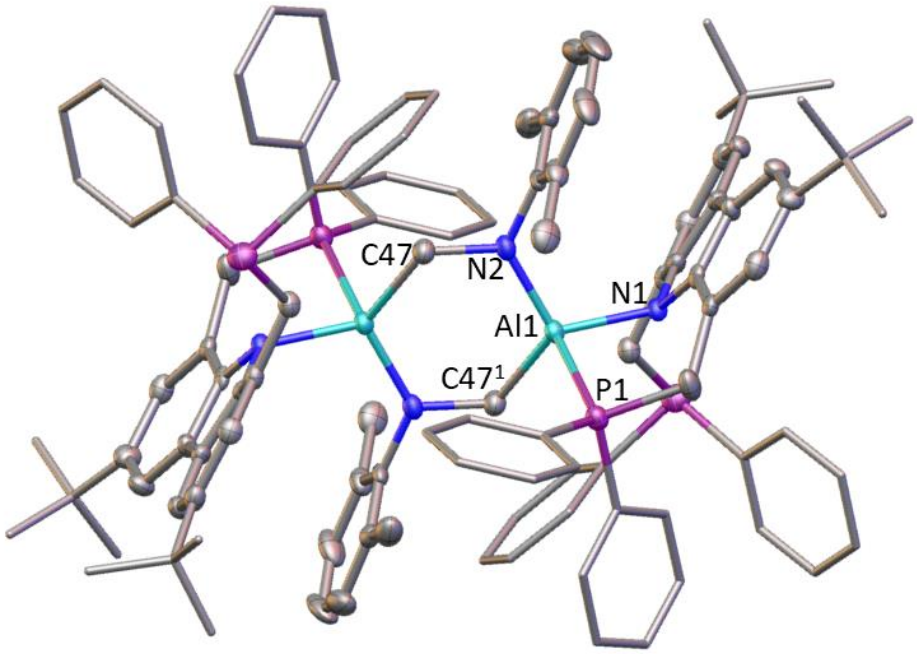

Figure 2.7 The solid-state structure of dimer **2.35**. H atoms are omitted for clarity. Thermal ellipsoids are set to 50% probability. Select bond lengths (Å) and angles (˚): Al1–N1 1.909(13), Al1–P1 2.5138(14), Al1–N2 1.993(4), Al1–C47^{1} 1.798(3), C47–N2 1.490(4), N1–Al1–P1 88.30(9), N2–Al1–C47^{1} 115.11(15), N1–Al1–N2 110.24(14), N1–Al1–C47^{1} 122.98(14).

A possible pathway to dimer **2.35** is detailed in scheme 2.14. It is suggested that the initial step of this reaction process, in which the isonitrile first coordinates to the aluminium centre, proceeds *via* insertion of the terminal carbon into the aluminium-hydrogen bond followed by hydride transfer to give an imine-containing aluminium hydride intermediate.[37] It is then proposed that a second molecule of the aluminium hydride intermediate reacts with the aluminium centre to form an Al–N bond, resulting in the transfer of the second hydride ligand to the carbon. This process also occurs at the second aluminium centre, leading to the formation of dimer **2.35**.

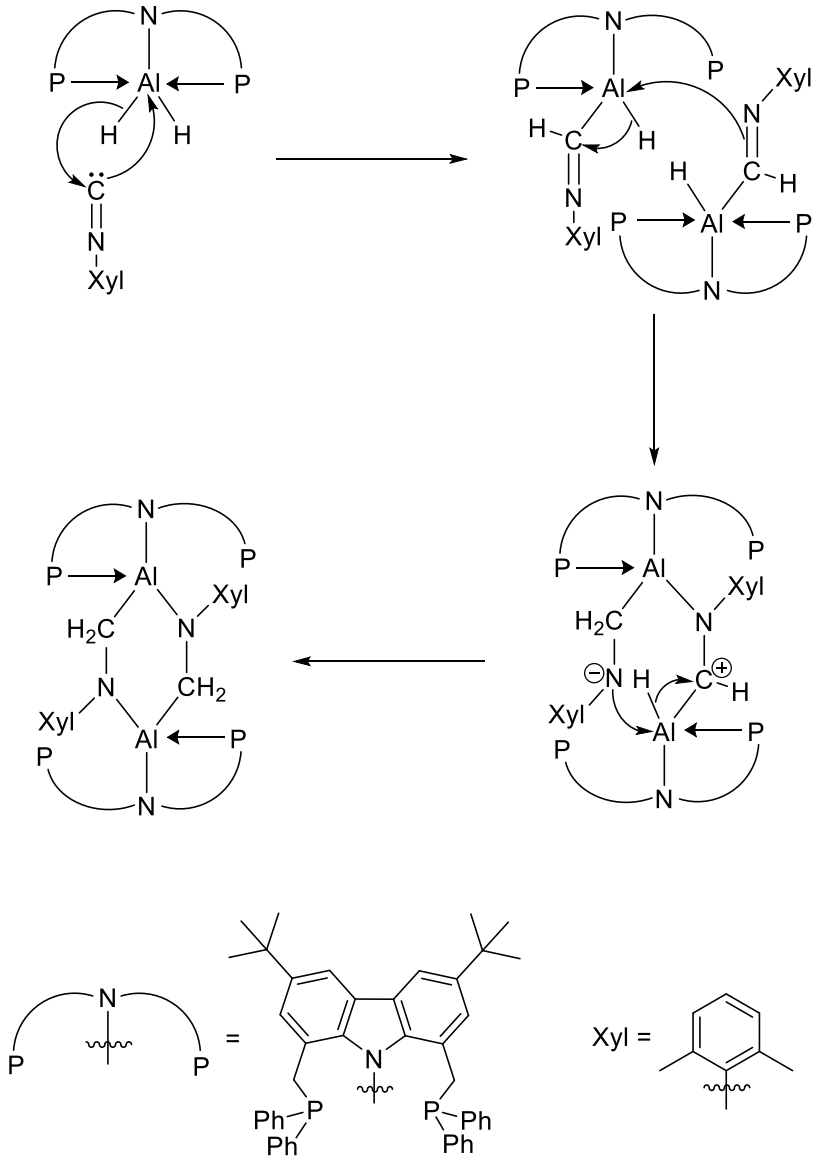

Scheme 2.14 A suggested pathway to dimer **2.35** by the reaction of (^{Ph}PNP)AlH$_2$ (**2.22**) and 2,6-xylylisonitrile.

However, a possible intramolecular rearrangement was also considered, which would result in a three-membered metallacycle followed by interactions with a second molecule of metallacyclic intermediate, leading to ring-opening and dimerization. Due to the extremely acute bond angles which would arise within the three-membered heterocycle, it is assumed that the pathway depicted in scheme 2.14 would be more favoured.

2.4.3 Reactivity with Palladium(0)

Palladium(0) complexes have been reported to partially dehydrogenate group 13 metal hydrides, and could provide an alternate pathway to low-oxidation state group 13 complexes, without the use of harsh reducing agents, such as KC_8.[40] Crimmin and co-workers showed that $Pd(PCy_3)_2$ (Cy = cyclohexyl) reacts with (^{Ar}NacNac)AlH_2 compounds, **1.28** (Ar = Mes) and **1.29** (Ar = 2,6-Xylyl), to produce heterobimetallic hydride complexes (scheme 2.15), formed by the loss of dihydrogen.[40] The solid-state structures of dehydrogenation products **2.36** and **2.37** revealed both to have a planar $\{Pd_2Al_2H_2\}$ core, with Pd–Pd and Pd–Al interactions and bridging hydride ligands (Al–H–Pd). Formal oxidation states of the metal centres of **2.36** and **2.37** are not assigned, but calculations do suggest a decrease in positive charge at aluminium upon dehydrogenation. Although the dehydrogenation of **1.28** and **1.29** resulted in complexes with H:Al ratios of 1:1, complete dehydrogenation of aluminium dihydride is not yet reported.

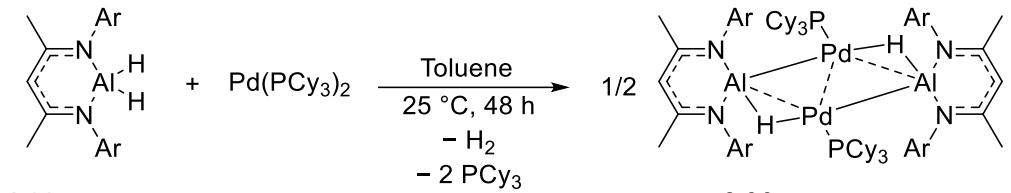

1.28, Ar = Mes
1.29, Ar = 2,6-Xylyl

2.36, Ar = Mes
2.37, Ar = 2,6-Xylyl

Scheme 2.15 Partial dehydrogenation of (^{Ar}NacNac)AlH_2 (**1.28** Ar = Mes, **1.29** Ar = 2,6-Xylyl) using $Pd(PCy_3)_2$.

The partial dehydrogenation of aluminium dihydrides **1.28** and **1.29** inspired investigations into the reactivity of $Pd(PCy_3)_2$ towards (^{Ph}PNP)AlH_2 (**2.22**). A benzene solution of aluminium dihydride **2.22** was added dropwise to one equivalent of $Pd(PCy_3)_2$ in benzene at room temperature (scheme 2.16). Gas evolution was observed, with an immediate colour change from colourless to orange, which became darker over 30 minutes.

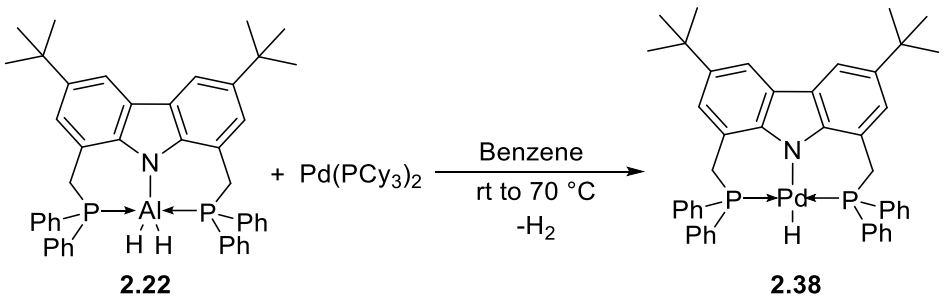

Scheme 2.16 The reaction of (^{Ph}PNP)AlH_2 (**2.22**) and $Pd(PCy_3)_2$ to give (^{Ph}PNP)PdH (**2.38**).

The reaction mixture of aluminium dihydride **2.22** and $Pd(PCy_3)_2$ was analysed by ^{31}P NMR spectroscopy, showing complete consumption of **2.22** (−33.5 ppm). A new broad doublet resonance is present at −0.2 ppm (J = 354 Hz), (figure 2.8). The singlet resonance at 9.93 ppm corresponds to dissociated PCy_3. In the ^{1}H NMR spectrum, a singlet resonance at 4.46 ppm corresponds to dihydrogen, suggesting that dehydrogenation has indeed occurred. Resonances relating to the PNP-ligand are only visible in the aryl region and are very broad. Thus, structural information for the PNP ligand-containing product could not be gained from NMR analysis.

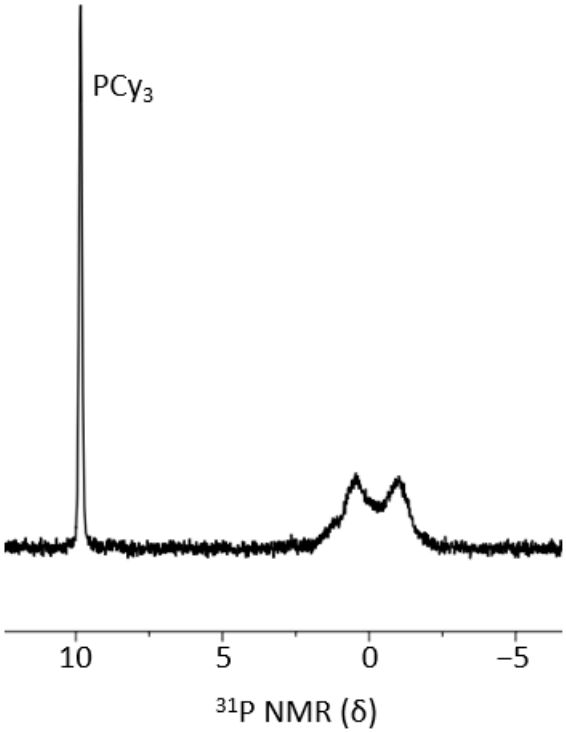

Figure 2.8 The ^{31}P NMR spectrum of the reaction of (^{Ph}PNP)AlH_2 (**2.22**) with $Pd(PCy_3)_2$ at ambient temperature.

Upon observing complete consumption of aluminium dihydride **2.22** and $Pd(PCy_3)_2$, the solution was then concentrated to precipitate a yellow solid, which was collected by cannula filtration. Recrystallisation from hot benzene afforded colourless crystals which were determined by X-ray crystallography to be (^{Ph}PNP)PdH, **2.38** (figure 2.9). The solid-state structure shows a monomeric complex with a four-coordinate palladium centre, coordinated by the PNP-ligand. The Pd–P distances of 2.2816(7) Å and 2.2835(7) Å, for Pd1–P1 and Pd1–P2 respectively, and a Pd1–N1 distance of 2.143(2) Å, are close in value to reported Pd–P and Pd–N bond lengths.[41,42] The P1–Pd1–P2 angle of 172.30(3)˚ and the N1–Pd1–P1 and N1–Pd1–P2 angles, 93.03(7)˚ and 93.60(7)˚ respectively, indicate palladium to have a distorted square-planar geometry.

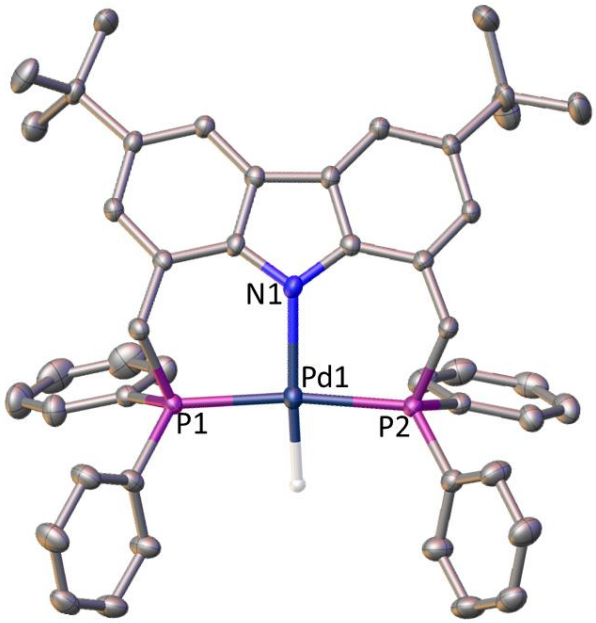

Figure 2.9 The solid-state structure of (^{Ph}PNP)PdH (**2.38**). The H atoms, except the hydride ligand, are omitted for clarity. The thermal ellipsoids are set to 50% probability. Select bond lengths (Å) and angles (˚): Pd1–N1 2.143(2), Pd1–P1 2.2816(7), Pd1–P2 2.2835(7), N1–Pd1–P1 93.03(7), N1–Pd1–P2 93.60(7), P1–Pd1–P2 172.29(3).

Palladium hydride **2.38** was independently generated from aminophosphine ligand **2.19** and $Pd(PCy_3)_2$ and analysed by ^{1}H and ^{31}P NMR spectroscopy. The ^{1}H NMR spectrum consists of a broad singlet resonance at −10.8 ppm for the Pd*H* environment. The ^{31}P NMR spectrum shows a singlet resonance at 40.7 ppm, assigned to the phosphorus environment of **2.38**. The resonances observed for **2.38** are not present in the NMR spectra of the reaction of aluminium dihydride **2.22** and $Pd(PCy_3)_2$. This suggests that palladium hydride **2.38** is either a minor component of the reaction mixture or formed under the conditions used for crystallisation of the product.

From the analytical data attained, it can be suggested that dehydrogenation of aluminium dihydride **2.22** had occurred, evident from the production of dihydrogen. However, the extent of dehydrogenation could not be determined as the aluminium-containing product was not identified. Due to the formation of palladium hydride **2.38** and

unsuccessful attempts to identify the aluminium-containing products, the dehydrogenation of aluminium dihydride **2.22** using $Pd(PCy_3)_2$ was not pursued further.

2.4.4 Reactivity with Magnesium(I)

Reported routes to low-oxidation state aluminium have been dominated by the reduction of aluminium halides using group 1 metals as reducing agents. However, a magnesium(I) dimer, $[(^{Mes}NacNac)Mg]_2$, has been reported to reduce aluminium hydrides **2.39** and **2.41** to produce aluminium(II) dimers **2.40** and **2.42** (scheme 2.17).[43,44] In addition to the preparation of aluminium(II) compounds, $[(^{Mes}NacNac)Mg]_2$ has also been used to access an aluminium(I) hydride cluster, $[(^{Mes}NacNac)Mg]_2[Al_6H_6(CH\{N^{Dipp}\}_2)_2]$ (**2.44**), through the reduction of aluminium hydride dimer $[(CH\{N^{Dipp}\}_2)AlH(\mu\text{-}H)]_2$ (**2.43**, scheme 2.17).[45]

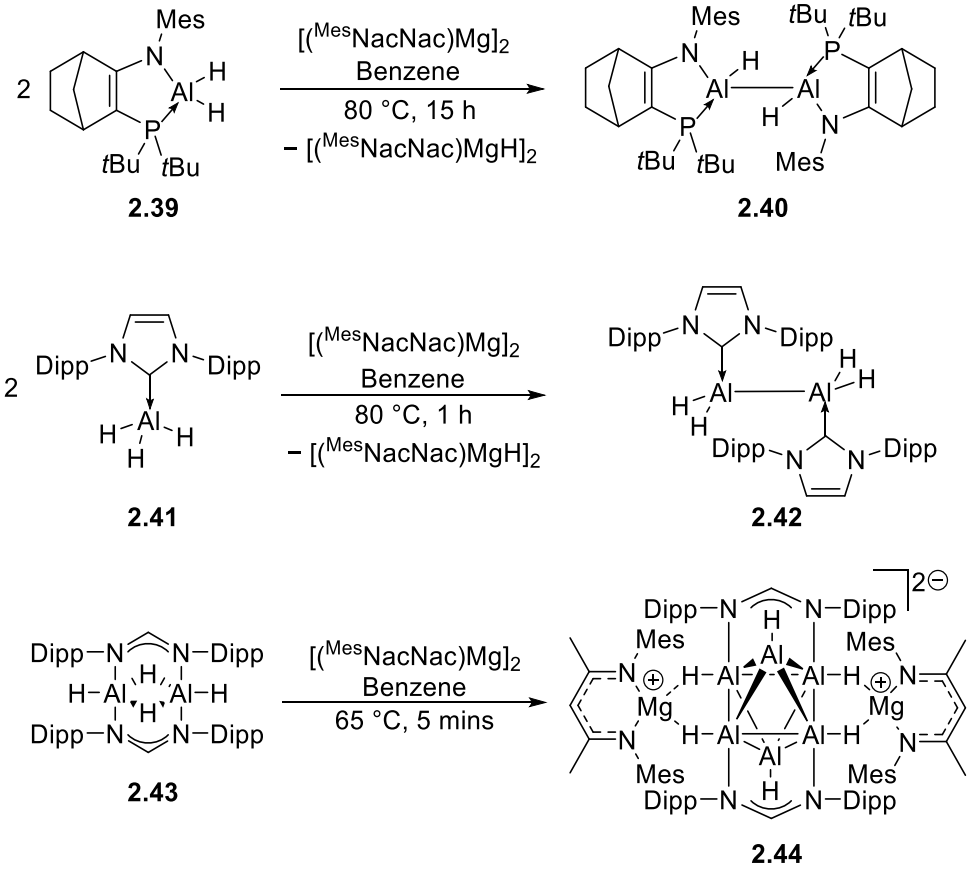

Scheme 2.17 The reductions of aluminium hydrides **2.39**, **2.41**, and **2.43** with $[(^{Mes}NacNac)Mg]_2$ to give aluminium(II) dimers **2.40** and **2.42**, and aluminium(I) cluster **2.44**.

The reduction of (^{Ph}PNP)AlH$_2$ (**2.22**) using [(^{Mes}NacNac)Mg]$_2$ was attempted. A toluene solution of aluminium dihydride **2.22** was added to one equivalent magnesium(I) dimer [(^{Mes}NacNac)Mg]$_2$ at ambient temperature. Upon complete addition, the reaction mixture was deep orange in colour. The ^{31}P NMR spectrum of an aliquot shows aluminium dihydride **2.22** had been fully consumed, indicated by the absence of a triplet resonance at −33.5 ppm, after approximately 30 minutes and consisted of only two new singlet resonances at −14.1 ppm and −26.3 ppm, which integrate to a ratio of 1:1 (figure 2.10). Due to the lack of phosphorus-hydrogen coupling observed, it is assumed that both hydride ligands in aluminium dihydride **2.22** have been removed, which gives rise to singlet resonances. The presence of two signals suggests that the two phosphorus centres of the PNP ligand are no longer equivalent which may be the result of dissociation of one phosphine donor from aluminium. The ^{1}H NMR spectrum consists of complex overlapping resonances which cannot be assigned.

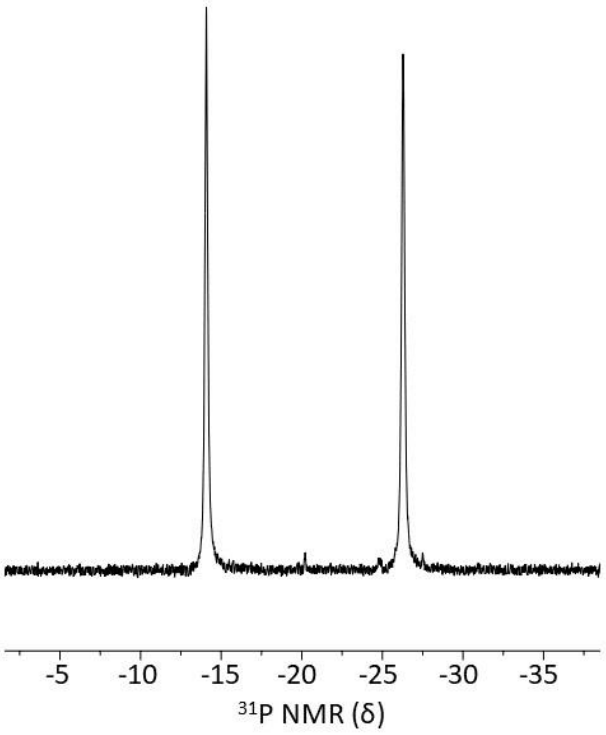

Figure 2.10 The ^{31}P NMR spectrum of reaction of (^{Ph}PNP)AlH$_2$ (**2.22**) with one equivalent of [(^{Mes}NacNac)Mg]$_2$.

Separation of products was attempted by fractional crystallisation from which colourless crystals were obtained and were determined by X-ray diffraction to be magnesium hydroxide dimer [(^{Mes}NacNac)MgOH]$_2$ (**2.45**, supporting figure SF1, section 5.6). The poor diffraction data for **2.45** precludes discussion of bond lengths and angles, but the connectivity is unambiguous. The presence of bridging hydroxyl groups is likely caused by the reaction of [(^{Mes}NacNac)MgH]$_2$ with trace amounts of water. Although attempts to crystallise the other products product were made, isolation and identification of the aluminium-containing product was not achieved.

To gain more information the reaction was repeated using half an equivalent of [(^{Mes}NacNac)Mg]$_2$ at ambient temperature. The ^{1}H NMR spectrum reveals complete consumption of the magnesium(I) dimer with resonances for the magnesium-containing product present, most notably the singlet resonances at 4.74 ppm, corresponding to the C*H* environment of the NacNac backbone, which is an upfield shift compared to [(^{Mes}NacNac)Mg]$_2$ (4.80 ppm).[46] Resonances for aluminium dihydride **2.22** are also present and comparison of integration of the magnesium product resonances suggest approximately 50% of **2.22** remains in solution. Broad signals are also observed which likely correlate to the aluminium-containing product. However, due to overlapping signals assignment of resonances for the aluminium-containing product was not possible. The ^{31}P NMR spectrum consists of two singlet resonances at −14.1 ppm and −26.3 ppm in a ratio of 1:1, corresponding to the product, as seen for the reaction of **2.22** with one equivalent of [(^{Mes}NacNac)Mg]$_2$, (figure 2.11). The triplet resonance at −33.5 ppm for aluminium dihydride **2.22**, accounting for approximately 50% (by integration) of the phosphorus environments present. Therefore, it can be suggested that the reaction of **2.22** and [(^{Mes}NacNac)Mg]$_2$ proceeds by the abstraction of both hydride ligands from aluminium rather than the removal of a single hydride ligand which would generate an aluminium(II) centre and would have resulted in complete consumption of aluminium dihydride **2.22**. However, the products of this reaction were not isolated and from the NMR analysis it is not possible to identify the aluminium-containing product.

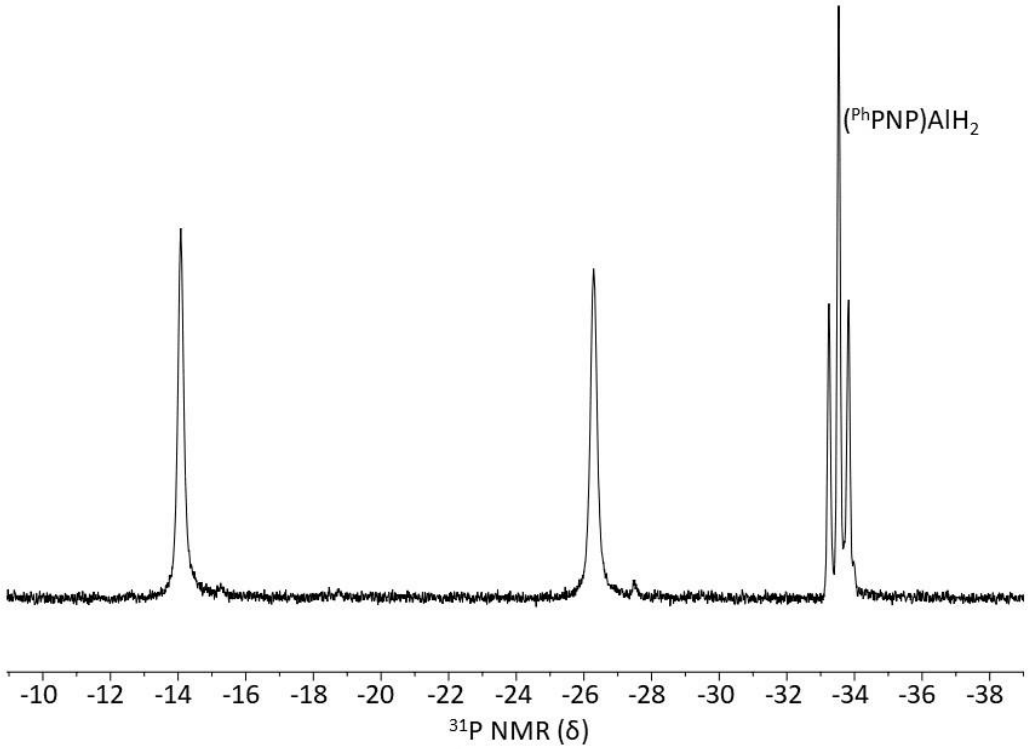

Figure 2.11 The ^{31}P NMR spectrum of the reaction of (^{Ph}PNP)AlH$_2$ (**2.22**) and 0.5 equivalents of [(^{Mes}NacNac)Mg]$_2$.

Due to issues surrounding isolation of products, the route to PNP-supported low-oxidation state aluminium compounds was not realised through the reduction of aluminium dihydride **2.22**. Hence, more established pathways to aluminium(I) from aluminium halide compounds were considered.

2.5 Synthesis of (^{Ph}PNP)AlX$_2$ (X = Br, I)

Reduction of organoaluminium halide species using group 1 metal reagents has become the most established pathway to organoaluminium(I) species.[47–51] The reaction of an aluminium halide precursor with group 1 metal reducing agent leads to the formation of salts, such as KI, which can easily be separated from the organoaluminium(I) product due to lack of solubility in organic solvents. Therefore, synthesis of the aluminium halide counterparts to (^{Ph}PNP)AlH$_2$ (**2.22**) was investigated with the intention of reducing these species to form aluminium(I).

2.5.1 Synthesis of (^{Ph}PNP)AlBr$_2$ (2.47)

Salt elimination is one of the most widely established routes to aluminium dihalide species, involving deprotonation of the ligand followed by a reaction with aluminium trihalide.[7,30,52] Deprotonation of (^{Ph}PNP)H (**2.19**) using alkyl lithiums such as nBuLi and MeLi proved problematic, as discussed in section 2.2. An excess of potassium hexamethyldisilazane (KHMDS) was reacted with aminophosphine **2.19** in benzene at ambient temperature to give (^{Ph}PNP)K (**2.44**) as a yellow solid, insoluble in benzene (scheme 2.18).

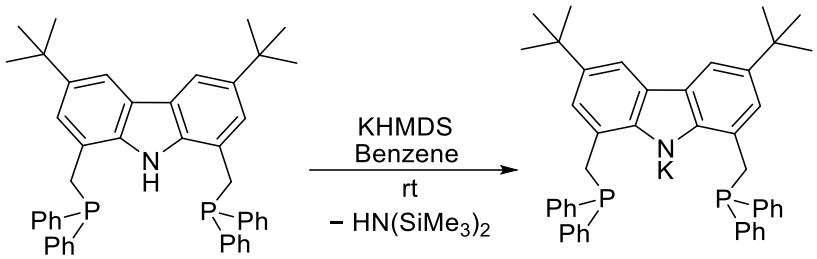

2.19 **2.46**

Scheme 2.18 Synthesis of (^{Ph}PNP)K (**2.46**) through the reaction of (^{Ph}PNP)H (**2.19**) with KHMDS at room temperature.

The ^{1}H NMR spectrum of potassium amide **2.46** in deuterated THF shows the absence of the N–H signal of aminophosphine **2.19** (8.01 ppm).[24] In the ^{31}P NMR spectrum, a singlet resonance at −13.2 ppm is present, showing both phosphorus donors to be chemically equivalent. The phosphorus centres resonate downfield compared to those of aminophosphine **2.19** (−18.1 ppm).[24]

Potassium amide **2.46** was then used to prepare (^{Ph}PNP)AlBr$_2$ (**2.47**). Initially **2.46** was reacted with AlBr$_3$.NEt$_3$ in THF at −78 ˚C. The reaction monitored using ^{1}H and ^{31}P NMR spectroscopy. The ^{31}P NMR spectrum consisted of a resonance at −34.9 ppm, a broad singlet, and is assigned to the desired product, aluminium dibromide **2.47**. A singlet resonance at −18.1 ppm was also observed and corresponds to (^{Ph}PNP)H (**2.19**), the major product. The ^{1}H NMR spectrum confirmed the presence of aminophosphine **2.19** by the broad N*H* signal at

8.01 ppm. It is assumed that the formation of aminophosphine **2.19** is a result of decomposition of highly sensitive aluminium dibromide **2.47**.

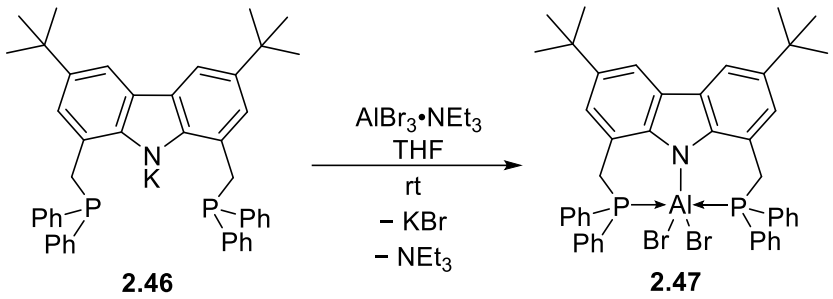

Scheme 2.19 The preparation of (^{Ph}PNP)AlBr$_2$ (**2.47**) through the reaction of (^{Ph}PNP)K (**2.46**) with AlBr$_3$•NEt$_3$ at room temperature.

To reduce formation of aminophosphine **2.19**, the synthesis of aluminium dibromide **2.47** was repeated within a glovebox under an argon atmosphere. The reaction of potassium amide **2.46** with AlBr$_3$•NEt$_3$ was carried out in THF at ambient temperature (scheme 2.19), and a colour change from orange to pale-yellow was observed. The product was extracted with toluene, and aluminium dibromide **2.47** was isolated by crystallisation in yields of up to 42%. Single crystals of quality suitable for X-ray diffraction were obtained through slow evaporation of a toluene solution.

The solid-state structure of aluminium dibromide **2.47** shows aluminium to be five-coordinate with a distorted trigonal bipyramidal geometry, resembling that of aluminium dihydride analogue **2.22**, with angles around aluminium ranging from 87.27(3)˚ to 125.16(3)˚ (figure 2.12). The Al–N distance is 1.8947(8) Å, comparable to Al–N distance of reported aluminium halide compounds.[12,21] The aluminium-phosphorus distances of 2.4874(5) Å and 2.4725(5) Å for P1–Al1 and P2–Al1 are similar to reported phosphine-stabilised aluminium halide compounds.[12,53] The P–Al bond lengths of aluminium dibromide **2.47** are slightly shorter than those of aluminium dihydride **2.22** (2.5823(5) Å and 2.6217(5) Å), suggesting a greater degree of donation from the phosphorus centres and stronger P–Al bonds. The P1–Al1–P2 angle is 175.386(13)˚, which is smaller than that of aluminium hydride **2.22**, showing a slightly higher degree of distortion of the trigonal bipyramidal geometry in aluminium

dibromide **2.47**. However, the P–Al–P angle remains larger than in other PNP-supported aluminium halides, such as (iPrPCH$_2$SiMe$_2$)$_2$NAlCl$_2$ (**2.8**) and (iPrPNP)AlCl$_2$ (**2.13b**) bearing P–Al–P angles of 171.8(3)˚ and 160.36(18)˚, respectively. The six-membered metallocycles of aluminium dibromide **2.47**, in contrast to the five-membered metallocycles of aluminium dichloride species **2.8** and **2.13b**, are the origin of the variation in the P–Al–P angles.

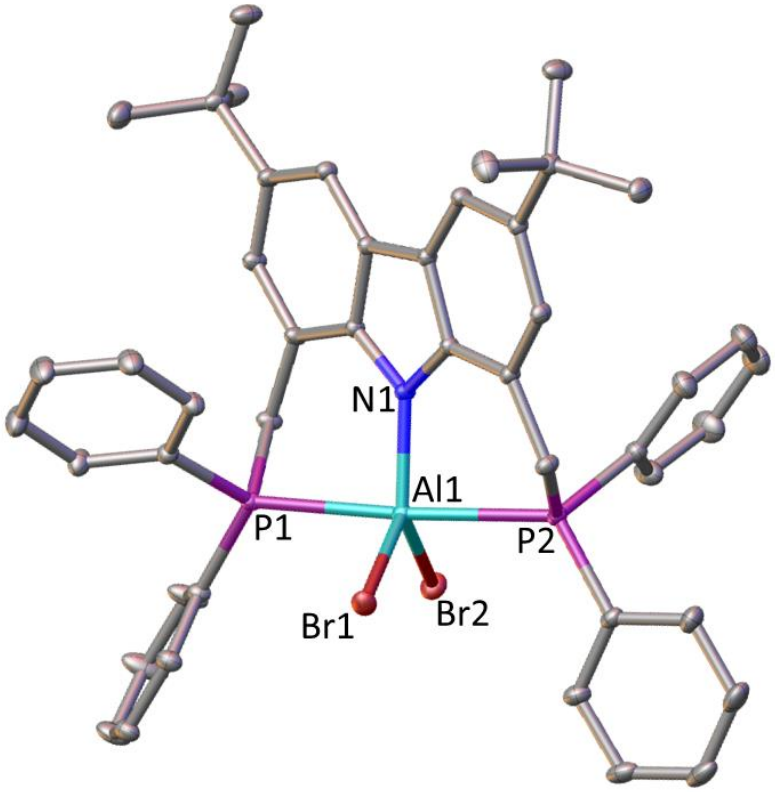

Figure 2.12 Solid-state structure of (^{Ph}PNP)AlBr$_2$ (**2.47**). The H atoms and solvent molecule are omitted for clarity. Thermal ellipsoids are set to 50% probability. Select bond lengths (Å) and angles (˚): N1–Al1 1.8947(8), P1–Al1 2.4874(5), P2–Al1 2.4725(5), Br1–Al1 2.3616(4), Br2–Al1 2.3470(4), P1–Al1–P2 175.386(13), Br1–Al1–Br2 115.551(15).

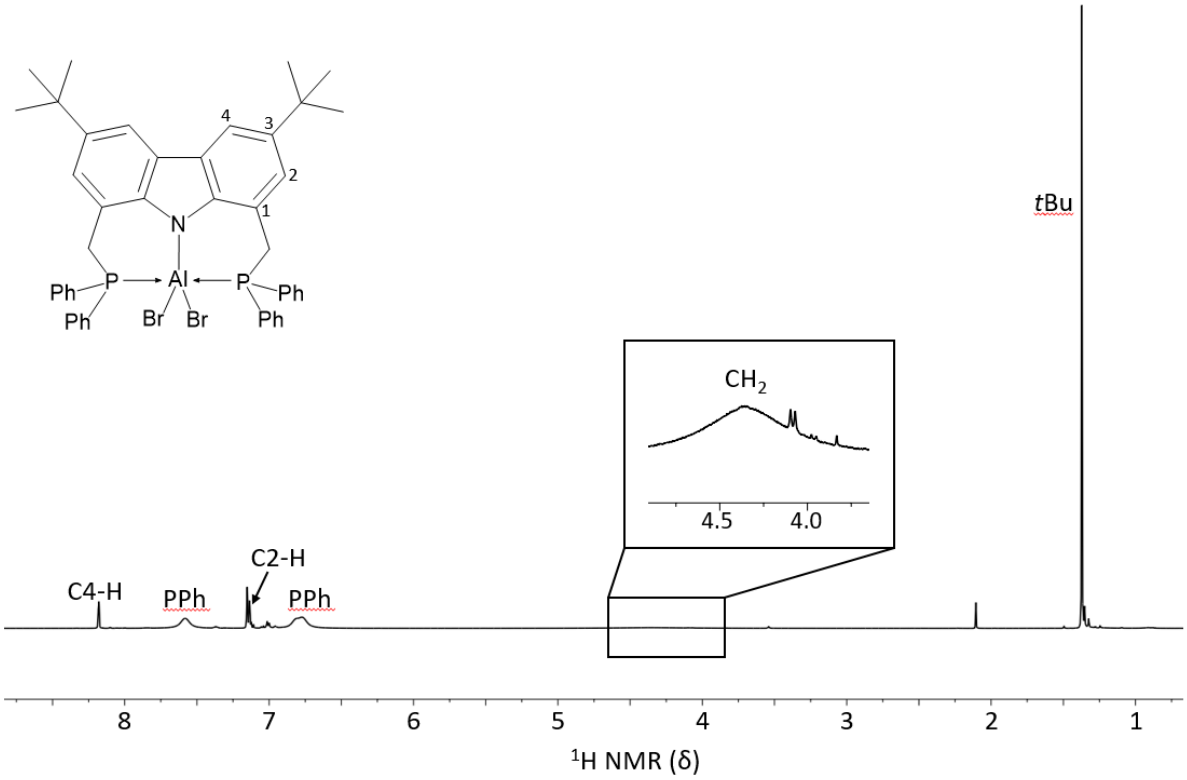

Figure 2.13 The ^{1}H NMR spectrum of (^{Ph}PNP)AlBr$_2$ (**2.47**) with a magnification of the C*H*$_2$ resonance.

The ^{1}H NMR spectrum of aluminium dibromide **2.47** shows new resonances for proton environments of the carbazole backbone, which are located slightly downfield in comparison to the analogous environments of protonated ligand **2.19** (figure 2.13). More notably, the signal at 4.34 ppm, corresponding to the C*H*$_2$ moieties, appears much broader than that of ligand **2.19** and aluminium dihydride **2.22**. This is also the case for the aryl protons of the phosphine groups, which may be due to the effect of the quadrupolar aluminium nucleus on the surrounding proton environments. The ^{31}P NMR spectrum consists of a broad singlet resonance at −35.0 ppm corresponding to the equivalent phosphorus centres of aluminium dibromide **2.47**.

Aiming to synthesise the aluminium(I) species (^{Ph}PNP)Al, a reduction of (^{Ph}PNP)AlBr$_2$ using an excess of KC$_8$ was attempted. After 24 hours stirring at room temperature, an aliquot was analysed by ^{31}P NMR spectroscopy, which showed no reaction had occurred. The reaction mixture was then heated to 65 ˚C for a further 24 hours, after which complete decomposition to (^{Ph}PNP)H was observed.

Although (^{Ph}PNP)AlBr$_2$ (**2.47**) was successfully synthesised, due to the complex requirements needed to synthesise and handle the highly sensitive aluminium dibromide **2.47**, along with its subdued reactivity towards reducing agents, it was concluded that alternate routes to (^{Ph}PNP)Al would need to be explored.

2.5.2 Synthesis of (^{Ph}PNP)AlI$_2$ (2.48)

Reported aluminium iodide compounds have been prepared by analogous routes to that presented for aluminium dibromide **2.47** but have also been prepared by reacting aluminium hydride compounds with RI (R = Me, I).[50,54] For example, (I^{i}Pr$_2$Me$_2$)AlTippH$_2$ (**1.84**) was reacted with an excess of methyliodide to produce the corresponding aluminium diiodide species (**1.85**), before undergoing a reduction reaction with KC_8 to form the aluminium(I) dimer [(I^{i}Pr$_2$Me$_2$)AlTipp]$_2$ (**1.86**) (discussed in section 1.4.1).[55]

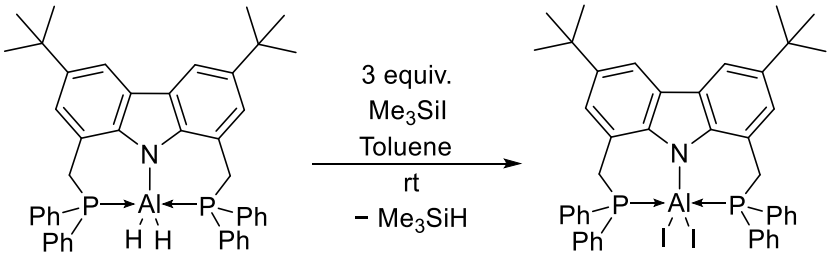

Scheme 2.20 Synthetic route to (^{Ph}PNP)AlI$_2$ (**2.48**) through the reaction of (^{Ph}PNP)AlH$_2$ (**2.22**) with trimethylsilyl iodide (Me_3SiI).

The synthesis of (^{Ph}PNP)AlI$_2$ (**2.48**) proceeds by reacting (^{Ph}PNP)AlH$_2$, **2.22**, with three equivalents of trimethylsilyl iodide (Me_3SiI), at room temperature, over a period of 16 days (scheme 2.20). After four days of stirring, the ^{31}P NMR spectrum of an aliquot showed complete consumption of aluminium dihydride **2.22** (figure 2.14, A). The doublet resonance at −35.6 ppm ($^2J_{H-P}$ = 75.8 Hz) corresponds to the aluminium iodide hydride intermediate (^{Ph}PNP)AlIH, (**2.49**), the major product at this stage of the reaction (56% by integration). The broad singlet resonance at −34.6 ppm correlates to aluminium diiodide **2.48**. This indicates

the reaction proceeds through the stepwise substitution of the hydride ligands and that the first substitution occurs much faster than the second. Over time, the formation of aluminium diiodide **2.48** continues and after 10 days, becomes the major species in solution (68% by integration, figure 2.14, B). After 14 days stirring at room temperature, the reaction had reached completion, evidenced by a broad singlet resonance at −33.8 ppm for aluminium diiodide **2.48** in the ^{31}P NMR spectrum (figure 2.14, C). After stirring for 16 days, the mixture was filtered and the volatiles were removed *in vacuo* to afford aluminium diiodide as an off-white solid. The ^{1}H NMR spectrum of **2.48** contains a singlet resonance at 1.36 ppm, which correspond to the *t*Bu of the carbazole backbone, and appears upfield compared to that of aluminium dihydride **2.22** (1.40 ppm) and aluminium dibromide **2.47** (1.38 ppm). The resonances for the aryl-*H* (PPh_2) environments are extremely broad and the C*H*$_2$ environments were not observed due to severe broadening of the resonance.

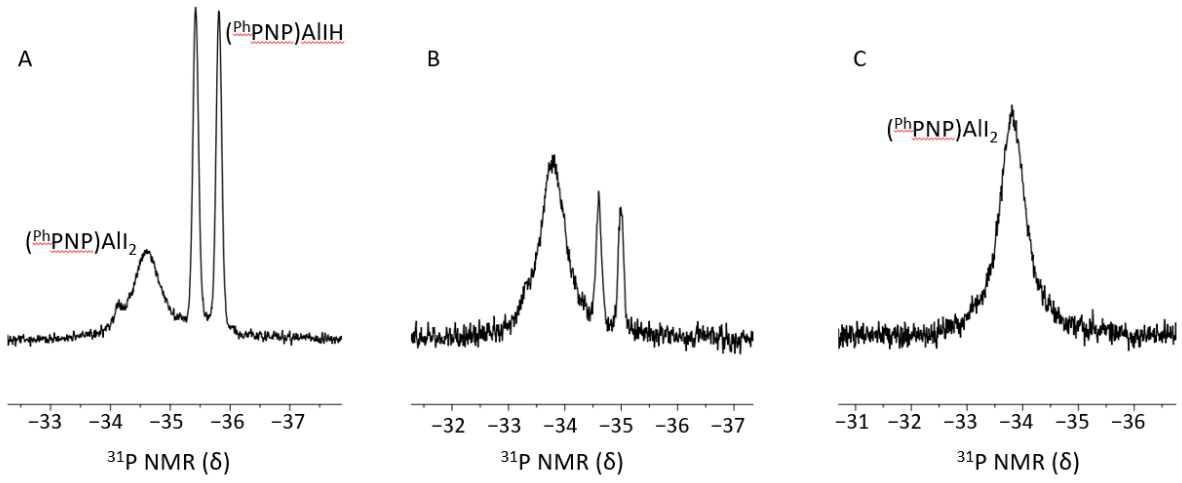

Figure 2.14 The ^{31}P NMR spectra of the reaction of (^{Ph}PNP)AlH_2 (**2.22**) with Me_3SiI, showing initial formation of (^{Ph}PNP)AlIH (**2.49**) and subsequent formation of (^{Ph}PNP)AlI_2 (**2.48**). Reactions times: A = 4 days, B = 10 days, C = 14 days.

Although the NMR spectroscopy data indicates formation of aluminium diiodide **2.48**, single crystals were not obtained and so the structure of **2.48** could not be determined by X-ray crystallography. Furthermore, isolation of **2.48** away from by-products, such as

aminophosphine **2.19**, was not achieved. However, preliminary reduction reaction of aluminium diiodide **2.48** using KC_8 were conducted. The ^{1}H and ^{31}P NMR analysis of the reactions reveal an intractable mixture, of which the products could not be identified. Attempts to isolate products through crystallisation and confirm their structures through X-ray crystallography were unsuccessful.

2.6 Synthesis of ($^{t\mathrm{Bu}}$PNP)AlH_2 and ($^{t\mathrm{Bu}}$PNP)AlHI

Ligands play a vital role in the stabilisation of metal centres, and a change in their properties can have a drastic effect on the characteristic of the compound, including its structure and reactivity. For example, $[Cp^*Al]_4$ (**1.70**) is a tetramer at room temperature and requires heat to dissociate into its monomeric form.[56] However, upon increasing the size of substituents on the Cp-ring, from five methyl groups to three *tert*-butyl groups, the aluminium(I) compound $Cp^{tBu3}Al$ (**1.75**) exists as a monomer at room temperature (discussed in section 1.4.1).[57]

Through varying the P-substituents of the carbazole-based PNP-ligand, the aim was to study the differences in synthesis, properties, and reactivity of the aluminium dihydride and diiodide compounds in comparison to the phenyl-substituted (^{Ph}PNP)AlH_2, **2.22**, and (^{Ph}PNP)AlI_2, **2.48**. Substitution of phenyl groups for *tert*-butyl groups results in more electron-rich phosphine donors which can affect the P–Al interactions and give rise to differences in reactivity. Factors that influenced the selection of *tert*-butyl (*t*Bu) groups as the P-substituents were based on the challenges that faced (^{Ph}PNP)AlX_2 (X = H, I). In particular, the separation of products of the reaction of aluminium dihydride **2.22** and magnesium(I) dimer $[(^{Mes}NacNac)Mg]_2$, and whether the presence of *tert*-butyl groups would induce a change in solubility great enough to overcome this obstacle.

2.6.1 Synthesis of ($^{t\mathrm{Bu}}$PNP)AlH_2 (2.50)

The preparation of (^{tBu}PNP)AlH_2 (**2.50**) (^{tBu}PNP = 3,6-di-*tert*-butyl-1,8-bis(di-*tert*-butylphosphinomethyl)carbazolide), like that of aluminium dihydride **2.22**, is achieved through the reaction of (^{tBu}PNP)H (**2.20**) with AlH_3•NMe_3 by elimination of H_2 (scheme 2.21).

However, unlike with aluminium dihydride **2.22** which forms at room temperature, the reaction of **2.20** and AlH_3•NMe_3 requires a much higher temperature of 80 ˚C. Aluminium dihydride **2.50** was isolated in yields of up to 83%, but a small quantity of aminophosphine **2.20** (ca. 5 - 10% by integration) is usually present.

The replacement of electron-withdrawing phenyl groups with electron-donating *tert*-butyl groups may reduce the acidity of the amine fragment of the PNP-ligand, decreasing the reactivity of aminophosphine **2.20** towards AlH_3•NMe_3. Furthermore, the larger size of *tert*-butyl groups may increase steric hindrance at the nitrogen centre of **2.20**, reducing access to the coordination site.

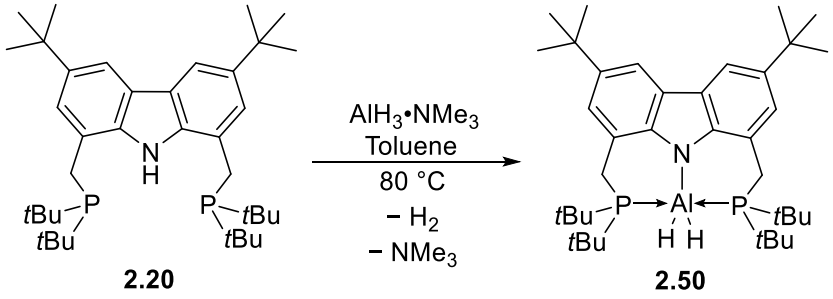

Scheme 2.21 The preparation of (^{tBu}PNP)AlH_2 (**2.50**) from the reaction of (^{tBu}PNP)H (**2.20**) with AlH_3•NMe_3.

The ^{1}H NMR spectrum of aluminium dihydride **2.50** reveals signals at 1.11 ppm and 1.54 ppm corresponding to *tert*-butyl groups of the phosphine fragments and the carbazole backbone, respectively. The aryl region consists of two resonances at 7.75 and 8.28 ppm correlating to aryl-H centres of the ligand. The signal at 5.32 ppm relates to AlH_2, resonating as a broad singlet, in contrast to the triplet observed at 5.85 ppm for AlH_2 of aluminium dihydride **2.22**. Further differences between aluminium dihydrides **2.22** and **2.50** are observed by ^{31}P NMR spectroscopy, with the phosphorus environment of aluminium dihydride **2.50** resonating as a broad singlet at 8.3 ppm, a downfield shift relative to the clearly defined triplet at −33.5 ppm for aluminium dihydride **2.22**.

The structural characteristics of aluminium dihydride **2.50**, specifically whether the P-donors are coordinated to aluminium, could not be easily interpreted due the lack of coupling

observed in both ^{31}P and ^{1}H NMR spectra. Therefore, variable temperature NMR analysis was conducted over a temperature range of 230 K to 300 K to reveal the $^{2}J_{H-P}$ coupling (figure 2.15). Between 300 K and 280 K the Al*H* environment resonates as a broad singlet in ^{1}H NMR spectrum. At 260 K, the Al*H* signal resolves to a triplet resonance ($^{2}J_{H-P}$ = 26 Hz), indicating that both phosphorus centres are coordinated to aluminium and are coupled to the hydride ligands. The triplet resonance of the Al*H* environment becomes more prominent as the temperature lowered to 230 K and a slight downfield shift was observed. However, the coupling constant ($^{2}J_{H-P}$ = 26 Hz) is much smaller compared to aluminium dihydride **2.22** ($^{2}J_{H-P}$ = 57 Hz), suggesting that the Al–P interactions of aluminium dihydride **2.50** are weaker than in **2.22**.

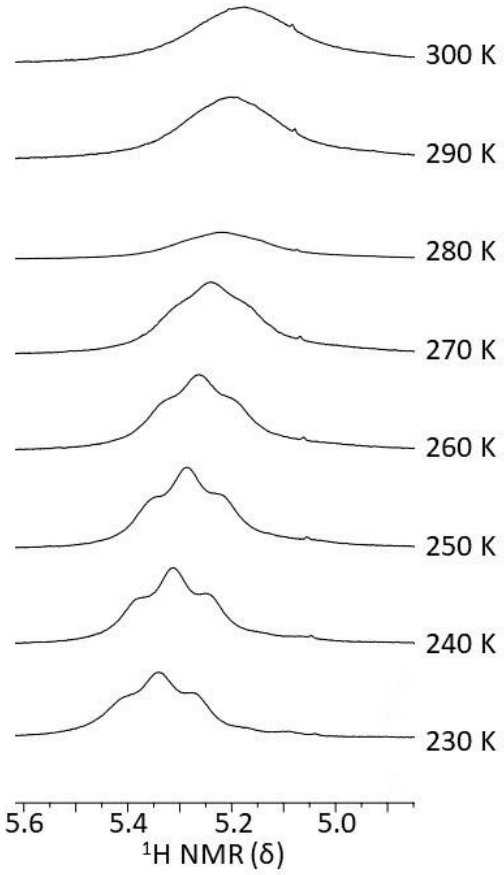

Figure 2.15 Variable temperature ^{1}H NMR of AlH_2 resonance of ($^{t\text{Bu}}$PNP)AlH_2 (**2.50**). Temperatures ranging from 230 K to 300 K.

IR spectroscopy reveals an Al–H stretching frequency at 1791 cm^{-1} for aluminium dihydride **2.50** which is comparable to reported terminal Al–H stretching frequencies and is greater than that of (^{Ph}PNP)AlH_2 (**2.22**) (1751 cm^{-1}).[17] This suggests that Al–H bonds are slightly stronger in **2.50** than **2.22**. To confirm the structural information gained from IR and NMR spectroscopy, X-ray crystallography could have been used to measure the Al–P bond lengths and angles. Unfortunately, single crystals of aluminium dihydride **2.50** could not be obtained, thus a solid-state structure of **2.50** was not determined.

Reduction of aluminium dihydride **2.50** using [(^{Mes}NacNac)Mg]$_2$ was attempted. A toluene solution of **2.50** was added to the magnesium(I) dimer at room temperature. NMR spectroscopy revealed no reaction had occurred and the reaction mixture was heated to 60 ˚C. However, even at elevated temperatures, no reaction was observed. Consequently, the aim to synthesise PNP-supported aluminium(I) was not realised through the reduction of aluminium dihydride **2.50**, and so the route to low-oxidation state aluminium using aluminium halide precursors needed to be explored.

2.6.2 Synthesis of (^{tBu}PNP)AlHI (2.51)

The reaction of (^{tBu}PNP)AlH_2 (**2.50**) and Me_3SiI was conducted to synthesise aluminium diiodide analogue (^{tBu}PNP)AlI_2, as demonstrated for the synthesis of aluminium diiodide **2.48**. However, upon treating aluminium dihydride **2.50** with three equivalents of Me_3SiI at ambient temperature, which was stirred for seven days, formation of (^{tBu}PNP)AlI_2 was not observed. Instead, it was found that iodoaluminium hydride (^{tBu}PNP)AlHI (**2.51**) was the major product (scheme 2.22).

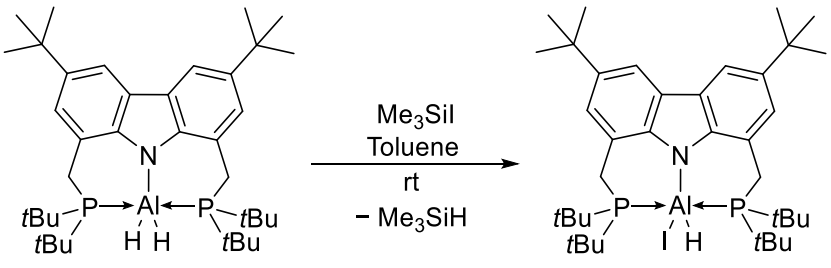

2.50 **2.51**

Scheme 2.22 Preparation of (^{tBu}PNP)AlIH (**2.51**) from the reaction of (^{tBu}PNP)AlH_2 (**2.50**) with Me_3SiI at room temperature.

The ^{31}P NMR spectrum of an aliquot shows aluminium dihydride **2.50** had been completely consumed and a broad singlet resonance is present at 9.8 ppm. The ^{1}H NMR spectrum consists of a sharp singlet resonance at 1.49 ppm corresponding to the *tert*-butyl fragments of the carbazole backbone. Two doublet resonances at 1.29 and 0.99 ppm, assigned to the *tert*-butyl P-substituents, suggest that the *tert*-butyl groups are not equivalent, in contrast to aluminium dihydride **2.50** for which only one resonance for the P*t*Bu$_2$ is observed. A broad singlet observed at 6.04 ppm, with an integral of one, indicates that only one hydride ligand is coordinated to aluminium. Thus, it is suggested that (^{tBu}PNP)AlIH (**2.51**) is the product of the reaction of aluminium dihydride **2.50** and Me_3SiI.

Although (^{tBu}PNP)AlHI (**2.51**) could be identified by NMR spectroscopy, the reaction of aluminium dihydride **2.50** and Me_3SiI does not proceed cleanly and isolation of **2.51** was not achieved. However, preliminary studies into reduction reactions of **2.51** to aluminium(II) hydride products were conducted. Upon formation of iodoaluminium hydride **2.51**, all volatiles were removed under reduced pressure, and then **2.51** was immediately used in a reaction with reducing agent KC_8. ^{1}H and ^{31}P NMR analysis of an aliquot of the reaction mixture reveals complete consumption of **2.51** and a mixture of unidentified products. However, the ^{1}H NMR spectrum contains a broad singlet at 5.40 ppm, indicative of an Al*H* environment, suggesting the hydride ligand remains coordinated to the aluminium centre. Attempts to isolate the products by crystallisation were unsuccessful, thus X-ray crystallography could not be used to identify the products.

2.7 Conclusions

The preparations of PNP-supported aluminium dihydrides (^{Ph}PNP)AlH_2 (**2.22**) and (^{tBu}PNP)AlH_2 (**2.50**) were carried out *via* the reaction of aminophosphines **2.19** and **2.20** with AlH_3•NMe_3, and their reactivity investigated. Aluminium dihydride **2.22** was found to be highly reactive towards organic molecules, such as anilines, through which the effects of the size of substrate on reactivity were studied. It was found that upon increasing the size of aniline, the reaction of aluminium dihydride **2.22** with only one equivalent of aniline was favoured. Moreover, the reduction of 2,6-xylylisonitrile with aluminium dihydride **2.22** led to the formation of dimeric product **2.35**, containing a six-membered metallocycle, resembling

previously reported compounds formed from the reaction of organoaluminium hydrides with isonitriles.

Dehydrogenation of aluminium dihydride **2.22** was investigated using $Pd(PCy_3)_2$. The formation of dihydrogen was observed by ^1H NMR spectroscopy which suggests dehydrogenation had occurred. Although the aluminium-containing product was not identified, (^{Ph}PNP)PdH (**2.38**) was crystallised from the reaction mixture and its structure determined by X-ray diffraction. Alternate reduction reactions of aluminium dihydride **2.22** were attempted using magnesium(I) dimer [(^{Mes}NacNac)Mg]$_2$. Although reactivity was observed by ^1H and ^{31}P NMR spectroscopy through the disappearance of the $^2J_{H-P}$ coupling of aluminium dihydride **2.22**, the aluminium-containing products were not identified. Aluminium dihydride **2.50** was not seen to react with [(^{Mes}NacNac)Mg]$_2$ at 60 ˚C.

Synthesis of (^{Ph}PNP)$AlBr_2$ (**2.47**) was performed through salt metathesis in yields of up to 42%. However, (^{Ph}PNP)AlI_2 (**2.48**) was prepared through the reaction of aluminium dihydride **2.22** with an excess of Me_3SiI. In contrast, the reaction of aluminium dihydride **2.50** with Me_3SiI achieved a single substitution to give ($^{t\text{Bu}}$PNP)AlIH (**2.51**). Aluminium iodide compounds **2.48** and **2.51** were synthesised *in situ* and immediately used in subsequent reactions. Reductions of **2.48** and **2.51** were attempted using KC_8, and whilst NMR analysis showed the consumption of starting material, the products of these reaction were not identified. However, further investigations into the reduction of aluminium iodide compounds **2.48** and **2.51**, varying condition and reducing agents, will be needed to realise the aim of synthesising PNP-supported aluminium(I) and aluminium(II) compounds.

2.8 References

(1) Peris, E.; Crabtree, R. H., *Chem. Soc. Rev.*, **2018**, *47*, 1959–1968.

(2) Kundu, S., *Chem. Asian J.*, **2020**, *15* , 3209–3224.

(3) Zhu, Q.; Qiu, R.; Dong, S.; Zeng, G.; Zhu, J. *Chem. Asian J.*, **2021**, *16*, 2063–2067.

(4) Wang, P.; Zhang, M.; Zhu, C., *Organometallics*, **2020**, *39* , 2732–2738.

(5) Leischner, T.; Spannenberg, A.; Junge, K.; Beller, M., *Chem. Cat. Chem.*, **2020**, *12*, 4543–4549.

(6) Sacconi, L.; Bertini, I., *J. Am. Chem. Soc.*, **1967**, *89*, 2235–2236.

(7) Fryzuk, M. D.; Giesbrecht, G. R.; Olovsson, G.; Rettig, S. J., *Organometallics*, **1996**, *15*, 4832–4841.

(8) Wang, L.; Cui, D.; Hou, Z.; Li, W.; Li, Y., *Organometallics*, **2011**, *30*, 760–767.

(9) You, F.; Zhai, J.; So, Y.-M.; Shi, X., *Inorg. Chem.*, **2021**, *60*, 1797–1805.

(10) Kessler, J. A.; Iluc, V. M., *Inorg. Chem.*, **2014**, *53*, 12360–12371.

(11) Kuriyama, S.; Arashiba, K.; Tanaka, H.; Matsuo, Y.; Nakajima, K.; Yoshizawa, K.; Nishibayashi, Y. *Angew. Chem. Int. Ed.*, **2016**, *55*, 14291–14295.

(12) Lee, P.-Y.; Liang, L.-C., *Inorg. Chem.*, **2009**, *48*, 5480–5487.

(13) Morris, A. L.; York, J. T., *J. Chem. Educ.*, **2009**, *86*, 1408.

(14) Allman, T.; Goel, R. G., *Can. J. Chem.*, **1982**, *60*, 716–722.

(15) Wu, K.; Doyle, A. G., *Nat. Chem.*, **2017**, *9*, 779–784.

(16) Wehmschulte, R. J.; Power, P. P., *Polyhedron*, **2000**, *19*, 1649–1661.

(17) Falconer, R. L.; Nichol, G. S.; Cowley, M. J., *Inorg. Chem.*, **2019**, *58*, 11439–11448.

(18) Contreras, L.; Cowley, A. H.; Gabbaï, F. P.; Jones, R. A.; Carrano, C. J.; Bond, M. R., *J. Organomet. Chem.*, **1995**, *489*, C1–C3.

(19) Chang, J.-C.; Hung, C.-H.; Huang, J.-H., *Organometallics*, **2001**, *20*, 4445–4447.

(20) Ouzounis, K.; Riffel, H.; Hess, H.; Kohler, U.; Weidlein, J., *Z. Anorg. Allg. Chem.*, **1983**, *504*, 67–76.

(21) Krossing, I.; Nöth, H.; Tacke, C.; Schmidt, M.; Schwenk, H., *Chem. Ber.*, **1997**, *130*, 1047–1052.

(22) Plundrich, G. T.; Wadepohl, H.; Gade, L. H., *Inorg. Chem.*, **2016**, *55*, 353–365.

(23) Xu, Y.; Rettenmeier, C. A.; Plundrich, G. T.; Wadepohl, H.; Enders, M.; Gade, L. H., *Organometallics*, **2015**, *34*, 5113–5118.

(24) Grüger, N.; Rodríguez, L.-I.; Wadepohl, H.; Gade, L. H., *Inorg. Chem.*, **2013**, *52*, 2050–2059.

(25) Grüger, N.; Wadepohl, H.; Gade, L. H., *Eur. J. Inorg. Chem.*, **2013**, *30*, 5358–5365.

(26) Higuchi, J.; Kuriyama, S.; Eizawa, A.; Arashiba, K.; Nakajima, K.; Nishibayashi, Y., *Dalton Trans.*, **2018**, *47*, 1117–1121.

(27) Zhang, X.; Liu, L. L., *Angew. Chem. Int. Ed.*, **2021**, *60*, 27062–27069.

(28) DeMott, J. C.; Guo, C.; Foxman, B. M.; Yandulov, D. V.; Ozerov, O. V., *Mendeleev Commun.*, **2007**, *17*, 63–65.

(29) Luo, B.; Kucera, B. E.; Gladfelter, W. L., *Dalton Trans.*, **2006**, 37, 4491.

(30) Lee, W.-Y.; Liang, L.-C., *Dalton Trans.*, **2005**, 11, 1952–1956.

(31) Diamond, S. E.; Szalkiewicz, A.; Mares, F., *J. Am. Chem. Soc.*, **1979**, *101*, 490–491.

(32) Crockett, M. P.; Wong, A. S.; Li, B.; Byers, J. A., *Angew. Chem. Int. Ed.*, **2020**, *59*, 5392–5397.

(33) Koller, J.; Bergman, R. G., *Organometallics*, **2010**, *29*, 3350–3356.

(34) Nako, A. E.; Gates, S. J.; Schädel, N.; White, A. J. P.; Crimmin, M. R., *Chem. Commun.*, **2014**, *50*, 9536–9538.

(35) Zhu, H.; Yang, Z.; Magull, J.; Roesky, H. W.; Schmidt, H.-G.; Noltemeyer, M., *Organometallics*, **2005**, *24*, 6420–6425.

(36) Zheng, W.; Stasch, A.; Prust, J.; Roesky, H. W.; Cimpoesu, F.; Noltemeyer, M.; Schmidt, H.-G. A., *Angew. Chem. Int. Ed.*, **2001**, *40*, 3461–3464.

(37) Wehmschulte, R. J.; Power, P. P., *Inorg. Chem.*, **1998**, *37*, 6906–6911.

(38) Wehmschulte, R. J.; Power, P. P., *Inorg. Chem.*, **1994**, *33*, 5611–5612.

(39) Knabel, K.; Nöth, H., *Z. Naturforsch B*, **2005**, *60*, 1027–1035.

(40) Hooper, T. N.; Lau, S.; Chen, W.; Brown, R. K.; Garçon, M.; Luong, K.; Barrow, N. S.; Tatton, A. S.; Sackman, G. A.; Richardson, C.; White, A. J. P.; Cooper, R. I.; Edwards, A. J.; Casely, I. J.; Crimmin, M. R., *Chem. Sci.*, **2019**, *10*, 8083–8093.

(41) Ozerov, O. V.; Guo, C.; Fan, L.; Foxman, B. M., *Organometallics*, **2004**, *23*, 5573–5580.

(42) Fan, L.; Yang, L.; Guo, C.; Foxman, B. M.; Ozerov, O. V., *Organometallics*, **2004**, *23*, 4778–4787.

(43) Bonyhady, S. J.; Collis, D.; Frenking, G.; Holzmann, N.; Jones, C.; Stasch, A., *Nat. Chem.*, **2010**, *2*, 865–869.

(44) Falconer, R. L.; Nichol, G. S.; Smolyar, I. V.; Cockroft, S. L.; Cowley, M. J., *Angew. Chem. Int. Ed.*, **2021**, *60*, 2047–2052.

(45) Bonyhady, S. J.; Collis, D.; Holzmann, N.; Edwards, A. J.; Piltz, R. O.; Frenking, G.; Stasch, A.; Jones, C., *Nat. Commun.*, **2018**, *9*, 3079.

(46) Hicks, J.; Juckel, M.; Paparo, A.; Dange, D.; Jones, C., *Organometallics*, **2018**, *37*, 4810–4813.

(47) Cui, C.; Roesky, H. W.; Schmidt, H.-G.; Noltemeyer, M.; Hao, H.; Cimpoesu, F., *Angew. Chem. Int. Ed.*, **2000**, *39*, 4274–4276.

(48) Bag, P.; Porzelt, A.; Altmann, P. J.; Inoue, S., *J. Am. Chem. Soc.*, **2017**, *139*, 14384–14387.

(49) Hicks, J.; Vasko, P.; Goicoechea, J. M.; Aldridge, S., *Nature*, **2018**, *557*, 92–95.

(50) Schwamm, R. J.; Coles, M. P.; Hill, M. S.; Mahon, M. F.; McMullin, C. L.; Rajabi, N. A.; Wilson, A. S. S., *Angew. Chem. Int. Ed.*, **2020**, *59*, 3928–3932.

(51) Queen, J. D.; Lehmann, A.; Fettinger, J. C.; Tuononen, H. M.; Power, P. P., *J. Am. Chem. Soc.* **2020**, *142*, 20554–20559.

(52) Stender, M.; Segerer, U.; Sieler, J.; Hey-Hawkins, E., *Z. Anorg. Allg. Chem.*, **1998**, *624*, 85–90.

(53) Burt, J.; Levason, W.; Light, M. E.; Reid, G., *Dalton Trans.*, **2014**, *43*, 14600–14611.

(54) Falconer, R. L.; Byrne, K. M.; Nichol, G. S.; Krämer, T.; Cowley, M. J., *Angew. Chem. Int. Ed.*, **2021**, *60*, 24702–24708.

(55) Weetman, C.; Porzelt, A.; Bag, P.; Hanusch, F.; Inoue, S., *Chem. Sci.*, **2020**, *11*, 4817–4827.

(56) Dohmeier, C.; Robl, C.; Tacke, M.; Schnöckel, H. *Angew. Chem. Int. Ed.*, **1991**, *30*, 564–565.

(57) Hofmann, A.; Tröster, T.; Kupfer, T.; Braunschweig, H., *Chem. Sci.*, **2019**, *10*, 3421–3428.

Chapter 3

NCN-Pincer Ligand-Supported Aluminium Dibromide

3.1 Introduction

Within the field of organoaluminium chemistry, very few examples of NCN-pincer ligand supported aluminium complexes have been reported. The NCN-ligands that have been used are anionic and bear a 2,6-xylene backbone with two neutral nitrogen-based donating groups. Slight variations within these ligands occur in the bonding of the nitrogen centres. For example, it is possible to have an amine donating group with C–N single bonds and two N-substituents, $^{-}C_6H_3\{CH_2NR_2\}_2$ (R = Me, ^{Me}NCN, **3.1**, or R = Et, ^{Et}NCN, **3.2**) (figure 3.1). [1] On the other hand, imine groups can be used instead, which have C=N double bonds and only one N-substituent per nitrogen centre, $^{-}C_6H_3\{C(H)=NDipp\}_2$ (**3.3**).[2,3] The C=N double bond reduces the degree of rotation that can occur, fixing the N-donor fragment in place, enhancing the rigidity of the ligand. Furthermore, imine groups can behave as both nucleophiles and electrophiles which may lead to possible side reactions occurring.[4] The size of N-substituent of these ligands varies drastically from small methyl and ethyl groups on the amine donors to larger Dipp (2,6-diisopropylphenyl) groups on the imine donors. Both types of NCN-ligand have been shown to coordinate aluminium halide and alkyl fragments and, in the case of the NCN-ligands **3.1** and **3.2**, aluminium hydride fragments (figure 3.1).[2,3,5,6]

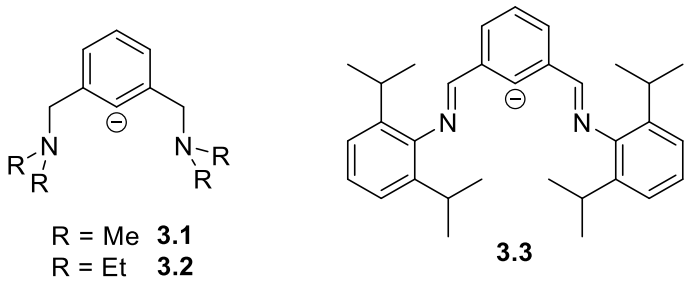

Figure 3.1 The NCN-type pincer ligands reported to stabilise AlX_2 fragments.

The reported synthesis of (^{Dipp}NCN)$AlCl_2$ (**3.7**) (^{Dipp}NCN = $^{-}C_6H_3\{C(H=NDipp\}_2$) proceeded by the reaction of (^{Dipp}NCN)Br (**3.4**) with nBuLi in THF to generate the lithium salt **3.5** through lithium-halogen exchange. This was followed by the addition of $AlCl_3$ to give aluminium dichloride THF-adduct **3.6**. The coordinated THF molecule was then removed under reduced pressure to afford aluminium dichloride **3.7** in a yield of 75% (scheme 3.1).

The solid-state structure of aluminium dichloride **3.7** shows the aluminium centre to be five-coordinate. The Al–C bond has a length of 1.9446(19) Å, the Al–N bond lengths are 2.1317(16) Å and 2.498(2) Å, and the Al–Cl distances are 2.1208(8) Å and 2.1382(7) Å. Aluminium dichloride **3.6** was then shown to react with $Na[BAr_4^F]$ to produce the aluminium cation $[(^{Dipp}NCN)AlCl(THF)][BAr_4^F]$, which was used as a Lewis acid precatalyst for Diels-Alder cycloadditions.[3]

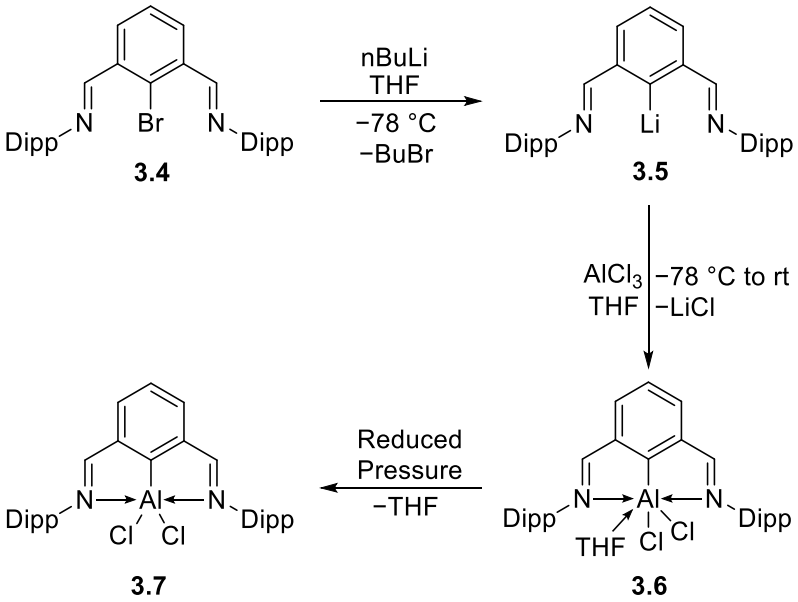

Scheme 3.1 The synthetic route to $(^{Dipp}NCN)AlCl_2$ (**3.7**).

A.H. Cowley and co-workers reported the preparation of $(^{Me}NCN)AlH_2$ (**3.9**). The initial route proceeds through salt metathesis as aryl lithium $(^{Me}NCN)Li$ (**3.8**) was reacted with $ClAlH_2{\bullet}NMe_3$ to give aluminium dihydride **3.9**, which was isolated in a yield of 55%. An alternate pathway requires the synthesis of the aluminium dichloride $(^{Me}NCN)AlCl_2$ (**3.10**) through the reaction of lithium amide **3.8** and one equivalent of $AlCl_3$. Aluminium dichloride **3.10** was then reacted with $LiAlH_4$ in a transmetallation reaction to give aluminium dihydride **3.9**. Gallium and indium dichloride analogues **3.11** and **3.12** have also been reacted with $LiAlH_4$ to synthesise aluminium dihydride **3.9** through transmetallation (scheme 3.2).[5]

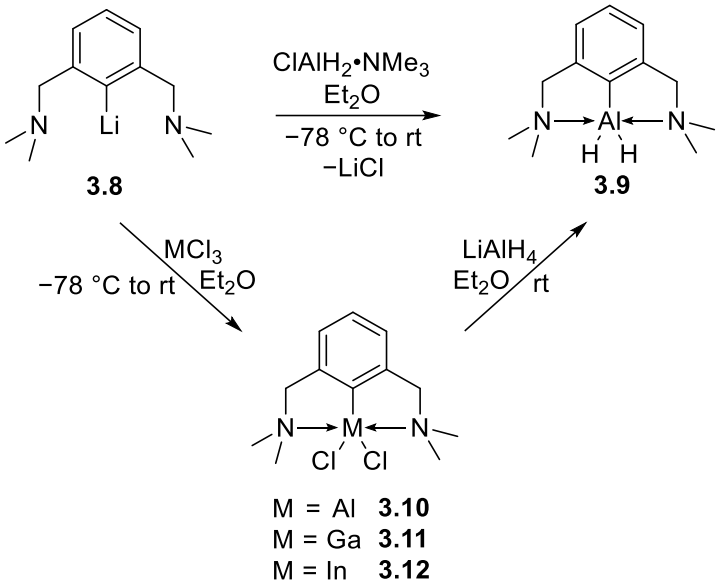

Scheme 3.2 The synthetic routes to (^{Me}NCN)AlH$_2$ (**3.9**) through salt metathesis or transmetallation pathways.

The identity of aluminium dihydride **3.9** was confirmed by X-ray crystallography. The solid-state structure revealed **3.9** to be monomeric with a pentacoordinate aluminium centre that has a distorted trigonal bipyramidal geometry. The H_2AlC moiety is planar, with the Al–H and Al–C centres residing in the equatorial plane. However, the N–Al–N fragment is non-linear, with an angle of 157.8(2)˚, which is attributed to the geometric constraints of the ligand. The N–Al bond lengths are 2.277(5) Å and 2.233(5) Å, which are comparable to those of ^{Dipp}NCN-aluminium dichloride **3.7**. The hydride ligands are located in the difference map and the Al–H distances are measured at 1.512(38) Å and 1.488(42) Å, similar to reported terminal aluminium-hydride bond lengths.[7–9] The solid-state structure aluminium dichloride analogue **3.10** was very similar to that of aluminium dihydride **3.9**, with average Al–N distances of 2.261(5) Å, and a marginally wider N–Al–N angle of 158.8(3)˚.

A slightly modified NCN-pincer ligand with larger N-substituents, increasing from methyl groups to ethyl groups, was used as the support system of analogues (^{Et}NCN)AlX$_2$ (X = Cl, Et, H).[6] Aluminium dichloride (^{Et}NCN)AlCl$_2$ (**3.14**) and aluminium diethyl (^{Et}NCN)AlEt$_2$ (**3.15**) were synthesised through reacting lithium amide (^{Et}NCN)Li (**3.13**) with ClAlX$_2$ (X = Cl or Et) and were isolated in yields of approximately 70%. Aluminium dihydride (^{Et}NCN)AlH$_2$ (**3.16**) was

prepared from the reaction of aluminium dichloride **3.14** with NaH and isolated in a high yield of 93% (scheme 3.3).

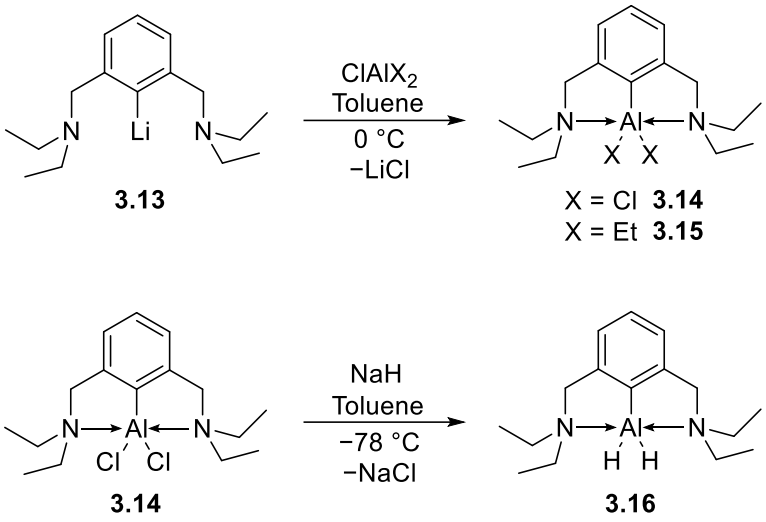

Scheme 3.3 The reported synthetic routes to (^{Et}NCN)AlCl$_2$ (**3.14**), (^{Et}NCN)AlEt$_2$ (**3.15**), and (^{Et}NCN)AlH$_2$ (**3.16**).

The solid-state structure of aluminium dichloride **3.14**, determined by X-ray crystallography, reveals a monomer containing a five-coordinate, distorted trigonal bipyramidal aluminium centre. The Al–N bond lengths are 2.321(3) Å and 2.296(3) Å, longer than those of aluminium dichloride **3.10**, and the N–Al–N angle of 158.19(10)˚ is similar to **3.10**. Likewise, the solid-state structure aluminium diethyl **3.15** is monomeric with a pentacoordinate aluminium. However, Al–N bond length (2.4640(11) Å) elongation was seen in comparison to aluminium dichloride **3.14** and are the longest distances for an Al–N dative bond of all reported (NCN)AlX$_2$ compounds. The N–Al–N angle of **3.15** is 152.88(9)˚, much more acute than aluminium dichloride **3.14**, and may be a result of the larger ethyl ligands bound to aluminium. The solid-state structure of aluminium dihydride **3.16** was not reported.

Although synthetic routes to NCN-stabilised aluminium halide, hydride and alkyl compounds are established, the reactivity of such compounds remains underexplored. The intramolecular-stabilisation of NCN-supported aluminium halide compounds may allow them to be used as potential precursors to low-oxidation state organoaluminium compounds. The majority of reported examples of organoaluminium(I) use large ligands to sterically protect

the aluminium centre.[10–13] In contrast, the ^{Me}NCN-ligand is much smaller, bearing methyl N-substituents, leaving the aluminium centre more open, which may lead to dimerisation. However, the tridentate manner in which ^{Me}NCN bonds to aluminium will also have an effect on the formation of the product.[14]

3.2 Aims and Outlooks

The aims of this work were:

- To synthesise and characterise the NCN-supported aluminium bromide (^{Me}NCN)AlBr$_2$.
- To study the reactivity of the ^{Me}NCN-aluminium dibromide compound towards reducing agents.
- To synthesise an ^{Me}NCN-supported aluminium(I) species and study the effects of using a smaller ligand system.

3.3 Synthesis of (^{Me}NCN)AlBr$_2$ (3.18)

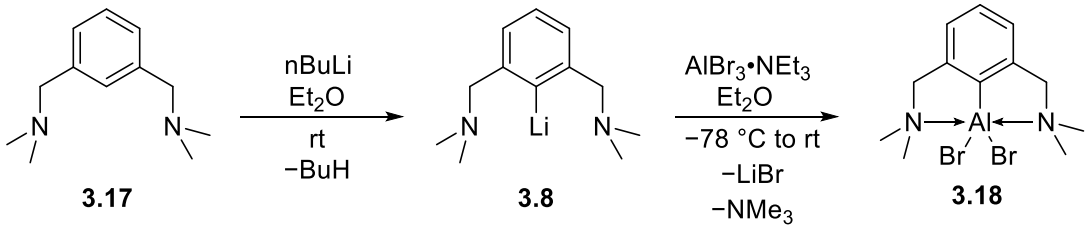

Scheme 3.4 Synthesis of (^{Me}NCN)AlBr$_2$ (**3.18**).

The preparation of (^{Me}NCN)AlBr$_2$ (^{Me}NCN = bis{dimethylaminomethyl}phenyl) proceeded through lithiation of (^{Me}NCN)H (**3.17**) followed by salt metathesis with AlBr$_3$•NEt$_3$. Protio ligand **3.17** was treated with nBuLi at room temperature to afford (^{Me}NCN)Li (**3.8**), resulting in a colour change from colourless to orange. Deprotonated ligand **3.8** was then

reacted with a toluene solution of $AlBr_3$•NEt_3 at −78 ˚C. The mixture was warmed slowly and stirred at room temperature for 48 hours, after which salts were removed *via* filtration and the product was extracted with benzene. (^{Me}NCN)$AlBr_2$ (**3.18**) was isolated as a yellow solid in a yield of 44% (scheme 3.4).

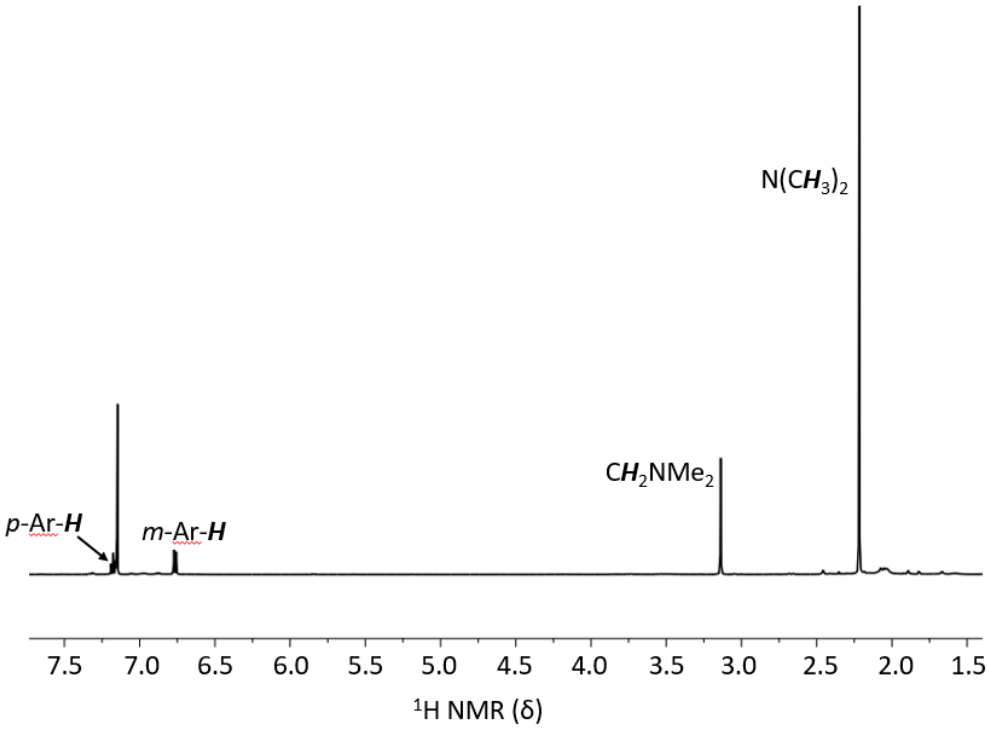

Figure 3.2 ^{1}H NMR spectrum of (^{Me}NCN)$AlBr_2$ (**3.18**).

The ^{1}H NMR spectrum of aluminium dibromide **3.18** consists of two singlet resonances at 2.23 ppm and 3.15 ppm, corresponding to the methyl N-substituents (N(CH_3)$_2$) and the methylene linkers (Ph-CH_2-NMe_2) (figure 3.2). The aromatic region shows a triplet resonance at 7.19 ppm ($^3J_{H–H}$ = 7.4 Hz), corresponding to the *para*-aromatic proton which is coupled to the aromatic protons in the *meta*-positions. A doublet of triplets at 6.78 ppm ($^3J_{H–H}$ = 7.4 Hz, $^4J_{H–H}$ could not be measured) correlates to the aromatic protons at the *meta*-positions. The splitting of the *m*-Ar-H signal arises from coupling to the *para*-aromatic proton, to give a doublet, with coupling to the protons of the methylene bridge, causing further splitting to weak triplets. Although splitting of the methylene signal at 3.15 ppm is not observed, a

crosspeak is present in the ^{1}H-^{1}H COSY NMR spectrum indicating coupling between the *m*-Ar-H and methylene proton environments.

The solid-state structure of aluminium dibromide **3.18** revealed the aluminium centre to be five-coordinate, with both nitrogen centres donating into the p-orbital at aluminium, and to have a distorted trigonal bipyramidal geometry (figure 3.3). The two Al–Br bond lengths are equal at 2.322(4) Å, similar to reported aluminium-bromine distances.[15] The Al1–C1 distance of 1.924(2) Å is slightly shorter than Al–C (1.949(5) Å) within the hydride analogue (^{Me}NCN)AlH$_2$ (**3.9**). The Al–N distances of aluminium dibromide **3.18** are 2.536(14) Å, which lies within the range observed for aluminium dihydride **3.9**, showing both N-donors to be datively bonded to aluminium at similar strengths. In contrast, aluminium dihydride **3.9** was reported to have a greater level of asymmetry with aluminium-nitrogen bond lengths of 2.277(5) Å and 2.233(5) Å for Al1–N1 and Al1–N2, respectively.[5]

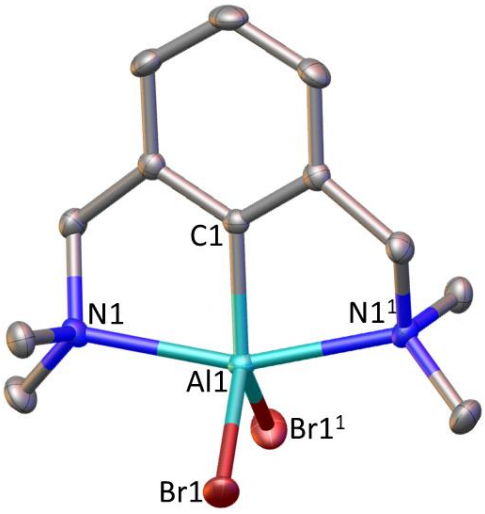

Figure 3.3 The solid-state structure of (^{Me}NCN)AlBr$_2$ (**3.18**). Hydrogen centres are omitted for clarity. Thermal ellipsoids are set to 50% probability. Select bond lengths (Å) and angles (˚): Al1–Br1 2.322(4), Al1–C1 1.924(2), Al1–N1 2.536(14), Br1–Al1–Br1^{1} 111.56(3), C1–Al1–Br1 124.219(15), and N1–Al–N1^{1} 158.31(8).

Further comparisons between aluminium dibromide **3.18** and aluminium dihydride **3.9** can be made from the bond angles around the aluminium centres. The Br1–Al1–Br1^{1} angle

(111.56(3)˚) of aluminium dibromide **3.18** is much narrower than the H1–Al1–H2 angle (118.8(21)˚) of aluminium dihydride **3.9** which may be due to longer Al–Br distances compared to Al–H lengths. The C1–Al1–Br angles in **3.18** are both 124.219(15)˚, which shows a higher level of distortion from a perfect trigonal bipyramidal geometry compared to **3.9**, with C–Al–H angles of 122.8(15)˚ and 118.4(15)˚.[5] However, the sum of angles around aluminium of aluminium bromide **3.18** is approximately 360˚, thus the carbon (C1) and bromide centres reside in the equatorial plane, while the nitrogen centres are at axial positions. The N1–Al1–N1[1] angle of 158.31(8)˚ reveals the extent of distortion observed in aluminium dibromide **3.18**, and is a result of ligand constraints with five-membered chelate rings.

3.4 Reactivity of (^{Me}NCN)AlBr$_2$ (3.18)

Organoaluminium halides are well-established precursors to low-oxidation state aluminium compounds. Group 1 metals are the most popular choice of reducing agent for accessing aluminium(I) or aluminium(II) species, as discussed in Chapter 1. Attempted reductions of (^{Me}NCN)AlBr$_2$ (**3.18**) in aromatic solvents were carried out using potassium mirror, potassium graphite (KC_8), sodium mirror, sodium/sodium chloride (Na/NaCl 5% w/w), and lithium powder, yet with each of these reducing agents, no reaction occurred.

3.4.1 Reactivity with Magnesium(I)

The low-oxidation state magnesium compound [(^{Ar}NacNac)Mg]$_2$ (Ar = Mes, Dipp) is known to reduce aluminium hydrides, as discussed in Chapter 2, generating magnesium hydride [(^{Ar}NacNac)MgH]$_2$.[16–18] Moreover, [(^{Ar}NacNac)Mg]$_2$ has also been reported to reduce main group halide complexes generating magnesium(II) halides [(^{Ar}NacNac)MgX]$_2$ (X = Cl, Br, I).[17,19] Therefore, [(^{Mes}NacNac)Mg]$_2$ was used in an attempt to reduce aluminium dibromide **3.18** to generate aluminium(I) derivative (^{Me}NCN)Al and [(^{Mes}NacNac)MgBr]$_2$ (**3.19**) as a by-product.

A toluene solution of aluminium dibromide **3.18** was added to [(^{Mes}NacNac)Mg]$_2$, in a ratio of 1:1, and at an elevated temperature of 60 ˚C, a colour change from pale-yellow to

orange occurred (scheme 3.5). After one hour of heating, a colourless precipitate had formed and isolated by filtration. ^{1}H NMR analysis of the reaction mixture shows almost complete consumption of magnesium(I) dimer [(^{Mes}NacNac)Mg]$_2$ and consists of resonances for magnesium bromide **3.19**, most notably for the C*H* of the backbone of the ^{Mes}NacNac ligand at 4.75 ppm, an upfield shift from [(^{Mes}NacNac)Mg]$_2$ (C*H*, 4.79 ppm).[20,21] Due to the complete consumption of [(^{Mes}NacNac)Mg]$_2$, it is possible that both bromide ligands of aluminium dibromide **3.18** have been abstracted from the aluminium centre. However, due to overlapping resonances, ^{1}H NMR spectroscopy did not give insight into the identity of the aluminium-containing product.

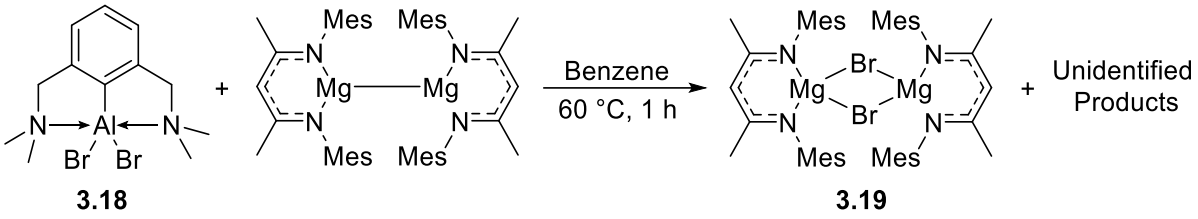

Scheme 3.5 The reaction of (^{Me}NCN)AlBr$_2$ (**3.18**) and [(^{Mes}NacNac)Mg]$_2$ to give [(^{Mes}NacNac)MgBr]$_2$ (**3.19**).

The colourless solid, which precipitated out of the reaction mixture, was recrystallised and, through X-ray crystallography, was identified as the magnesium bromide by-product **3.19**. It is worth noting that magnesium bromide **3.19** has been mentioned as a by-product in the reduction of a dibromosilane, but characterisation of **3.19** has not been reported.[19,22,23] The solid-state structure reveals magnesium bromide **3.19** has a dimeric structure with two bridging bromine centres linking the NacNac-magnesium fragments (figure 3.4). The magnesium centres have distorted tetrahedral geometries, observed through the bond angles around magnesium, ranging from 96.72(2)˚ to 121.38(6)˚. A marginal difference in the Mg–Br bond lengths of 2.5191(7) Å and 2.5381(7) Å for Br1–Mg1 and Br1–Mg1^{1}, respectively, is observed. This is concordant with the reported solid-state structures of NacNac-supported magnesium halide dimers.[24,25] Due to the ease at which magnesium bromide **3.19** can crystallise, isolation of the aluminium-containing products was attempted through fractional

crystallisation. However, only magnesium bromide **3.19** was isolated and the aluminium-containing products were not identified.

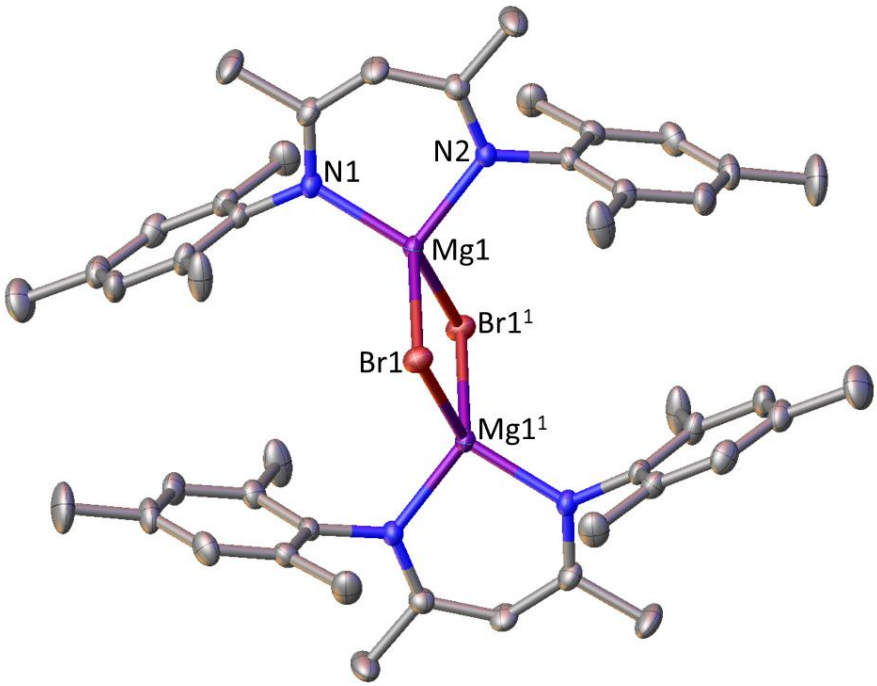

Figure 3.4 The solid-state structure of [(^{Mes}NacNac)MgBr]$_2$ (**3.19**). Hydrogen centres are omitted for clarity. Thermal ellipsoids are set to 50% probability. Select bond lengths (Å) and angles (˚): Mg1–Br1 2.5191(7), Mg1^1–Br1 2.5381(7), Mg1–N1 2.0005(17), Mg1–N2 2.0030(17), Br1–Mg1–Br1^1 96.72(2), N1–Mg1–N2 96.95(7), N1–Mg1–Br1 111.26(5), and N2–Mg1–Br1 121.38(6).

3.4.2 Reactivity with Potassium Naphthalenide

Attempts to reduce aluminium dibromide **3.18** were also carried out using potassium naphthalenide, [($C_{10}H_8$)K], a soluble reducing agent. An excess of [($C_{10}H_8$)K] in THF was added to a toluene solution of aluminium dibromide **3.18** at ambient temperature and stirred for 14 hours resulting in a colour change from pale-yellow to dark-orange (scheme 3.6). The volatiles were removed under reduced pressure and the residues dissolved in toluene before removing the insoluble salts *via* filtration.

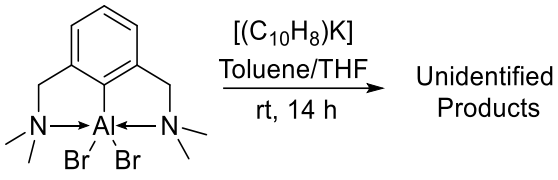

3.18

Scheme 3.6 The reaction of (^{Me}NCN)AlBr$_2$ (**3.18**) with potassium naphthalenide in THF.

The ^{1}H NMR spectrum of the reaction of aluminium dibromide **3.18** with an excess of [($C_{10}H_8$)K] showed complete consumption of **3.18**. The multiplet resonances at 7.24 ppm and 7.62 ppm correspond to naphthalene. However, signals for the NCN-containing product were not observed in the ^{1}H NMR spectrum. Therefore, it is not possible to suggest how the reaction proceeded or the products that have formed. Attempts were made to identify the aluminium-containing product through X-ray crystallography, but no single crystals of any product were obtained.

Although NMR spectroscopic data revealed that aluminium bromide **3.18** reacts with [($C_{10}H_8$)K], further detail into the reaction was lacking. Furthermore, isolation and identification of the aluminium-containing product proved difficult, which may have been a result of the presence of naphthalene. Thus, the use of other alkali metal reducing agents was explored.

3.4.3 Reactivity with Sodium-Potassium Alloy

The alloy of sodium and potassium metals, known as NaK, although not as commonly used as potassium within main group chemistry, has been reported to reduce metal halide precursors.[13,26] The eutectic alloy is liquid at room temperature at room temperature as a result of differing atomic radii of potassium and sodium, leading to lower efficiency of cation packing and weaker metallic bonding. The weaker forces between the metals may promote greater reactivity with aluminium dibromide **3.18** compared to pure potassium or sodium, with which no reaction occurred.

A THF solution of aluminium dibromide **3.18** was added to an excess (greater than two equivalents) of NaK (50% potassium by mass) at ambient temperature (scheme 3.7). After stirring for one hour, the reaction mixture turned deep orange from pale yellow. The mixture was then dissolved in toluene and filtered to remove the metal bromide salts. The volatiles were removed and the pale yellow solid obtained was recrystallised from a 1:1 mixture of benzene and THF. Colourless single crystals were obtained and using X-ray crystallography, the product was identified as aluminium bromide dimer $[(NCO)AlBr]_2$ (**3.20**) (NCO = 2-$(Me_2NCH_2)C_6H_3$-6-$CH(C_4H_9)O$). The transformation of **3.18** to **3.20** involves removal of one bromide ligand from aluminium. Activation of THF and a reaction with the NCN ligand occurs, resulting in the loss of an N-donor group, and formation of an asymmetric NCO ligand. The overall product is a dimeric aluminium(III) bromide species.

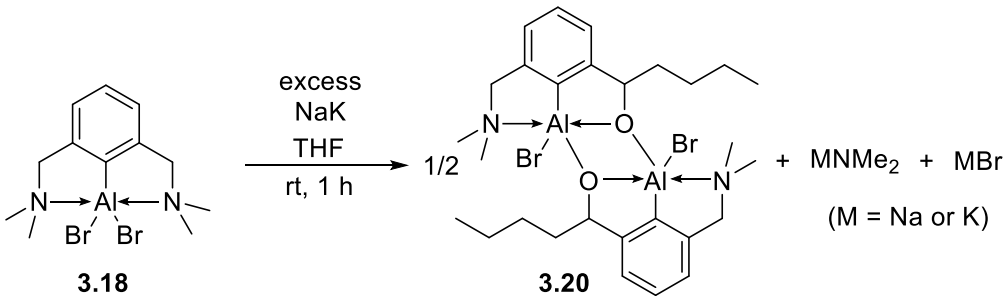

3.18 **3.20**

Scheme 3.7 The reaction of $(^{Me}NCN)AlBr_2$ (**3.18**) with NaK in THF at ambient temperature to give dimer $[(NCO)AlBr]_2$ (**3.20**).

The solid-state structure of aluminium bromide dimer **3.20** revealed the aluminium centre to be five-coordinate and to have a distorted trigonal bipyramidal geometry (figure 3.5). The NCO ligand is bonded to aluminium in a tridentate meridional manner. The covalent Al–C bond has a distance of 1.9150(17) Å (Al1–C1[1]), while the dative Al–N and Al–O bonds have lengths of 2.1934(16) Å (Al1–N1[1]) and 2.0279(13) Å (Al1–O1[1]). The Al–N bond is marginally shorter than that of aluminium dibromide **3.18** (2.2536(14) Å) suggesting a slightly stronger interaction between aluminium and nitrogen in dimer **3.20**. One bromide ligand remains coordinated to the aluminium centre and has a bond length of 2.3291(5) Å, similar to that of aluminium dibromide **3.18**. The aluminium centre is also covalently bonded to an

oxygen centre and has a typical Al–O distance of 1.7897(12) Å (Al1–O1), considerably shorter than the dative Al1–O1^{1} bond.[27] The aluminium and oxygen centres form a four-membered heterocycle with Al1–O1–Al1^{1} and O1–Al1–O1^{1} angles of 98.77(5)˚ and 81.23(5)˚ respectively.

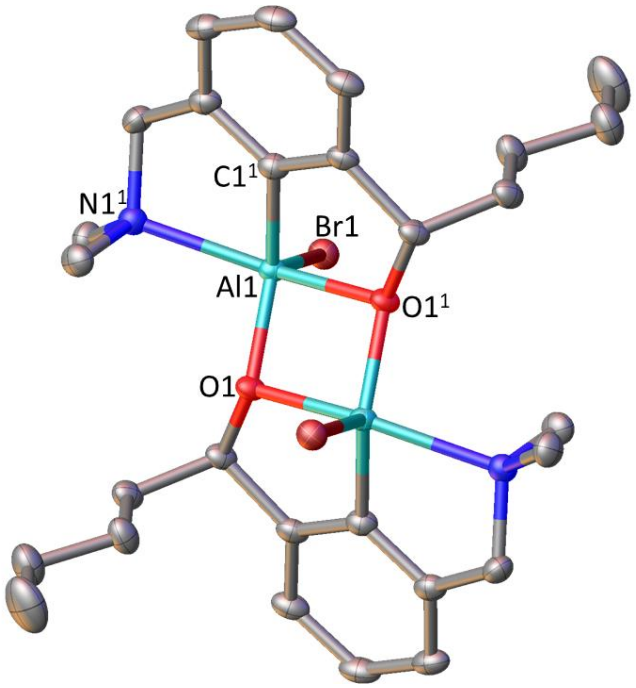

Figure 3.5 The solid-state structure of aluminium bromide dimer **3.20**. Hydrogen centres and solvent molecule are omitted for clarity. Thermal ellipsoids are set to 50% probability. Select bond lengths (Å) and angles (˚): Al1–Br1 2.3291, Al1–O1 1.7897(12), Al1–C1^{1} 1.9150(17), Al1–N1^{1} 2.1934(16), Al1–O1^{1} 2.0279(13), Al1–O1–Al1^{1} 98.77(5), O1–Al1–O1^{1} 81.23(5), N1^{1}–Al1–O1^{1} 154.72(6), Br1–Al1–O1 107.37(4).

The ^{1}H NMR spectrum of the crude product consists of two singlet resonances at 2.11 ppm and 3.31 ppm which correlate to the N-methyl groups and the methylene linker, slight upfield shifts compared to aluminium dibromide **3.18** (figure 3.6). The aryl region shows three multiplet resonances at between 6.88 ppm and 7.33 ppm corresponding to the aryl-H environments of the phenyl backbone of the NCO ligand, showing the lack symmetry of **3.20**. However, the signals for the proton environments of the alkyl chain and OC***H*** were not observed which suggests that dimer **3.20** may be a minor component of the crude solid.

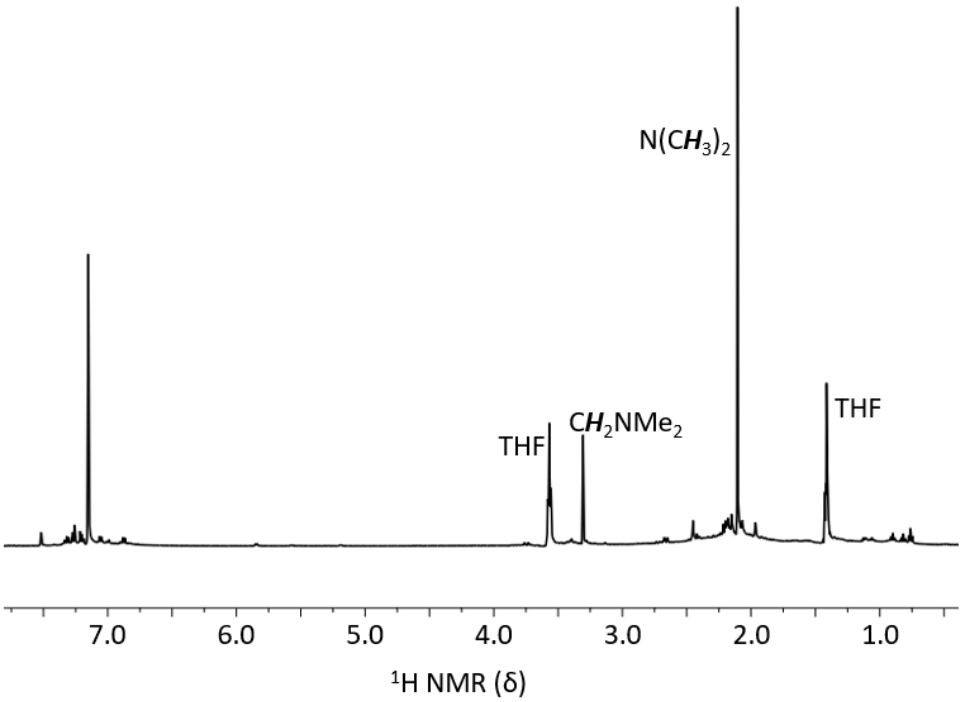

Figure 3.6 The ^{1}H NMR spectrum of the crude solid obtained from the reaction of (^{Me}NCN)AlBr$_2$ (**3.18**) and NaK in THF.

The mechanism of the reaction of aluminium dibromide **3.18** with NaK in the presence of THF is not immediately obvious, but it is suggested that loss of a hydrogen centre from the methylene linker is required to form intermediate **3.21** (scheme 3.8). The acidity of the α-hydrogen of tertiary amines increases when the nitrogen centre is coordinated to a Lewis acid, in this case RAlBr$_2$.[28] The CH$_2$ linker is also bonded to the phenyl backbone, causing the hydrogen centres of the linker fragment to be more acidic compared to those of the terminal methyl groups, making them more vulnerable to deprotonation. Behrle and co-workers reported the deprotonation of dimethylbenzylamine (C$_6$H$_5$CH$_2$NMe$_2$) at the α-position in the presence of KO*t*Bu and nBuLi to give the aminobenzyl potassium counterpart (C$_6$H$_5$CHKNMe$_2$).[29] It is worth noting that only alkyl metal bases have been reported to be used in this deprotonation reaction. Thus, it is suggested that C–H activation occurs to generate carbanion intermediate **3.21** and metal hydride MH (M = Na or K). Carbanion intermediate **3.21** could then react with a molecule of THF through nucleophilic attack from the carbanionic centre of **3.21** to the carbon located adjacent to oxygen in THF, cleaving the C–O bond causing ring opening to occur to give oxide intermediate **3.22**. An intramolecular rearrangement could

then occur through cyclisation, resulting in the cleavage of the C–N bond, to give intermediate **3.23** and $MNMe_2$ (M = Na or K) as a by-product. Intermediate **3.23** could then react with MH, which was generated in the first step, to give oxide intermediate **3.24**, which may then undergo salt elimination with another molecule of intermediate **3.24** to afford dimeric product **3.21** and two equivalents of MBr (M = Na or K).

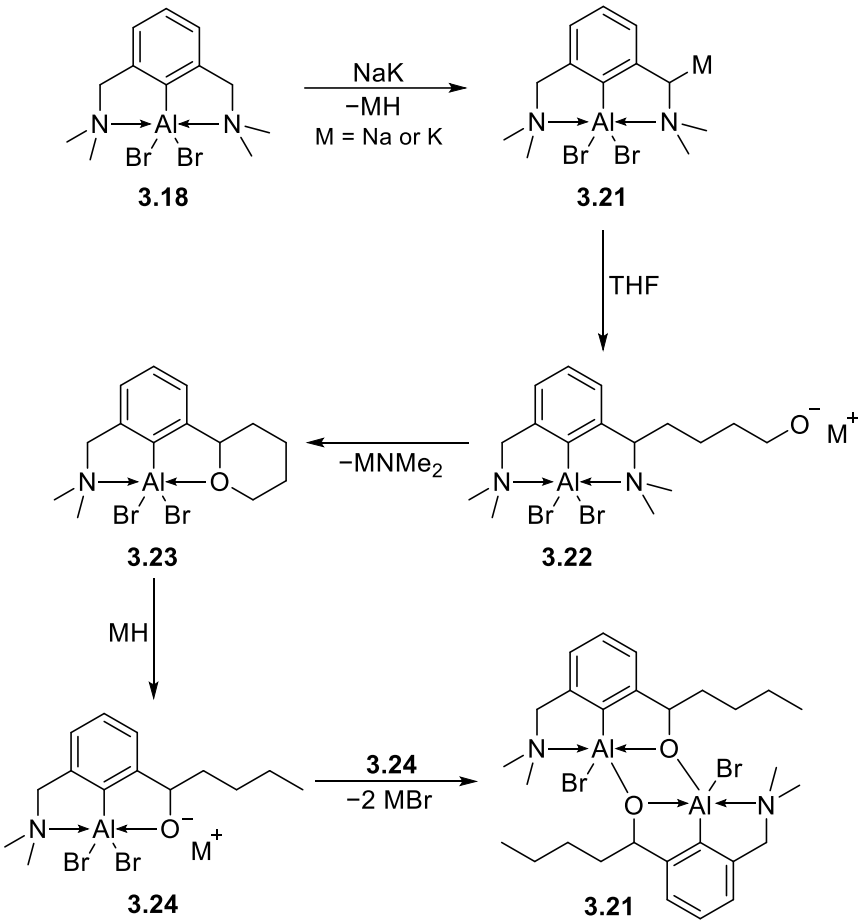

Scheme 3.8 The suggested pathway for the reaction of (^{Me}NCN)$AlBr_2$ (**3.18**) with NaK and THF to give $[(NCO)AlBr]_2$ (**3.20**), MBr and $MNMe_2$ (M = Na or K).

3.5 Conclusions

NCN-pincer ligand 2,6-bis(dimethylaminomethyl)benzene (**3.17**) was used as a support system for aluminium dibromide. (^{Me}NCN)$AlBr_2$ (**3.18**) was synthesised from the reaction of lithium salt (^{Me}NCN)Li (**3.8**) with $AlBr_3$•NEt_3 in Et_2O and isolated as a pale yellow solid in moderate yields. The solid-state structure revealed the aluminium centre to be five-coordinate, with a distorted trigonal bipyramidal geometry, as both nitrogen centres of the NCN ligand donate into the p-orbital at aluminium.

The reactivity of aluminium dibromide **3.18** towards reducing agents was explored. **3.18** reacted with magnesium(I) dimer [(^{Mes}NacNac)Mg]$_2$ at 60 ˚C to give magnesium bromide [(^{Mes}NacNac)MgBr]$_2$ (**3.19**) as a by-product, identified by X-ray crystallography. The formation of **3.19** suggests that [(^{Mes}NacNac)Mg]$_2$ has indeed reduced the aluminium centre of aluminium dibromide **3.18**. However, the aluminium-containing product was not identified. Alkali metal reducing agents, such as K(mirror), KC_8, Na(mirror), Na/NaCl (5% wt. Na), were used to reduce aluminium dibromide **3.18**, but all resulted in no reaction. Moreover, aluminium dibromide **3.18** was reacted with soluble reducing agent K[$C_{10}H_8$] which led to the formation of a new NCN-containing product, observed by ^{1}H NMR. From the reaction mixture the product was not isolated, thus its identity remains unknown. The reaction of aluminium dibromide **3.18** with sodium/potassium alloy (NaK) resulted in the formation of dimer [(NCO)AlBr]$_2$ (**3.20**). A speculative mechanism has been proposed for the formation of dimer **3.20** in which C–H activation of the NCN-ligand leads to the activation of THF, followed by intramolecular rearrangement and dimerisation.

Although aluminium dibromide **3.18** showed reactivity towards a small number of reducing agents, the aim of producing an NCN-supported aluminium(I) species was not realised.

3.6 References

(1) Cowley, A. H.; Gabbaie, F. P.; Atwood, D. A.; Carrano, C. J.; Mokry, L. M.; Bond, M. R., *J. Am. Chem. Soc.*, **1994**, *116*, 1559–1560.

(2) Liu, Z.; Gao, W.; Zhang, J.; Cui, D.; Wu, Q.; Mu, Y., *Organometallics*, **2010**, *29*, 5783–5790.

(3) Liu, Z.; Ganguly, R.; Vidović, D., *Dalton Trans.*, **2017**, *46*, 753–759.

(4) Das, T. K.; Biju, A. T., *Chem. Commun.*, **2020**, *56*, 8537–8552.

(5) Contreras, L.; Cowley, A. H.; Gabbaï, F. P.; Jones, R. A.; Carrano, C. J.; Bond, M. R., *J. Organomet. Chem.*, **1995**, *489*, C1–C3.

(6) Stender, M.; Segerer, U.; Sieler, J.; Hey-Hawkins, E., *Z. Anorg. Allg. Chem.*, **1998**, *624*, 85–90.

(7) Wehmschulte, R. J.; Power, P. P., *Inorg. Chem.*, **1994**, *33*, 5611–5612.

(8) Wehmschulte, R. J.; Grigsby, W. J.; Schiemenz, B.; Bartlett, R. A.; Power, P. P., *Inorg. Chem.*, **1996**, *35*, 6694–6702.

(9) Vogel, U.; Timoshkin, A. Y.; Scheer, M., *Angew. Chem. Int. Ed.*, **2001**, *40*, 4409–4412.

(10) Cui, C.; Roesky, H. W.; Schmidt, H.-G.; Noltemeyer, M.; Hao, H.; Cimpoesu, F., *Angew. Chem. Int. Ed.* **2000**, *39*, 4274–4276.

(11) Hofmann, A.; Tröster, T.; Kupfer, T.; Braunschweig, H., *Chem. Sci.*, **2019**, *10*, 3421–3428.

(12) Hicks, J.; Vasko, P.; Goicoechea, J. M.; Aldridge, S., *Nature*, **2018**, *557*, 92–95.

(13) Falconer, R. L.; Byrne, K. M.; Nichol, G. S.; Krämer, T.; Cowley, M. J., *Angew. Chem. Int. Ed.*, **2021**, *60*, 24702–24708.

(14) Caise, A.; Crumpton, A. E.; Vasko, P.; Hicks, J.; McManus, C.; Rees, N. H.; Aldridge, S., *Angew. Chem.* **2022**, *134*, e202114926.

(15) Li, X.-W.; Su, J.; Robinson, G. H., *Chem. Commun.*, **1998**, 12, 1281–1282.

(16) Falconer, R. L.; Nichol, G. S.; Smolyar, I. V.; Cockroft, S. L.; Cowley, M. J., *Angew. Chem. Int. Ed.*, **2021**, *60*, 2047–2052.

(17) Jones, C., *Nat. Rev. Chem.*, **2017**, *1*, 1–9.

(18) Green, S. P.; Jones, C.; Stasch, A., *Science*, **2007**, 318, 1754–1757.

(19) Asay, M.; Inoue, S.; Driess, M., *Angew. Chem. Int. Ed.*, **2011**, *50*, 9589–9592.

(20) Bonyhady, S. J.; Jones, C.; Nembenna, S.; Stasch, A.; Edwards, A. J.; McIntyre, G. J., *Chem. Eur. J.*, **2010**, *16*, 938–955.

(21) Hicks, J.; Juckel, M.; Paparo, A.; Dange, D.; Jones, C., *Organometallics*, **2018**, *37*, 4810–4813.

(22) Stasch, A. *Angew. Chem. Int. Ed.*, **2014**, *53*, 10200–10203.

(23) Braunschweig, H.; Damme, A.; Dewhurst, R. D.; Vargas, A., *Nat. Chem.*, **2013**, *5*, 115–121.

(24) Dove, A. P.; Gibson, V. C.; Hormnirun, P.; Marshall, E. L.; Segal, J. A.; White, A. J. P.; Williams, D. J., *Dalton Trans.*, **2003**, 15, 3088–3097.

(25) MacNeil, C. S.; Johnson, K. R. D.; Hayes, P. G.; Boeré, R. T., *Acta Crystallogr. Sect. E Crystallogr. Commun.*, **2016**, *72*, 1754–1756.

(26) Kurumada, S.; Takamori, S.; Yamashita, M., *Nat. Chem.*, **2020**, *12*, 36–39.

(27) Braune, W.; Ma, H.; Spaniol, T. P.; Okuda, J., *Organometallics*, **2005**, *24*, 1953–1958.

(28) Asakura, M.; Ōki, M.; Toyota, S., *Organometallics*, **2000**, *19*, 206–208.

(29) Behrle, A. C.; Schmidt, J. A. R., *Organometallics*, **2011**, *30*, 3915–3918.

Chapter 4

Diphosphide Ligands for Aluminium

4.1 Introduction

Aluminyl anions, featuring a formally negatively charged aluminium(I) centre, have gained increasing interest in the past 5 years due to their strong reducing properties and use as novel ligand systems.[1] Isoelectronic with carbenes, this class of compounds has ambiphilic potential with frontier orbitals typically involving an aluminium centred lone-pair of electrons (HOMO) and an orthogonal vacant p-type orbital (LUMO).[2,3] Analogous to N-heterocyclic carbenes (NHCs),[4] the first examples of isolable aluminyl anions utilised the secondary π-donator properties of bulky dianionic diamide scaffolds to stabilise the highly reactive aluminium centre. Efforts to increase the nucleophilicity of these species and reduce the stabilising properties of the ligand systems have involved substitution of one or both nitrogen donors with weaker π-donor substituents; this has been limited to the incorporation of carbon-based ligands that form one or two Al–C bonds.[5,6]

4.1.1 Diamide Ligand-Supported Aluminyl Anions

To date, there are only four examples of diamide-supported aluminyl anions, in which the ligand is bonded to aluminium through two Al–N covalent bonds (figure 4.1). The first reported aluminyl complex, $[K\{(NON)Al\}]_2$ (**1.92**), features a dimethylxanthene-derived diamide ligand coordinated to the aluminium in a tridentate fashion through two covalent Al–N bonds and a dative O→Al bond.[7] Calculations were used to show that donation from oxygen to aluminium is vital for the stabilisation of the aluminyl anion, with population of the orthogonal p-type orbital at aluminium leading to a large HOMO-LUMO gap. However, the reported examples that followed showed that a secondary neutral donor interaction with the aluminium is not necessary to form a stable aluminyl anion, with the use of bidentate diamide ligands providing sufficient stabilisation to access isolable aluminyl anions. Chelating diamide ligands linked through siloxane and 1,2-disilylethane bridges were demonstrated to provide access to the related two-coordinate aluminyl species **1.95** and **1.96**, respectively.[2,3] More recently, an aluminyl species, **1.97**, featuring an unsaturated carbon chain backbone derived from ^{Dipp}NacNac was isolated.[8] In all cases, these complexes utilise sterically demanding nitrogen substituents (e.g. Dipp or Mes) to protect the highly reactive aluminium centre.

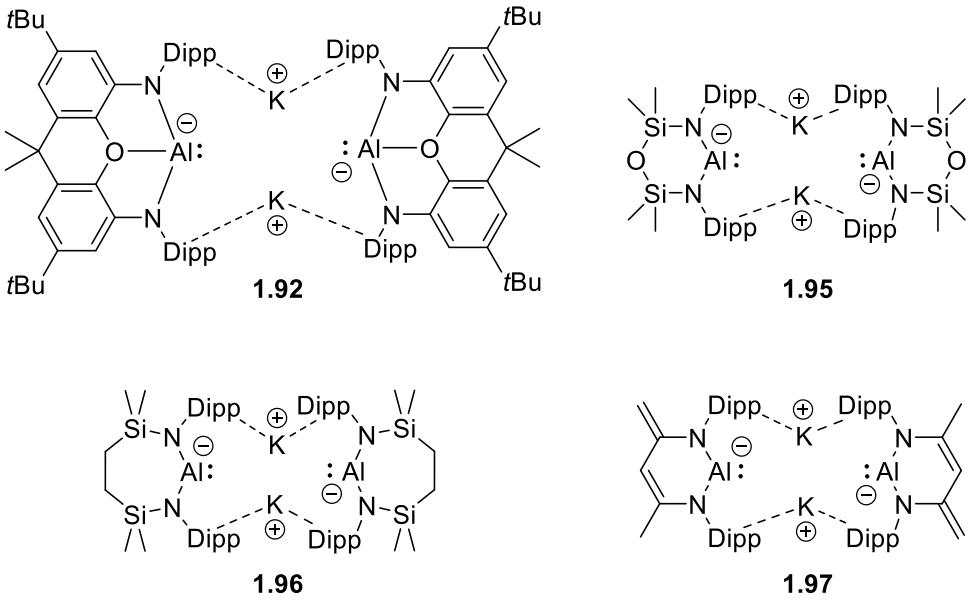

Figure 4.1 The reported diamide-supported aluminyl anions.

The balancing cation (typically a group 1 metal: Li, Na, K) has been shown to play a role in the structural features of these complexes and subsequently their reactivity. In all cases, the diamide aluminyl complexes **1.92**, **1.95** to **1.97** adopt a dimer structure in the solid-state linked through cation-π interactions between the group 1 metal cation and the flanking aryl substituents, a feature that is also retained in the solution-state. The dimeric structure is proposed to provide both kinetic and thermodynamic stabilising properties to the highly reactive aluminium(I) centre and there is considerable interest in altering the stabilising effect. Interchanging between group 1 metals is demonstrated to have a significant impact on the nature of the cation-π interactions (e.g. ring slipping) resulting in differing associations and relative arrangements of the individual aluminium centres and interactions with the cations.[9] Indeed, further partial and complete sequestration of the cation from the aluminyl anion allows isolation of the monomeric species, which have demonstrated reactivity pathways distinct from their dimeric forms.[10,11]

Synthetic pathways to aluminium(I) species typically involve the reduction of an aluminium(III) halide precursor using a group 1 metal reducing agent. Access to **1.92** was first achieved through reduction of the corresponding aluminium(III) iodide species (NON)AlI (**1.91**) using excess potassium graphite (KC_8). In a similar manner, **1.95** and **1.96** were

prepared in good yields by reduction of the aluminium(III) iodide species {OSiN}AlI, (OSiN = O{SiMe$_2$N(Dipp)}$_2$), and {SiN^{Dipp}}AlI (**4.3**), (SiN^{Dipp} = {CH$_2$SiMe$_2$N(Dipp)}$_2$), over a potassium mirror in hexane. Access to the aluminium(III) iodide pre-cursors may be achieved through either a double salt-elimination reaction between metalated ligand systems, or deprotonation reaction with trimethylaluminium (AlMe$_3$), followed by substitution of the methyl ligand with an iodide (scheme 4.1). In contrast, **1.97** was synthesised by C–H deprotonation of the ligand backbone in the reported aluminium(I) species (^{Dipp}NacNac)Al (**1.33**) using bulky potassium amide or alkyl bases, KHMDS or K(CH{SiMe$_3$}$_2$), respectively.

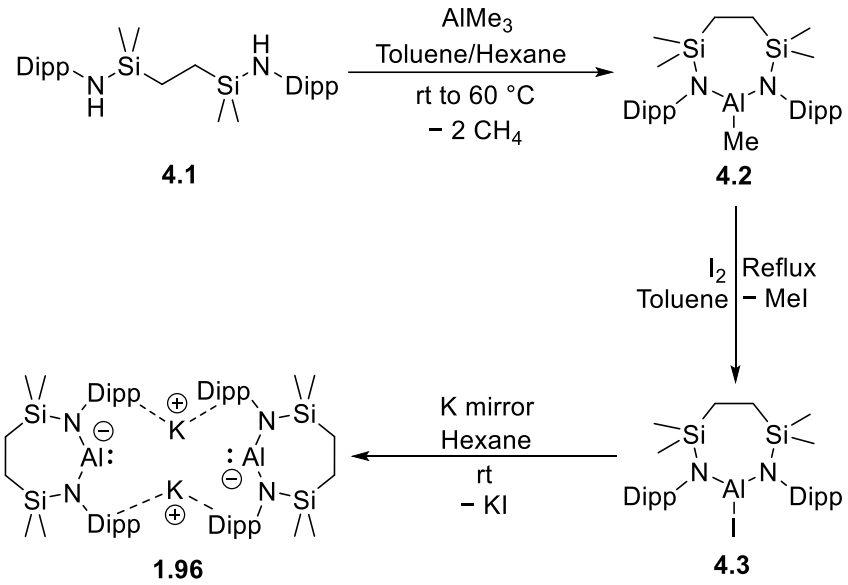

Scheme 4.1 The synthesis of aluminyl anion [K{SiN^{Dipp}}Al]$_2$ (**1.96**).

4.1.2 Diamide vs. Diphosphide Ligands

Nitrogen-based supporting scaffolds have allowed the synthesis and isolation of many otherwise inaccessible or unstable compound classes.[12] Among the most notable of these is the N-heterocyclic carbenes which utilise favourable secondary π-stabilisation provided by the adjacent nitrogen centres (figure 4.2).[13] Diamide ligands, featuring two anionic nitrogen centres linked through a connecting backbone, have been shown to provide similar stabilising properties to metal centres, allowing the isolation of unusual low coordinate and low oxidation state metal complexes.[8,11,14]

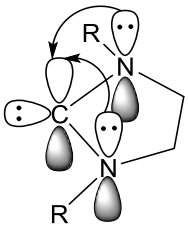

Figure 4.2 General representation of π-donation of the lone pair of electrons at nitrogen to the p-type orbital at a carbene centre of an N-heterocyclic carbene (NHC).

Despite the popularity of diamide ligands, the analogous diphosphide ligands have not received as much attention. Although belonging to the pnictogens and being directly below nitrogen in the periodic table, phosphorus ligands display markedly different ligating and stabilising properties. These can be attributed to differences in the fundamental properties between nitrogen and phosphorus:

i) Size: The atomic radius of nitrogen (1.55 Å) is significantly smaller than the atomic radius of phosphorus (1.80 Å). The relative size (or radial extension) of a ligated atom has a significant influence on the metric parameters within a ligated metal complex. For example, the M–P bond is expected to be significantly longer than an analogous M–N bond (e.g. sum of covalent radii – Al–P: 2.28 Å, Al–N: 1.92 Å). In the case of chelating diphosphide ligands, this would give rise to a decreased bite angle of the ligand. In addition, increased removal of the ligating atoms from the coordination sphere of the metal can result in a decreased steric effect imposed by flanking substituents on the N and P.

ii) Electronegativity: The Pauling electronegativity of nitrogen (3.04) is significantly larger than phosphorus (2.19). This results in greater polarisation of covalent bonding interactions between nitrogen and electropositive metal centres compared to phosphorus. In addition, the polarity of N–H bonds is significantly increased over P–H bonds resulting in greater acidity for amines. The relative polarity of M–P/M–N bonds and P–H/N–H bonds plays a vital role in establishing the highly polarised four-membered transition states required for σ-bond metathesis reactivity (e.g. protonolysis).

iii) Hybridisation and Orbital Overlap: Hybridisation theory is a powerful qualitative tool for better understanding the behaviour of the p-block elements. The frontier atomic orbitals of nitrogen and phosphorus are comprised of 2s/p and 3s/p orbitals, respectively. The first-row elements, including nitrogen, are distinct from their heavier congeners in that the 2s and 2p orbitals occupy similar spatial positions.[15] As the periodic table is descended, the valence np orbitals become more diffuse and the spatial overlap with the valence s-orbitals decreases considerably, due in part to Pauli repulsion between the valence p-orbitals and the core p-orbitals.[15] For example, the valence p-orbitals of phosphorus extend almost 30% further from the nucleus compared to the 3s orbital. In contrast, the 2p orbitals of nitrogen extend only 10% further than the corresponding 2s orbital.[15] This has several implications for s-p orbital hybridisation with respect to nitrogen and phosphorus: 1) The enhanced orbital overlap gained by forming hybrid orbitals is enhanced in nitrogen, which would otherwise be hindered by poor radial extension of the valence p-orbitals, 2) The introduction of p-character into the lone-pair on nitrogen reduces electron repulsion between bonding orbitals and the lone-pair, and 3) wider bonding angles in sp^3-hybridised orbitals reduce electron repulsion between bonding orbitals. As a result, s-p hybridisation at nitrogen is very effective for bond formation and it is often energetically unfavourable to form hybridised orbitals at phosphorus.[15]

iv) Geometry: As discussed above, the tendency towards s-p hybridisation at nitrogen can result in considerable differences in geometry between nitrogen and phosphorus centres. For example, ammonia (NH_3) adopts a trigonal pyramidal geometry with the H–N–H angles of approximately 104° increments about the central nitrogen, close to the idealise sp^3-hybrid orbital geometry of 109°. Phosphine (PH_3) also adopts a pyramidal geometry. However, the H–P–H angles of 94° are significantly more acute, more closely resembling the angles for pure p-orbitals (90°). In addition to having greater pyramidalization, the barrier to inversion processes at phosphorus is greatly increased.[16]

v) Hyperconjugation: Nitrogen-silicon hyperconjugation occurs through the donation of the lone pair of electrons at nitrogen into the antibonding orbital of the neighbouring Si-R bond, causing a stabilising effect. The ability for phosphorus to partake in such hyperconjugation may be diminished in comparison. This is due to a lack of energetic benefit associated with hybridisation of the orbitals of phosphorus compared to nitrogen, resulting

in a lone pair of electrons with greater s-character which have little directionality and have reduced opportunity for overlap with the adjacent Si-R antibonding orbital.[17] Therefore, phosphorus-silicon hyperconjugation is less likely to occur.

Overall, these fundamental differences are expected to result in significantly different ligating properties for diamide and diphosphide ligands.

4.2 Aims and Outlooks

The aims of this project are:

- To synthesise novel diphosphines with bulky phosphorus substituents linked through a disilylethane bridge, and their diphosphide counterparts.
- To investigate the reactivity of the diphosphines towards alkyl aluminium species.
- To synthesise a diphosphide- supported aluminium halide species and probe its reactivity towards reducing agents.
- To synthesise aluminium hydride species supported by diphosphide ligands.

4.3 Synthesis of Novel Diphosphines

4.3.1 Synthesis and Characterisation of Diphosphine {SiP^{Tipp}}H$_2$ (4.4)

Diphosphine {SiP^{Tipp}}H$_2$ (**4.4**), ({SiP^{Tipp}}H$_2$ = (TippP(H)SiMe$_2$CH$_2$)$_2$, Tipp = 2,4,6-tri*iso*propylphenyl), was synthesised through an initial lithiation of the primary phosphine TippPH$_2$ with nBuLi in hexane to give the mono-lithiate TippPHLi as a yellow solid in a 88% yield. TippPHLi was then reacted with 1,2-bis(chlorodimethylsilyl)ethane, (ClSiMe$_2$CH$_2$)$_2$, in Et$_2$O at −78 ˚C and allowed to warm to room temperature. Diphosphine **4.4** was isolated as a colourless solid in an 85% yield after workup (scheme 4.2).

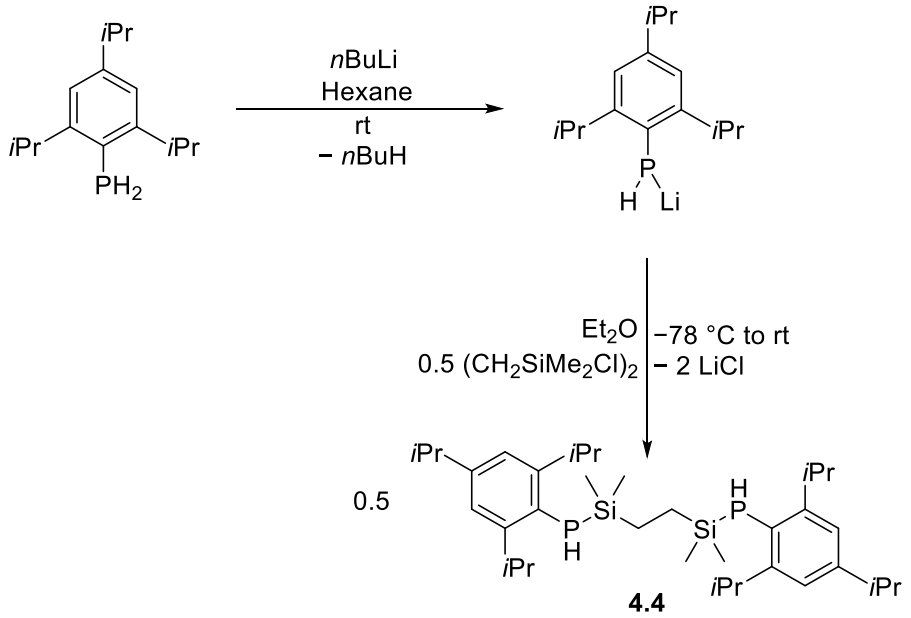

Scheme 4.2 The synthesis of lithium phosphide TippPHLi and subsequent reaction with $(ClSiMe_2CH_2)_2$ to give diphosphine $\{SiP^{Tipp}\}H_2$ (**4.4**).

The ^{1}H NMR spectrum of diphosphine **4.4** in C_6D_6 contains two overlapping doublet resonances from 0.12 – 0.15 ppm and a singlet resonance at 0.69 ppm which correlate to the Si*Me*$_2$ and Si*CH*$_2$ protons, respectively. A doublet resonance at 1.22 ppm corresponds to the methyl groups of the para-*iso*-propyl fragments, whilst the methyl groups of the ortho-*iso*-propyl moieties resonate at 1.27 ppm and 1.36 ppm. The septet resonances at 2.78 ppm and 3.62 ppm relate to the methine environment of the para-*iso*-propyl and ortho-*iso*-propyl groups respectively. A doublet resonance at 3.64 ppm ($^1J_{H–P}$ = 207 Hz) correlates to the P*H* protons, with the ^{31}P coupling confirmed by ^{1}H{^{31}P} spectroscopy showing a singlet at 3.64 ppm. The P*H* shift and coupling constant ($^1J_{H–P}$) are comparable to reported secondary aryl silylphosphines, such as DippP(H)SiMe$_3$ (3.46 ppm, $^1J_{H–P}$ = 211 Hz).[18] The doublet signal at 7.12 ppm is assigned to the C_6H_2 protons of the aryl ring, revealing weak coupling between the phosphorus and C_6H_2 protons.

The resonance observed at 0.12 – 0.15 ppm in the ^{1}H NMR spectrum may be explained by inequivalent Si*Me*$_2$ protons resulting in two overlapping doublets due to three-bond coupling with a ^{31}P nucleus ($^3J_{H–P}$ = 3.6 Hz). The inequivalence of these protons may be a consequence of restricted rotation around the P–Si bond. Variable temperature ^{1}H NMR spectroscopy reveals that, at 333 K, the methyl groups become magnetically equivalent

resonating as a single doublet ($^3J_{H-P}$ = 3.6 Hz, figure 4.3). The $^1H\{^{31}P\}$ NMR spectrum confirms the P–H coupling as the Si*Me*$_2$ resonates as a singlet at 0.13 ppm at 333 K.

The $^{31}P\{^1H\}$ NMR spectrum of diphosphine **4.4** consists of a singlet resonance at −169.7 ppm which corresponds to the phosphorus centres (figure 4.3). In the ^{31}P NMR spectrum, the phosphorus environment resonates as a doublet, revealing the strong P–H coupling with a $^1J_{H-P}$ of 208 Hz. The ^{29}Si NMR spectrum of **4.4** has a doublet resonance at 6.0 ppm ($^1J_{P-Si}$ = 25.7 Hz) consistent with single bond coupling between ^{29}Si and ^{31}P and the presence of P–Si bonds.

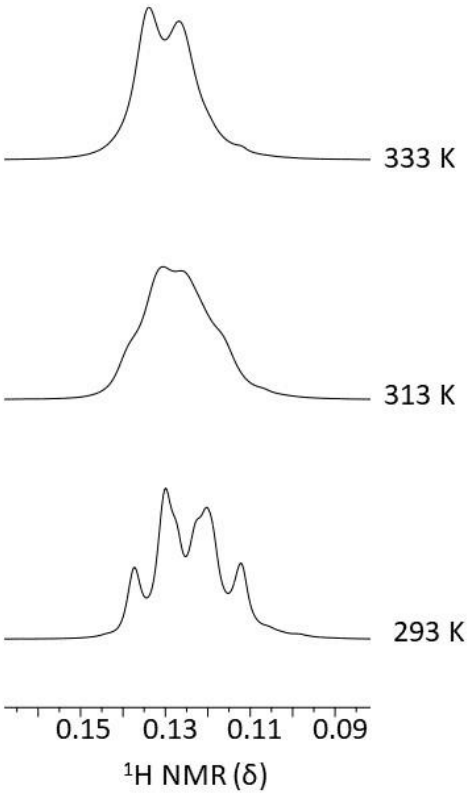

Figure 4.3 The variable temperature ^1H NMR spectrum of $\{SiP^{Tipp}\}H_2$ (**4.4**), showing the resonance of the Si*Me*$_2$ environments at 293K, 313 K and 333 K.

4.3.2 Synthesis and Characterisation of Diphosphine $\{SiP^{Mes*}\}H_2$ (4.5)

Diphosphine $\{SiP^{Mes*}\}H_2$ (**4.5**), ($\{SiP^{Mes*}\}H_2$ = $(Mes^*P(H)SiMe_2CH_2)_2$, Mes* = 2,4,6-tri-*tert*-butylphenyl), was synthesised through a similar method to that detailed for diphosphine

4.4 by initial lithiation of primary phosphine Mes*PH_2, followed by a double salt elimination reaction with $(ClSiMe_2CH_2)_2$ (scheme 4.3). A solution of primary phosphine Mes*PH_2 in Et_2O was treated with nBuLi at −78 ˚C and allowed to warm to room temperature to generate Mes*PHLi *in-situ*. A solution of $(ClSiMe_2CH_2)_2$ was added dropwise to the solution of Mes*PHLi at −78 ˚C and slowly warmed to room temperature to give the diphosphine {SiP^{Mes*}}H_2 (**4.5**) as a colourless solid in a yield of 64 % after workup.

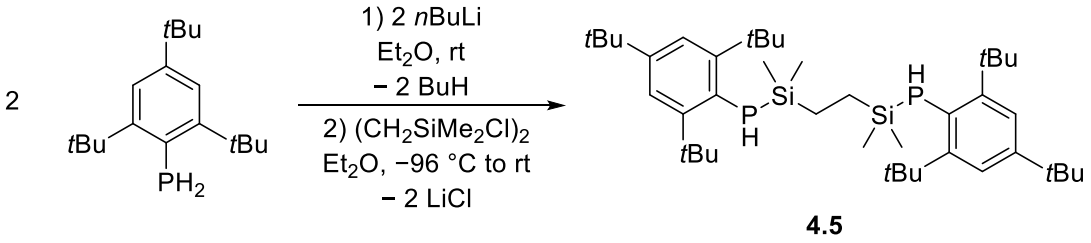

4.5

Scheme 4.3 The synthesis of {SiP^{Mes*}}H_2 (**4.5**).

The ^{1}H NMR spectrum of diphosphine **4.5** in C_7D_8 consists of four overlapping doublet resonances at −0.07 – 0.03 ppm and a multiplet resonance at 0.43 – 0.55 ppm corresponding to the Si*Me*$_2$ and SiC*H*$_2$ protons, respectively. The *tert*-butyl groups of the Mes*-substituents resonate as two singlets at 1.33 ppm (para-*t*Bu) and 1.63 ppm (ortho-*t*Bu) with relative integrations of 1 : 2. The doublet resonance at 4.34 ppm ($^1J_{H–P}$ = 214 Hz) corresponds to P*H* protons, shifted significantly downfield compared to the analogous resonance in **4.4**. The aryl-C$_6$*H*$_2$ protons appear as a doublet at 7.43 ppm ($^4J_{H–P}$ = 2.3 Hz).

The ^{31}P{^{1}H} NMR spectrum of diphosphine **4.5** shows two singlet resonances at −132.9 and −133.0 ppm. The ^{31}P NMR spectrum reveals the coupling between the phosphorus and hydrogen centres with two overlapping doublet resonances at −132.9 ppm ($^1J_{H–P}$ = 213 Hz) and −132.0 ppm ($^1J_{H–P}$ = 214 Hz). The ^{29}Si NMR spectrum consists of a doublet resonance at 11.0 ppm ($^1J_{P–Si}$ = 25.3 Hz), which supports the presence of P–Si bonds within **4.5**.

The presence of two resonances in the ^{31}P{^{1}H} NMR spectrum is a result of the stereoisomers of diphosphine **4.5**, which possesses phosphorus stereocentres that have pyramidal geometries with inversion barriers that are too high in energy to overcome on the NMR timescale at room temperature (figure 4.4). Therefore, the diastereomers of **4.5**, RR or

SS and meso (RS and SR isomers are achiral, thus are considered to be the same isomer described as meso), can be observed by NMR spectroscopy. It is worth noting, that in contrast to diphosphine **4.5**, the stereoisomers of the disphosphine **4.4** are not distinguishable by ^{31}P NMR spectroscopy, suggesting that size of the P-substituent is a key-factor in these observations. Furthermore, in the ^{1}H NMR spectrum, the $SiCH_2$ and $SiMe_2$ groups of **4.5** are both observed to be inequivalent. Unlike the $SiMe_2$ groups of diphosphine **4.4**, which resonate as two overlapping doublets, within **4.5**, four overlapping doublets are observed for the $SiMe_2$ groups. This is due to lack of inversion of the pyramidal phosphorus centres on the NMR timescale, as well as restricted rotation around the P–Si bond.

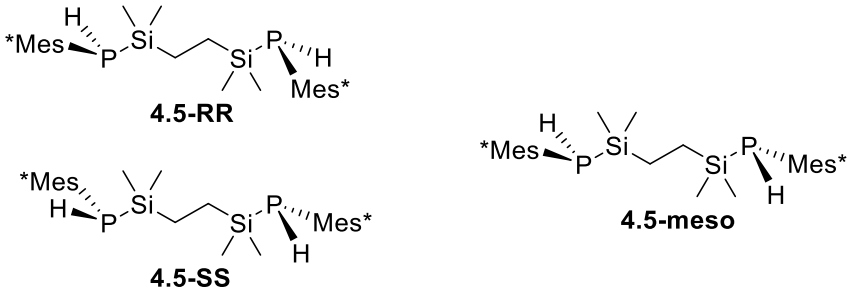

Figure 4.4 The possible diastereomers of diphosphine $\{SiP^{Mes*}\}H_2$ (**4.5**).

Variable temperature ^{31}P and $^{31}P\{^{1}H\}$ NMR spectroscopy shows that upon heating a solution of diphosphine **4.5** from 293 K to 333 K, the diastereomers exchange rapidly on the NMR timescale. At 333 K, the $^{31}P\{^{1}H\}$ shows the resonances for the diastereomers of **4.5** coalesce, forming a singlet at −132.0 ppm (figure 4.5). Similarly, the ^{31}P NMR spectrum consists of a single resonance, a doublet, at −132.0 ppm ($^{1}J_{H–P}$ = 214 Hz).

The ^{1}H NMR spectrum reveals that, at 333 K, the $SiCH_2$ environments resonates as a broad singlet. The $SiMe_2$ groups are observed as a doublet ($^{3}J_{H–P}$ = 3.0 Hz) and as a singlet in the $^{1}H\{^{31}P\}$ NMR (figure 4.6). This suggests that, at 333 K, inversion at the phosphorus stereocentres is occurring in diphosphine **4.5**, observed by ^{31}P NMR spectroscopy, along with free rotation around the Si–P bond, observed by ^{1}H NMR spectroscopy.

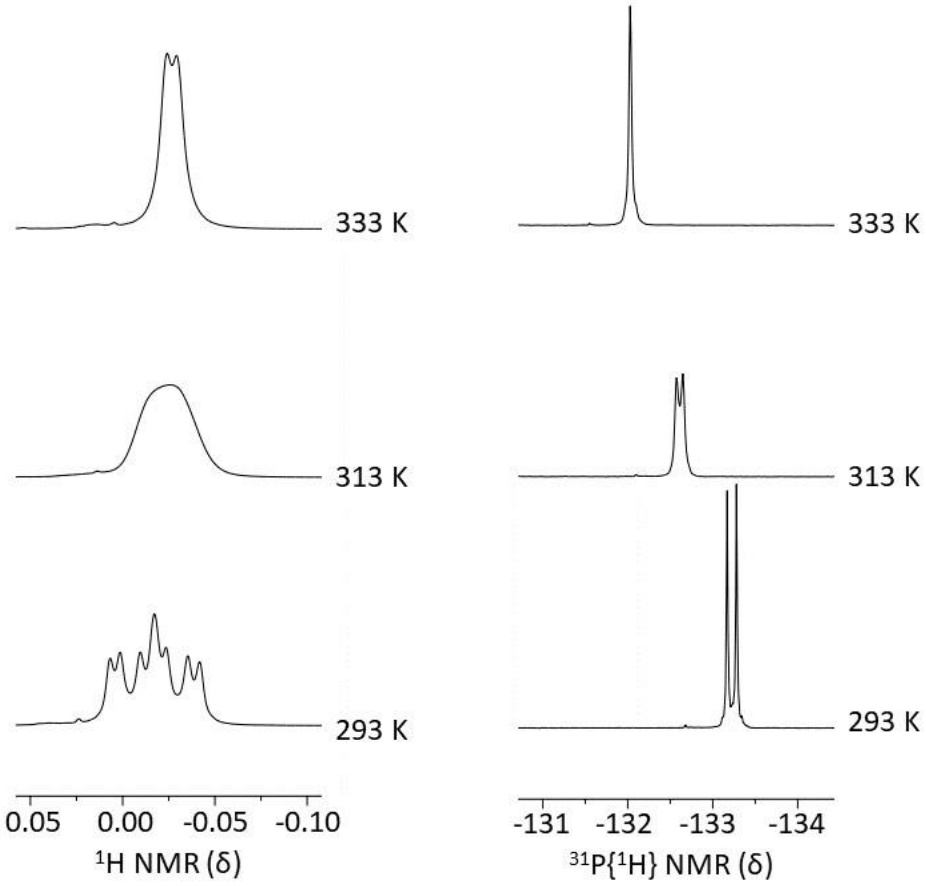

Figure 4.5 The variable temperature ^{1}H and ^{31}P{^{1}H} NMR spectra of **4.5**, showing the coalescence of resonances for the Si*Me*$_2$ environments and the phosphorus environments of diastereomers of **4.5**, respectively, upon increasing the temperature from 293 K to 333 K.

Single crystals of **4.5** suitable for analysis by single crystal X-ray diffraction were grown from a saturated C_6D_6 solution and were used to determine the solid-state structure of **4.5** (figure 4.6). The solid-state structure of **4.5** confirms formation of the diphosphine, crystallising in the $P2_1/c$ space group with two essentially identical half molecules within the asymmetric unit related to their symmetry equivalent through an inversion centre. Only one of the molecular units will be discussed. The phosphorus centres have a trigonal pyramidal geometry with a C4–P1–Si1 angle of 101.62(6)˚. The P1–Si1 distance of 2.2889(7) Å lies within the range of typical P–Si single bond lengths.[19,20] The H atom bonded to P1 was disordered over two sites, consistent with peaks in the difference map. The solid-state structure, shown in figure 4.6, reveals that the stereoisomer **4.5-meso** (figure 4.4) had crystallised, which is achiral and centrosymmetric, consistent with the X-ray diffraction data.

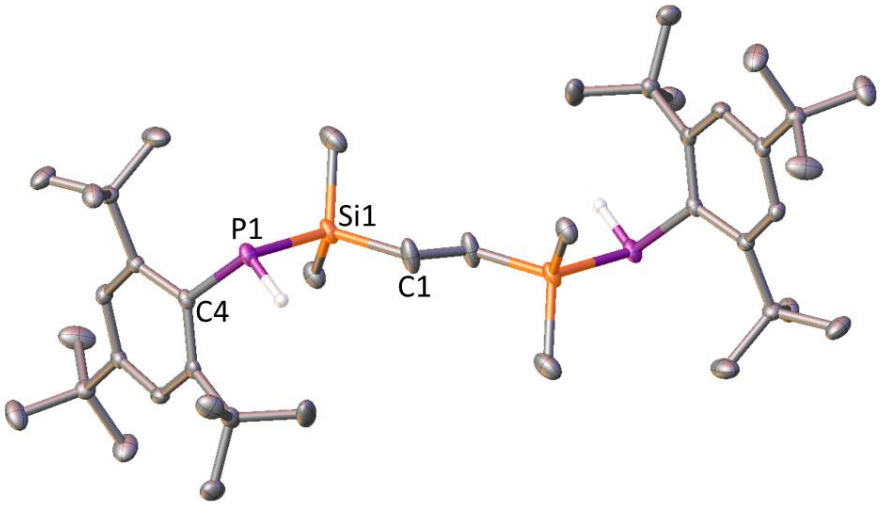

Figure 4.6 The solid-state structure of {SiP^{Mes*}}H_2 (**4.5-meso**). H atoms, except PH, are omitted are omitted for clarity. Thermal ellipsoids are set to 50% probability. Select bond lengths (Å) and angles (˚): P1–Si1 2.2889(7), P1–C4 1.8589(18), Si1–C1 1.883(2), C4–P1–Si1 101.62(6), P1–Si1–C1 106.49(7).

4.4 Synthesis of Alane-Phosphine Adducts

To explore whether deprotonation of the diphosphine pre-ligands and direct metalation by aluminium can be achieved from organoaluminium species, the reaction of the diphosphines with simple commercially available organoaluminium reagents $AlMe_2Cl$ and $AlMe_3$ was attempted.

4.4.1 Synthesis and Characterisation of {SiP^{Tipp}}H_2•$(AlMe_2Cl)_2$ (4.7)

The reaction of diphosphine **4.4** with $AlMe_2Cl$ was carried out in an attempt to deprotonate the diphosphine P−H protons and generate the diphosphidoaluminium chloride species {SiP^{Tipp}}AlCl (**4.6**) (SiP^{Tipp} = $(TippPSiMe_2CH_2)_2$), in a similar manner to that observed for

diamine **4.1** and $AlMe_3$ to give **4.2** (scheme 4.1). Initial investigation of this pathway was probed through the addition of two equivalents of $AlMe_2Cl$ to a toluene solution of diphosphine **4.4** at room temperature. However, deprotonation of the diphosphine ligand was not observed, instead the bis-dimethylaluminium chloride-phosphine adduct, $\{SiP^{Tipp}\}H_2 \bullet (AlMe_2Cl)_2$ (**4.7**), is formed. Adduct **4.7** was isolated as a colourless solid in a yield of 81% (scheme 4.4).

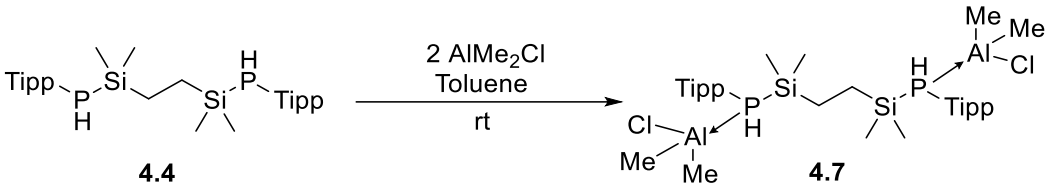

4.4 **4.7**

Scheme 4.4 The synthesis of $\{SiP^{Tipp}\} \bullet (AlMe_2Cl)_2$ (**4.7**) through the reaction of $\{SiP^{Tipp}\}H_2$ (**4.4**) with $AlMe_2Cl$.

The ^1H NMR spectrum of adduct **4.7** consists of a singlet resonance at −0.11 ppm corresponding to the Al*Me* protons, a downfield shift compared to free $AlMe_2Cl$ (−0.27 ppm).[21] The relative integration shows 12 protons for each diphosphine ligand, which is consistent with two $AlMe_2Cl$ fragments per disphosphine. A multiplet between 0.14 ppm and 0.28 ppm is assigned to inequivalent Si*Me*$_2$ protons. In contrast, a broad singlet resonance at 0.87 ppm corresponds to the SiC*H*$_2$ protons. The doublet resonance at 1.12 ppm corresponds to the para-CH(C*H*$_3$)$_2$ groups, while the multiplet resonances at 1.20 ppm and 1.30 ppm correlate to the ortho-CH(C*H*$_3$)$_2$ groups of the aryl P-substituents. The multiplet resonances at 2.68 ppm and 3.27 ppm correspond to the para- and ortho-C*H*$(CH_3)_2$ environments, respectively. Two overlapping doublet resonances at 4.52 ppm and 4.56 ppm correspond to the P–H environments and suggest two diastereomers may be present in solution, analogous to that discussed for **4.5**. A doublet at 7.07 ppm correlates to the C$_6$*H*$_2$ protons of the Tipp fragments.

The $^{31}P\{^1H\}$ NMR spectrum of adduct **4.7** consists of a singlet at −142.0 ppm, shifted significantly downfield compared to the free diphosphine ligand **4.4** (−169.7 ppm). In the ^{31}P

NMR spectrum, the phosphorus environment of **4.7** resonates as a doublet with a coupling constant ($^1J_{H-P}$) of 280 Hz.

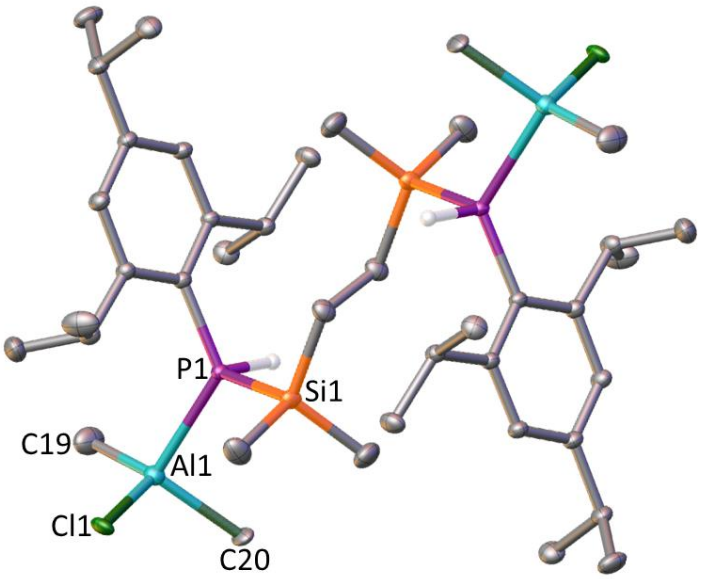

Figure 4.7 The solid-state structure of {SiP^{Tipp}}H$_2$•(AlMe$_2$Cl)$_2$ (**4.7**). H atoms, except PH, are omitted for clarity. Thermal ellipsoids set to 50% probability. Select bond lengths (Å) and angles (˚): Al1–C19 2.0698(7), Al1–P1 2.4725(5), C19–Al1–P1 99.01(2).

Single crystals of **4.7** suitable for analysis by single crystal X-ray diffraction were grown from a concentrated toluene solution and were used to determine the solid-state structure of **4.7**. The solid-state structure of **4.7** confirms the formation of a diphosphine bridged bis(chlorodimethylaluminium) adduct (figure 4.7). The asymmetric unit contains one half molecule, for which the bond lengths and angles will be discussed, with the other half consisting of symmetry equivalent atoms. The aluminium centre is four-coordinate with a distorted tetrahedral geometry.[22] The Al–C distance, 2.0698(7) Å (Al1–C19), is comparable to reported Al–C bond lengths (range = 1.9 – 2.1 Å).[23,24] It is worth noting that disorder of the chloride (Cl1) and methyl (C20) positions decrease the accuracy of the bond lengths and angles around aluminium, thus precluding their discussion. The Al1–P1 distance is 2.4725(5) Å which lies within the typical range for P→Al dative bond lengths (2.4 – 2.8 Å).[25,26] The bond angles around phosphorus are in the range of 108.97(3)˚ to 124.74(3)˚, suggesting

phosphorus to have a tetrahedral geometry. However, as the hydrogen centres at phosphorus were not located in the difference map.

4.4.2 Synthesis and Characterisation of {SiP^{Tipp}}H$_2$•AlMe$_3$ (4.8)

In a similar manner to the synthesis of **4.8**, the reaction between diphosphine **4.4** and one equivalent of $AlMe_3$ does not result in deprotonation of the diphosphine ligand. The dropwise addition of a solution of $AlMe_3$ in hexane to a solution of **4.4** at room temperature followed by the removal of the volatile components gave the trimethylaluminium-diphosphine adduct {SiP^{Tipp}}H$_2$•AlMe$_3$ as a colourless powder in a high yield (80%).

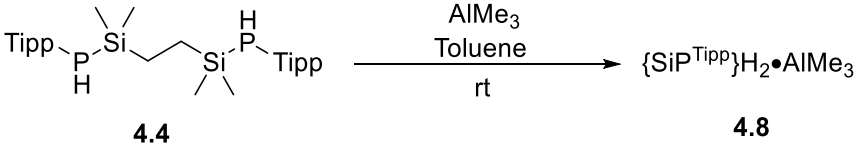

4.4 **4.8**

Scheme 4.5 The preparation of {SiP^{Tipp}}H$_2$•AlMe$_3$ (**4.8**).

The ^{1}H NMR spectrum for adduct **4.8** consists of a singlet resonance for the aluminium methyl fragments at −0.20 ppm, a downfield shift compared to free $AlMe_3$ (−0.37 ppm),[27] with an integration indicative of one $AlMe_3$ fragment per diphosphine unit. Two doublet resonances at 4.12 ppm and 4.13 ppm ($^1J_{H-P}$ = 253 Hz) confirm the P–H bonds of the diphosphine remain intact and suggests the presence of two diastereomers in solution. In comparison to uncoordinated diphosphine **4.4** (3.65 ppm, $^1J_{H-P}$ = 207 Hz), the P–H resonance of adduct **4.8** is shifted downfield, consistent with coordination to an electropositive centre. The signals for the diphosphine ligand show three doublet resonances at 1.16 ppm, 1.22 ppm and 1.34 ppm in a 1 : 1 : 1 ratio corresponding to the *p*-CH(C*H*$_3$)$_2$ and *o*-CH(C*H*$_3$)$_2$ protons, and indicating asymmetry in the *ortho*-substituents. In contrast, the C*H*(CH$_3$)$_2$ methine protons appear as a septet and multiplet at 2.71 ppm and 3.39 ppm, respectively. The aryl C–H of the Tipp substituents appear as a doublet at 7.09 ppm.

In the $^{31}P\{^{1}H\}$ NMR spectrum of adduct **4.8**, only a singlet resonance at −150.6 ppm is present, showing the phosphorus centres to be magnetically equivalent, and the resonance is shifted downfield compared to free diphosphine **4.4**. The ^{31}P NMR spectrum of **4.8** reveals the P–H coupling as the phosphorus centres resonate as a doublet with a coupling constant ($^{1}J_{H-P}$) of 252 Hz.

These data confirm coordination of the diphosphine to the aluminium centre through a donor-acceptor interaction. The symmetric nature of the ligand and the single phosphorus environments suggests either rapid interconversion of monodentate coordination through a single phosphorus centre to the aluminium, or bidentate coordination to give a 5-coordinate aluminium centre (figure 4.8). Attempts to crystallise **4.8** were unsuccessful, preventing analysis of the solid-state structure.

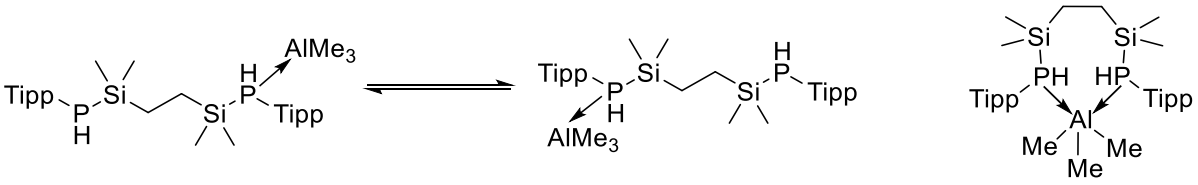

Figure 4.8 The possible coordination modes of $\{SiP^{Tipp}\}H_2 \bullet AlMe_3$ of either interconversion of monodentate coordination (left) or bidentate coordination (right).

4.4.3 Synthesis and Characterisation of $\{SiP^{Tipp}\}H_2 \bullet (AlMe_3)_2$ (4.9)

The reaction of **4.4** and two equivalents of $AlMe_3$ gave rise to the formation of bis(trimethylalane)-diphosphine adduct, $\{SiP^{Tipp}\}H_2 \bullet (AlMe_3)_2$ (**4.9**), which was isolated as a colourless solid in moderate yields (49%, scheme 4.6).

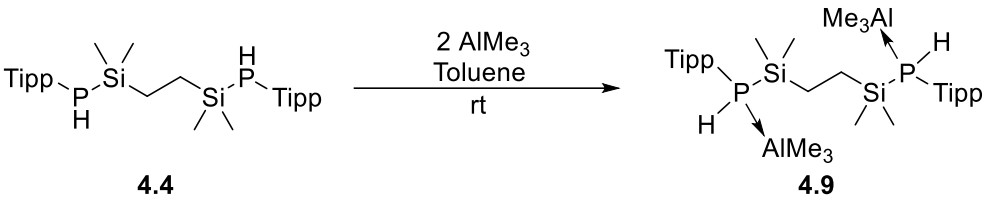

4.4 **4.9**

Scheme 4.6 The preparation of {SiP^{Tipp}}H$_2$•(AlMe$_3$)$_2$ (**4.9**).

The ^{1}H NMR spectrum of **4.9** is similar to **4.8**, suggesting a similar species is present in solution. The Al*Me* protons resonate as a singlet at −0.22 ppm, with relative integrals indicating 18 protons per equivalent of ligand, consistent with the formation of a bis(trimethylaluminium) adduct. The only other significant difference from the ^{1}H NMR spectrum of **4.8** is in the P*H* resonance, which appears at 4.26 and 4.27 ppm ($^1J_{H–P}$ = 266 Hz) for **4.9**, slightly downfield from that of **4.8**. The spectral similarities between **4.9** and **4.8** may be representative of similar interactions between the diphosphine ligand and aluminium centre. The ^{31}P NMR spectrum of **4.9** shows a doublet at −144.9 ppm, shifted slightly downfield from that of **4.8**.

Single crystals of **4.9** were isolated from a concentrated pentane solution at −27 °C and were analysed by single crystal X-ray diffraction. The solid-state structure identified the crystalline species as bis(trimethylaluminium)-phosphine adduct {SiP^{Tipp}}H$_2$•(AlMe$_3$)$_2$ (**4.9**) (figure 4.9). The aluminium centre is four-coordinate with C–Al–C angles of 113.41(6)˚, 115.65(7)˚, and 116.78(7)˚, and C–Al–P bond angles ranging from 97.02(4)˚ to 107.00(4)˚. The bond angles around aluminium of **4.9** are similar to those of dimethyl aluminium chloride adduct **4.7**. Thus, the aluminium centre of **4.9** also has a distorted tetrahedral geometry (τ_4 = 0.90, τ'_4 = 0.91). The Al–P bond distance of **4.9** is 2.5357(4) Å which is longer than that of **4.7**, indicating a weaker donor-acceptor interaction. This coincides with the expected reduction in Lewis acidity of the aluminium centre when a chloride ligand is replaced with an electron donating methyl ligand.

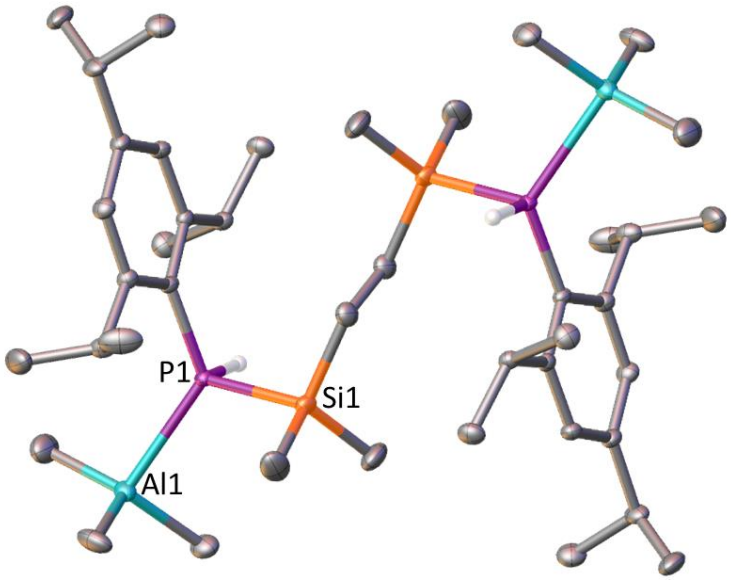

Figure 4.9 The solid-state structure of {SiP^{Tipp}}H$_2$•(AlMe$_3$)$_2$ (**4.9**). H atoms, except PH, are omitted for clarity. Thermal ellipsoids are set to 50% probability. Select bond lengths (Å) and angles (˚): Al1–C16 1.9627(15), Al1–C17 1.9739(14), Al1–C18 1.9832(13), Al1–P1 2.5357(4), C16–Al1–C17 116.78(7), C16–Al1–C18 115.65(7), C17–Al1–C18 113.41(6), C16–Al1–P1 103.97(5).

4.4.4 Synthesis and Characterisation of {SiP^{Mes*}}H$_2$•AlMe$_2$Cl (4.10)

The synthesis of the aluminium-phosphine adducts was extended to the Mes*-substituted diphosphine {SiP^{Mes*}}H$_2$ (**4.5**). One equivalent of AlMe$_2$Cl was added to a toluene solution of **4.5** at room temperature. After five hours, the volatiles were removed under vacuum to afford {SiP^{Mes*}}H$_2$•AlMe$_2$Cl (**4.10**) as a colourless solid (scheme 4.7).

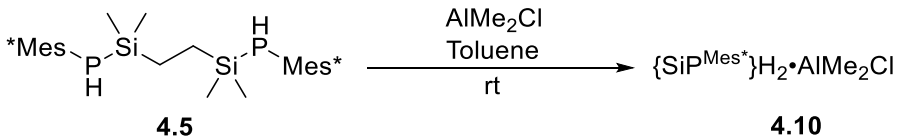

4.5 **4.10**

Scheme 4.7 The preparation of {SiP^{Mes*}}H$_2$•AlMe$_2$Cl (**4.10**) by the reaction of {SiP^{Mes*}}H$_2$ (**4.5**) and AlMe$_2$Cl.

The ^{1}H NMR spectrum of adduct **4.10** consists of a singlet resonance at −0.06 ppm for Al*Me*$_2$, a downfield shift compared to free $AlMe_2Cl$ (−0.27 ppm). The Al*Me*$_2$ resonance has an integral of six, suggesting that only one $AlMe_2Cl$ unit is present per disphosphine molecule. The doublet resonances at 0.02 and 0.03 ppm correspond to Si*Me*$_2$ protons, split by three bond coupling to the ^{31}P nucleus, while a multiplet at 0.53 ppm corresponds to the SiC*H*$_2$ protons. The doublet resonance at 4.67 ppm ($^{1}J_{H-P}$ = 240 Hz) indicates the P–H bonds remain intact. Resonances for the Mes* environments are also present at 1.31 ppm and 1.60 ppm for the para- and ortho-*t*Bu groups, respectively, and at 7.46 ppm which relates to the aryl-H environments.

The ^{31}P{^{1}H} NMR spectrum contains a singlet resonance at −125.5 ppm, which becomes broad in the ^{31}P NMR spectrum. The presence of only a single resonance suggests that both phosphorus centres are magnetically equivalent on an NMR timescale and may correspond to a time-averaged signal for the rapid exchange of dimethylchloroalane between each phosphorus centre, or bidentate coordination of the ligand to the aluminium, analogous to **4.9**.

Attempts to crystallise **4.10** were unsuccessful, preventing analysis of the molecular structure in the solid state. Crystals isolated from a concentrated toluene solution of the product were identified as the free diphosphine **4.5** by single crystal X-ray diffraction, suggesting the presence of an equilibrium between the adduct and free diphosphine/$AlMe_2Cl$.

4.4.5 Synthesis and Characterisation of {SiP^{Mes*}}H$_2$•AlMe$_3$ (4.11)

The trimethylaluminium adduct {SiP^{Mes*}}H$_2$•$AlMe_3$ (**4.11**) was prepared in a similar manner to adduct **4.8**. One equivalent of $AlMe_3$ in hexane was added to a toluene solution of diphosphine **4.5**. Upon complete consumption of starting material, the volatiles were removed under reduced pressure to afford adduct **4.11** as a colourless solid in 77% yield.

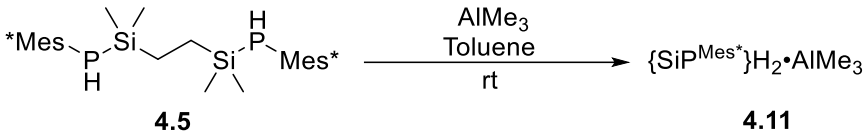

4.5 **4.11**

Scheme 4.8 The synthesis of {SiP^{Mes*}}H_2•$AlMe_3$ (**4.11**).

The ^{1}H NMR spectrum of adduct **4.11** resembles that of adduct **4.10**. The coordinated Al*Me*$_3$ resonates as a singlet at −0.16 ppm, with the relative integration showing 9 protons for each diphosphine ligand, suggesting coordination of the diphosphine to one $AlMe_3$ fragment. The doublet resonance at 4.66 ppm ($^1J_{H–P}$ = 230 Hz) confirms the retention of two P–H protons. The ligand backbone proton environments resonate as two doublets at 0.00 and 0.01 ppm for Si*Me*$_2$, and a multiplet at 0.53 ppm for the SiC*H*$_2$ protons, consistent with the presence of multiple diastereomers. The doublet splitting in the Si*Me*$_2$ protons arises due to three bond coupling with a ^{31}P nucleus, indicated by loss of the splitting in the ^{1}H{^{31}P} NMR spectrum. The resonances at 1.30 ppm (para-*t*Bu), 1.58 ppm (ortho-*t*Bu), and 7.46 ppm (Ar-*H*) correspond to the Mes* substituent. The ^{31}P{^{1}H} NMR spectrum of **4.11** consists of a singlet at −122.8 ppm, whilst the ^{31}P NMR spectrum shows a doublet resonance ($^1J_{H–P}$ = 230 Hz), further supporting that the P–H bonds are intact.

Analogous to dimethylchloroaluminium analogue **4.10**, attempts to crystallise **4.11** from a concentrated solution of toluene were unsuccessful. Instead, only crystals of the free diphosphine **4.5** were isolated, suggesting the presence of a similar equilibrium to that proposed for **4.10**, whereby the donor-acceptor interaction is fluxional resulting in a mixture of **4.11**, free trimethylaluminium and diphosphine **4.5** in solution.

4.4.6 Attempted Deprotonation Reactivity of Diphosphine-Alane Adducts

The deprotonation of the diphosphine ligands **4.4** and **4.5** using organoaluminium reagents $AlMe_2Cl$ and $AlMe_3$ does not occur spontaneously at room temperature. In addition, heating solutions of **4.7** - **4.11** in C_6D_6 does not result in methane elimination and formation of Al–P covalent bonds, with no reaction observed even after heating samples to 75 °C for 48

hours. This contrasts to the synthetic pathway used for the corresponding diamine system, {SiN^{Dipp}}H$_2$ (scheme 4.1). The lack of deprotonation may correspond to decreased polarity of the P–H bond, and subsequent reduction in the acidity compared to the N−H bonds of {SiN^{Dipp}}H$_2$. The lack of dipole moment in the P−H bond presents a significant challenge when considering the highly polarised transition state that would typically be required for protonolysis reactivity.[28] The potential for the phosphorus centres in **4.4** and **4.5** to behave as σ-donor ligands at aluminium has been demonstrated in this section. Coordination of a bulky Lewis base to the aluminium centre may also hinder the reactivity at the Al–C bonds, preventing the formation of the concerted four-centre transition states typically required for protonolysis.

4.5 Synthesis and Reactivity of {SiP^R}AlX (R = Tipp, Mes*; X = Cl, Br, I)

Following the reported preparation of diamide supported aluminyl anions (scheme 4.1), a synthetic pathway to [{SiP^R}Al]$^-$ species involving initial preparation of diphosphide supported aluminium(III) halides followed by reduction with a group 1 metal was devised. As discussed in section 4.4, a diphosphidoaluminium species was not accessible by direct deprotonation of diphosphines **4.4** and **4.5** using AlMe$_2$Cl or AlMe$_3$. Thus, the diphosphide aluminium halide synthesis was attempted through a double salt elimination route. Diphosphines {SiP^{Tipp}}H$_2$ (**4.4**) and {SiP^{Mes*}}H$_2$ (**4.5**) may be deprotonated at both phosphorus centres to give the analogous diphosphide using a suitable base, which can then be reacted with aluminium trihalides to access the desired aluminium halide precursors.

4.5.1 Synthesis of Diphosphide {SiP^{Tipp}}M$_2$ (M = Li, 4.12; K, 4.13)

The deprotonation of diphosphine **4.4** using two equivalents of nBuLi in Et$_2$O proceeds with the formation of a yellow solution. Removal of the solvent *in vacuo* gave the diphosphide species {SiP^{Tipp}}Li$_2$•(Et$_2$O)$_3$ (**4.12**) as a yellow solid after work-up in 61 % yield (scheme 4.9).

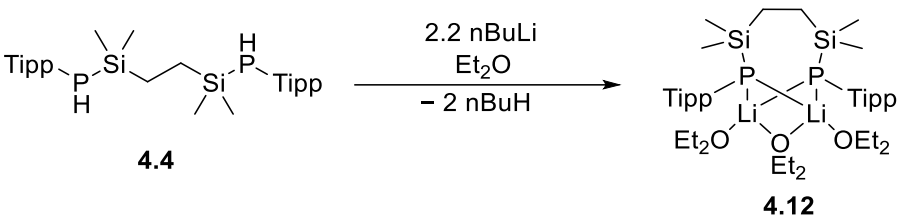

4.4 **4.12**

Scheme 4.9 The preparation of {SiP^{Tipp}}Li$_2$•(Et$_2$O)$_3$ (**4.12**) from the reaction of {SiP^{Tipp}}H$_2$ (**4.4**) with 2.2 equivalents of nBuLi.

The ^{1}H NMR spectrum of **4.12** shows a high field singlet at 0.36 ppm corresponding to the Si*Me$_2$* protons, while the SiC*H$_2$* protons appear as a triplet at 1.15 ppm. The *p*-CH(C*H$_3$*)$_2$ and *o*-CH(C*H$_3$*)$_2$ protons resonate as doublets at 1.31 and 1.40 ppm, while the corresponding methine resonances appear at 2.91 and 4.88 ppm, respectively. The C$_6$*H$_2$* protons of the Tipp substituent appear as a singlet at 7.24 ppm. Resonances corresponding to coordinated Et$_2$O molecules are also observed at 1.07 and 3.19 ppm, with relative integrals indicating three molecules per equivalent of ligand.

The ^{31}P NMR spectrum shows a septet at −212.3 ppm, indicative of coupling to two identical ^{7}Li (nuclear spin = 3/2) centres with a coupling constant of 62.8 Hz (figure 4.10). The ^{7}Li NMR spectrum shows a triplet at 2.6 ppm, with the splitting caused by coupling to two identical ^{31}P centres (figure 4.10). These data are consistent with the formation of the dilithium diphosphide species {SiP^{Tipp}}Li$_2$•(Et$_2$O)$_3$ (**4.12**). The splitting observed in the ^{31}P and ^{7}Li NMR spectra suggest that the solution state structure of **4.12** consists of a bridging bonding mode featuring a P$_2$Li$_2$ metallacycle.

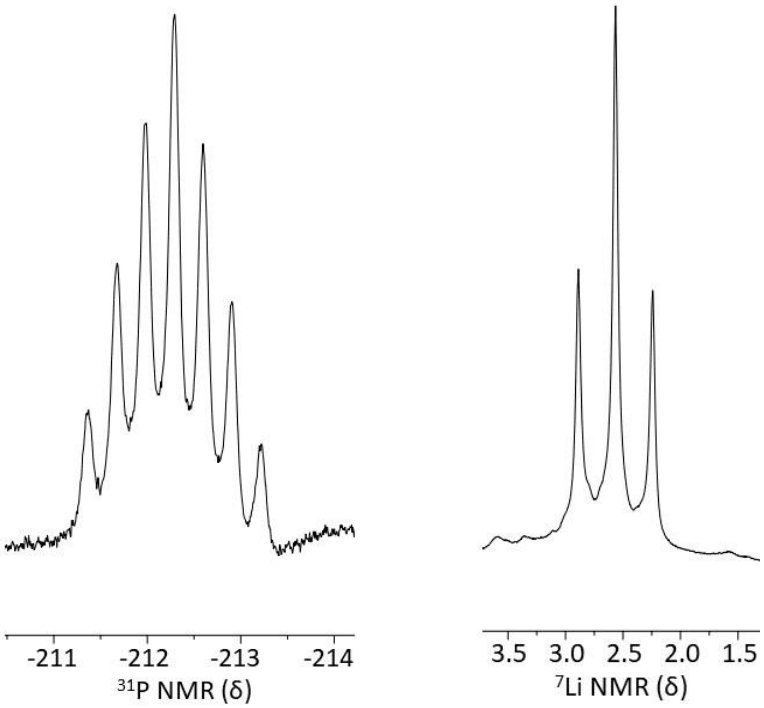

Figure 4.10 The ^{31}P (left) and ^{7}Li (right) NMR spectra of $\{SiP^{Tipp}\}Li_2\bullet(Et_2O)_3$ (**4.12**).

Diphosphine **4.4** can also be deprotonated with $K[N(SiMe_3)_2]$ (KHMDS, HMDS = $N(SiMe_3)_2$) at room temperature. Upon the addition of a benzene solution of diphosphine **4.4** to 2.2 equivalents KHMDS, a colour change from colourless to yellow was observed. The reaction was monitored using ^{31}P NMR spectroscopy and complete formation of the corresponding potassium diphosphide $\{SiP^{Tipp}\}K_2$ (**4.13**) was observed after one hour at room temperature. The potassiated diphosphide **4.13** can also be cleanly accessed using $K(CH_2Ph)$ as a base, allowing for easy separation of poorly soluble unreacted KCH_2Ph and reaction by-products (toluene), and was used for further reactivity without purification.

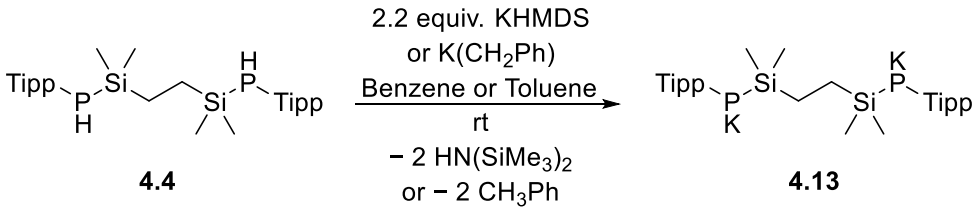

Scheme 4.10 The preparation of $\{SiP^{Tipp}\}K_2$ (**4.13**) from the reaction of $\{SiP^{Tipp}\}H_2$ (**4.4**) with 2.2 equivalents of KHMDS or $K(CH_2Ph)$.

The ^{1}H NMR spectrum of the reaction mixture has a sharp singlet resonance at 0.09 ppm indicating the formation of $HN(SiMe_3)_2$.[29] The singlets at 0.30 ppm and 0.83 ppm correspond the Si*Me*$_2$ and SiC*H*$_2$ protons, respectively. Doublet resonances at 1.24 ppm and 1.35 ppm correspond to the methyl groups of the para- and ortho-CH(C*H*$_3$)$_2$ fragments of the P-substituents. The C*H*$(CH_3)_2$ environments resonate as multiplets at 2.80 ppm (para) and 4.88 ppm (ortho), while the broad singlet resonance at 7.08 ppm corresponds to the C$_6$*H*$_2$ protons of the Tipp groups. The ^{31}P NMR spectrum of the reaction mixture consists of a singlet resonance at −206.4 ppm, corresponding to diphosphide **4.13**, similar to that observed for the dilithium species **4.12**. No proton-coupled resonances were observed in the spectrum, indicating complete consumption of the diphosphine **4.4** and formation of **4.13**.

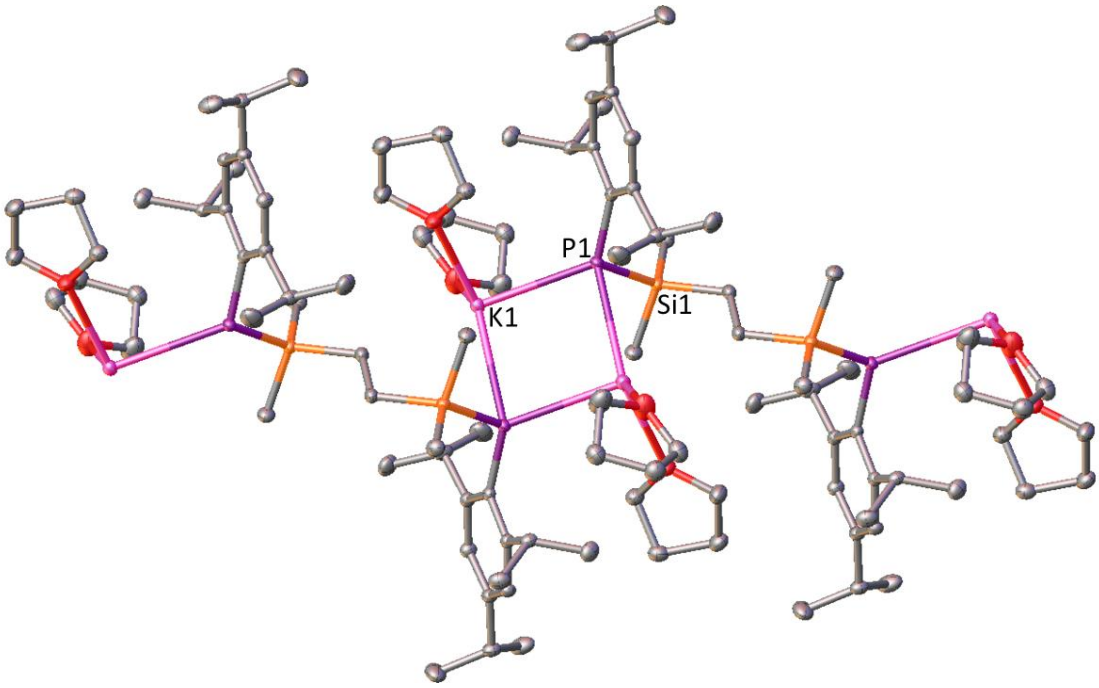

Figure 4.11 The solid-state structure of {SiP^{Tipp}}K$_2$•(THF)$_4$ (**4.13-THF**). H atoms are omitted for clarity. Thermal ellipsoids are set to 50% probability. Select bond lengths (Å) and angle (˚): P1–K1 3.1636(5), P1–Si1 2.1861(5), K1–P1–Si1 119.050(18).

A few colourless crystals of {SiP^{Tipp}}K$_2$•(THF)$_4$ (**4.13-THF**), the THF-adduct of **4.13**, were obtained from a concentrated THF solution and its solid-state structure was determined by X-ray crystallography. The asymmetric unit contains one half of a molecule of **4.13-THF** with the

other half consisting of symmetry equivalent atoms. The data also reveals that **4.13-THF** forms an oligomeric structure in the solid-state, in which the diphosphide fragments are linked through two bridging potassium centres, forming four-membered [P_2K_2] metallacycles. A section of the solid-state structure in **4.13-THF** is shown in figure 4.11. The phosphorus centres have a trigonal pyramidal geometry with a K1–P1–Si1 angle of 119.050(18)˚. The P1–K1 distance is 3.1636(15) Å and two units of THF are coordinated to each potassium. The P1–Si1 distance of 2.1861(5) Å lies within in the typical range of a P–Si bond.[19,20]

4.5.2 Synthesis of {SiP^{Tipp}}AlBr(THF) (4.14)

Diphosphide **4.13** in benzene was added to $AlBr_3$•NEt_3 at room temperature and an immediate colour change from orange to yellow was observed, which turned colourless over a period of 10 minutes. After 30 minutes, the ^{31}P NMR spectrum of an aliquot revealed complete consumption of diphosphide **4.13**. The new major resonance appears as a broad singlet at −192.8 ppm. In addition, broad resonances in the range of −177 ppm to −190 ppm suggest the presence of unidentified impurities or other products that are being formed. Attempts made to separate and identify reaction products from the reaction mixture by crystallisation were unsuccessful.

Further investigation revealed that the outcome of the reaction is heavily influenced by the choice of reaction solvent. Repeating the reaction in THF resulted in a more selective reaction pathway allowing the isolation of the diphosphidoaluminium bromide {SiP^{Tipp}}AlBr(THF) (**4.14**). Diphosphide **4.13** was dissolved in THF and added to $AlBr_3$•NEt_3 at room temperature. An immediate change from a clear orange solution to a colourless suspension was observed. The reaction was stirred for one hour, the volatiles were then removed under reduced pressure and pentane was added before filtration to remove the insoluble salts. Pentane was then removed under reduced pressure to afford the aluminium bromide THF adduct **4.14** as a colourless solid (scheme 4.11).

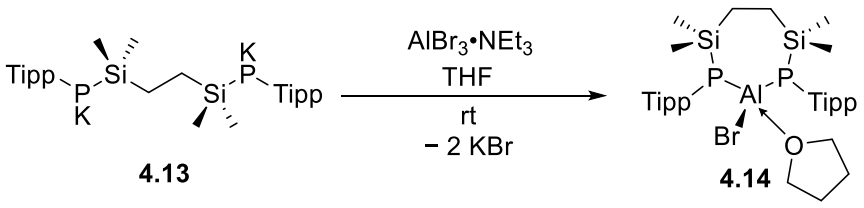

Scheme 4.11 The preparation of {SiP^{Tipp}}AlBr(THF) (**4.14**) from the reaction of {SiP^{Tipp}}K$_2$ (**4.13**) and AlBr$_3$•NEt$_3$ in THF at room temperature.

The ^{1}H NMR spectrum of aluminium bromide **4.14** consists of a high field singlet and triplet resonance for the Si*Me$_2$* environments at 0.47 and 0.52 ppm, respectively (figure 4.12). The doublet resonances at 1.19 and 1.20 ppm are assigned to the para-CH(C*H$_3$*)$_2$, integrating to a sum of 12 protons. The doublet resonances at 1.34 and 1.59 ppm correspond to the ortho-CH(C*H$_3$*)$_2$, each integrating to six protons. The broad resonance at 1.46 ppm, integrating to 12 protons, is thought to be two overlapping doublets, corresponding to the remaining ortho-CH(C*H$_3$*)$_2$. The septet resonance for the para-*i*Pr methine environment is observed at 2.78 ppm. The ortho-*i*Pr methine fragments are magnetically inequivalent, with one above and one below the P–Al–P plane and correspond to broad multiplets at 4.51 and 4.90 ppm. The broad resonances at 7.19 and 7.20 ppm correspond to the aryl-*H* environments. The THF resonances at 0.82 and 3.79 ppm are shifted compared to free THF (1.40 ppm and 3.57 ppm), suggesting the coordination of THF to the aluminium centre, while integration indicates the presence of one THF fragment per disphosphide ligand. The resonances for the SiC*H$_2$* groups could not be easily assigned in the ^{1}H NMR spectrum due to overlapping resonances. However, in the ^{1}H-^{1}H COSY NMR spectrum, the crosspeaks between the Si*Me$_2$* and SiC*H$_2$* environments allow for the assignment of the SiC*H$_2$* at 1.22 and 1.43 ppm. The assignment of the resonances for the *i*Pr groups are confirmed by the observed coupling between the *i*Pr methine and methyl groups. The ^{31}P NMR spectrum of aluminium bromide **4.14** has a singlet resonance at −194.4 ppm.

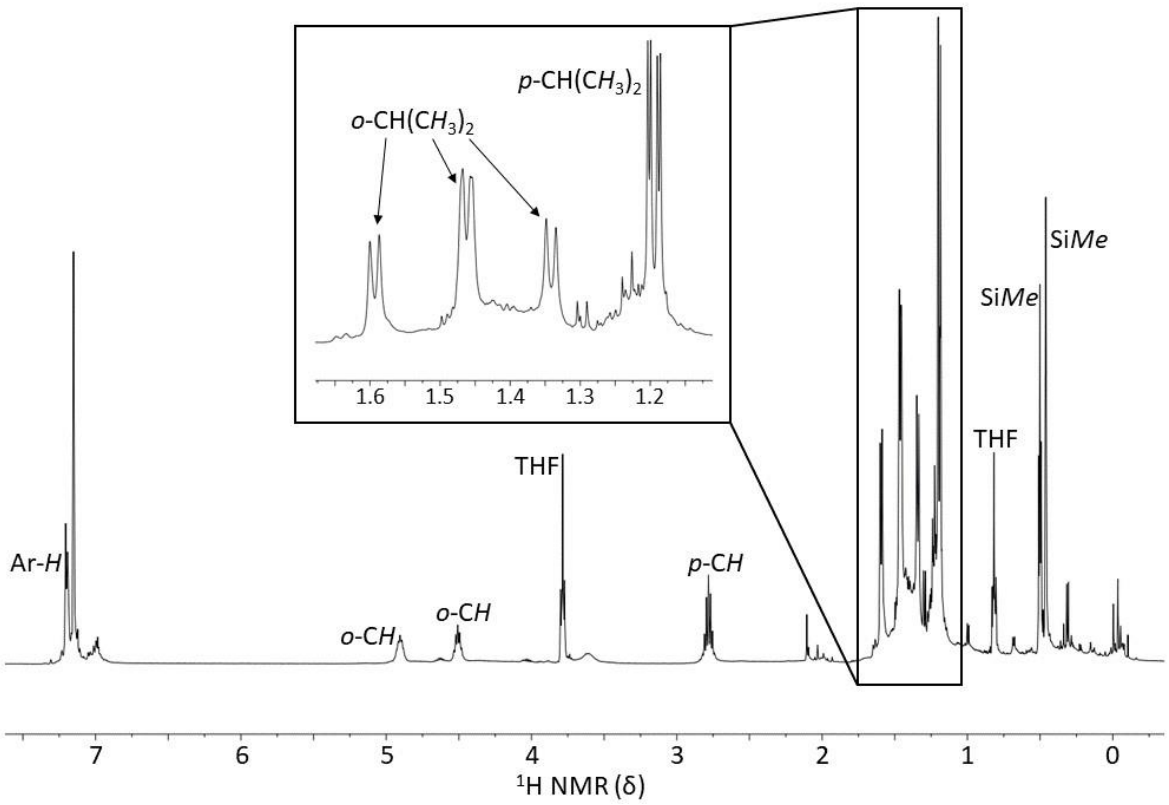

Figure 4.12 The ^{1}H NMR spectrum of {SiP^{Tipp}}AlBr(THF) (**4.14**).

The number of resonances observed for the methyl groups of the *i*Pr fragments of the P-substituents indicate that the Tipp groups are no longer magnetically equivalent, suggesting a loss of symmetry within the molecule. This is also reinforced by the presence of two distinct environments for the Si*Me*$_2$ protons. However, the phosphorus centres remain magnetically equivalent. This can be explained by bidentate coordination of the diphosphide to a tetrahedral aluminium centre with the remaining positions occupied by two different substituents resulting in an averaged C_S-symmetric species, whereby the mirror plane dissects the molecule along the Al–Br/Al–O bonds. In addition, rotation along the P–C bonds must be energetically inaccessible at room temperature, or rotating slower than the NMR timescale, to allow observation of the independent *ortho*-CH(CH$_3$)$_2$ substituents. These data, and the identification of coordinated THF in the ^{1}H NMR spectrum, are consistent with the formation of bidentate coordination of a diphosphide ligand to a tetrahedral aluminium, with the remaining sites occupied by a coordinated THF molecule and a bromide ligand. Unfortunately, attempts to obtain single crystals of **4.14** were unsuccessful, preventing confirmation of the

structure by X-ray crystallography. However, mass spectrometry analysis of the sample identified an ion fragment consistent with aluminium bromide **4.14**.

4.5.3 Synthesis of {SiP^{Tipp}}AlBr(DMAP) (4.15)

The inclusion of a coordinated THF molecule was predicted to lead to complications during reduction reactions, as previous aluminium(I) species have been demonstrated to activate THF through a reductive ring-opening process.[3] Therefore, substitution of the THF adduct was performed using the more robust Lewis base dimethylaminopyridine (DMAP). A toluene solution of aluminium bromide **4.14** was added to DMAP at room temperature and stirred for 48 hours, after which the suspension was filtered and the solid collected to afford {SiP^{Tipp}}AlBr(DMAP) (**4.15**) as a colourless solid (32 %, scheme 4.12).

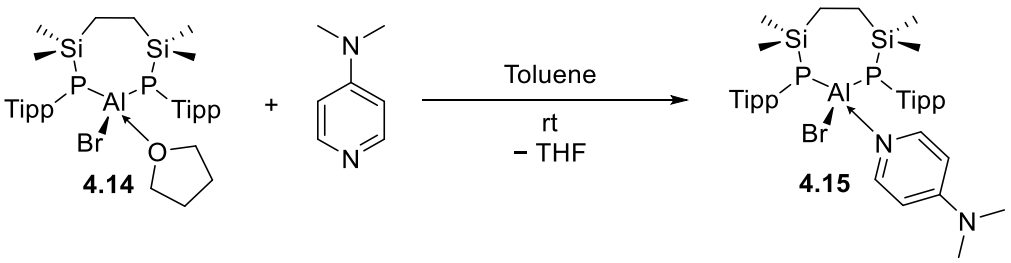

Scheme 4.12 The preparation of {SiP^{Tipp}}AlBr(DMAP) (**4.15**) from the reaction of {SiP^{Tipp}}AlBr(THF) (**4.14**) and DMAP.

The ^{1}H NMR spectrum (figure 4.13), the resonances for the diphosphine ligand closely resemble those observed for aluminium bromide **4.14**. A triplet resonance at 0.58 ppm and singlet at 0.61 ppm correspond to the Si*Me*$_2$ protons, similar to that observed for **4.14** and indicative of asymmetry in the diphosphide backbone. The CH(C*H*$_3$)$_2$ protons of the Tipp fragments appear as a series of doublets, with the para-substituents appearing as two overlapping doublets at 1.13 ppm and 1.14 ppm and the ortho-substituents appearing as four distinct doublets at 1.28 ppm, 1.50 ppm, 1.55 ppm and 1.57 ppm. The C*H*(CH$_3$)$_2$ resonances appear as a septet at 2.74 ppm for the para-substituents, while the ortho-substituents appear as two distinct multiplets at 4.80 and 4.97 ppm. Loss of the THF resonances and the

observation of resonances relating to the protons of a coordinated DMAP confirm replacement of the Lewis base. The singlet resonance at 1.63 ppm corresponds to the NMe_2 fragment, while the two doublet resonances at 5.36 ppm and 8.48 ppm correspond to the aryl C-H protons. The ^{31}P NMR spectrum of **4.15** has a singlet resonance at −191.8 ppm, slightly downfield from aluminium bromide-THF adduct **4.14** (−194.4 ppm). These data are similar to that observed for **4.14**, and are consistent with the retention of a C_S-symmetric species which has a tetrahedral aluminium chelated by the bidentate diphosphide ligand. The remaining positions are occupied by a DMAP ligand and a bromide ligand.

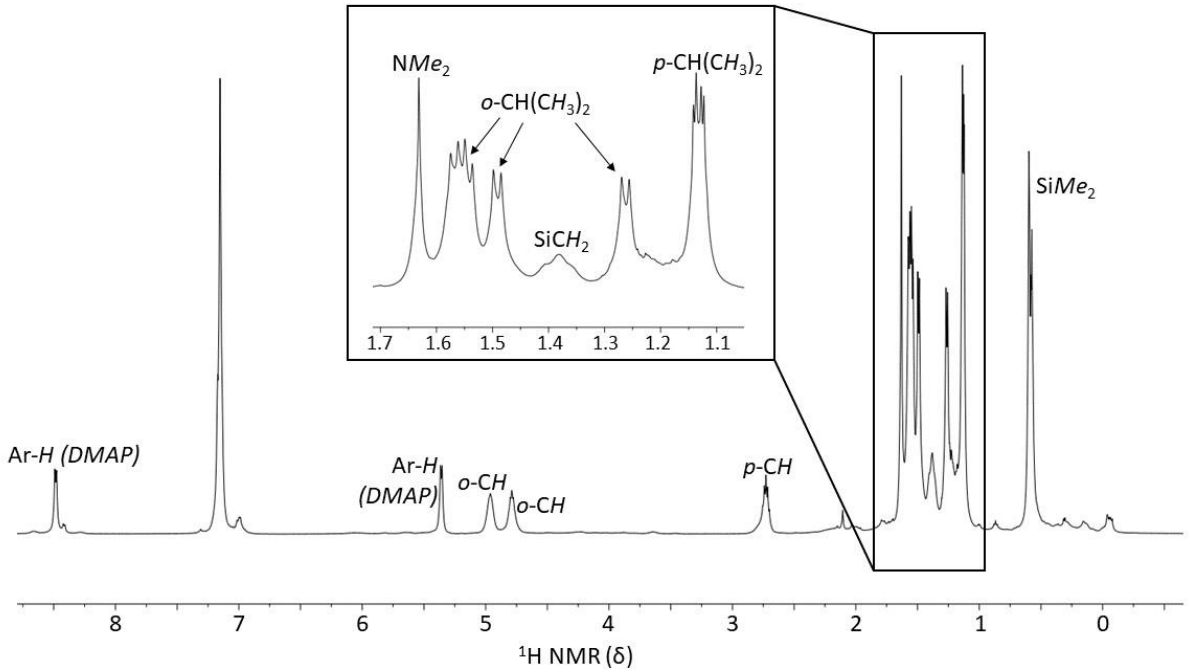

Figure 4.13 The ^{1}H NMR spectrum of {SiP^{Tipp}}AlBr(DMAP) (**4.15**).

Attempts to synthesise the aluminium iodide counterpart proceeded by adding a benzene solution of diphosphide **4.13** dropwise to AlI_3 suspended in toluene at −40 ˚C. Upon complete addition, the reaction mixture was warmed to room temperature resulting in a colour change from orange to yellow and deposition of a colourless solid. However, an aliquot of the solution was analysed by ^{31}P NMR spectroscopy indicating decomposition of the ligand to the primary phosphine TippPH_2 had occurred. As there was no evidence of {SiP^{Tipp}}AlI being formed, investigations into preparing the aluminium iodide were not continued.

4.5.4 Synthesis of Diphosphide {SiP^{Mes*}}M$_2$ (M = Li, 4.16; K, 4.18)

Diphosphine **4.5** can be deprotonated in an analogous manner to **4.4**, using *n*BuLi. To a solution of diphosphine **4.5** in Et_2O, two equivalents of nBuLi were added dropwise at −78 ˚C, and a colour change from colourless to yellow was observed. The reaction mixture was then allowed to warm to room temperature and stirred for four hours. The volatiles were removed and the solid washed with hexane and dried to give diphosphide **4.16** (scheme 4.13).

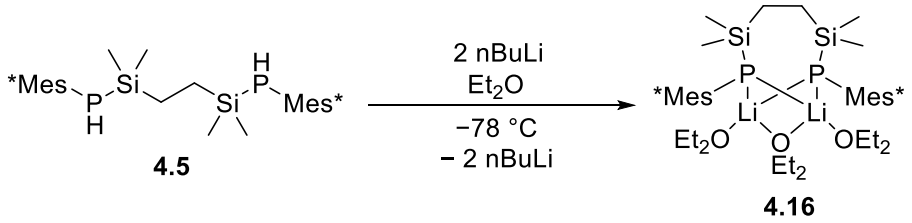

Scheme 4.13 The reaction of {SiP^{Mes*}}H_2 (**4.5**) and two equivalents of nBuLi to give {SiP^{Mes*}}Li_2•$(Et_2O)_3$ (**4.16**).

The ^{1}H NMR spectrum of diphosphide **4.16** consists of a singlet resonance at 0.07 ppm for Si*Me*$_2$ and a multiplet resonance at 0.82 ppm for SiC*H*$_2$. The singlet resonances at 1.41 and 1.93 ppm correspond to the para- and ortho-*t*Bu groups, respectively, whilst the singlet resonance at 7.50 ppm relates to the aryl-*H* environments of Mes*. Integration of resonances at 1.13 ppm (triplet) and 3.24 ppm (quartet) reveal that three molecules of Et_2O are coordinated to the lithium diphosphide. The absence of a P*H* resonance is consistent with deprotonation at both phosphorus centres.

The ^{31}P NMR spectrum of **4.16** (figure 4.14) consists of a septet at −162.2 ppm indicating the phosphorus centres to be magnetically equivalent. The splitting is due to phosphorus coupling to two magnetically equivalent ^{7}Li centres. The ^{7}Li NMR spectrum shows a triplet resonance at 3.02 ppm, indicating that each lithium centre is coupled to two phosphorus centres (figure 4.14). These data are similar to the analogous dilithiate species **4.12**, suggesting a similar solution-state structure.

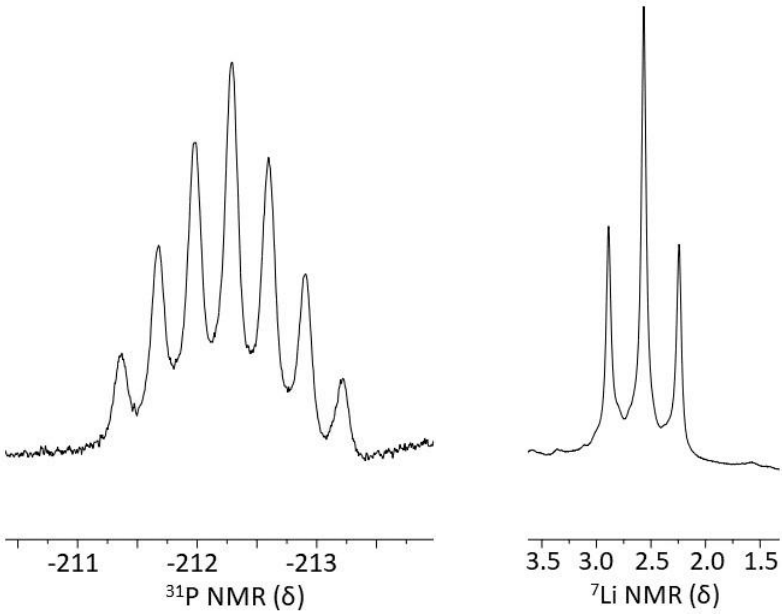

Figure 4.14 The ^{31}P (left) and ^{7}Li (right) NMR spectra of {SiP^{Mes*}}Li_2•$(Et_2O)_3$ (**4.16**).

Crystallisation of the **4.16** gave colourless crystals suitable for analysis using single crystal X-ray diffraction and allowing determination of the solid-state structure (figure 4.15). The solid-state structure reveals that **4.16** crystallises as the mono-etherate adduct {SiP^{Mes*}}Li_2•(Et_2O) (**4.16a**), losing two equivalents of Et_2O through the crystallisation process. The geometries of the phosphorus centres are intermediate between tetrahedral and see-saw (P1: τ_4 = 0.72, τ'_4 = 0.66; P2: τ_4 = 0.66, τ'_4 = 0.60), with angles around P1 and P2 ranging from 73.27(12)˚ to 138.78(10)˚ and from 73.68(12)˚ to 142.69(10)˚, respectively. The P–Li1 distances are shorter than P–Li2, suggesting stronger interactions between the phosphorus centres and Li1, which may be due to the presence of coordinated Et_2O at Li2.

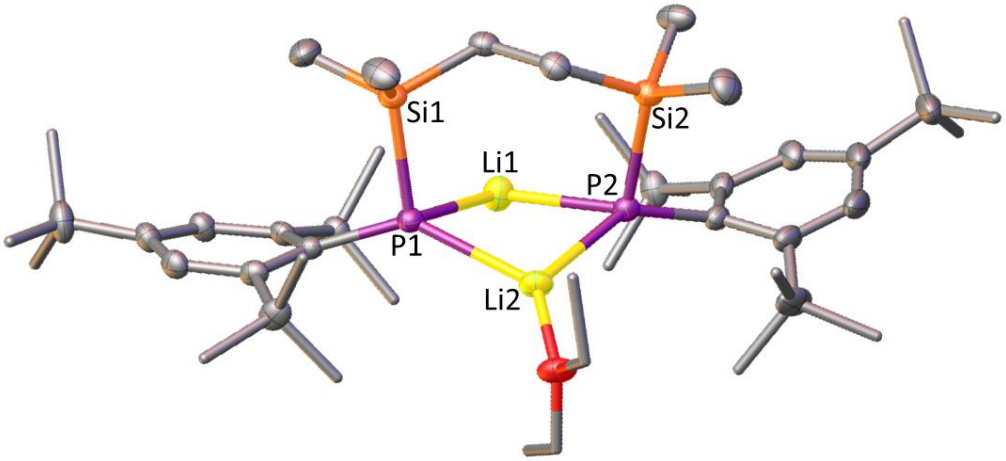

Figure 4.15 The solid-state structure of {SiP^{Mes*}}Li$_2$(Et$_2$O) (**4.16a**). H atoms are omitted for clarity. Thermal ellipsoids are set to 50% probability. Select bond lengths (Å) and angles (˚): P1–Li1 2.441(3), P1–Li2 2.505(4), P2–Li1 2.428(4), P2–Li2 2.494(3), P1–Li1–P2 104.24(13), Li1–P1–Li2 73.27(12).

The deprotonation of {SiP^{Mes*}}H$_2$ (**4.5**) was also attempted using KHMDS. A solution of KHMDS in benzene was added to a benzene solution of diphosphine **4.5** at room temperature. In contrast to the analogous reaction involving diphosphine **4.4** and KHMDS which is complete within one hour, the reaction of **4.5** is extremely slow. The ^{1}H NMR spectrum reveals unreacted KHMDS (Si*Me$_3$*, s, 0.12 ppm) and diphosphine **4.5** (P*H*, d, 4.39 ppm) to be the major species in solution after one hour at room temperature. However, a doublet resonance at −132.0 ppm ($^1J_{H–P}$ = 216 Hz) indicates the formation of a new phosphine species. In addition, a singlet resonance at −148.8 ppm is observed, consistent with deprotonation of a phosphine and formation of a phosphide centre. The integrals for the new doublet and singlet resonances are in a ratio of 1:1, suggesting that the partially deprotonated intermediate {SiP^{Mes*}}(H)K (**4.17**, scheme 4.14) was being generated. After four days, ^{31}P NMR spectroscopy reveals complete consumption of diphosphine **4.5**. Along with the resonances for intermediate **4.17**, the broad singlet resonance at −153.1 ppm corresponds to the fully deprotonated diphosphide {SiP^{Mes*}}K$_2$ (**4.18**) and is in a ratio of approximately 1:1 (**4.17**:**4.18**).

After 10 days, diphosphide **4.18** was the major species in solution (ca. 64 % by integration), but intermediate **4.17** was still present indicating the slow rate of complete deprotonation of the phosphorus centres of disphosphine **4.5**. Heating the reaction of **4.5** and KHMDS to 60 °C for one hour led to the formation of a mixture of phosphorus containing products demonstrating the thermal lability of the ligand framework.

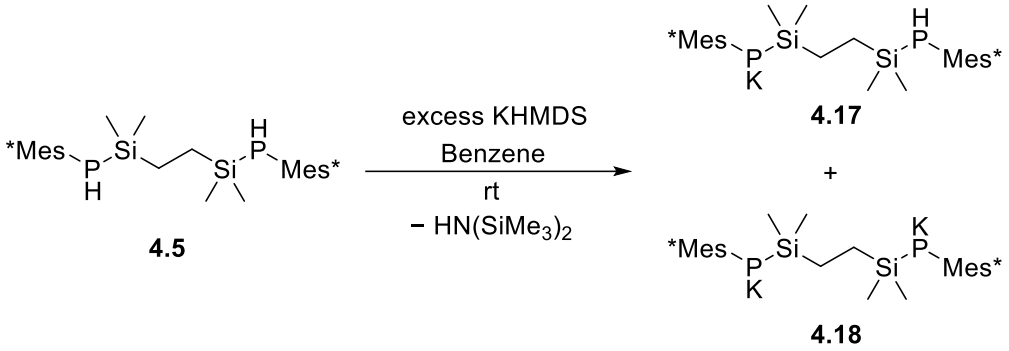

Scheme 4.14 The deprotonation of {SiP^{Mes*}}H$_2$ (**4.5**) using KHMDS to give {SiP^{Mes*}}K$_2$ (**4.18**), with partial deprotonation intermediate **4.17** observed by NMR spectroscopy.

The differences in the rate of deprotonation of two diphosphines may be due to different steric profiles of the phosphorus substituents allowing differing access to the P–H moiety. The slow progress of the reaction for the Mes* derivative may indicate a kinetic limitation imposed by the use of the relatively bulky base KHMDS.

4.5.5 Attempted Synthesis of {SiP^{Mes*}}AlX (X = Cl, Br, I)

Attempts to synthesise aluminium halide species {SiP^{Mes*}}AlX (X = Cl, Br, I) by a double salt-elimination reaction between the dilithiate species **4.16** and corresponding aluminium trihalide AlX$_3$ were unsuccessful, instead resulting in the formation of diphosphine **4.5** and primary phosphine Mes*PH$_2$, which were observed by ^{31}P NMR spectroscopy. This may reflect the importance of the cation in the salt-elimination process, and the limitations of using the dilithiate species **4.16** for this reactivity.

4.6 Towards the Reduction of {SiP^{Tipp}}AlBr(L) (L = THF, DMAP)

The aluminium bromide species {SiP^{Tipp}}AlBr(L) (L = THF, **4.14**; L = DMAP, **4.15**) were explored as pre-cursors to the targeted diphosphide supported aluminyl anion [{SiP^{Tipp}}Al]$^{-}$. Previous examples of diamide supported aluminyl complexes indicate the need for strong reducing agents and correct solvent conditions to achieve clean reduction products. Group 1 metals and non-coordinating solvents have typically been required to allow isolation of the desired aluminyl complexes. In addition, the ligand system is required to be relatively robust to survive the harsh reduction conditions.

The preliminary reduction reactions of {SiP^{Tipp}}AlBr(THF) (**4.14**) were carried out using potassium containing reducing agents such as potassium graphite (KC_8), potassium mirror, and potassium-crown ether complex K[18-c-6][$C_{10}H_8$] (18-c-6 = $[C_2H_4O]_6$) which is partially soluble in aromatic solvents. Solutions of aluminium bromide **4.14** in benzene or toluene were stirred over the reducing agents at room temperature. The ^{1}H and ^{31}P NMR spectra of the reaction mixtures reveals an intractable mixture of products. In the reactions with KC_8, the presence of potassium diphosphide **4.13** is also observed, suggesting that the Al–P bond is susceptible to cleavage by a group 1 metal and is weaker than Al–N of the diamido ligands of **1.92** and **1.95** – **1.97**. Attempts to isolate the products through crystallisation were not successful, thus the products of the reactions were not identified.

The reduction of {SiP^{Tipp}}AlBr(DMAP) (**4.15**) was also attempted using KC_8. Reminiscent to the reactivity observed for aluminium bromide **4.14**, the ^{1}H and ^{31}P NMR spectra show a mixture of products form including potassium diphosphide **4.13**.

4.7 Synthesis of Diphosphide-Supported Aluminium Hydrides

Aluminium hydrides present an alternative route into low oxidation state aluminium compounds through reductive processes. Trimethylamine-alane (**1.3**) has previously been reported to undergo deprotonation reactivity when introduced to a suitably acidic proton source.[30] For example, the reaction of **1.3** with primary aniline H_2NDipp was demonstrated to

result in formation of amido- and imidoalanes and loss of H_2.[31] In contrast, no reaction was observed between diphosphides **4.4** or **4.5** and **1.3** in C_6D_6, even when the reaction mixture was heated to 70 °C for 24 hours. The decreased acidity of P–H compared to their lighter amine congeners, in addition to the kinetic stabilisation provided by the bulky phosphine substituents may disfavour deprotonation through this route.

An alternative route to ligated alane species from **1.3** and metalated ligand systems has also been reported for systems with weakly acidic binding sites. For example, Cowley and co-workers highlighted that access to alane species may be achieved by the reaction of two equivalents of **1.3** with a lithium amidophosphine species, utilising the formation $LiAlH_4$ as a driving force for hydride displacement (scheme 4.15).[32] However, access to alane species through this route has not yet been reported using a dilithium salt. This method was explored in an attempt to generate aluminium hydrides supported by diphosphide ligands $[\{SiP^{Tipp}\}]^-$ and $[\{SiP^{Mes*}\}]^-$.

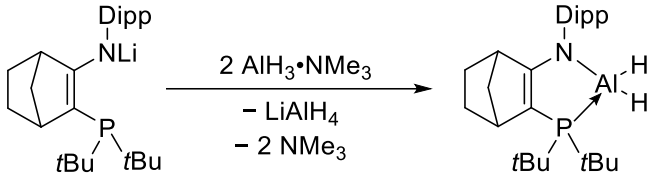

Scheme 4.15 The reaction of a lithium amidophosphine species with two equivalents of AlH_3•NMe_3 (**1.3**) to give an aluminium dihydride species by elimination of $LiAlH_4$.

4.7.1 Attempted synthesis of {SiP^{Tipp}}AlH (4.19)

The reaction of dilithium salt **4.12** with trimethylamine-alane **1.3** was investigated. Addition of a solution of two equivalents of **1.3** in Et_2O to a solution of **4.12** in Et_2O resulted in the formation of a new species. Removal of the volatile components and recrystallisation from a mixture of toluene with a few drops of THF gave colourless crystals of the diphosphido(alane) lithate $\{SiP^{Tipp}\}(AlH_2)Li•(THF)_2$ (**4.20**, 56% yield, scheme 4.16).

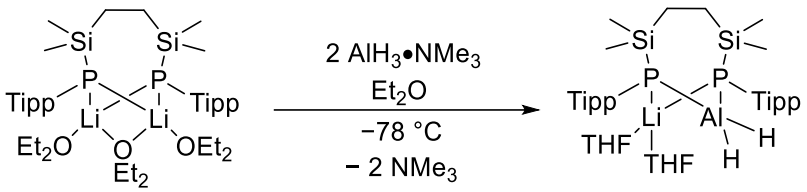

4.12 **4.20**

Scheme 4.16 The reaction of {SiP^{Tipp}}Li$_2$•(Et$_2$O)$_3$ (**4.12**) and two equivalents of AlH$_3$•NMe$_3$ to give {SiP^{Tipp}}(AlH$_2$)Li•(THF)$_2$ (**4.20**).

The ^{1}H NMR spectrum of **4.20** contains a high field singlet at 0.35 ppm corresponding to the Si*Me$_2$* protons of the ligand backbone, while the SiC*H$_2$* protons appear significantly downfield as a triplet at 1.15 ppm. The *p*-CH(C*H$_3$*)$_2$ and *o*-CH(C*H$_3$*)$_2$ protons appear as doublets at 1.24 and 1.52 ppm, respectively. The methine protons *p*-CH(C*H$_3$*)$_2$ and *o*-CH(C*H$_3$*)$_2$ are observed as a septet and multiplet at 2.82 and 4.56 ppm, respectively. A broad singlet resonance at 5.11 ppm corresponds to Al*H* ligands, with relative integrals indicating two hydride ligands are present for every diphosphide ligand. Two multiplet resonances at 1.26 ppm and 3.59 ppm correspond to coordinated THF ligands, with relative integrals indicating two coordinated THF molecules per diphosphide unit.

The ^{31}P NMR spectrum shows a single broad resonance at −200.3 ppm, shifted slightly downfield compared to the dilithate **4.12**. The ^{7}Li NMR shows a broad singlet at 1.0 ppm, indicating the presence of lithium within the molecular structure. The solid-state IR spectrum shows two peaks at 1790 and 1725 cm^{-1}, consistent with Al–H stretches for a hydride ligand.

The solid-state structure of **4.20** was investigated using single crystal X-ray diffraction, confirming the formation of the {SiP^{Tipp}}(AlH$_2$)Li•(THF)$_2$ (Figure 4.16). Unfortunately, due to the poor quality of the X-ray diffraction data, the accurate discussion of the bond lengths and angles is not possible. However, the molecular connectivity is unambiguous, confirming the coordination of the diphosphide ligand to both the aluminium and lithium centres through a bridging bonding mode at both phosphorus atoms. This provides the first structural evidence that chelation of the diphosphide ligand to an aluminium centre is possible.

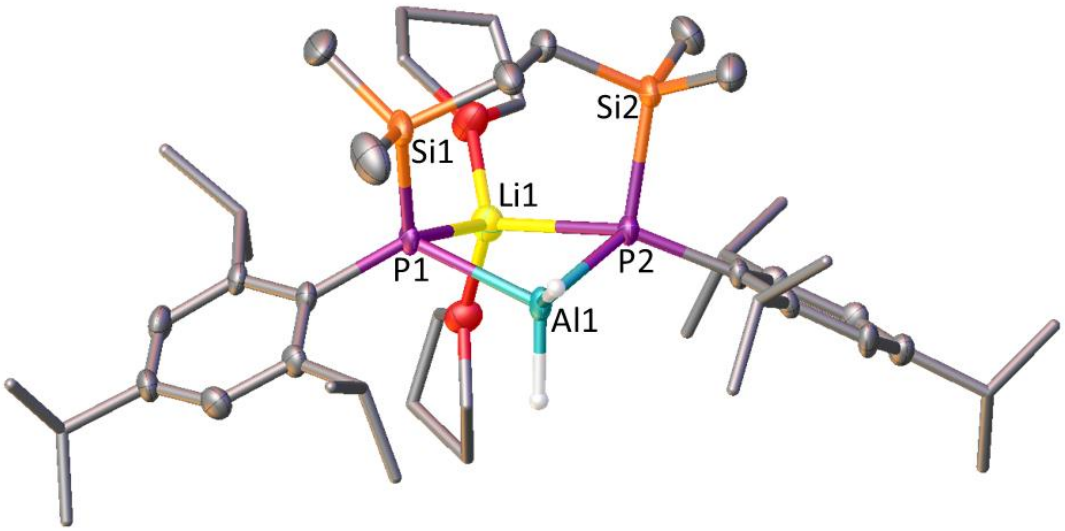

Figure 4.16 The solid-state structure of {SiP^{Tipp}}(AlH_2)Li•$(THF)_2$ (**4.20**). H atoms, except for AlH, are omitted for clarity. Thermal ellipsoids are set to 50% probability.

The formation of **4.20** can be considered as an intermediate in the pathway towards $LiAlH_4$ elimination and the formation of {SiP^{Tipp}}AlH (**4.19**) through further reaction with **1.3** (scheme 4.17). Addition of one equivalent of **1.3** to a solution of **4.20** in C_6D_6 resulted in the deposition of a colourless solid. However, ^{1}H NMR spectroscopy revealed the formation of a mixture of products. Two major species can be identified in the ^{31}P NMR spectrum appearing at −183.3 and −196.6 ppm. The ^{7}Li NMR spectrum indicates loss of the lithium resonance, consistent with the deposition of $LiAlH_4$. Attempts to access **4.19** directly by reaction of **4.12** with 4 equivalents of **1.3** were unsuccessful, instead giving an intractable mixture of products.

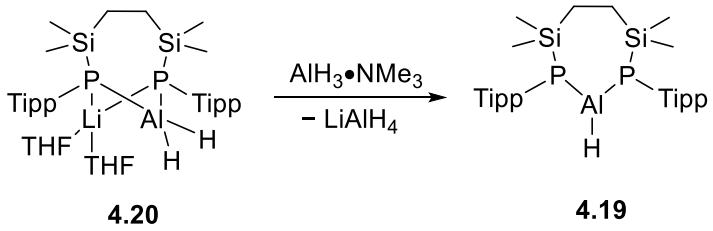

4.20 **4.19**

Scheme 4.17 Proposed synthetic pathway to {SiP^{Tipp}}AlH (**4.19**).

4.7.2 Attempted synthesis of {SiP^{Mes*}}AlH (4.21)

The reactivity of **4.16** with AlH_3•NMe_3 (**1.3**) was also investigated, with the addition of two equivalents of **1.3** to **4.16** in Et_2O resulting in the slow deposition of a colourless precipitate over an hour at room temperature. The precipitate was isolated and investigated using NMR spectroscopy. The ^{1}H NMR spectrum shows a broad high field singlet at 0.05 ppm corresponding to the 12 Si*Me*$_2$ protons. The SiC*H*$_2$ protons appear as a broad resonance at 1.15, while singlets corresponding to the C(C*H*$_3$)$_3$ protons appear at 1.38 and 1.94 ppm. A broad resonance at 3.71 ppm corresponds to Al*H* ligands, with relative integration indicating six hydride ligands for each diphosphide ligand. Resonances corresponding to coordinated Et_2O molecules are also present at 1.11 and 3.32 ppm, with integration consistent with four coordinated molecules retained.

The ^{31}P NMR spectrum shows a single broad resonance at −170.4 ppm, while the ^{7}Li NMR spectrum shows a broad resonance at 0.53 ppm, indicating retention of lithium within the molecular structure. These data are consistent with the formation of a diphosphido bis(alane) adduct {SiP^{Mes*}}$(AlH_3)_2Li_2$•$(Et_2O)_4$ (**4.22**), formed through loss of two equivalents of trimethylamine (scheme 4.18). The solid-state IR spectrum shows a broad peak at 1751 cm^{-1}, within the region expected for Al–H vibrations.

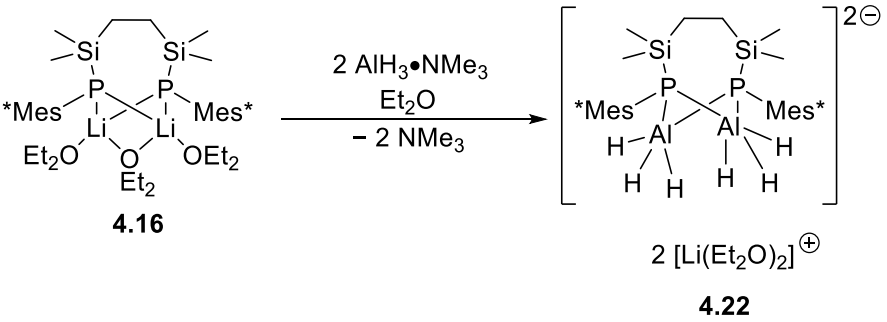

Scheme 4.18 The reaction of {SiP^{Mes*}}Li_2•$(Et_2O)_3$ (**4.16**) and two equivalents of AlH_3•NMe_3 to give {SiP^{Mes*}}$(AlH_3)Li_2$•$(Et_2O)_4$ (**4.22**).

This species may be an intermediate towards a $LiAlH_4$ elimination reaction. Heating a sample of **4.22** in C_6D_6 to 60 °C resulted in gradual conversion to a complex mixture of

products, including the free diphosphine ligand **4.5**. In contrast, the addition of excess **1.3** to a solution of **4.22** in C_6D_6 resulted in the deposition of a colourless solid and formation of a single new species. The ^{1}H NMR spectrum of the reaction mixture showed a high field doublet at 0.27 ppm and singlet at 0.78 ppm corresponding to the Si*Me*$_2$ and SiC*H*$_2$ resonances, respectively. The observed doublet resolves into a sharp singlet in the ^{1}H{^{31}P} NMR spectrum consistent with $^3J_{P–H}$ coupling of 4.7 Hz. The C(C*H*$_3$)$_3$ resonances appear as singlets at 1.92 and 1.37 ppm, while the C_6H_2 resonance of the phosphorus substituent appears as a doublet at 7.54 ppm. Free trimethylamine is observed in the ^{1}H NMR spectrum, appearing as a singlet at 2.05 ppm, while excess **1.3** was observed at 1.89 ppm (N*Me*$_3$) and 4.10 ppm (Al*H*).[33] The relative integrals reveal two equivalents of trimethylamine are present for every ligand, suggesting reaction of **4.22** with two equivalents of **1.3**. A broad resonance at 4.37 ppm may correspond to the Al*H* of a new alane species. However, overlapping of the Al*H* resonances of the product and **1.3** prevents accurate integration. The ^{31}P NMR spectrum contains a singlet at −162.3 ppm, while the ^{7}Li NMR spectrum consists of a single minor resonance at 0.26 ppm, attributed to the presence of a small amount of lithium containing impurity.

These data are consistent with the formation of a new diphosphido alane species and may correspond to the formation of {SiP^{Mes*}}(AlH$_2$)$_2$ (**4.23**) formed through the loss of two equivalents of LiAlH$_4$ (scheme 4.19). However, further investigation is required to confirm the identity of this species.

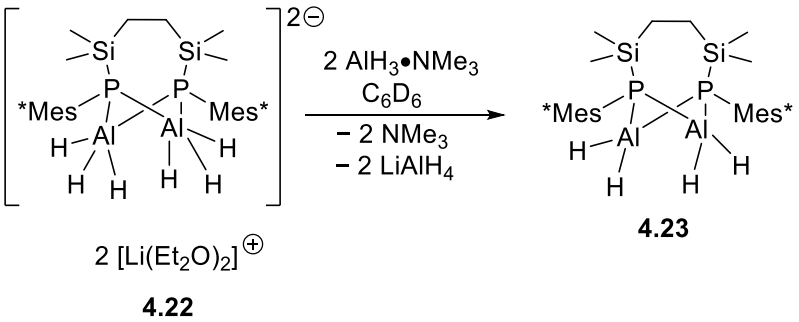

4.22 **4.23**

Scheme 4.19 Proposed reaction of {SiP^{Mes*}}(AlH$_3$)Li$_2$•(Et$_2$O)$_4$ (**4.22**) with two equivalents of AlH$_3$•NMe$_3$ to give {SiP^{Mes*}}(AlH$_2$)$_2$ (**4.23**).

4.8 Conclusions

This chapter discusses the attempted synthesis of a diphosphide-supported aluminyl species. The synthesis of two novel diphosphine ligand systems {SiP^{Tipp}}H$_2$ (**4.4**) and {SiP^{Mes*}}H$_2$ (**4.5**) is reported. These ligand systems display structural difference in comparison to their diamine counterpart **4.1**, most notably the phosphorus centres have pyramidal geometries which allows the formation of diastereomers, observed by NMR spectroscopy.

Attempts to deprotonate the ligands using AlMe$_2$Cl and AlMe$_3$ instead gave diphosphine adducts **4.7** – **4.11**, with both P–H bonds still intact. Therefore, organo- and amido-group 1 complexes were explored as metalating reagents. The metalation reaction was found to be dependent on the phosphorus substituents and the base. Diphosphine **4.4**, featuring a Tipp substituent, was readily deprotonated by nBuLi and the milder potassium amide KHMDS to give the corresponding lithium and potassium diphosphides **4.12** and **4.13**. Diphosphine **4.5** may also be readily deprotonated using nBuLi to give **4.16**, while reaction with KHMDS gave a mixture of the singly deprotonated species **4.17** and potassium diphosphide **4.18** over an extended period of time. The latter case is proposed to be due to the increased steric encumbrance provided by the Mes* substituent.

Reactivity of diphosphides **4.13** and **4.16** towards aluminium halides was investigated with the aim to synthesise a diphosphido aluminium halide complex. Reactions of lithium diphosphide **4.16** with AlX$_3$ (X = Cl, Br, I) resulted in decomposition of starting materials and the generation of diphosphine **4.5**. Similar reactivity was observed for the reaction of potassium diphosphide **4.13** with AlX$_3$, with the exception of AlBr$_3$. It was also found that solvent selection is crucial for the synthesis of the chelated aluminium bromide, requiring a coordinating solvent such as THF. The reaction of potassium diphosphide **4.13** with AlBr$_3$•NEt$_3$ in THF results in the formation of {SiP^{Tipp}}AlBr(THF) (**4.14**), in which one molecule of THF is coordinated to aluminium, giving rise to a four-coordinate metal centre and asymmetry in the diphosphido ligand, observed by NMR spectroscopy. The THF fragment can be displaced using stronger coordinating base DMAP to give aluminium bromide **4.15**, whilst retaining its chelate structure and ligand asymmetry. Preliminary reactions into the reduction of aluminium bromide **4.14** and **4.15** resulted in either P–Al cleavage to form potassium diphosphide **4.13** or an intractable mixture of products which could not be identified.

The dilithium diphosphide species **4.12** and **4.16** also show reactivity with trimethylamine-alane **1.3**, resulting in ligation of the diphosphide ligand and the formation of new alane species **4.20** and **4.22**, featuring Al–H bonds.

4.9 References

(1) Hicks, J.; Vasko, P.; Goicoechea, J. M.; Aldridge, S., *Angew. Chem. Int. Ed.*, **2021**, *60*, 1702–1713.

(2) Schwamm, R. J.; Anker, M. D.; Lein, M.; Coles, M. P., *Angew. Chem. Int. Ed.*, **2019**, *58*, 1489–1493.

(3) Schwamm, R. J.; Coles, M. P.; Hill, M. S.; Mahon, M. F.; McMullin, C. L.; Rajabi, N. A.; Wilson, A. S. S. *Angew. Chem. Int. Ed.*, **2020**, *59*, 3928–3932.

(4) Fantasia, S.; Petersen, J. L.; Jacobsen, H.; Cavallo, L.; Nolan, S. P., *Organometallics*, **2007**, *26*, 5880–5889.

(5) Kurumada, S.; Takamori, S.; Yamashita, M., *Nat. Chem.*, **2020**, *12*, 36–39.

(6) Koshino, K.; Kinjo, R., *J. Am. Chem. Soc.*, **2020**, *142*, 9057–9062.

(7) Hicks, J.; Vasko, P.; Goicoechea, J. M.; Aldridge, S., *Nature*, **2018**, *557*, 92–95.

(8) Grams, S.; Eyselein, J.; Langer, J.; Färber, C.; Harder, S., *Angew. Chem. Int. Ed.*, **2020**, *59*, 15982–15986.

(9) Evans, M. J.; Anker, M. D.; McMullin, C. L.; Neale, S. E.; Coles, M. P. *Angew. Chem. Int. Ed.* **2021**, *60*, 22289–22292.

(10) Hicks, J.; Vasko, P.; Goicoechea, J. M.; Aldridge, S., *J. Am. Chem. Soc.*, **2019**, *141*, 11000–11003.

(11) Schwamm, R. J.; Hill, M. S.; Liu, H.-Y.; Mahon, M. F.; McMullin, C. L.; Rajabi, N. A., *Chem. Eur. J.*, **2021**, *27*, 14971–14980.

(12) Kays, D. L., *Chem. Soc. Rev.*, **2016**, *45*, 1004–1018.

(13) Hopkinson, M. N.; Richter, C.; Schedler, M.; Glorius, F., *Nature*, **2014**, *510*, 485–496.

(14) Schwamm, R. J.; Anker, M. D.; Lein, M.; Coles, M. P.; Fitchett, C. M., *Angew. Chem. Int. Ed.*, **2018**, *57*, 5885–5887.

(15) Kutzelnigg, W. *Angew. Chem. Int. Ed.*, **1984**, *23*, 272–295.

(16) Ferao, A. E.; Alcaraz, A. G., *New J. Chem.*, **2020**, *44*, 8763–8770.

(17) Magnusson, E., *J. Am. Chem. Soc.*, **1986**, *108*, 11–16.

(18) Boeré, R. T.; Masuda, J. D., *Can. J. Chem.*, **2002**, *80*, 1607-1617.

(19) Dykema, K. J.; Truong, T. N.; Gordon, M. S., *J. Am. Chem. Soc.*, **1985**, *107*, 4535–4541.

(20) Kapitein, M.; Balmer, M.; Niemeier, L.; Hänisch, C. von., *Dalton Trans.*, **2016**, *45*, 6275–6281.

(21) Atiya, G. A.; Grady, A. S.; Jackson, S. A.; Parker, N.; Russel, D. K., *J Organomet. Chem.*, **1989**, *378*, 307–316.

(22) Yang, L.; Powell, D. R.; Houser, R. P., *Dalton Trans.*, **2007**, 9, 955–964.

(23) Melton, C. E.; Dube, J. W.; Ragogna, P. J.; Fettinger, J. C.; Power, P. P., *Organometallics*, **2014**, *33*, 329–337.

(24) Fettinger, J. C.; Gray, P. A.; Melton, C. E.; Power, P. P., *Organometallics*, **2014**, *33*, 6232–6240.

(25) Bennett, F. R.; Elms, F. M.; Gardiner, M. G.; Koutsantonis, G. A.; Raston, C. L.; Roberts, N. K., *Organometallics*, **1992**, *11*, 1457–1459.

(26) Fryzuk, M. D.; Giesbrecht, G. R.; Olovsson, G.; Rettig, S. J., *Organometallics*, **1996**, *15*, 4832–4841.

(27) Watson, I. C.; Zhou, Y.; Ferguson, M. J.; Kränzlein, M.; Rieger, B.; Rivard, E., *Z. Anorg. Allg. Chem.*, **2020**, *646*, 547–551.

(28) Waterman, R., *Organometallics*, **2013**, *32*, 7249–7263.

(29) Yu, C.; Guo, C.; Jiang, L.; Gong, M.; Luo, Y,. *Organometallics*, **2021**, *40*, 1201–1206.

(30) Bauer, T.; Schulz, S.; Hupfer, H.; Nieger, M., *Organometallics*, **2002**, *21*, 2931–2939.

(31) Aldridge, S.; Downs, A. J., *Chem. Rev.*, **2001**, *101*, 3305–3366.

(32) Falconer, R. L.; Nichol, G. S.; Cowley, M. J., *Inorg. Chem.*, **2019**, *58*, 11439–11448.

(33) Itazaki, M.; Ueda, K.; Nakazawa, H., *Angew. Chem. Int. Ed.*, **2009**, *48*, 3313–3316.

Summary and Outlook

Summary and Outlook

This thesis has explored the synthesis and reactivity of bi- and tri-dentate ligand-supported aluminium hydrides and halides.

Chapter 2 reports the preparation of PNP-pincer ligand-supported aluminium dihydrides (^{Ph}PNP)AlH$_2$ (**2.22**) and (^{tBu}PNP)AlH$_2$ (**2.50**). The reactivity of **2.22** towards organic anilines was explored and revealed that upon increasing the steric bulk of the aniline, the single dehydrocoupled product, (^{Ph}PNP)AlH(NHAr), was favoured. The attempted dehydrogenation of **2.22** using Pd(PCy$_3$)$_2$ resulted in formation of (^{Ph}PNP)PdH (**2.38**). However, dihydrogen was observed by ^{1}H NMR spectroscopy indicating dehydrogenation had occurred. The reduction of **2.22** was attempted using [(^{Mes}NacNac)Mg]$_2$. Although the ^{31}P NMR spectrum suggests formation of a single product with inequivalent phosphorus centres, the aluminium-containing product was not identified. Generation of (^{Ph}PNP)AlI$_2$ (**2.48**) and (^{tBu}PNP)AlHI (**2.51**) from the corresponding aluminium dihydrides with trimethylsilyl iodide was also achieved. The reductions of the aluminium iodide species with group 1 metal reducing agents were investigated but the aluminium-containing products were not identified. While the aim of synthesising and isolating low oxidation state aluminium species supported by a ^{R}PNP-ligand system was not realised, several key pieces of information about how this ligand bonds to aluminium has been revealed. This chapter demonstrates that the ^{R}PNP-pincer ligand can chelate to aluminium with a tridentate bonding mode. The pendant phosphorus donors provide a demonstrable steric and electronic effect, evidenced by the different reaction products obtained from the reaction of the dihydrides **2.22** and **2.50** with trimethylsilyl iodide. In addition, the suggestion of lability of phosphorus donor coordination to aluminium has been made based on fluxional behaviour observed in solution in addition to loss of the donor-acceptor interaction in the solid-state structure of **2.35**. In addition to further attempts at the reduction of aluminium iodide species **2.48** and **2.51**, future work related to this chapter could focus on modification of the pincer scaffold. Carbazole ligands have been demonstrated to stabilise aluminium(I) species through the inclusion of bulky substituents in the 1,8-positions of the carbazole unit. Recent advances have demonstrated a direct relationship between the strength of σ-donation and the energy of the lone pair of electrons on a monomeric aluminium(I) species. Therefore, future work may investigate the

effect of different pendant σ-donor groups at aluminium. The inclusion of poorer σ-donor ligands may facilitate a more stabilised aluminium(I) centre, while a stronger σ-donor will result in a more reactive aluminium(I) species.

Chapter 3 studies the use of an NCN-pincer ligand in the preparation of (^{Me}NCN)AlBr$_2$ (**3.18**). Investigations into the reduction of **3.18** using [(^{Mes}NacNac)Mg]$_2$ revealed the reaction proceeds at 60 ˚C to give by-product [(^{Mes}NacNac)MgBr]$_2$. However, the aluminium-containing products were not identified. The reaction of **3.18** and sodium/potassium alloy, NaK, in THF results in the activation of THF and substitution of the donating arm of the ligand to afford dimer [(NCO)AlBr]$_2$ (**3.20**). A proposed mechanism for this reaction was discussed. This chapter highlights the possible side-reactions available to NCN-pincer ligands at the side-arm CH_2-units and the importance of using robust ligand systems for the relatively harsh reducing conditions typically required to access aluminium(I) species. Future work derived from this chapter should focus on the development of novel ligand systems with robust linkers for reactions that require harsh reducing conditions (see section 1.5.2, figure 1.11, **Y**). Replacing the benzylic CH_2-linkers with a more substituted linker (e.g. CMe_2) may prevent the undesirable side-reactions observed during reduction.

Chapter 4 explores the preparation of novel diphosphine ligands {SiP^{Tipp}}H$_2$ (**4.4**) and {SiP^{Mes*}}H$_2$ (**4.5**). Attempts to deprotonate diphosphine ligands **4.4** and **4.5** using ClAlMe$_2$ and AlMe$_3$ were unsuccessful, instead resulting in the formation of adducts **4.7** – **4.11**, in which the diphosphine acts as a Lewis base. Deprotonation of **4.4** and **4.5** was achieved using n-butyllithium, KHMDS or benzylpotassium to afford the corresponding lithium or potassium diphosphides. Aluminium bromide {SiP^{Tipp}}AlBr(THF) (**4.14**) was synthesised from {SiP^{Tipp}}K$_2$ and AlBr$_3$•NEt$_3$ and subsequently reacted with dimethylaminopyridine (DMAP) to give {SiP^{Tipp}}AlBr(DMAP) (**4.15**). Preliminary investigations into the reductions of **4.14** and **4.15** were conducted and reactivity towards group 1 metal reducing agents was observed, but the products were not identified. Research into the preparation of diphosphide-supported aluminium hydride species was also conducted, reacting lithium diphosphides **4.12** and **4.16** with AlH$_3$•NMe$_3$. The solid-state structure of {SiP^{Tipp}}AlH$_2$Li•(THF)$_2$ (**4.20**) reveals the first structural evidence of the coordination of these diphosphide ligands to an aluminium centre. Further work should focus on the synthesis of the aluminium hydride species {SiP^{Ar}}AlH which can then undergo substitution of the hydride ligand to give the corresponding aluminium

halide species, followed by investigations into reactivity towards reducing agents. In contrast to the now widespread chemistry of diamide ligands, well-defined bulky diphosphide ligands are rare. The coordination chemistry of the diphosphide ligands reported in this chapter may be explored at other metal centres, in particular for the low oxidation state chemistry of the p-block elements.

In the past 25 years, there has been a surge in interest towards novel ligand systems capable of providing unusual stabilising and destabilising effects to main group element centres. Multidentate ligands are capable of providing significant control over the geometry, electronic and steric properties, and reactivity of a metal centre. In addition to the future work discussed with each chapter summary, this work seeks to highlight the importance of further investigation and development of novel ligand systems at main group elements.

The design of future ligand systems should seek to promote greater control over the reactivity of metal centres. The stabilisation of reactive metal species using sterically demanding ligands has seen considerable success in the last 30 years by providing control over the coordination sphere of the metal centre. An alternate approach to controlling the reactivity of the metal centre may lie in the introduction of ligands with greater denticity, allowing for finer tuning of the steric and electronic environment of the metal centre. Monodentate and bidentate ligands dominate the field of main group chemistry. In contrast, the ability of tridentate ligands to stabilise reactive main group element centres has not yet been fully realised. The development of tridentate ligand systems could lead to the introduction of hemilabile coordination of the metal centre, akin to those already well-established in transition metal chemistry. Strategies to incorporate this bonding motif will involve a combination of weak σ-donors and flexible linkers, aiding the dissociation and re-association of neutral donors. These ligand systems may play a defining role in the progression of reversible redox chemistry within the main group elements through dynamic interactions allowing changes to the coordination sphere of the metal centre *in situ*. Therefore, further studies into multidentate ligand systems are vital for promoting greater understanding of the effects ligands have on metal centres and the advancement of main group chemistry.

Chapter 5

Experimental Methods

5.1 General Considerations

All manipulations were carried out under an argon atmosphere using standard Schlenk or glovebox techniques. Solvents were obtained from an Inert solvent purification system or distilled under argon from sodium and benzophenone and stored over 4 Å molecular sieves. Deuterated solvents were distilled from potassium and stored over 4 Å sieves.

NMR spectra were recorded on Bruker PRO 500 MHz, AVA 600 MHz, AVA 500 MHz, or AVA 400 MHz spectrometers. ^{1}H and ^{13}C NMR spectra were referenced to residual solvent signals.[1] ^{31}P NMR spectra were referenced to 85% H_3PO_4 in D_2O as an external standard. ^{29}Si NMR spectra were referenced to an external standard of tetramethylsilane ($SiMe_4$). All IR spectra are of solid-state samples and were recorded on SHIMADZU IRSpirit FTIR spectrophotometer. Elemental analysis was performed by Stephen Boyer at London Metropolitan University or Elemental Microanalysis Ltd. Mass spectrometry was performed by Alan Taylor at the University of Edinburgh.

The following compounds were prepared according to literature procedures: trimethylamine-alane adduct (AlH_3•NMe_3),[2] (^{Ph}PNP)H (**2.19**),[3] di-*tert*-butylphosphine (*t*Bu_2PH),[4] ($^{t\text{Bu}}$PNP)H (**2.20**),[5] bis-(tricyclohexylphosphine)palladium ($Pd(PCy_3)_2$),[6] [(^{Mes}NacNac)Mg]$_2$,[7] (^{Me}NCN)H (**3.17**),[8] tri*iso*propylphenylphosphine ($TippPH_2$),[9] and Tri-*tert*-butylphenylphosphine (Mes^*PH_2).[10]

Trimethylsilyl iodide was distilled under argon from copper wire prior to use.

5.2 Experimental Details for Chapter 2

5.2.1 Generation of (^{Ph}PNP)Li (2.21)

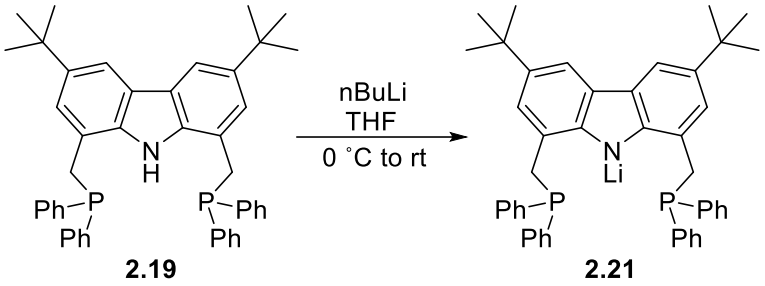

2.19 **2.21**

A solution of (^{Ph}PNP)H (**2.19**, 200 mg, 0.30 mmol) in THF (35 mL) was cooled to 0 ˚C, to which a solution of nBuLi (2.5 M in hexanes, 0.15 mL, 0.35 mmol) was added dropwise to give an orange solution. After 25 minutes stirring at 0 ˚C, the solution was allowed to warm to room temperature and was stirred for a further 15 minutes to generate (^{Ph}PNP)Li (**2.21**) *in situ*. The solution of **2.21** was used in subsequent reactions with $ClAlH_2$•NMe_3 from which colourless crystals were obtained from a concentrated toluene solution at room temperature. X-ray diffraction revealed **2.21** co-crystallised with **2.19** in a 1:1 ratio.

^{31}P NMR (162.0 MHz, THF-d_8, 300 K): δ −10.5

5.2.2 Synthesis of (^{Ph}PNP)AlH_2 (2.22)

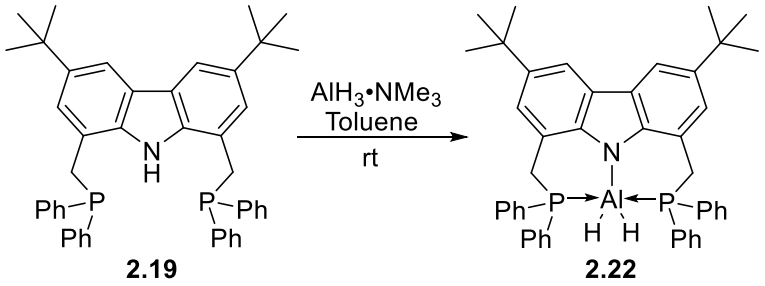

2.19 **2.22**

A solution of (^{Ph}PNP)H (500 mg, 0.74 mmol) in 20 mL toluene was added to AlH_3•NMe_3 (80 mg, 0.89 mmol) at room temperature and stirred for 5 days. The solution was filtered, and all volatiles removed under vacuum. The residue was washed with pentane and dried *in vacuo* to yield (^{Ph}PNP)AlH_2 as a colourless solid (476 mg, 91%).

^{1}H NMR (500.2 MHz, C_6D_6, 300 K): δ 8.12 (C^{carb}***H***, d, *J* = 1.79 Hz, 2 H), 7.43 (o-Ar ***H***, m, 8 H), 7.09 (m-,p-Ar ***H***, m, 12 H), 6.85 (C^{carb}***H***, d, *J* = 1.52, 2 H), 5.84 (Al***H***, t, $^{2}J_{H-P}$ = 56 Hz, 2 H), 4.11 ($C\boldsymbol{H_2}PPh_2$, s, 4 H), 1.40 ($C(C\boldsymbol{H_3})_3$, s, 18 H).

^{13}C{^{1}H} NMR (125.8 MHz, C_6D_6, 300 K): δ 31.7 ($C(\boldsymbol{C}H_3)_3$, s), 31.9 ($\boldsymbol{C}H_2$, m), 34.0 ($\boldsymbol{C}(CH_3)_3$, s), 114.6 ($\boldsymbol{C}^{carb}$H, s), 118.8 ($\boldsymbol{C}^{carb}CH_2$, m), 125.6 ($\boldsymbol{C}^{carb}$H, m), 127.3 ($\boldsymbol{C}^{carb}$, s), 128.3 ($\boldsymbol{C}^{m\text{-}Ph}$H, m), 129.6 ($\boldsymbol{C}^{p\text{-}Ph}$H, s), 130.7 ($\boldsymbol{C}^{i\text{-}Ph}$, m), 133.1 ($\boldsymbol{C}^{o\text{-}Ph}$H, m), 140.1 ($\boldsymbol{C}^{carb}$, s), 144.9 ($\boldsymbol{C}^{carb}C(CH_3)_3$, s).

^{31}P{^{1}H} NMR (202.5 MHz, C_6D_6, 300 K): δ −33.5

IR (solid): 1751 cm^{-1} (Al–H stretch)

Mass Peak Analysis: Calculated mass for $C_{46}H_{48}NP_2Al$ for most abundant isotopes: 703.30720 Da. Observed mass peak: 703.30817 Da

Elemental Analysis: Calc. for $C_{46}H_{48}NP_2Al$ (%): C, 78.50; H, 6.87; N, 1.99. Found: C, 78.42; H, 6.74; N, 1.98.

5.2.3 Reaction of (^{Ph}PNP)AlH_2 (2.22) with Aniline

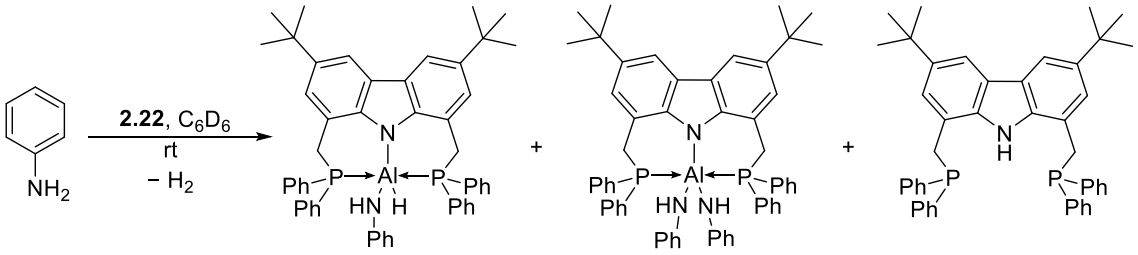

$PhNH_2$ (1.95 µL, 21.3 µmol) was added to (^{Ph}PNP)AlH_2 (**2.22**, 15.0 mg, 21.3 µmol) in C_6D_6 at room temperature and evolution of H_2 was observed. The products (^{Ph}PNP)AlH(NHPh) (**2.23**) and (^{Ph}PNP)Al$(NHPh)_2$ (**2.24**) observed by NMR spectroscopy.

^{1}H NMR (500.2 MHz, C_6D_6, 300 K):* δ 8.19 (N***H***, br s, 1 H), 8.16 (C^{carb}***H***, d, J_{H-P} = 1.7 Hz, 2 H), 7.29 (Ar-***H***, m, 8 H), 6.46 – 6.56 (Ar-***H***, m, 8 H), 1.38 ($C(C\boldsymbol{H_3})_3$, s, 18 H). *resonances given are for products **2.23** or **2.24**. Not all environments assigned due to overlapping resonances.

^{31}P NMR (202.5 MHz, C_6D_6, 300 K): δ −33.5 (**2.22**, t, $^2J_{H–P}$ = 60.3 Hz, 19%), −31.1 (**2.23**, d, $^2J_{H–P}$ = 55.0 Hz, 19%), −26.8 (**2.24**, s, 7%), −18.1 (**2.19**, s, 55%)

5.2.4 Reaction of (^{Ph}PNP)AlH_2 (2.22) with 2,4,6-trimethylaniline

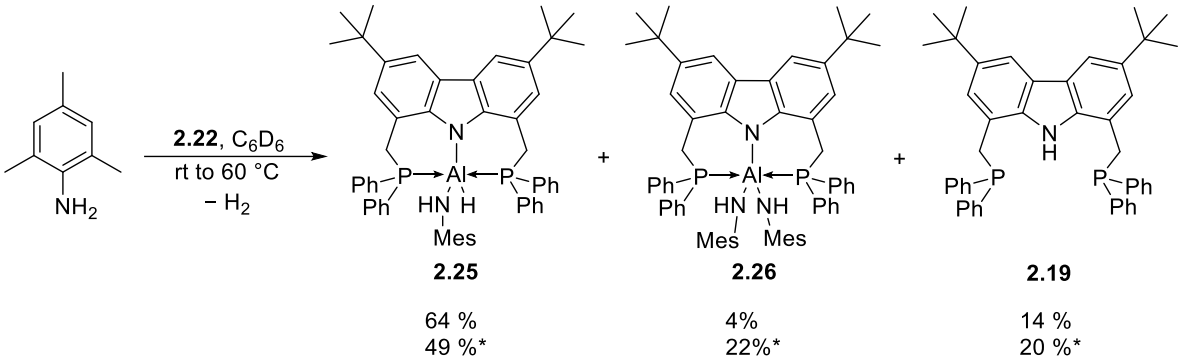

$MesNH_2$ (2.8 µL, 19.9 µmol) was added to a C_6D_6 solution of (^{Ph}PNP)AlH_2 (**2.22**, 14 mg, 19.9 µmol) at room temperature. After 24 hours at room temperature, the solution was heated to 60 °C for 3 days. The products, (^{Ph}PNP)AlH(NHMes) (**2.25**) and (^{Ph}PNP)Al(NHMes)$_2$ (**2.26**), were observed by NMR spectroscopy and ratios of products are given before and after (*) heating.

^{1}H NMR (500.2 MHz, C_6D_6, 300 K): * δ 8.26 (N***H***, br s, 1 H), 8.16 (C^{carb}***H***, d, $J_{H–P}$ = 1.6 Hz, 2 H), 4.15 (C***H*$_2$, br s, 4 H), 2.16 (*p*-C***H*$_3$, s, 3 H), 2.02 (*o*-C***H*$_3$, s, 6 H), 1.38 (C(C***H*$_3$)$_3$, s, 18 H). * Resonances given are for product **2.25**, not all environments are assigned due to overlapping resonances.

^{31}P NMR (202.5 MHz, C_6D_6, 300 K): δ −33.5 (**2.22**, t, $^2J_{H–P}$ = 60.8 Hz, 18%, 0%*), −31.1 (**2.25**, d, $^2J_{H–P}$ = 51.3 Hz, 64%, 49%*), −26.8 (**2.26**, s, 4%, 22%*), −18.1 (**2.19**, s, 55%, 20%*).

5.2.5 Reaction of (^{Ph}PNP)AlH$_2$ (2.22) with 2,6-Di*iso*propylaniline

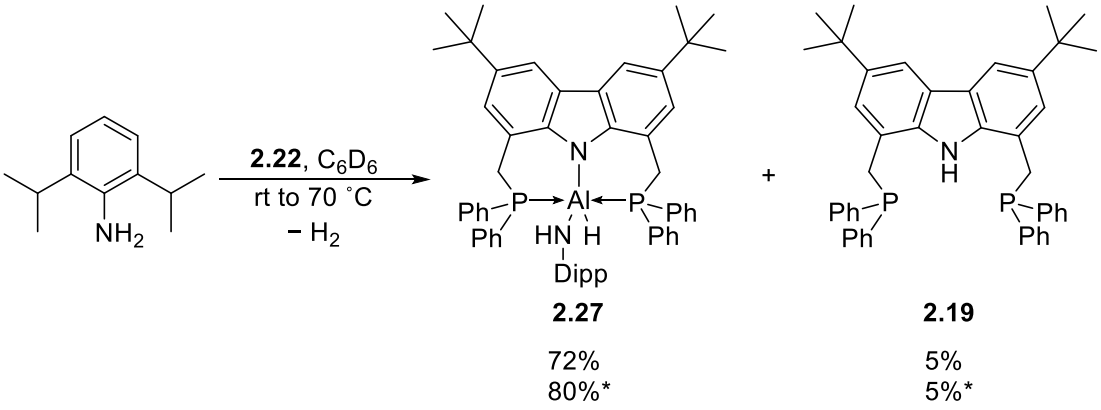

DippNH$_2$ (4.0 µL, 21.3 µmol) was added to a solution of (^{Ph}PNP)AlH$_2$ (**2.22**, 15.0 mg, 21.3 µmol) in C_6D_6 and, after 48 hours at room temperature, the mixture was heated to 70 °C for three hours. The product, (^{Ph}PNP)AlH(NHDipp) (**2.27**), was observed by NMR spectroscopy and their ratios given before and after ($^{\#}$) heating.

^{1}H NMR (500.2 MHz, C_6D_6, 300 K):* δ 8.07 (**2.27**, C^{carb}***H***, d, $J_{H–P}$ = 1.4 Hz, 2 H), 7.35 (**2.27**, Ar-*H*, m, 8 H), 7.11 (**2.27**, C^{carb}***H***, s, 2 H), 7.04 (**2.27**, Ar-***H***, m, 3 H), 6.92 (**2.27**, Ar-*H*, m, 12 H), 5.83 (**2.27**, Al***H***, br s, 1 H), 4.05 (**2.27**, C***H*$_2$**, d, $^{2}J_{H–P}$ = 2.8 Hz, 4 H), 3.08 (**2.27**, C*H*(CH$_3$)$_2$, sept, $^{3}J_{H–H}$ = 6.5, 2 H), 1.36 (**2.27**, C(C***H*$_3$**)$_3$, s, 18 H), 0.94 (**2.27**, CH(C***H*$_3$**)$_2$, d, $^{3}J_{H–H}$ = 6.6 Hz, 12 H). *N***H*** resonance not observed.

^{31}P NMR (202.5 MHz, C_6D_6, 300 K): δ −33.5 (**2.22**, t, $^{2}J_{H–P}$ = 58.0 Hz, 23%, 7%*), −27.8 (**2.27**, d, $^{2}J_{H–P}$ = 41.1 Hz, 72%, 80%*), −18.1 (**2.19**, s, 5%, 5%*).

5.2.6 Reaction of (^{Ph}PNP)AlH$_2$ (2.22) with 4-(Trifluoromethyl)aniline

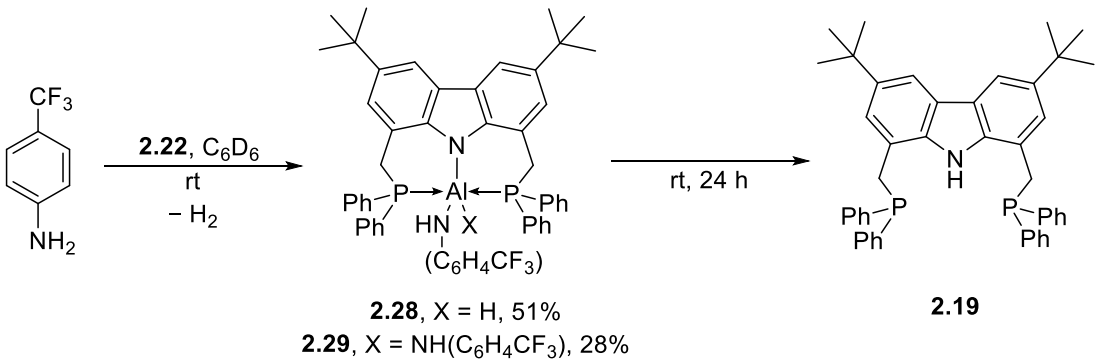

A C_6D_6 solution of (^{Ph}PNP)AlH_2 (15.0 mg, 21.3 µmol) was treated with 4-(CF_3)$C_6H_4NH_2$ (2.7 µL, 21.3 µmol) at room temperature and the products, (^{Ph}PNP)$AlH(NHC_6H_4CF_3)$ (**2.28**) and (^{Ph}PNP)$Al(NHC_6H_4CF_3)_2$ (**2.29**), were observed by NMR spectroscopy after one hour. After 24 hours, only (^{Ph}PNP)H (**2.19**) and unidentified by-products were observed.

^{1}H NMR (500.2 MHz, C_6D_6, 300 K):* δ 1.38 (C(C***H*₃**)₃ of **2.28**, s), 1.35 (C(C***H*₃**)₃ of **2.29**, s). *Due to overlapping resonances, only select resonances could be assigned.

^{31}P NMR (202.5 MHz, C_6D_6, 300 K): δ −33.5 (**2.22**, t, $^2J_{H-P}$ = 55.1 Hz, 9%), −32.1 (**2.28**, d, $^2J_{H-P}$ = 59.4 Hz, 51%), −27.7 (**2.29**, s, 28%), −18.1 (**2.19**, s, 25%).

^{19}F NMR (202.5 MHz, C_6D_6, 300 K): δ −60.5 (**2.29**), −60.2 (**2.28**)

5.2.7 Reaction of $(PNP)AlH_2$ (2.22) with 4-Cyanoaniline

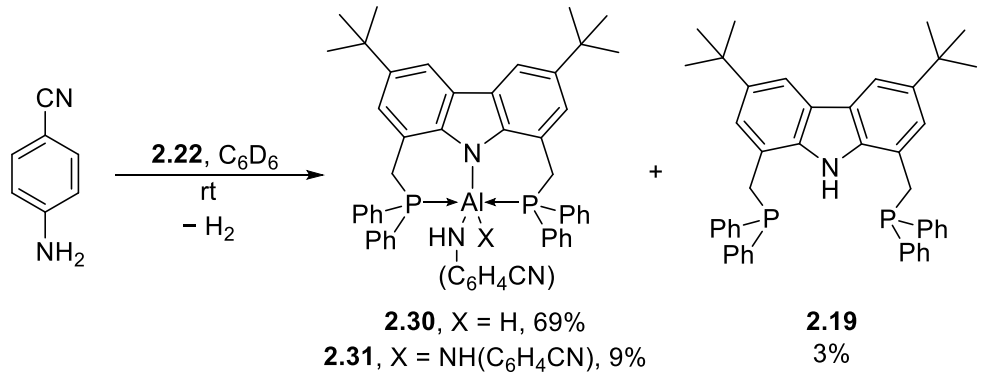

A C_6D_6 solution of (^{Ph}PNP)AlH_2 (**2.22**, 15.0 mg, 21.3 µmol) was added to $H_2NC_6H_4CN$ (2.5 mg, 21.3 µmol) at room temperature and the products (^{Ph}PNP)$AlH(NHC_6H_4CN)$ (**2.30**) and (^{Ph}PNP)$Al(NHC_6H_4CN)_2$ (**2.31**) were observed by NMR spectroscopy.

^{1}H NMR (500.2 MHz, C_6D_6, 300 K):* δ 8.24 (N***H***, br s, 1 H), 8.19 (C^{carb}***H***, d, J_{H-P} = 1.8 Hz, 2 H), 7.29 (Ar-***H***, br s, 8H), 7.10 (C^{carb}***H***, s, 2 H), 6.73 (Ar-***H***, d, $^3J_{H-H}$ = 9.4 Hz, 2 H), 6.07 (Ar-***H***, d, $^3J_{H-H}$ = 9.1 Hz), 3.66 (C***H*₂**, s, 4 H), 1.38 (C(C***H*₃**)₃, s, 18 H). *Only resonances for **2.30** are reported. Due to overlapping resonances not all aryl protons could be assigned.

^{31}P NMR (202.5 MHz, C_6D_6, 300 K): δ −33.5 (**2.22**, t, $^2J_{H-P}$ = 61.8 Hz, 19%), −32.4 (**2.30**, d, $^2J_{H-P}$ = 63.5 Hz, 69%), −28.1 (**2.29**, s, 9%), −18.1 (**2.19**, s, 3%).

5.2.8 Reaction of (PNP)AlH_2 (2.22) with 4-Cyano-2,6-dimethylaniline

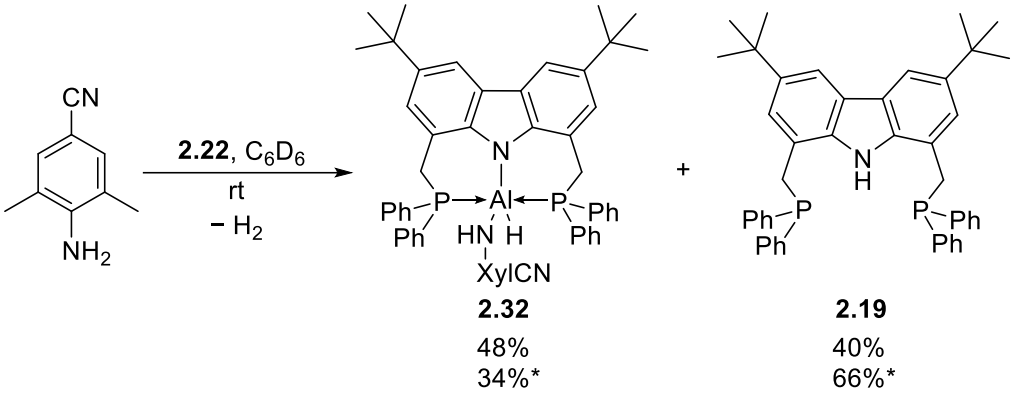

A C_6D_6 solution of (PNP)AlH_2 (**2.22**, 15.0 mg, 21.3 µmol) was added to H_2N(XylCN) (3.1 mg, 21.3 µmol) at room temperature. After three days, the reaction was heated to 60 ˚C for 15 hours and upon cooling to room temperature a precipitate formed. The product (^{Ph}PNP)AlH(NH{XylCN}) (**2.32**) was observed by NMR spectroscopy. The ratios of observed phosphorus environments, before and after ($^{\#}$) heating, are only indicative of species in solution.

^{1}H NMR (500.2 MHz, C_6D_6, 300 K): * δ 1.45 (**2.32**, C(C***H*₃**)₃, s, 18 H), 1.73 (**2.32**, *o*-C***H*₃**, s, 6 H).
*Only selected proton environments could be assigned due to overlapping and broadening of resonances.

^{31}P NMR (202.5 MHz, C_6D_6, 300 K): δ −33.5 (**2.22**, t, $^2J_{H-P}$ = 60.6 Hz, 11%, 0%$^{\#}$), −30.8 (**2.30**, d, $^2J_{H-P}$ = 56.6 Hz, 48%, 34%$^{\#}$), −18.1 (**2.19**, s, 40%, 66%$^{\#}$).

5.2.9 Reaction of (PNP)AlH_2 (2.22) with 2,6-Xylylisonitrile

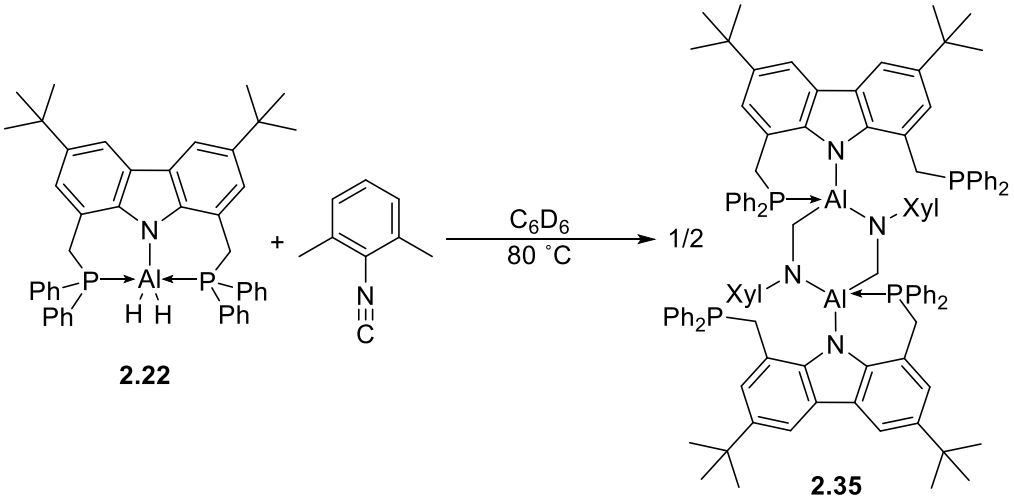

(PNP)AlH_2 (15 mg, 21.3 µmol) was dissolved in C_6D_6 and added to XylCN (2.8 mg, 21.3 µmol) and the mixture was heated to 80 °C for one hour. A colour change from colourless to dark orange was observed. The ^1H and ^{31}P NMR spectra revealed a complex mixture of products and could not be assigned. A colourless crystal was obtained by slow evaporation of a toluene solution of the reaction mixture and the structure of [(^{Ph}PNP)AlN(Xyl)CH_2]$_2$ (**2.35**) was determined by X-ray crystallography. However, insufficient material prevented characterisation by NMR spectroscopy.

5.2.10 Reaction of (PNP)AlH_2 (2.22) with $Pd(PCy_3)_2$

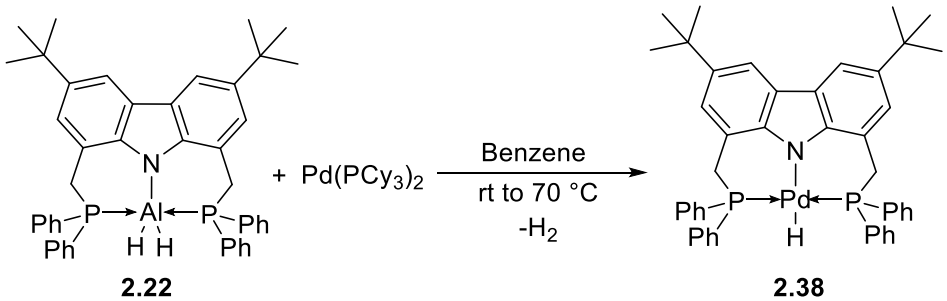

(^{Ph}PNP)AlH_2 (**2.22**, 60 mg, 85.2 µmol) in 3 mL benzene was added to $Pd(PCy_3)_2$ (57 mg, 85.2 µmol) at room temperature resulting in a dark brown solution. The NMR spectrum of an aliquot of the crude reaction mixture was taken revealing the formation of a complex mixture of products. After two days, the solution filtered and the solid was dissolved in a minimal

amount of benzene. The solution was heated to 70 ˚C and cooled slowly to afford a few colourless X-ray quality crystals of (^{Ph}PNP)PdH (**2.38**).

5.2.11 Independent Generation of (^{Ph}PNP)PdH (2.38)

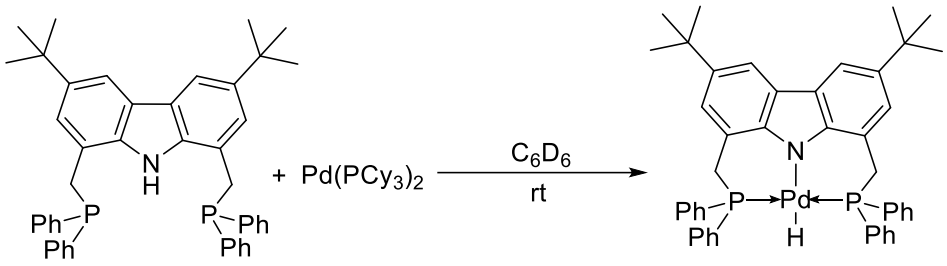

2.22 **2.38**

A C_6D_6 solution of (^{Ph}PNP)H (**2.19**) (15 mg, 22.2 µmol) was added to $Pd(PCy_3)_2$ (15 mg, 22.2 µmol) at room temperature. A colour change from colourless to yellow was observed, which turned orange over three days. The generation of (^{Ph}PNP)PdH (**2.38**) was observed by NMR spectroscopy.

^{1}H NMR (500.2 MHz, C_6D_6, 300 K): δ 8.37 (C^{carb}***H***, d, *J* = 1.47 Hz, 2 H), 7.63 (o-Ar ***H***, m, 8 H), 7.23 (C^{carb}***H***, s, 2 H), 6.93 (m-,p-Ar ***H***, m, 12 H), 3.79 (C***H***$_2$, t, *J* = 2.7 Hz, 4 H), 1.52 ($C(C$***H***$_3)_3$, s, 18 H), −10.9 (Pd***H***, s, 1 H).

^{31}P NMR (202.5 MHz, C_6D_6, 300 K): δ 40.7

5.2.12 Attempted Reduction of (PNP)AlH_2 (2.22) with [(^{Mes}NacNac)Mg]$_2$

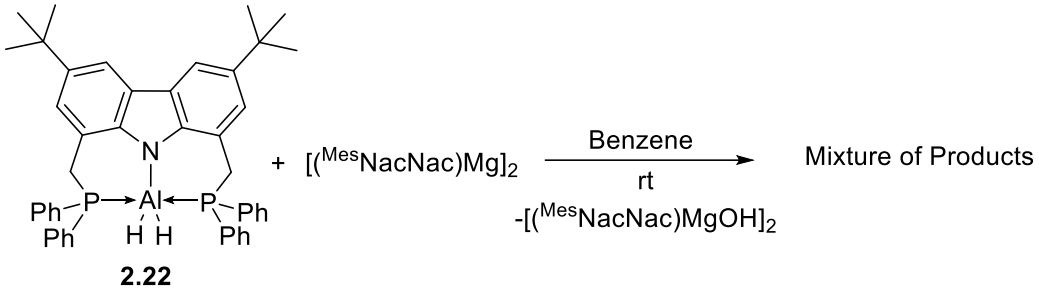

2.22

(PNP)AlH_2 (500 mg, 0.71 mmol) was dissolved in benzene (50 mL) and added to [(CH{C(Me)N(Mes)}$_2$)Mg]$_2$ (508 mg, 0.71 mmol) at room temperature and stirred for 48 hours. The volatiles were removed under reduced pressure and the residue dissolved in 5 mL benzene and filtered. The filtrate was concentrated to ca. 1 mL and hexane (15 mL) was added. After filtration, all volatiles were removed under vacuum. Pentane (12 mL) was added, the solution was filtered and concentrated to ca. 4 mL and cooled to −20 °C.

The aluminium containing product was not isolated or identified. However, [(^{Mes}NacNac)MgOH]$_2$ (**2.43**) was identified by X-ray diffraction as the by-product. The ^{1}H NMR spectrum of the reaction mixture revealed a complex mixture of products and could not be assigned. The ^{31}P NMR spectrum contains two singlets for the phosphorus-containing product.

The reaction was repeated using 0.5 equivalent of [(CH{C(Me)N(Mes)}$_2$)Mg]$_2$: A C_6D_6 solution of (^{Ph}PNP)AlH_2 (**2.22**, 15.0 mg, 21.3 µmol) was added to [(CH{C(Me)N(Mes)}$_2$)Mg]$_2$ (7.6 mg, 10.7 µmol). The ^{31}P NMR spectrum consisted of the same signals as seen for the reaction with one equivalent of [(^{Mes}NacNac)Mg]$_2$, along with a resonance at −33.5 ppm for unreacted aluminium dihydride **2.22**.

^{31} P NMR (202.5 MHz, C_6D_6, 300 K): δ −26.3, −14.1

5.2.13 Generation of (^{Ph}PNP)K (2.46)

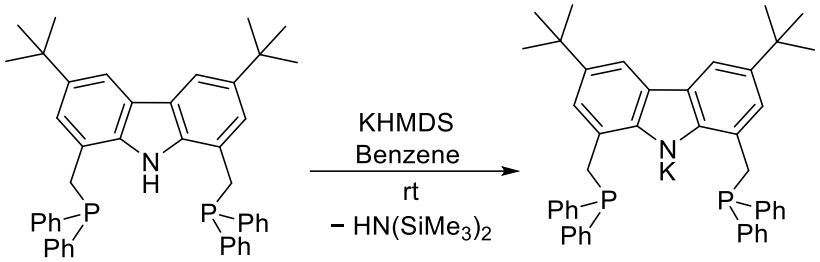

2.19 **2.46**

To KHMDS (89 mg, 0.44 mmol) was added a solution of (^{Ph}PNP)H (**2.19**) (200 mg, 0.30 mmol) in benzene (15 mL) at room temperature. The solution was stirred for 75 minutes and the resulting precipitate was allowed to settle overnight. The solution was filtered, and the precipitate dried to give (^{Ph}PNP)K (**2.46**) as a yellow solid (172 mg, 82%).

^{1}H NMR (500.2 MHz, THF-d$_8$, 300 K): δ 7.79 (C^{carb}***H***, t, *J* = 1.8 Hz, 2 H), 7.60 (o-Ar ***H***, m, 8 H), 7.29 (m-,p-Ar ***H***, m, 12 H), 6.68 (C^{carb}***H***, t, *J* = 2.2, 2 H), 4.08 (C***H*****$_2$**PPh$_2$, d, *J* = 3.3 Hz, 4 H), 1.24 (C(C***H*****$_3$**)$_3$, s, 18 H).

^{31}P NMR (202.5 MHz, THF-d$_8$, 300 K): δ −13.2

5.2.14 Synthesis of (PNP)AlBr$_2$ (2.47)

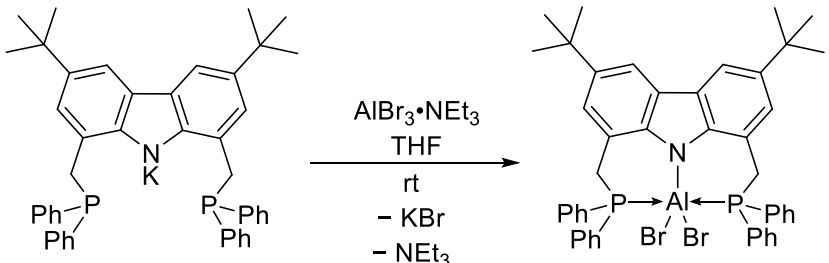

2.46 **2.47**

In a glovebox, (^{Ph}PNP)K (**2.46**) (200 mg, 0.28 mmol) was dissolved in 10 mL THF, to which a solution of AlBr$_3$•NEt$_3$ (103 mg, 0.28 mL) in 5 mL THF was added dropwise at ambient temperature. After stirring for 22 hours, the volatiles were removed under vacuum and the residue was dissolved in 20 mL toluene and stirred vigorously for 20 minutes. The solution was filtered and the precipitate washed with toluene (2 x 5 mL). The combined filtrate and washings were concentrated to ca. 1 mL and cooled to −30 °C overnight. The solid was isolated and washed with hexane (2 x 0.5 mL) to give (^{Ph}PNP)AlBr$_2$ (**2.47**) as a colourless solid. The

combined filtrate and washings were further concentrated and cooled to −30 °C to afford a second crop of (^{Ph}PNP)AlBr$_2$ (**2.47**) as a colourless solid (101 mg, 42% combined).

^{1}H NMR (500.2 MHz, C_6D_6, 300 K): δ 8.19 (C^{carb}***H***, d, *J* = 1.5 Hz, 2 H), 7.59 (o-Ar ***H***, br. s, 8 H), 7.14 (C^{carb}***H***, d, *J* = 1.1 Hz, 2 H), 6.78 (m-,p-Ar ***H***, br. s, 12 H), 4.35 (C***H*****$_2$**PPh$_2$, br. s, 4 H), 1.38 (C(C***H*****$_3$**)$_3$, s, 18 H).

^{13}C{^{1}H} NMR (125.8 MHz, C_6D_6, 300 K): δ 31.5 (***C***H$_2$, m), 31.9 (C(***C***H$_3$)$_3$, s), 34.4 (***C***(CH$_3$)$_3$, s), 115.2 (***C*****^{carb}**H, s), 118.4 (***C*****^{carb}**CH$_2$, s), 125.7 (***C*****^{carb}**H, s), 126.8 (***C*****^{carb}**, m), 128.6 (***C*****^{Ph}**H, m), 129.1 (***C*****^{Ph}**H, s), 129.3 (***C*****^{Ph}**, m), 133.1 (***C*****^{Ph}**H, m), 140.1 (***C*****^{carb}**, s), 144.9 (***C*****^{carb}**C(CH$_3$)$_3$, s).

^{31}P NMR (202.5 MHz, C_6D_6, 300 K): δ −35.0

Mass Peak Analysis: Calculated mass for $C_{46}H_{46}NP_2AlBr_2$ for most abundant isotopes: 859.12822 Da. Observed mass peak: 859.12712 Da.

5.2.15 Generation of (^{Ph}PNP)AlI$_2$ (2.48)

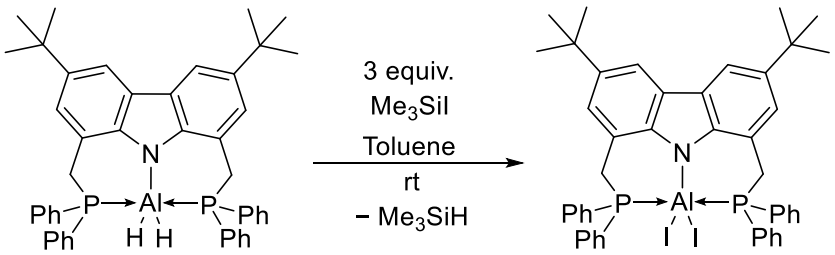

2.22 **2.48**

Me$_3$SiI (0.18 mL, 1.28 mmol) was added at room temperature to (^{Ph}PNP)AlH$_2$ (300 mg, 0.43 mmol) solution in 20 mL toluene and stirred for 16 days. All volatiles were removed under reduced pressure to give (^{Ph}PNP)AlI$_2$ (**2.48**) as an off-white solid, which was used immediately in subsequent reactions without further purification.

^{1}H NMR (500.2 MHz, C_6H_6, 300 K): δ 8.23 (C^{carb}***H***, d, *J* = 1.5 Hz, 2 H), 7.60 (o-Ar ***H***, br. s, 8 H), 7.11 (C^{carb}***H***, s, 2 H), 6.83 (m-,p-Ar ***H***, br. s, 12 H), 1.36 (C(C***H*****$_3$**)$_3$, s, 18 H).

^{13}C{^{1}H} NMR (125.8 MHz, C_6D_6, 300 K): δ 31.9 (C(***C***H$_3$)$_3$, s), 32.1 (***C***H$_2$, m), 34.4 (***C***(CH$_3$)$_3$, s), 115.1 (***C*****^{carb}**H, s), 118.4 (***C*****^{carb}**CH$_2$, s), 125.8 (***C*****^{carb}**, s), 127.1 (***C*****^{carb}**H, m), 128.5 (***C*****^{Ph}**H, s), 129.3 (***C*****^{Ph}**H, s), 130.6 (***C*****^{Ph}**H, s), 134.4 (***C*****^{Ph}**, m), 142.3 (***C*****^{carb}**, s), 144.9 (***C*****^{carb}**C(CH$_3$)$_3$, s).

^{31}P NMR (202.5 MHz, C_6D_6, 300 K): δ −33.8

5.2.16 Attempted Reduction of (^{Ph}PNP)AlI$_2$ (2.48) with KC$_8$

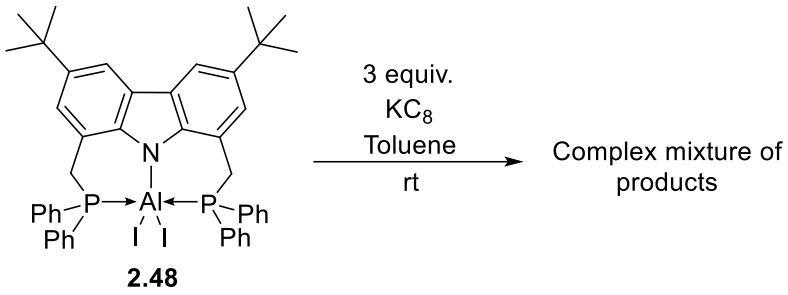

2.48

(^{Ph}PNP)AlH$_2$ (**2.22**) (300 mg, 0.43 mmol) was dissolved in toluene (20 mL) and was treated with Me$_3$SiI (0.18 mL, 1.28 mmol) at ambient temperature and stirred for 14 days to generate (^{Ph}PNP)AlI$_2$ (**2.48**). The volatiles were removed under reduced pressure, the residue dissolved in toluene (20 mL), and added to KC$_8$ (173 mg, 1.28 mmol) at room temperature. The suspension was stirred for 16 days and then the solution was collected *via* filtration. The volatiles were removed under vacuum to give a yellow solid. NMR analysis of the solid obtained revealed a complex mixture of products which could not be identified.

5.2.17 Synthesis of (^{tBu}PNP)AlH$_2$ (2.50)

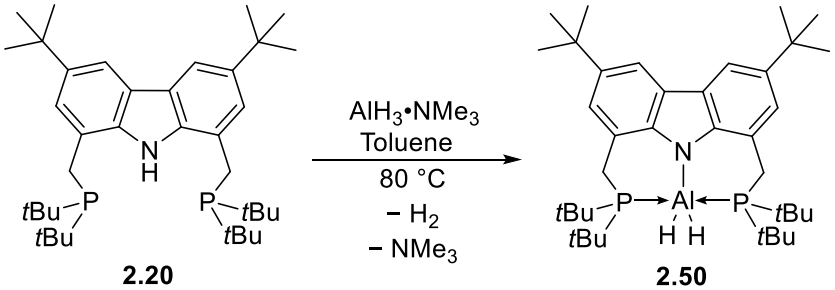

2.20 **2.50**

A solution of (^{tBu}PNP)H (**2.20**, 1.00 g, 1.68 mmol) in 35 mL toluene was added to AlH$_3$•NMe$_3$ (195 mg, 2.18 mmol) and the solution heated to 80 °C for 4 days. The solution was then filtered and all volatiles removed under reduced pressure. To the residue was added 20 mL pentane and the resulting solution was filtered. The filtrate was concentrated under vacuum to attain (^{tBu}PNP)AlH$_2$ (**2.50**) as a colourless solid (865 mg, 83%).

^{1}H NMR (500.2 MHz, C_6D_6, 300 K): δ 8.28 (C^{carb}***H***, d, *J* = 2.0 Hz, 2 H), 7.75 (C^{carb}***H***, s, 2 H), 5.32 (Al***H***, br. s, 2 H), 3.62 (C***H***$_2$, d, *J* = 3.9 Hz, 4 H), 1.54 (C(C***H***$_3$)$_3$, s, 18 H), 1.11 (PC(C***H***$_3$)$_3$, d, *J* = 11.8 Hz, 36 H).

^{13}C{^{1}H} NMR (125.8 MHz, C_6D_6, 300 K): δ 29.4 (PC(***C***H$_3$)$_3$, d, J_{P-C} = 7.2 Hz), 32.3 (C(***C***H$_3$)$_3$, s), 32.6 (P***C***(CH$_3$)$_3$, d, J_{P-C} = 4.0 Hz), 34.8 (***C***H$_2$, s), 46.6 (***C***(CH$_3$)$_3$, s), 114.7 ($\boldsymbol{C}^{carb}$H, s), 121.7 ($\boldsymbol{C}^{carb}$CH$_2$, s), 125.5 ($\boldsymbol{C}^{carb}$H s), 127.1 ($\boldsymbol{C}^{carb}$, s), 141.1 ($\boldsymbol{C}^{carb}$, s), 146.1 ($\boldsymbol{C}^{carb}$C(CH$_3$)$_3$, s).

^{31}P NMR (202.5 MHz, C_6D_6, 300 K): δ 8.3

IR (solid): 1791 cm^{-1} (Al–H stretch)

Mass Peak Analysis: Calculated mass for $C_{38}H_{64}NP_2Al$ for most abundant isotopes: 623.43240 Da. Observed mass peak: 623.43149 Da.

5.2.18 Generation of (^{tBu}PNP)AlHI (2.51)

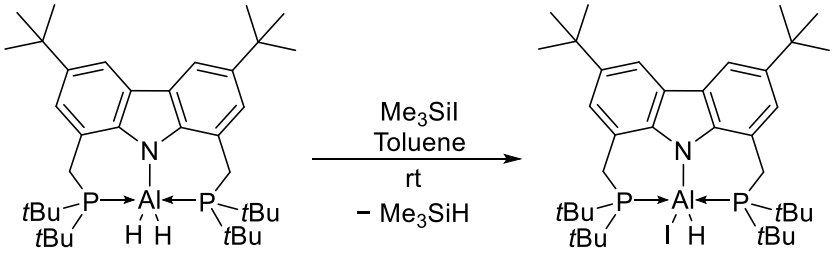

(^{tBu}PNP)AlH$_2$ (**2.50**, 500 mg, 0.80 mmol) was dissolved in 15 mL toluene to which Me$_3$SiI (0.34 mL, 2.40 mmol) was added dropwise at room temperature. The solution was stirred for seven days and all volatiles removed under reduced pressure to give (^{tBu}PNP)AlHI (**2.51**) as an off-white solid which was used in reduction reactions without further purification.

^{1}H NMR (400.1 MHz, C_6D_6, 300 K): δ 8.15 (C^{carb}***H***, s, 2 H), 7.77 (C^{carb}***H***, s, 2 H), 6.04 (Al***H***, br. s, 1 H), 3.77 (C***H***$_2$, d, *J* = 14.7 Hz, 2 H), 3.54 (C***H***$_2$, br. m, 2 H), 1.49 (C(C***H***$_3$)$_3$, s, 18 H), 1.29 (PC(C***H***$_3$)$_3$, d, *J* = 12.3 Hz, 18 H), 0.99 (PC(C***H***$_3$)$_3$, d, *J* = 12.3 Hz, 18 H).

^{31}P NMR (162.0 MHz, C_6D_6, 300 K): δ 9.8

5.2.19 Reduction of (^{tBu}PNP)AlHI (2.51) with KC_8

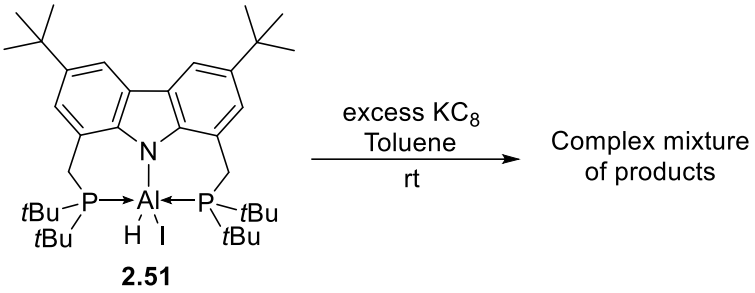

2.51

Me_3SiI (0.35 mL, 2.40 mmol) was added dropwise to a solution of (^{tBu}PNP)AlH_2 (**2.50**, 500 mg, 0.80 mmol) in 15 mL toluene and stirred at room temperature for two days, generating (^{tBu}PNP)AlHI (**2.51**). All volatiles were removed under reduced pressure and the residue dissolved in 15 mL toluene. The solution of (^{tBu}PNP)AlHI (**2.51**) was transferred to a flask charged with KC_8 (240 mg, 1.76 mmol) at room temperature and stirred for three days. After filtration, the volatiles were removed *in vacuo* and the oily residue was dissolved in 10 mL pentane. The solvent was removed under reduced pressure to give a yellow solid (313 mg). NMR spectroscopy shows complete consumption of **2.51** and a complex mixture of products which could not be identified.

5.3 Experimental Details for Chapter 3

5.3.1 Synthesis of (^{Me}NCN)AlBr$_2$ (3.18)

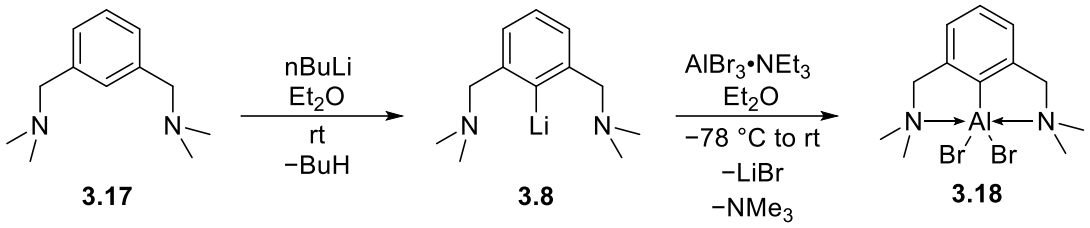

3.17 **3.8** **3.18**

To a solution of (^{Me}NCN)H (**3.17**, 5.00 g, 26.0 mmol) in Et_2O (50 mL) was treated with nBuLi (11.5 mL, 28.6 mmol, 2.5 M in hexanes) at ambient temperature and stirred for one hour. The deep orange mixture was added dropwise to $AlBr_3$.NEt_3 (9.56 g, 26.0 mmol) in toluene (60 mL) at -78 °C. The solution was allowed to warm slowly overnight and stirred at room temperature for 48 hours. The volatiles were removed under reduced pressure, the residue dissolved in benzene and stirred for a further 48 hours. The solvent was removed *in vacuo* and the residue washed with pentane to afford (^{Me}NCN)$AlBr_2$ (**3.18**) as a yellow solid (4.40 g, 44%). Colourless crystals of **3.18** were obtained from a benzene/pentane solution at room temperature and the structure determined by X-ray diffraction.

^{1}H NMR (500.2 MHz, C_6D_6, 300 K): δ 7.19 (p-Ar-***H***, t, $^3J_{H–H}$ = 7.4 Hz, 1 H), 6.78 (m-Ar-***H***, dt, $^3J_{HH}$ = 7.4, 2 H)*, 3.15 (C***H**$_2$N(CH$_3$)$_2$, s, 4 H), 2.23 (N(C***H**$_3$)$_2$, s, 12 H). * $^4J_{H–H}$ could not be measured.

^{13}C{^{1}H} NMR (151.1 MHz, C_6D_6): δ 145.0 (ortho-***C***, s), 130.0 (para-***C***H, s), 128.6 (ipso-***C***, s), 123.4 (meta-***C***H, s), 65.2 (***C***H$_2$, s), 47.4 (N(***C***H$_3$)$_2$, s).

Mass Peak Analysis: Calculated mass for $C_{12}H_{19}N_2AlBr_2$ for most abundant isotopes: 375.97249 Da. Observed mass peak: 375.97437 Da.

Elemental Analysis Calc for $C_{12}H_{19}N_2AlBr_2$: C, 38.12; H, 5.07; N, 7.14. Found: C, 38.96; H, 5.00; N, 5.46.

5.3.2 Reaction of (^{Me}NCN)AlBr$_2$ (3.18) with [(^{Mes}NacNac)Mg]$_2$

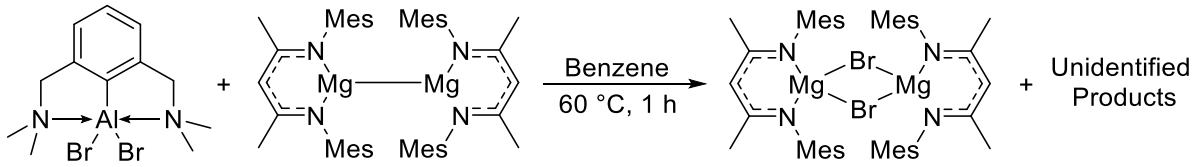

3.18 **3.19**

A toluene (40 mL) solution of (^{Me}NCN)AlBr$_2$ (**3.18**, 250 mg, 0.66 mmol) was added to solution of [(^{Mes}NacNac)Mg]$_2$ in toluene and the mixture was heated to 60 °C for one hour. The resulting deep orange suspension was cooled to room temperature and filtered. The filtrate was concentrated to an orange residue and washed with hexane. NMR analysis shows a complex mixture of products. Colourless x-ray-quality crystals, obtained from a toluene/hexane solution at room temperature, were identified as [(^{Mes}NacNac)MgBr]$_2$ by X-ray diffraction. The aluminium-containing product was not identified.

The ^{1}H NMR spectrum for [(^{Mes}NacNac)MgBr)]$_2$ (**3.19**):

^{1}H NMR (400.1 MHz, Tol-d$_8$, 300 K): δ 6.76 (NCC***H***$_3$, s, 8 H), 4.75 (C***H***, s, 2 H), 2.34 (C***H***$_3$, s, 12 H), 2.01 (C***H***$_3$, s, 24 H), 1.47 (C***H***$_3$, s, 12 H).

5.3.3 Reaction of (^{Me}NCN)AlBr$_2$ with Potassium Naphthalenide

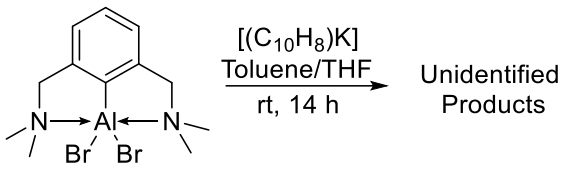

3.18

A THF (40 mL) solution of naphthalene (331 mg, 2.58 mmol) was added to potassium metal (100 mg, 2.58 mmol) and stirred for 14 hours at room temperature, generating potassium naphthalenide. The potassium naphthalenide solution was added dropwise to (^{Me}NCN)AlBr$_2$ (**3.18**, 500 mg, 1.29 mmol) in toluene (40 mL) at room temperature and stirred for 48 hours. Volatiles were removed under reduced pressure and the residue washed with a minimal amount of benzene and hexane to give a yellow oil. NMR spectroscopy revealed complete consumption of (^{Me}NCN)AlBr$_2$ (**3.18**). The NCN-ligand-containing product was not observed by NMR spectroscopy and could not be isolated.

5.3.4 Reaction of (^{Me}NCN)AlBr$_2$ (3.18) with NaK alloy in THF

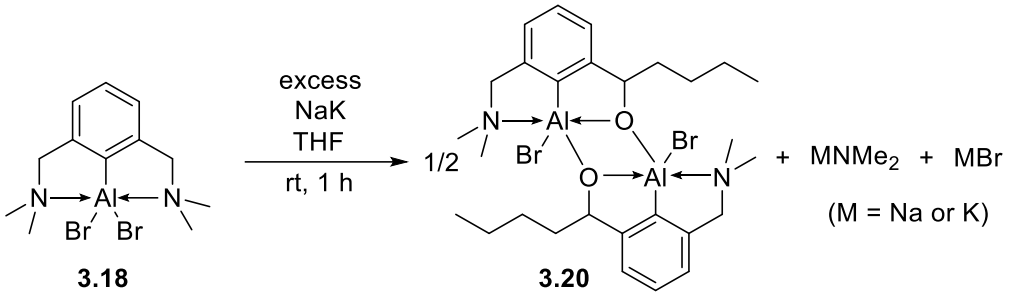

3.18 **3.20**

A solution of (NCN)AlBr$_2$ (**3.18**, 500 mg, 1.59 mmol) in THF (30 mL) was transferred to a flask charged with NaK (175 mg, 1:1 by mass) at ambient temperature and stirred vigorously for one hour. The solution was filtered, and volatiles removed under vacuum. The residue was washed with hexane (20 mL) and the resulting pale yellow solid was dried *in vacuo* (215 mg). Single crystals of **3.20** were attained from a concentrated benzene/THF solution cooled to 2 °C and its structure was determined by X-ray diffraction. The ^{1}H NMR spectrum of the crude pale yellow solid was not in concordance with the solid-state structure of **3.20**, thus it is assumed **3.20** is a minor product in the reaction of aluminium dibromide **3.18** and NaK alloy.

^{1}H NMR (500.2 MHz, C$_6$D$_6$, 300 K):* δ 7.33 (p-Ar ***H***, m, 1 H), 7.06 (m-Ar ***H***, d, $J_{H–H}$ = 7.6 Hz, 1 H), 7.3 (m-Ar ***H***, d, $J_{H–H}$ = 7.3 Hz, 1 H), 3.31 (C***H***$_2$, s, 2 H), 2.11 (N(C***H***$_3$)$_2$, s, 6 H). *Proton environments for pentyl fragment not observed.

5.4 Experimental Details for Chapter 4

5.4.1 Synthesis of {SiP^{Tipp}}H$_2$ (4.4)

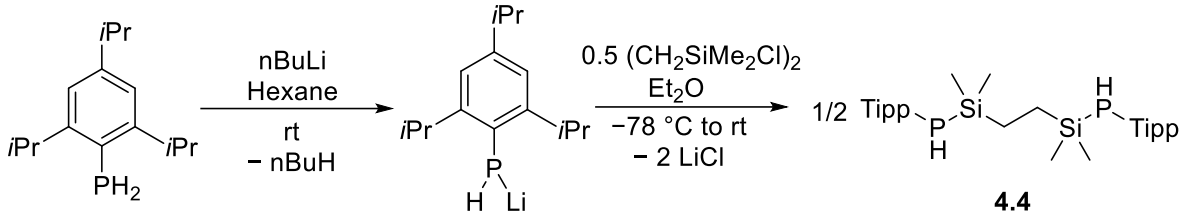

A solution of *n*BuLi in hexane (2.6 mL of a 2.5M solution, 6.60 mmol) was added dropwise to a stirring solution of TippPH$_2$ (1.55 g, 6.60 mmol) in hexane at room temperature and stirred for 2 hours resulting in the formation of a pale-yellow precipitate. The off-white precipitate was isolated by filtration (1.38 g, 88%) and dissolved in 40 mL of Et$_2$O to give a clear yellow solution. This solution was cooled to −78 °C and a solution of bis(chlorosilane) (ClSiMe$_2$CH$_2$)$_2$ (0.61 g, 2.86 mmol) in Et$_2$O (15 mL) was added dropwise to the stirring solution. The solution was allowed to warm to room temperature and stirred for 12 hours resulting in the formation of a pale-yellow suspension. Filtration and collection of the colourless filtrate followed by removal of the volatiles *in vacuo* gave a colourless precipitate. This solid was extracted into hexane, filtered and the volatiles removed to give {SiP^{Tipp}}H$_2$ (**4.4**) as a colourless powder (1.48 g, 85%).

^{1}H NMR (500.2 MHz, C$_6$D$_6$, 298 K): δ 7.12 (*m*-C$_6$***H$_2$***, d, *J* = 2.7 Hz, 4 H), 3.64 (P***H***, d, $^1J_{PH}$ = 207 Hz, 2 H), 3.62 (*o*-C***H***(CH$_3$)$_2$, m, 4H), 2.78 (*p*-C***H***(CH$_3$)$_2$, sept, *J* = 6.8 Hz, 2 H) 1.36 (*o*-CH(C***H$_3$***)$_2$, dd, *J* = 6.8 Hz, 12 H), 1.28 (*o*-CH(C***H$_3$***)$_2$, d, *J* = 6.8 Hz, 12 H), 1.22 (*p*-CH(C***H$_3$***)$_2$, d, *J* = 6.8 Hz, 12H), 0.69 (SiC***H$_2$***, s, 4H), 0.15 - 0.12 (SiC***H$_3$***, m, 12H).

^{13}C{^{1}H} NMR (125.8 MHz, C$_6$D$_6$, 298 K): δ 152.2 (P***C$_6$***H$_2$, d), 148.0 (P***C$_6$***H$_2$, s), 125.9 (P***C$_6$***H$_2$, d), 121.4 (P***C$_6$***H$_2$, d), 34.6 (*p*-***C***H(CH$_3$)$_2$, s), 33.8 (*o*-***C***H(CH$_3$)$_2$, d), 24.2 (CH(***C***H$_3$)$_2$, d), 24.2 (CH(***C***H$_3$)$_2$, d), 9.9 (Si***C***H$_2$, dd), -1.7 (Si***C***H$_3$, d), -1.9 (Si***C***H$_3$, d).

^{31}P NMR (202.5 MHz, C$_6$D$_6$, 298 K): δ –169.7 (d, $^1J_{PH}$ = 207 Hz).

^{29}Si NMR (99.4 MHz, C$_6$D$_6$, 298 K): δ 6.0 (d).

Mass Peak Analysis: Calculated mass for $C_{36}H_{64}P_2Si_2$ for most abundant isotopes: 614.40164 Da. Observed mass peak: 614.39976 Da.

5.4.2 Synthesis of {SiP ^{Mes*}}H_2 (4.5)

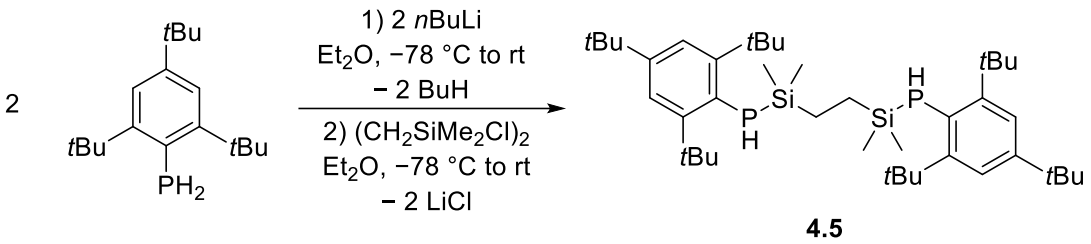

4.5

A solution of *n*BuLi in hexane (6.3 mL of a 2.5M solution, 0.0158 mol) was added dropwise to a stirring solution of Mes*PH_2 (4.00 g, 0.0143 mol) in Et_2O (50 mL) at −78 ˚C and was then allowed to warm to room temperature resulting in the formation of an orange suspension over 2 hours. A solution of bis(chlorosilane) $(ClSiMe_2CH_2)_2$ (1.53 g, 0.0072 mol) in Et_2O (15 mL) was then added dropwise to the stirring solution at −78 °C resulting in the immediate formation of a colourless solid. The suspension was allowed to warm to room temperature and stirred for 12 hours, followed by filtration and collection of the colourless filtrate. Removal of the volatiles *in vacuo* gave a colourless precipitate which was extracted into toluene, filtered and the volatile components removed to give {SiP^{Mes*}}H_2 (**4.5**) as a colourless powder (3.22 g, 64%). A colourless crystal of **4.5** suitable for analysis by single crystal X-ray diffraction was grown by cooling a saturated solution of toluene at −35 °C.

^{1}H NMR (500.2 MHz, C_7D_8, 298 K): δ 7.43 (*m*-C_6***H*$_2$**, d, *J* = 2.5 Hz, 4 H), 4.34 (P***H***, d, $^1J_{PH}$ = 214 Hz, 2 H), 1.63 (*o*-C(C***H*$_3$**)$_3$, br s, 36 H), 1.33 (*p*-C(C***H*$_3$**)$_3$, s, 18 H), 0.55 - 0.43 (SiC***H*$_2$**, m, 4 H), −0.03 - −0.07 (SiC***H*$_3$**, m, 12 H).

^{13}C{^{1}H} NMR (125.8 MHz, C_7D_8, 298 K):* δ 155.5 (P***C*$_6$**H_2, s), 147.7 (P***C*$_6$**H_2, s), 122.7 (P***C*$_6$**H_2, br), 38.2 (*o*-***C***H$(CH_3)_3$, br s), 34.9 (*p*-***C***H$(CH_3)_3$, s), 33.7 (*o*-CH(***C***$H_3)_3$, d), 31.6 (*p*-CH(***C***$H_3)_3$, s), 9.7 (Si***C***H_2, dd), −1.7 (Si***C***H_3, m). *one of the ***C*$_6$**H_2 resonances not observed due to overlapping d8-toluene resonance.

^{31}P NMR (202.5 MHz, C_7D_8, 298 K): δ −132.9 (d, $^1J_{PH}$ = 214 Hz), −133.0 (d, $^1J_{PH}$ = 214 Hz).

^{29}Si NMR (99.4 MHz, C_7D_8, 298 K): δ 12.3 (d, *J* = 25.0 Hz).

Mass Peak Analysis: Calculated mass for $C_{42}H_{76}NP_2Si_2$ for most abundant isotopes: 698.49554 Da. Observed mass peak: 698.49408 Da

5.4.3 Synthesis of {SiP^{Tipp}}H$_2$•(AlMe$_2$Cl)$_2$ (4.7)

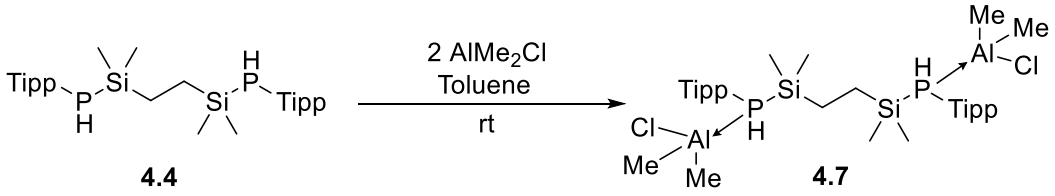

4.4 **4.7**

A solution of AlMe$_2$Cl in hexane (1.0 mL of a 1 M solution, 1.02 mmol) was added dropwise to a stirring solution of {SiP^{Tipp}}H$_2$ (300 mg, 0.49 mmol) in toluene (10 mL) at room temperature. After three hours stirring at room temperature, the volatile components were removed to give a colourless powder of **4.7** (317 mg, 81%). Colourless crystals of **4.7** were grown from slow evaporation of a saturated toluene solution at room temperature.

^{1}H NMR (500.2 MHz, C$_6$D$_6$, 298 K): δ 7.07 (*m*-C$_6$***H$_2$***, d, *J* = 2.7 Hz, 4 H), 4.56, 4.52 (P***H***, d, $^{1}J_{PH}$ = 280 Hz, 1H), 3.27 (*o*-C***H***(CH$_3$)$_2$, br, 4 H), 2.68 (*p*-C***H***(CH$_3$)$_2$, sept, *J* = 7.0 Hz, 2 H) 1.30 (*o*-CH(C***H$_3$***)$_2$, dd, *J* = 6.7 and 2.2 Hz, 12 H), 1.20 (*o*-CH(C***H$_3$***)$_2$, dd, *J* = 6.7 and 3.7 Hz, 12 H), 1.12 (*p*-CH(C***H$_3$***)$_2$, d, *J* = 7.0 Hz, 12 H), 0.87 (SiC***H$_2$***, m, 4 H), 0.28 - 0.14 (SiC***H$_3$***, m, 12 H), –0.11 (AlC***H$_3$***, s, 12 H).

^{13}C{^{1}H} NMR (125.8 MHz, C$_6$D$_6$, 298 K): δ 152.5 (P***C$_6$***H$_2$, s), 150.7 (P***C$_6$***H$_2$, s), 122.4 (P***C$_6$***H$_2$, s), 118.2 (P***C$_6$***H$_2$, br), 34.4 (*p*-***C***H(CH$_3$)$_2$), 34.4 (*o*-***C***H(CH$_3$)$_2$, d), 24.7 (CH(***C***H$_3$)$_2$, s), 24.6 (CH(***C***H$_3$)$_2$, s), 24.0 (CH(***C***H$_3$)$_2$, s), 23.9 (*p*-CH(***C***H$_3$)$_2$, d), 9.2 (Si***C***H$_2$, t), –2.2 (Si***C***H$_3$, m), –5.3 (Al***C***H$_3$, s).

^{31}P NMR (202.5 MHz, C$_6$D$_6$, 298 K): δ –142.0 (d, $^{1}J_{PH}$ = 282 Hz).

Mass Peak Analysis: Calculated mass for C$_{40}$H$_{76}$P$_2$Si$_2$Al$_2$Cl$_2$ for most abundant isotopes: 399.19789 Da. Observed mass peak: 399.19912 Da

5.4.4 Synthesis of {SiP^{Tipp}}H$_2$•AlMe$_3$ (4.8)

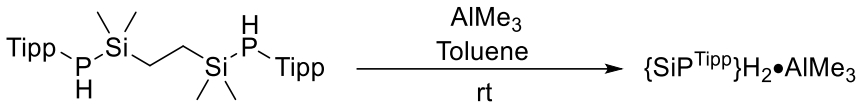

4.4 **4.8**

A solution of AlMe$_3$ in hexane (0.12 mL of a 2.0 M solution, 0.244 mmol) was added to a stirring solution of {SiP^{Tipp}}H$_2$ (150 mg, 0.244 mmol) in benzene (10 mL) at room temperature. After 4 hours stirring at room temperature, the volatile components were removed *in vacuo* to give a colourless powder of **4.8** (135 mg, 80%).

^{1}H NMR (500.2 MHz, C$_6$D$_6$, 298 K): δ 7.09 (*m*-C$_6$***H$_2$***, d, *J* = 2.7 Hz, 4 H), 4.13, 4.12 (P***H***, d, $^1J_{PH}$ = 252 Hz, 1 H), 3.39 (*o*-C***H***(CH$_3$)$_2$, m, 4 H), 2.71 (*p*-C***H***(CH$_3$)$_2$, sept, *J* = 7.0 Hz, 2 H), 1.34 (*o*-CH(C***H$_3$***)$_2$, d, *J* = 6.7 Hz, 12 H), 1.22 (*o*-CH(C***H$_3$***)$_2$, dd, *J* = 6.7 and 1.7 Hz, 12 H), 1.16 (*p*-CH(C***H$_3$***)$_2$, d, *J* = 7.0 Hz, 12 H), 0.66 (SiC***H$_2$***, m, 4 H), 0.18 - 0.10 (SiC***H$_3$***, m, 12 H) , –0.20 (AlC***H$_3$***, s, 9H).

^{13}C{^{1}H} NMR (125.8 MHz, C$_6$D$_6$, 298 K): δ 152.3 (P***C$_6$***H$_2$, d), 149.5 (P***C$_6$***H$_2$, s), 122.0 (P***C$_6$***H$_2$, d), 121.2 (P***C$_6$***H$_2$, br), 34.5 (*p*-***C***H(CH$_3$)$_2$, s), 34.1 (*o*-***C***H(CH$_3$)$_2$, d), 24.6 (CH(***C***H$_3$)$_2$, d), 24.4 (CH(***C***H$_3$)$_2$, d), 24.1 (CH(***C***H$_3$)$_2$, s), 24.0 (*p*-CH(***C***H$_3$)$_2$, d), 9.4 (Si***C***H$_2$, dd), -2.1 (Si***C***H$_3$, m), -6.2 (Al***C***H$_3$, s).

^{31}P NMR (202.5 MHz, C$_6$D$_6$, 298 K): δ –150.6 (d, $^1J_{PH}$ = 252 Hz).

5.4.5 Synthesis of {^{Tipp}SiP}H$_2$•(AlMe$_3$)$_2$ (4.9)

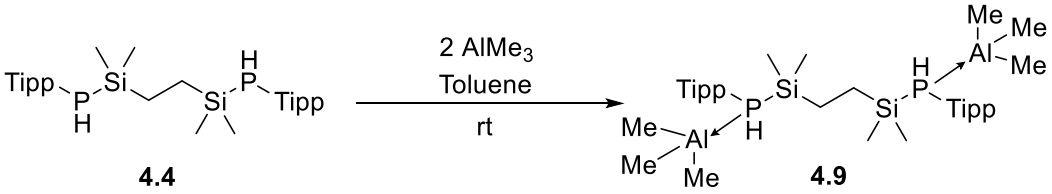

4.4 **4.9**

A solution of AlMe$_3$ in hexane (0.40 mL of a 2.0 M solution, 0.804 mmol) was added dropwise to a stirring solution of {SiP^{Tipp}}H$_2$ (250 mg, 0.402 mmol) in toluene (10 mL) at room temperature. After 2 hours stirring at room temperature, the volatile components were removed *in vacuo* to give a colourless powder of **4.9** (150 mg, 49%).

^{1}H NMR (500.2 MHz, C_6D_6, 298 K): δ 7.08 (*m*-C_6***H*****$_2$**, d, *J* = 2.7 Hz, 4 H), 4.27, 4.26 (P***H***, d, $^{1}J_{PH}$ = 266 Hz, 1 H), 3.32 (*o*-C***H***$(CH_3)_2$, br, 4 H), 2.70 (*p*-C***H***$(CH_3)_2$, sept, *J* = 7.0 Hz, 2 H) 1.32 (*o*-CH(C***H*****$_3$**$)_2$, dd, *J* = 6.7 Hz, 12 H), 1.21 (*o*-CH(C***H*****$_3$**$)_2$, dd, *J* = 6.7 and 1.7 Hz, 12 H), 1.14 (*p*-CH(C***H*****$_3$**$)_2$, d, *J* = 7.0 Hz, 12 H), 0.67 (SiC***H*****$_2$**, m, 4 H), 0.18, 0.16, 0.14, 0.12 (SiC***H*****$_3$**, d, $^{3}J_{PH}$ = 5.5, 3 H) , –0.22 (AlC***H*****$_3$**, s, 18 H).

^{13}C{^{1}H} NMR (125.8 MHz, C_6D_6, 298 K): δ 152.3 (P***C*****$_6$**H_2, d), 149.9 (P***C*****$_6$**H_2, t), 122.2 (P***C*****$_6$**H_2, d), 119.9 (P***C*****$_6$**H_2, q), 34.5 (*p*-***C***$H(CH_3)_2$), 34.2 (*o*-***C***$H(CH_3)_2$, d), 24.8 (CH(***C***$H_3)_2$, s), 24.5 (CH(***C***$H_3)_2$, s), 24.0 (CH(***C***$H_3)_2$, s), 23.9 (*p*-CH(***C***$H_3)_2$, d), 9.3 (Si***C***H_2, t), –2.0 (Si***C***H_3, d), –2.1 (Si***C***H_3, d), –2.2 (Si***C***H_3, d), –2.3 (Si***C***H_3, d), –6.3 (Al***C***H_3, s).

^{31}P NMR (202.5 MHz, C_6D_6, 298 K): δ –144.9 (d, $^{1}J_{PH}$ = 266 Hz).

^{29}Si NMR (99.4 MHz, C_6D_6, 298 K): δ –7.8 (t).

Mass Peak Analysis: Calculated mass for $C_{42}H_{82}P_2Si_2Al_2$ for most abundant isotopes: 379.25251 Da. Observed mass peak: 379.25339 Da.

5.4.6 Synthesis of {^{Mes*}SiP}H_2 • $AlMe_2Cl$ (4.10)

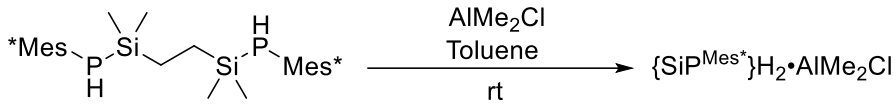

4.5 **4.10**

A solution of $AlMe_2Cl$ in toluene (0.43 mL of a 1.0 M solution, 0.43 mmol) was added dropwise to a stirring suspension of {SiP^{Mes*}}H_2 (300 mg, 0.429 mmol) in toluene (10 mL) at room temperature. After stirring for 4 hours at room temperature, the volatile components were removed to give a colourless powder of **4.10** (294 mg, 87%).

^{1}H NMR (500.2 MHz, C_6D_6, 298 K): δ 7.46 (*m*-C_6***H*****$_2$**, d, *J* = 2.5 Hz, 4 H), 4.67 (P***H***, d, $^{1}J_{PH}$ = 240 Hz, 2 H), 1.60 (*o*-C(C***H*****$_3$**$)_3$, br s, 36 H), 1.31 (*p*-C(C***H*****$_3$**$)_3$, s, 18 H), 0.53 (SiC***H*****$_2$**, m, 4 H), 0.03, 0.02 (SiC***H*****$_3$**, d, $^{3}J_{PH}$ = 3.6 Hz, 6 H), –0.06 (AlC***H*****$_3$**, s, 6 H).

^{13}C{^{1}H} NMR (125.8 MHz, C_6D_6, 298 K): δ 155.9 (P***C*****$_6$**H_2, s), 148.6 (P***C*****$_6$**H_2, s), 126.6 (P***C*****$_6$**H_2, q), 122.2 (P***C*****$_6$**H_2, d), 38.2 (*o*-***C***$H(CH_3)_3$, br s), 34.9 (*p*-***C***$H(CH_3)_3$, s), 33.7 (*o*-CH(***C***$H_3)_3$, d), 31.5 (*p*-CH(***C***$H_3)_3$, s), 9.5 (Si***C***H_2, dd), –1.9 (Si***C***H_3, m), –5.0 (Al***C***H_3, s).

^{31}P NMR (202.5 MHz, C_6D_6, 298 K): δ -125.5 (br d, $^{1}J_{PH}$ = 240 Hz).

^{29}Si NMR (99.4 MHz, C_6D_6, 298 K): δ 12.3 (d).

5.4.7 Synthesis of {SiP^{Mes*}}H_2•$AlMe_3$ (4.11)

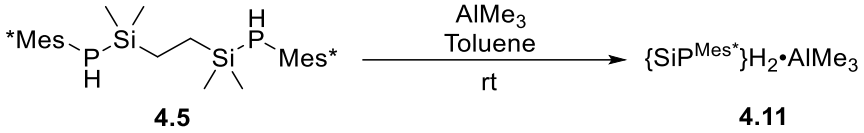

4.5 **4.11**

A solution of $AlMe_3$ in hexane (0.29 mL of a 2 M solution, 0.58 mmol) was added dropwise to a stirring solution of {SiP^{Mes*}}H_2 (402 mg, 0.572 mmol) in toluene (10 mL) at room temperature. After 4 hours stirring at room temperature, the volatile components were removed to give a colourless powder of **4.11** (340 mg, 77%).

^{1}H NMR (500.2 MHz, C_6D_6, 298 K): δ 7.46 (*m*-C_6***H*$_2$**, d, *J* = 2.5 Hz, 4 H), 4.66 (P***H***, d, $^{1}J_{PH}$ = 230 Hz, 2H), 1.58 (*o*-C(C***H*$_3$**)$_3$, br s, 36 H), 1.30 (*p*-C(C***H*$_3$**)$_3$, s, 18 H), 0.53 (SiC***H*$_2$**, m, 4 H), 0.01, 0.00 (SiC***H*$_3$**, d, $^{3}J_{PH}$ = 3.7 Hz, 6 H), –0.16 (AlC***H*$_3$**, s, 6 H).

^{13}C{^{1}H} NMR (125.8 MHz, C_6D_6, 298 K): δ 155.0 (P***C*$_6$H$_2$, s), 148.8 (P***C*$_6$H$_2$, s), 125.7 (P***C*$_6$H$_2$, q)*, 122.3 (P***C*$_6$H$_2$, d), 38.3 (*o*-***C***H(CH$_3$)$_3$, br s), 34.9 (*p*-***C***H(CH$_3$)$_3$, s), 33.7 (*o*-CH(***C***H$_3$)$_3$, d), 31.5 (*p*-CH(***C***H$_3$)$_3$, s), 9.3 (Si***C***H$_2$, dd), –1.9 (Si***C***H$_3$, m), –5.7 (Al***C***H$_3$, s). *overlapping with residual toluene impurity resonance.

^{31}P NMR (202.5 MHz, C_6D_6, 298 K): δ -122.8 (d, $^{1}J_{PH}$ = 230 Hz).

^{29}Si NMR (99.4 MHz, C_6D_6, 298 K): δ 12.9 (s).

5.4.8 Synthesis of {SiP^{Tipp}}$Li_2(Et_2O)_{2.5}$ (4.12)

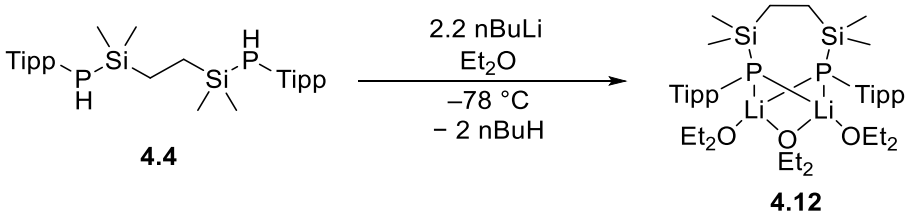

4.4 **4.12**

A solution of *n*BuLi in hexane (1.15 mL of a 2.5 M solution, 2.88 mmol) was added dropwise to a stirring solution of {SiP^{Tipp}}H$_2$ (800 mg, 1.31 mmol) in Et$_2$O (10 mL) at –78 °C resulting in the formation of a yellow solution. After the addition, the reaction mixture was allowed to warm to room temperature and stirred for 3 hours. Removal of the volatiles *in vacuo* gave **4.12** as a pale-yellow powder (680 mg, 61%).

^{1}H NMR (500.2 MHz, C$_6$D$_6$, 298 K): δ 7.24 (*m*-C$_6$***H$_2$***, s, 4 H), 4.88 (*o*-C***H***(CH$_3$)$_2$, m, 4 H), 3.19 (OC***H$_2$***CH$_3$, q, *J* = 7.0 Hz, 10 H), 2.91 (*p*-C***H***(CH$_3$)$_2$, sept, *J* = 7.0 Hz, 2 H), 1.40 (*o*-CH(C***H$_3$***)$_2$, d, *J* = 6.9 Hz, 24H), 1.31 (*p*-CH(C***H$_3$***)$_2$, d, *J* = 7.0 Hz, 12H), 1.15 (SiC***H$_2$***, t, $^3J_{PH}$ = 4.1 Hz, 4 H), 1.07 (OCH$_2$C***H$_3$***, t, *J* = 7.0 Hz, 15H), 0.36 (SiC***H$_3$***, s, 12H).

^{13}C{^{1}H} NMR (125.8 MHz, C$_6$D$_6$, 298 K): δ 155.1 (P***C$_6$***H$_2$, t), 145.2 (P***C$_6$***H$_2$, s), 120.9 (P***C$_6$***H$_2$, d), 120.6 (P***C$_6$***H$_2$, s), 66.7 (O***C***H$_2$CH$_3$, s), 34.7 (*p*-***C***H(CH$_3$)$_2$, s), 34.1 (*o*-***C***H(CH$_3$)$_2$, t), 25.1 (CH(***C***H$_3$)$_2$, s), 24.5 (CH(***C***H$_3$)$_2$, s), 14.7 (OCH$_2$***C***H$_3$ and Si***C***H$_2$, overlapping s and d), 3.6 (Si***C***H$_3$, d).

^{31}P NMR (202.5 MHz, C$_6$D$_6$, 298 K): δ –212.3 (sept, $^1J_{PLi}$ = 62.8 Hz).

^{29}Si NMR (99.4 MHz, C$_6$D$_6$, 298 K): δ 4.0 (s).

^{7}Li NMR (194.0 MHz, C$_6$D$_6$, 298 K): δ 2.6 (t, $^1J_{PLi}$ = 62.8 Hz).

5.4.9 Generation of {SiP^{Tipp}}K$_2$ (4.13)

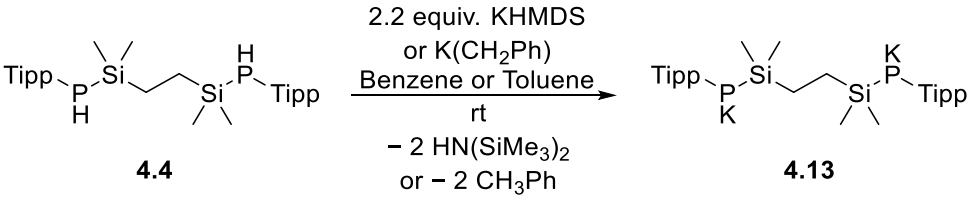

Method 1: A benzene solution of KHMDS (64 mg, 0.32 mmol) was added dropwise to a stirring solution of {SiP^{Tipp}}H$_2$ (90 mg, 0.15 mmol) in benzene (10 mL) at room temperature resulting in the formation of a yellow solution. After the addition, the reaction mixture was stirred for 3 hours and then filtered. The volatiles were removed and **4.13** was immediately used in subsequent reactions without further purification

Method 2: A solution of {SiP^{Tipp}}H_2 (150 mg, 0.24 mmol) in toluene was added to K[$CH_2C_6H_5$] (70 mg, 0.54 mmol) resulting in the formation of a yellow solution. After the addition, the reaction mixture was stirred for 3 hours and then filtered. The volatiles were removed and **4.13** was used immediately in subsequent reactions without further purification.

^{1}H NMR (500.2 MHz, C_6D_6, 298 K):* δ 4.90 (*o*-C***H***$(CH_3)_2$, br, 4 H), 2.80 (*p*-C***H***$(CH_3)_2$, m, 2 H), 1.36 (*o*-CH(C***H*****$_3$**$)_2$, d, *J* = 6.7 Hz, 24 H), 1.24 (*p*-CH(C***H*****$_3$**$)_2$, d, *J* = 7.0 Hz, 12 H), 0.87 (SiC***H*****$_2$**, br, 4H), 0.32 (SiC***H*****$_3$**, s, 12 H). *C_6***H_2** not observed due to overlap with residual toluene solvent.

^{31}P NMR (202.5 MHz, C_6D_6, 298 K): δ –206.4 (s).

5.4.10 Synthesis of {SiP^{Tipp}}AlBr(THF) (4.14)

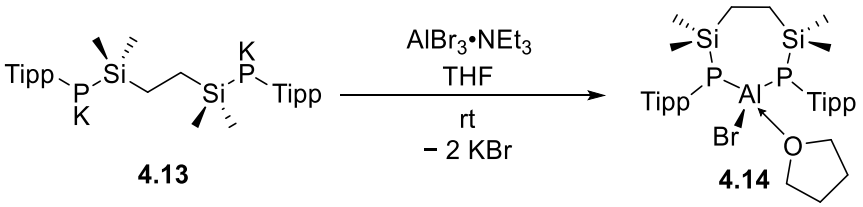

A THF (100 mL) solution of {SiP^{Tipp}}K_2, generated by method 2 (**4.4**, 1.00 g, 1.63 mmol; K[$CH_2C_6H_5$], 466 mg, 3.58 mmol), was added to $AlBr_3$•NEt_3 (780 mg, 2.12 mmol) at room temperature resulting in a colourless suspension. After the addition, the reaction mixture was stirred for four hours. The volatiles were removed under reduced pressure. 100 mL pentane was added to give a colourless suspension, which was vigorously stirred for 20 minutes, and then filtered. Removal of the volatiles *in vacuo* gave **4.14** as a colourless solid (977 g, 76%).

^{1}H NMR (500.2 MHz, C_6D_6, 298 K): δ 7.20 (*m*-C_6***H*****$_2$**, s, 4 H), 4.90, 4.52 (*o*-C***H***$(CH_3)_2$, m, 2 H), 3.79 (OC***H*****$_2$**CH_2, m, 4H), 2.79 (*p*-C***H***$(CH_3)_2$, sept, *J* = 7.0 Hz, 2 H), 1.61 (*o*-CH(C***H*****$_3$**$)_2$, d, *J* = 6.7 Hz, 6 H), 1.47 (*o*-CH(C***H*****$_3$**$)_2$, d, *J* = 6.7 Hz, 12H), 1.35 (*o*-CH(C***H*****$_3$**$)_2$, d, *J* = 6.7 Hz, 6 H), 1.20 (SiC***H*****$_2$** and *p*-CH(C***H*****$_3$**$)_2$, m, 4 H), 1.07 (OCH_2C***H*****$_2$**, m, 4 H), 0.52 (SiC***H*****$_3$**, t, 6 H), 0.47 (SiC***H*****$_3$**, s, 6 H).

^{13}C{^{1}H} NMR (125.8 MHz, C_6D_6, 298 K): δ 155.7 (P***C*****$_6$**H_2, m), 147.9 (P***C*****$_6$**H_2, s), 146.3 (P***C*****$_6$**H_2, s), 121.5 (P***C*****$_6$**H_2, m), 120.7 (P***C*****$_6$**H_2, s), 73.2 (O***C***H_2CH_3, s), 34.8 (*p*-***C***$H(CH_3)_2$, s), 34.3 – 34.0

(*o*-***C***H(CH$_3$)$_2$, m), 25.4 - 23.7 (OCH$_2$***C***H$_3$ and CH(***C***H$_3$)$_2$, m), 14.2 (Si***C***H$_2$, t), 1.9 - 1.1 (Si***C***H$_3$, m).

^{31}P NMR (202.5 MHz, C$_6$D$_6$, 298 K): δ –194.4 (s).

^{29}Si NMR (99.4 MHz, C$_6$D$_6$, 298 K): δ 3.4 (s).

5.4.11 Synthesis of {SiP^{Tipp}}AlBr(DMAP) (4.15)

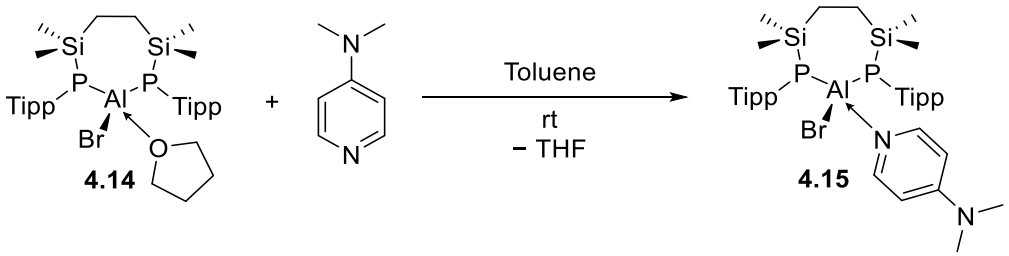

A toluene (20 mL) solution of {SiP^{Tipp}}AlBr(THF) (250 mg, 0.32 mmol) was added to DMAP (40 mg, 0.33 mmol) at room temperature resulting in the formation of a pale yellow solution. After the addition, the reaction mixture was stirred for 48 hours. The volatiles were removed under reduced pressure, pentane (15 mL) was added, and the solution concentrated to ca. 3 mL and a precipitate formed. After filtration, the residual volatiles were removed *in vacuo* to afford **4.15** as a colourless powder (86 mg, 32%).

^{1}H NMR (500.2 MHz, C$_6$D$_6$, 298 K): δ 8.49 (C$_5$***H$_4$***N, d, *J* = 7.5 Hz, 2H), 7.16 (*m*-C$_6$***H$_2$***, d, 4H), 5.36 (C$_5$***H$_4$***N, d, *J* = 7.5 Hz, 2H), 4.97 (*o*-C***H***(CH$_3$)$_2$, br, 2H), 4.80 (*o*-C***H***(CH$_3$)$_2$, m, 2H), 2.74 (*p*-C***H***(CH$_3$)$_2$, sept, *J* = 7.0 Hz, 2H), 1.64 (N(C***H$_3$***)$_2$, s, 6H), 1.57, 1.55, 1.50 (*o*-CH(C***H$_3$***)$_2$, d, *J* = 6.7 Hz, 6H), 1.39 (SiC***H$_2$***, br, 4H), 1.28 (*o*-CH(C***H$_3$***)$_2$, d, J = 6.7 Hz, 6H), 1.14, 1.13 (*p*-CH(C***H$_3$***)$_2$, d, *J* = 6.7 Hz, 6 H), 0.60 (SiC***H$_3$***, s, 6 H), 0.58 (SiC***H$_3$***, t, 6 H).

^{13}C{^{1}H} NMR (125.8 MHz, C$_6$D$_6$, 298 K): δ 156.2 (P***C$_6$***H$_2$, m), 155.2 (***C$_5$***H$_4$N, s), 147.7 (P***C$_6$***H$_2$, s), 147.1 (P***C$_6$***H$_2$ and ***C$_5$***H$_4$N, m), 121.9 (P***C$_6$***H$_2$, s), 121.2 (P***C$_6$***H$_2$, s), 120.7 (P***C$_6$***H$_2$, s), 106.1 (***C$_5$***H$_4$N, s), 38.0 (N(***C***H$_3$)$_2$, s), 35.1 (*p*-***C***H(CH$_3$)$_2$, s), 34.5 (*p*-***C***H(CH$_3$)$_2$, s), 34.2 (*p*-***C***H(CH$_3$)$_2$, t), 27.4 (CH(***C***H$_3$)$_2$, d), 25.6 (CH(***C***H$_3$)$_2$, d), 25.4 (CH(***C***H$_3$)$_2$, d), 24.5 (CH(***C***H$_3$)$_2$, d), 24.2 (CH(***C***H$_3$)$_2$, d, 24.1(CH(***C***H$_3$)$_2$, d), 14.3 (Si***C***H$_2$, t), 2.0 (Si***C***H$_3$, m).

^{31}P NMR (202.5 MHz, C$_6$D$_6$, 298 K): δ –191.8 (s).

^{29}Si NMR (99.4 MHz, C_6D_6, 298 K): δ 3.9 (s).

5.4.12 General Procedure for attempted reduction of {SiP^{Tipp}}AlBr(L) (L = THF, 4.14; L = DMAP, 4.15)

A solution of {SiP^{Tipp}}AlBr(L) in toluene was stirred over KC_8 or K(mirror) (4 equivalents) at room temperature for 48 – 72 hours. The solution was filtered and the volatiles removed under reduced pressure. The resulting solid or residue was analysed using NMR spectroscopy.

5.4.13 Synthesis of {SiP^{Mes*}}Li$_2$(Et$_2$O)$_{2.5}$ (4.16)

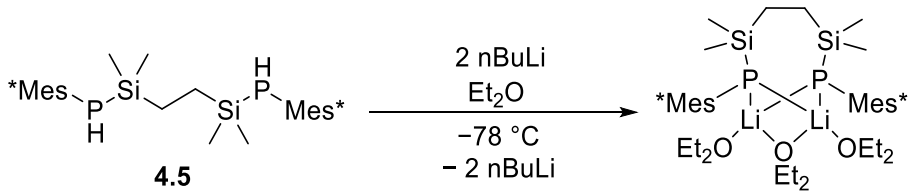

A solution of *n*BuLi in hexane (1.2 mL of a 2.5 M solution, 3.0 mmol) was added dropwise to a stirring solution of {SiP^{Mes*}}H_2 (1.00 g, 1.43 mmol) in Et_2O (10 mL) at –78 °C resulting in the formation of a yellow solution. After the addition, the reaction mixture was allowed to warm to room temperature and stirred for 4 hours. Removal of the volatiles *in vacuo* gave **4.16** as a pale-yellow powder (851 mg, 66%).

^{1}H NMR (500.2 MHz, C_6D_6, 298 K): δ 7.51 (*m*-C_6***H*$_2$**, s, 4 H), 3.24 (OC***H*$_2$**CH_3, q, *J* = 7.0 Hz, 10 H), 1.94 (*o*-C(C***H*$_3$**)$_3$, br s, 36 H), 1.43 (*p*-C(C***H*$_3$**)$_3$, s, 18 H), 1.14 (OCH_2C***H*$_3$**, t, *J* = 7.0 Hz, 15 H), 0.83 (SiC***H*$_2$**, t, $^{3}J_{PH}$ = 4.9 Hz, 4 H), 0.08 (SiC***H*$_3$**, s, 12 H).

^{13}C{^{1}H} NMR (125.8 MHz, C_6D_6, 298 K): δ 156.7 (P***C*$_6$**H_2, s), 145.8 (P***C*$_6$**H_2, s), 137.7 (P***C*$_6$**H_2, q), 120.4 (P***C*$_6$**H_2, s), 66.4 (O***C***H_2CH_3, s), 38.9 (*o*-***C***H$(CH_3)_3$, s), 34.8 (*p*-***C***H$(CH_3)_3$, s), 34.0 (*o*-CH(***C***H$_3$)$_3$, m), 31.8 (*p*-CH(***C***H$_3$)$_3$, s), 15.1 (OCH_2***C***H_3, s), 14.5 (Si***C***H_2, t), 2.8 (Si***C***H_3, s).

^{31}P NMR (202.5 MHz, C_6D_6, 298 K): δ –162.2 (sept, $^{1}J_{PLi}$ = 63 Hz).

^{29}Si NMR (99.4 MHz, C_6D_6, 298 K): δ 5.7 (t, *J* = 14.8 Hz).

^{7}Li NMR (194.0 MHz, C_6D_6, 298 K): δ 3.0 (t, $^{1}J_{PLi}$ = 63 Hz).

5.4.14 Synthesis of {SiP^{Tipp}}(AlH$_2$)Li(THF)$_2$ (4.20)

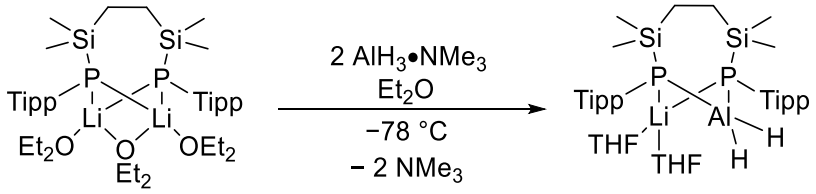

4.12 **4.20**

A solution of AlH_3•NMe_3 (53 mg, 0.592 mmol) in Et_2O (5 mL) was added dropwise to a stirring solution of **4.12** (250 mg, 0.296 mmol) in Et_2O (10 mL) at room temperature. The solution was stirred for 5 hours at room temperature, followed by removal of the volatiles *in vacuo* to give a colourless oil. Addition of toluene and a few drops of THF, followed by storage at -35 °C for 24 hours resulted in the formation of colourless crystals of **4.20** which were isolated by filtration and dried *in vacuo* (0.10 g, 56 %).

^{1}H NMR (500.2 MHz, C_6D_6, 298 K): δ 7.22 (*m*-C_6***H*****$_2$**, s, 4 H), 5.11 (Al***H***, br, 2 H), 4.56 (*o*-C***H***$(CH_3)_2$, m, 4 H), 3.59 (OC***H*****$_2$**CH_2, m, 8 H), 2.82 (*p*-C***H***$(CH_3)_2$, sept, *J* = 7.0 Hz, 2 H), 1.52 (*o*-CH(C***H*****$_3$**$)_2$, d, 24 H), 1.26 (OCH_2C***H*****$_2$**, m, 8 H), 1.24 (*p*-CH(C***H*****$_3$**$)_2$, d, *J* = 7.0 Hz, 12 H), 1.15 (SiC***H*****$_2$**, t, $^3J_{PH}$ = 4.1 Hz, 4 H), 0.35 (SiC***H*****$_3$**, s, 12 H).

^{13}C{^{1}H} NMR (125.8 MHz, C_6D_6, 298 K):* δ 155.7 (P***C*****$_6$**H_2, s), 147.2 (P***C*****$_6$**H_2, s), 121.8 (P***C*****$_6$**H_2, t), 67.0 (O***C***H_2CH_2, s), 34.5 (*p*-***C***$H(CH_3)_2$, s), 34.4 (*o*-***C***$H(CH_3)_2$, t), 25.3 ($CH(\boldsymbol{C}H_3)_2$, s), 24.3 ($CH(\boldsymbol{C}H_3)_2$, s), 21.5 ($OCH_2\boldsymbol{C}H_2$, s), 9.67 (Si***C***H_2, t), 1.0 (Si***C***H_3, t). *quaternary C_6H_2 not observed.

^{31}P NMR (202.5 MHz, C_6D_6, 298 K): δ –200.3 (br).

^{29}Si NMR (99.4 MHz, C_6D_6, 298 K): δ 5.7 (t).

^{7}Li NMR (194.0 MHz, C_6D_6, 298 K): δ 1.0 (br).

IR (solid): 1789, 1725 cm^{-1} (Al–H stretch)

5.4.15 Synthesis of {SiP^{Mes*}}(AlH$_3$)$_2$Li$_2$ (4.22)

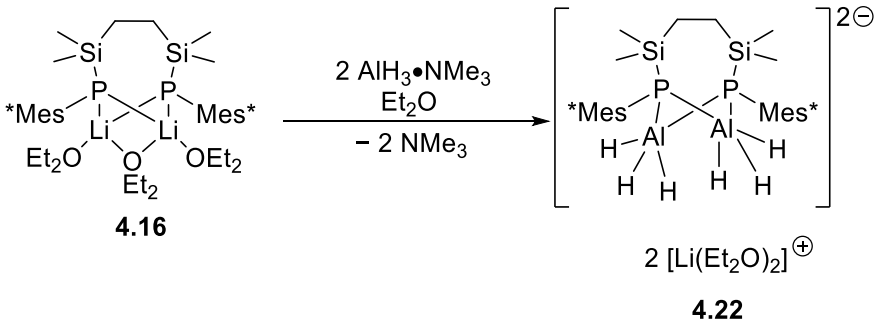

4.16 **4.22**

A solution of *n*BuLi in hexane (0.36 mL of a 2.5 M solution, 0.91 mmol) was added dropwise to a stirring solution of {SiP^{Mes*}}H$_2$ (0.30 g, 0.429 mmol) in Et$_2$O (10 mL) at -78 °C resulting in the formation of a colourless solution. After the addition, the reaction mixture was allowed to warm to room temperature and stirred for 3 hours. A solution of AlH$_3$•NMe$_3$ (0.11 g, 1.29 mmol) was then added dropwise to the reaction mixture at room temperature, resulting in an immediate colour change to colourless. After stirring at room temperature for 30 minutes, a colourless precipitate was deposited. The reaction mixture was filtered and the remaining solid residue was dried *in vacuo* to give **4.22** as a colourless powder (0.13 g, 29% based on {SiP^{Mes*}}(AlH$_3$)$_2$Li$_2$(Et$_2$O)$_{3.5}$).

^{1}H NMR (500.2 MHz, C$_6$D$_6$, 298 K): δ 7.55 (*m*-C$_6$***H$_2$***, m, 4 H), 3.71 (Al***H***, br, 6 H), 3.32 (OC***H$_2$***CH$_3$, q, *J* = 7.0 Hz, 14 H), 1.94 (*o*-C(C***H$_3$***)$_3$, br s, 36 H), 1.38 (*p*-C(C***H$_3$***)$_3$, s, 18 H), 1.11 (OCH$_2$C***H$_3$***, t, *J* = 7.0 Hz, 21 H), 1.15 (SiC***H$_2$***, br s, 4 H), 1.07 (OCH$_2$C***H$_3$***, t, *J* = 7.0 Hz, 15 H), 0.05 (SiC***H$_3$***, s, 12 H).

^{13}C{^{1}H} NMR (125.8 MHz, C$_6$D$_6$, 298 K):* δ 158.1 (P***C$_6$***H$_2$, s), 147.7 (P***C$_6$***H$_2$, s), 121.1 (P***C$_6$***H$_2$, t), 66.0 (O***C***H$_2$CH$_3$, s), 47.9 (*o*-***C***H(CH$_3$)$_3$, s), 39.2 (*p*-***C***H(CH$_3$)$_3$, s), 34.6 (*o*-CH(***C***H$_3$)$_3$, m), 31.6 (*p*-CH(***C***H$_3$)$_3$, s), 15.3 (OCH$_2$***C***H$_3$, s), 13.4 (Si***C***H$_2$, br), 0.4 (Si***C***H$_3$, t). *quaternary C$_6$H$_2$ not observed.

^{31}P NMR (202.5 MHz, C$_6$D$_6$, 298 K): δ –170.4 (br).

^{29}Si NMR (99.4 MHz, C$_6$D$_6$, 298 K): Not observed.

^{7}Li NMR (194.0 MHz, C$_6$D$_6$, 298 K): δ 0.53 (br).

IR (solid): 1751 cm^{-1} (Al–H stretch)

5.4.16 Reaction of {^{Mes*}SiP}(AlH_3)$_2$$Li_2$ (4.22) with AlH_3•NMe_3 (1.3)

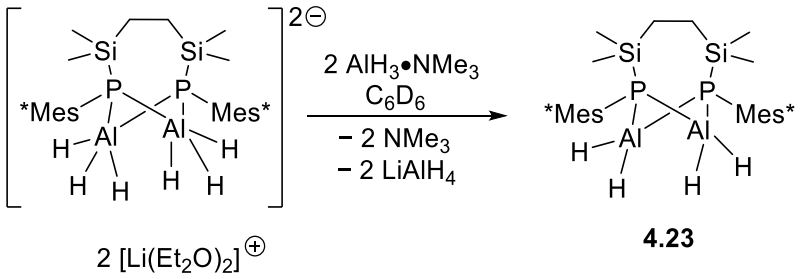

4.22 **4.23**

A J. Young's NMR tube was charged with **4.22** (0.015 g, 0.0163 mmol) and **1.3** (0.007 g, 0.082 mmol) and C_6D_6 was added. The resulting colourless suspension was monitored by NMR spectroscopy revealing immediate formation of a new species.

^{1}H NMR (500 MHz, C_6D_6, 298 K): δ 7.54 (*m*-C_6***H*$_2$**, d, *J* = 2.4 Hz, 4 H), 4.37 – 3.80 (br, Al*H* and Al*H* of **1.3**, 12 H)*, 3.28 (OC***H*$_2$**CH_3, q, *J* = 7.0 Hz, 10 H), 2.05 (free N(C***H*$_3$**$)_3$, s, 18 H), 1.92 (*o*-C(C***H*$_3$**$)_3$, s, 36 H), 1.89 (N(C***H*$_3$**$)_3$ of **1.3**, s, 27 H), 1.37 (*p*-C(C***H*$_3$**$)_3$, s, 18 H), 1.15 (OCH_2C***H*$_3$**, t, *J* = 7.0 Hz, 15 H), 0.78 (SiC***H*$_2$**, s, 4 H), 0.27 (SiC***H*$_3$**, s, 12 H). *two overlapping resonances

^{13}C{^{1}H} NMR (125.76 MHz, C_6D_6, 298 K): δ 158.4 (P***C*$_6$**H_2, d), 147.4 (P***C*$_6$**H_2, d), 130.6 (P***C*$_6$**H_2, d), 121.1 (P***C*$_6$**H_2, d), 66.9 (O***C***H_2CH_3, s), 47.8 (free N(C***H*$_3$**$)_3$), 47.6 (N(C***H*$_3$**$)_3$ of **1.3**), 39.4 (*o*-***C***H$(CH_3)_3$, s), 34.8 (*p*-***C***H$(CH_3)_3$, s) 34.6 (*o*-CH(***C***H$_3)_3$, s), 31.7 (*p*-CH(***C***H$_3)_3$, s), 15.6 (OCH_2***C***H_3, s), 12.0 (Si***C***H_2, dd), –0.1 (Si***C***H_3, d).

^{31}P NMR (202.50 MHz, C_6D_6, 298 K): δ –162.4 (br).

^{29}Si NMR (99 MHz, C_6D_6, 298 K): 9.1 (d, *J* = 10.3 Hz).

^{7}Li NMR (194 MHz, C_6D_6, 298 K): δ 0.26 (br, impurity).

5.5 Crystallography Data

Crystallography was performed by Dr Gary Nichol.

Full crystallographic data are available at the end of this section.

5.5.1 (^{Ph}PNP)Li (2.21)

Experimental

Single colourless block-shaped crystals of **2.21** were recrystallised from toluene by slow cooling. A suitable crystal 0.13×0.10×0.08 mm^3 was selected and mounted on a MITIGEN holder in Paratone oil. on an Rigaku Oxford Diffraction SuperNova diffractometer. The crystal was kept at a steady T = 120.0 K during data collection. The structure was solved with the XT (Sheldrick, 2015) structure solution program using the Intrinsic Phasing solution method and by using **Olex2** (Dolomanov et al., 2009) as the graphical interface. The model was refined with version 2018/3 of **ShelXL** (Sheldrick, 2015) using Least Squares minimisation.

Crystal Data

$C_{46}H_{45.5}Li_{0.5}NP_2$, M_r = 677.74, triclinic, P-1 (No. 2), a = 12.8944(7) Å, b = 13.2672(9) Å, c = 13.8915(7) Å, α = 112.533(5)°, β = 114.314(5)°, γ = 91.748(5)°, V = 1949.7(2) $Å^3$, T = 120.0 K, Z = 2, Z' = 1, μ(MoKα) = 0.143, 21191 reflections measured, 7116 unique (R_{int} = 0.0686) which were used in all calculations. The final wR_2 was 0.1487 (all data) and R_1 was 0.0774 (I > 2(I)).

Structure

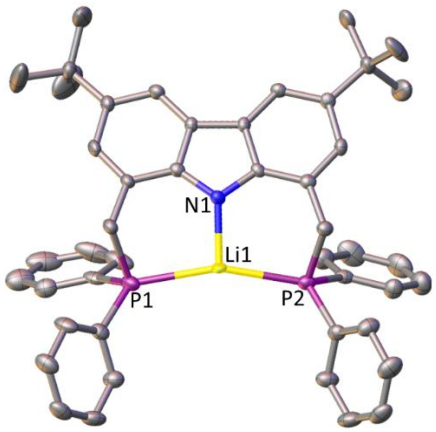

Molecule of **2.19** and H atoms are omitted. Thermal ellipsoids are set 50% probability.

5.5.2 (^{Ph}PNP)AlH_2 (2.22)

Experimental

Single colourless block-shaped crystals of **2.22** were recrystallised from a mixture of pentane and toluene by slow evaporation. A suitable crystal 0.32×0.29×0.15 mm^3 was selected and mounted on a MITIGEN holder in Paratone oil. on an Bruker D8 VENTURE diffractometer. The crystal was kept at a steady T = 120.0 K during data collection. The structure was solved with the **ShelXT** (Sheldrick, 2015) structure solution program using the Intrinsic Phasing solution method and by using **Olex2** (Dolomanov et al., 2009) as the graphical interface. The model was refined with version 2018/3 of **ShelXL** (Sheldrick, 2015) using Least Squares minimisation.

Crystal Data

$C_{46}H_{48}AlNP_2$, M_r = 703.77, monoclinic, $P2_1/c$ (No. 14), a = 23.7789(14) Å, b = 8.2780(5) Å, c = 20.3929(11) Å, β = 106.889(2)°, α = γ = 90°, V = 3841.0(4) Å^3, T = 120.0 K, Z = 4, Z' = 1, μ(MoK_α) = 0.169, 113817 reflections measured, 10337 unique (R_{int} = 0.0490) which were used in all calculations. The final wR_2 was 0.1146 (all data) and R_1 was 0.0407 (I > 2(I)).

Structure

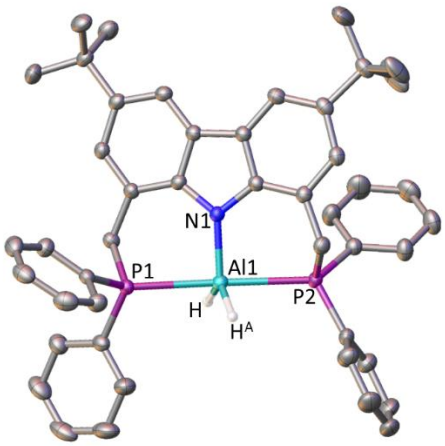

H atoms (except AlH) are omitted. Thermal ellipsoids are set 50% probability.

5.5.3 [(^{Ph}PNP)AlN(Xyl)CH_2]$_2$ (2.35)

Experimental

Single translucent light colourless block-shaped crystals of **2.35** recrystallised from d6-benzene by slow evaporation. A suitable crystal with dimensions 0.53 × 0.34 × 0.27 mm^3 was selected and mounted on a MITIGEN holder in Paratone oil on a Rigaku Oxford Diffraction XCalibur diffractometer. The crystal was kept at a steady T = 120.0 K during data collection. The structure was solved with the **ShelXT** (Sheldrick, 2015) solution program using dual methods and by using **Olex2** 1.5-beta (Dolomanov et al., 2009) as the graphical interface. The model was refined with **ShelXL** 2018/3 (Sheldrick, 2015) using full matrix least squares minimisation on F^2.

Crystal Data

$C_{110}H_{114}Al_2N_4P_4$, M_r = 1669.89, monoclinic, $P2_1/n$ (No. 14), a = 13.7243(9) Å, b = 16.5767(10) Å, c = 20.9538(13) Å, β = 104.389(7)°, α = γ = 90°, V = 4617.5(5) Å^3, T = 120.0 K, Z = 2, Z' = 0.5, μ(MoK$_\alpha$) = 0.152, 31298 reflections measured, 21838 unique (R_{int} = 0.1306) which were used in all calculations. The final wR_2 was 0.1253 (all data) and R_1 was 0.0581 (I≥2 σ(I)).

Structure

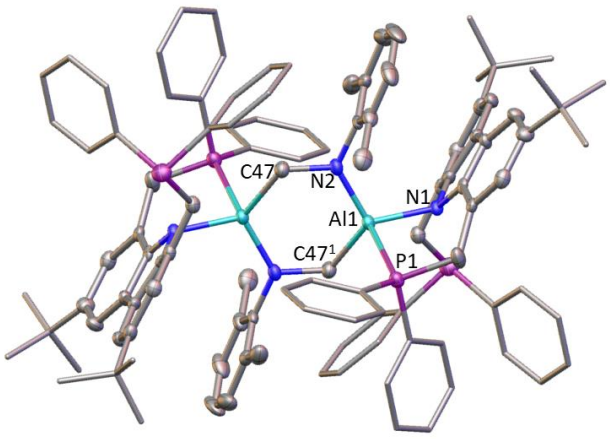

H atoms are omitted. Thermal ellipsoids are set 50% probability.

5.5.4 (^{Ph}PNP)PdH (2.38)

Experimental

Single colourless prism-shaped crystals of **2.38** were used as supplied. A suitable crystal with dimensions 0.14 × 0.07 × 0.05 mm^3 was selected and mounted on a MITIGEN holder in Paratone oil. on a Rigaku Oxford Diffraction SuperNova diffractometer. The crystal was kept at a steady T = 120.0 K during data collection. The structure was solved with the **ShelXT** 2018/2 (Sheldrick, 2018) solution program using dual methods and by using **Olex2** 1.5-beta (Dolomanov et al., 2009) as the graphical interface. The model was refined with **ShelXL** 2018/3 (Sheldrick, 2015) using full matrix least squares minimisation on F^2.

Crystal Data

$C_{46}H_{47}NP_2Pd$, M_r = 782.18, triclinic, P-1 (No. 2), a = 12.6359(4) Å, b = 13.0530(3) Å, c = 13.9318(5) Å, α = 112.057(3)°, β = 112.870(3)°, γ = 90.507(2)°, V = 1929.76(12) Å^3, T = 120.0 K, Z = 2, Z' = 1, μ(Cu Kα) = 4.902, 31587 reflections measured, 7955 unique (R_{int} = 0.0648) which were used in all calculations. The final wR_2 was 0.1281 (all data) and R_1 was 0.0474 (I≥2 σ(I)).

Structure

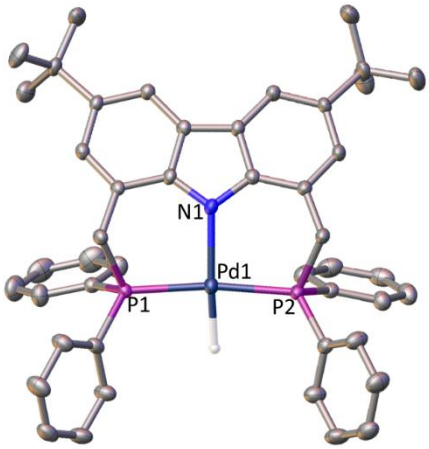

H atoms (except PdH) are omitted. Thermal ellipsoids are set 50% probability.

5.5.5 (^{Ph}PNP)AlBr$_2$ (2.47)

Experimental

Single colourless block crystals of **2.47** recrystallised from toluene by slow evaporation. A suitable crystal with dimensions 0.47 × 0.30 × 0.26 mm^3 was selected and mounted on a MITIGEN holder in Paratone oil. on a Bruker D8 VENTURE diffractometer. The crystal was kept at a steady T = 100.0 K during data collection. The structure was solved with the **ShelXT** 2018/2 (Sheldrick, 2018) solution program using dual methods and by using **Olex2** (Dolomanov et al., 2009) as the graphical interface. The model was refined with **ShelXL** 2018/3 (Sheldrick, 2015) using full matrix least squares minimisation on F^2.

Crystal Data

$C_{53}H_{54}AlBr_2NP_2$, M_r = 953.71, triclinic, P-1 (No. 2), a = 9.9572(15) Å, b = 12.528(3) Å, c = 19.156(4) Å, α = 89.898(6)°, β = 81.416(6)°, γ = 74.714(6)°, V = 2277.3(7) Å^3, T = 100.0 K, Z = 2, Z' = 1, μ(MoKα) = 1.907, 239893 reflections measured, 22118 unique (R_{int} = 0.0609) which were used in all calculations. The final wR_2 was 0.0696 (all data) and R_1 was 0.0257 (I > 2(I)).

Structure

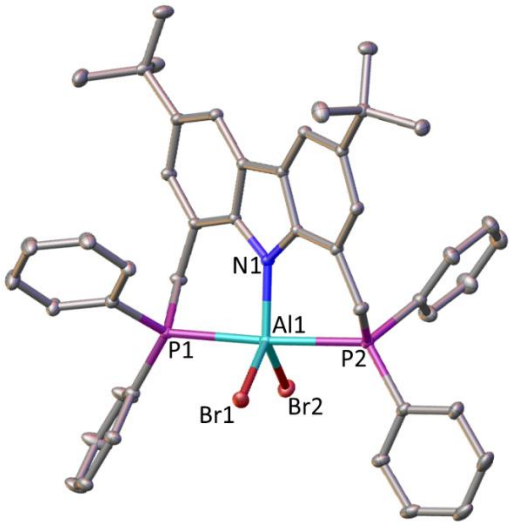

H atoms are omitted. Thermal ellipsoids are set 50% probability.

5.5.6 (^{Me}NCN)AlBr$_2$ (3.18)

Experimental

Single colourless block-shaped crystals of **3.18** were recrystallised from toluene by slow cooling. A suitable crystal 0.37×0.28×0.15 mm^3 was selected and mounted on a MITIGEN holder in Paratone oil. on an Rigaku Oxford Diffraction SuperNova diffractometer. The crystal was kept at a steady T = 120.0 K during data collection. The structure was solved with the **ShelXT** (Sheldrick, 2015) structure solution program using the Intrinsic Phasing solution method and by using **Olex2** (Dolomanov et al., 2009) as the graphical interface. The model was refined with version 2018/3 of **ShelXL** (Sheldrick, 2015) using Least Squares minimisation.

Crystal Data

$C_{19}H_{27}AlBr_2N_2$, M_r = 470.22, monoclinic, $P2_1/c$ (No. 14), a = 8.1702(3) Å, b = 17.6393(5) Å, c = 14.3444(5) Å, β = 96.818(3)°, α = γ = 90°, V = 2052.65(12) Å^3, T = 120.0 K, Z = 4, Z' = 1, μ(MoKα) = 3.996, 18827 reflections measured, 4998 unique (R_{int} = 0.0396) which were used in all calculations. The final wR_2 was 0.0805 (all data) and R_1 was 0.0385 (I > 2(I)).

Structure

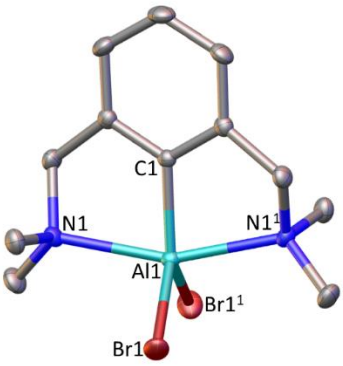

H atoms are omitted. Thermal ellipsoids are set 50% probability.

5.5.7 [(^{Mes}NacNac)MgBr]$_2$ (3.19)

Experimental

Single colourless plate-shaped crystals of **3.19** were recrystallised from d6-benzene by slow evaporation. A suitable crystal 0.26×0.16×0.05 mm^3 was selected and mounted on a MITIGEN holder in Paratone oil. on an Rigaku Oxford Diffraction SuperNova diffractometer. The crystal was kept at a steady T = 120.0 K during data collection. The structure was solved with the **ShelXT** (Sheldrick, 2015) structure solution program using the Intrinsic Phasing solution method and by using **Olex2** (Dolomanov et al., 2009) as the graphical interface. The model was refined with version 2018/3 of **ShelXL** (Sheldrick, 2015) using Least Squares minimisation.

Crystal Data

$C_{46}H_{58}Br_2Mg_2N_4$, M_r = 875.40, triclinic, P-1 (No. 2), a = 8.5459(3) Å, b = 10.4384(4) Å, c = 13.5803(5) Å, α = 69.090(3)°, β = 83.757(3)°, γ = 81.578(3)°, V = 1117.36(7) Å^3, T = 120.0 K, Z = 1, Z' = 0.5, μ(MoKα) = 1.877, 24855 reflections measured, 5680 unique (R_{int} = 0.0344) which were used in all calculations. The final wR_2 was 0.0813 (all data) and R_1 was 0.0363 (I >2(I)).

Structure

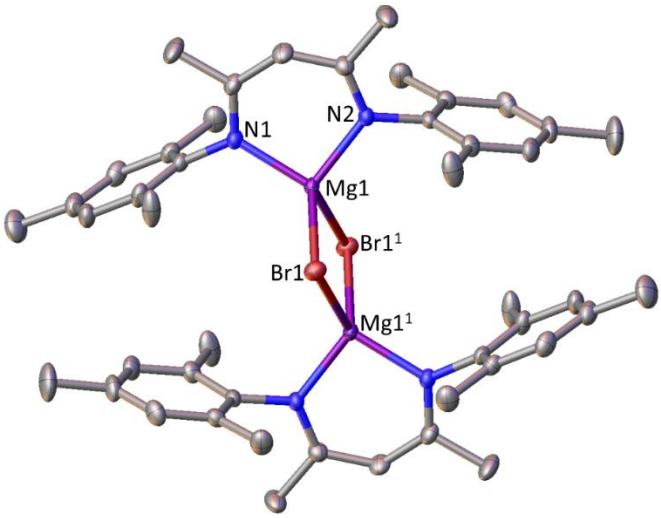

H atoms are omitted. Thermal ellipsoids are set 50% probability.

5.5.8 $[(NCO)AlBr]_2$ (3.20)

Experimental

Single colourless block crystals of **3.20** recrystallised from a mixture of benzene and THF by slow evaporation. A suitable crystal with dimensions 0.16 × 0.13 × 0.07 mm^3 was selected and mounted on a MITIGEN holder in Paratone oil on a Rigaku Oxford Diffraction SuperNova diffractometer. The crystal was kept at a steady T = 120.00(10) K during data collection. The structure was solved with the ShelXT 2018/2 (Sheldrick, 2018) solution program using dual methods and by using Olex2 (Dolomanov et al., 2009) as the graphical interface. The model was refined with ShelXL 2018/3 (Sheldrick, 2015) using full matrix least squares minimisation on F^2.

Crystal Data

$C_{40}H_{54}Al_2Br_2N_2O_2$, M_r = 808.63, monoclinic, $P2_1/c$ (No. 14), a = 12.59270(10) Å, b = 8.28970(10) Å, c = 19.8508(2) Å, β = 106.9610(10)°, α = γ = 90°, V = 1982.08(4) $Å^3$, T = 120.00(10) K, Z = 2, Z' = 0.5, μ(Cu Kα) = 3.292, 21283 reflections measured, 4126 unique (R_{int} = 0.0607) which were used in all calculations. The final wR_2 was 0.1090 (all data) and R_1 was 0.0413 (I≥2 σ(I)).

Structure

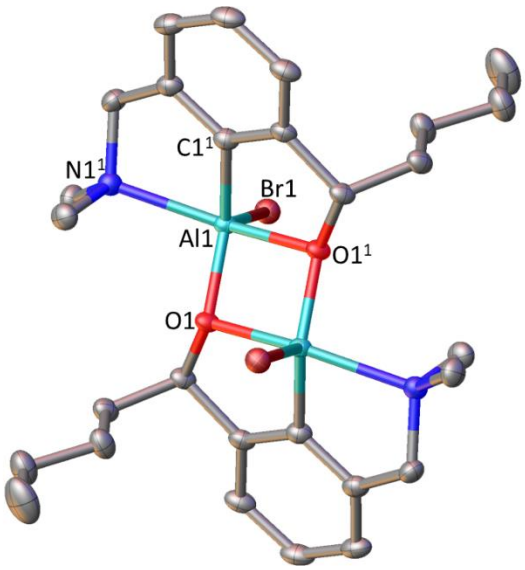

H atoms are omitted. Thermal ellipsoids are set 50% probability.

5.5.9 {SiP^{Mes*}}H_2 (4.5)

Experimental

Single colourless plate-shaped crystals of **4.5** recrystallised from toluene by slow cooling. A suitable crystal with dimensions 0.34 × 0.19 × 0.06 mm^3 was selected and mounted on a MITIGEN holder in Paratone oil on a Rigaku Oxford Diffraction SuperNova diffractometer. The crystal was kept at a steady T = 120.01(10) K during data collection. The structure was solved with the **ShelXT** 2018/2 (Sheldrick, 2018) solution program using dual methods and by using **Olex2** 1.5-beta (Dolomanov et al., 2009) as the graphical interface. The model was refined with **ShelXL** 2018/3 (Sheldrick, 2015) using full matrix least squares minimisation on F^2.

Crystal Data

$C_{42}H_{76}P_2Si_2$, M_r = 699.14, monoclinic, $P2_1/c$ (No. 14), a = 14.4936(4) Å, b = 10.7623(3) Å, c = 27.8072(9) Å, β = 91.189(3)°, $\alpha = \gamma$ = 90°, V = 4336.6(2) Å^3, T = 120.01(10) K, Z = 4, Z' = 1, μ(Mo Kα) = 0.182, 50393 reflections measured, 10745 unique (R_{int} = 0.0528) which were used in all calculations. The final wR_2 was 0.1109 (all data) and R_1 was 0.0522 (I≥2 σ(I)).

Structure

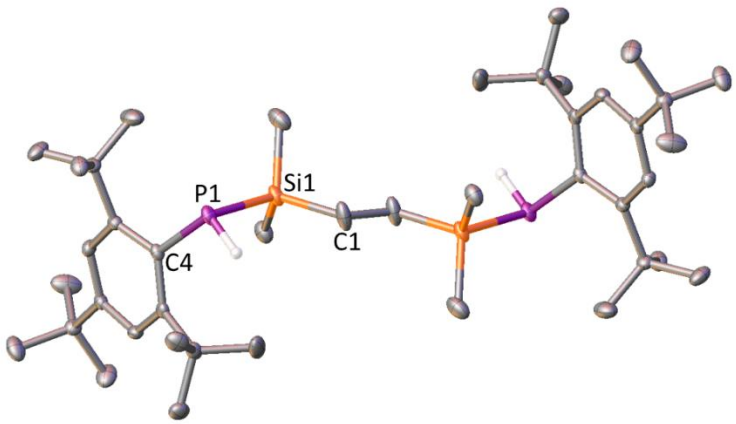

H atoms (except PH) are omitted. Thermal ellipsoids are set 50% probability.

5.5.10 {SiP^{Tipp}}H$_2$•(AlMe$_2$Cl)$_2$ (4.7)

Experimental

Single colourless block crystals of **4.7** recrystallised from toluene by slow evaporation. A suitable crystal with dimensions 0.50 × 0.43 × 0.38 mm^3 was selected and mounted on a MITIGEN holder in Paratone oil. on a Bruker D8 VENTURE diffractometer. The crystal was kept at a steady T = 100.0 K during data collection. The structure was solved with the ShelXT 2018/2 (Sheldrick, 2018) solution program using dual methods and by using Olex2 (Dolomanov et al., 2009) as the graphical interface. The model was refined with ShelXL 2018/3 (Sheldrick, 2015) using full matrix least squares minimisation on F^2.

Crystal Data

$C_{40}H_{76}Al_2Cl_2P_2Si_2$, M_r = 799.98, triclinic, P-1 (No. 2), a = 9.6003(8) Å, b = 10.3467(8) Å, c = 14.1226(12) Å, α = 70.483(3)°, β = 79.523(3)°, γ = 64.775(3)°, V = 1194.85(17) Å^3, T = 100.0 K, Z = 1, Z' = 0.5, μ(MoKα) = 0.315, 122016 reflections measured, 12494 unique (R_{int} = 0.0299) which were used in all calculations. The final wR_2 was 0.1432 (all data) and R_1 was 0.0436 (I≥2 σ(I)).

Structure

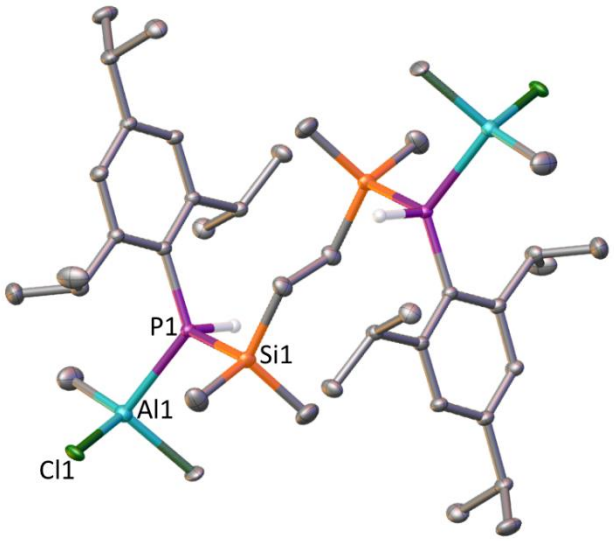

H atoms (except PH) are omitted. Thermal ellipsoids are set 50% probability. The chloride (Cl1) and methyl (C20) positions were refined as disordered.

5.5.11 $\{SiP^{Tipp}\}H_2 \bullet (AlMe_2)_3$ (4.9)

Experimental

Single colourless block crystals of **4.9** recrystallised from slow cooling by pentane. A suitable crystal with dimensions 0.37 × 0.21 × 0.15 mm^3 was selected and mounted on a MITIGEN holder in Paratone oil on a Rigaku Oxford Diffraction XCalibur diffractometer. The crystal was kept at a steady T = 100.0(2) K during data collection. The structure was solved with the ShelXT 2018/2 (Sheldrick, 2018) solution program using dual methods and by using Olex2 (Dolomanov et al., 2009) as the graphical interface. The model was refined with ShelXL 2018/3 (Sheldrick, 2015) using full matrix least squares minimisation on $\boldsymbol{F^2}$.

Crystal Data

$C_{42}H_{82}Al_2P_2Si_2$, M_r = 759.15, triclinic, P-1 (No. 2), a = 9.6084(3) Å, b = 10.3966(3) Å, c = 14.0690(5) Å, α = 70.397(3)°, β = 79.599(2)°, γ = 66.801(3)°, V = 1215.01(8) $Å^3$, T = 100.0(2) K, Z = 1, Z' = 0.5, μ(Mo Kα) = 0.200, 38787 reflections measured, 7136 unique (R_{int} = 0.0301) which were used in all calculations. The final wR_2 was 0.0950 (all data) and R_1 was 0.0368 (I≥2 σ(I)).

Structure

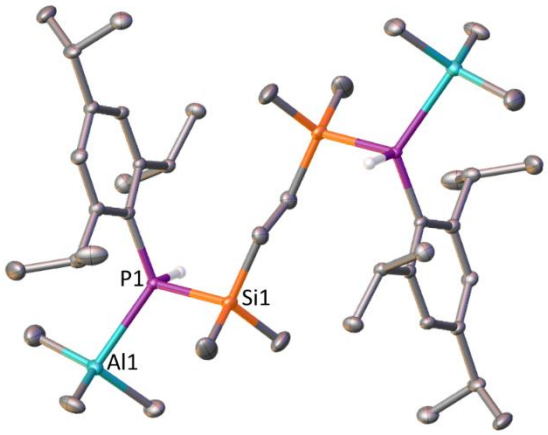

H atoms (except PH) are omitted. Thermal ellipsoids are set 50% probability.

5.5.12 {SiP^{Mes*}}$Li_2(Et_2O)$ (4.16a)

Experimental

Single colourless plate-shaped crystals of **4.16a** recrystallised from a mixture of toluene and diethyl ether by slow cooling. A suitable crystal with dimensions 0.18 × 0.06 × 0.04 mm^3 was selected and mounted on a MITIGEN holder in Paratone oil on a Rigaku Oxford Diffraction SuperNova diffractometer. The crystal was kept at a steady T = 120.01(10) K during data collection. The structure was solved with the **ShelXT** 2018/2 (Sheldrick, 2018) solution program using dual methods and by using **Olex2** 1.5-beta (Dolomanov et al., 2009) as the graphical interface. The model was refined with **ShelXL** 2018/3 (Sheldrick, 2015) using full matrix least squares minimisation on F^2.

Crystal Data

$C_{60}H_{100}Li_2OP_2Si_2$, M_r = 969.39, triclinic, P-1 (No. 2), a = 10.7047(3) Å, b = 16.7340(6) Å, c = 18.7341(7) Å, α = 108.791(3)°, β = 91.685(2)°, γ = 100.297(2)°, V = 3112.19(19) Å^3, T = 120.01(10) K, Z = 2, Z' = 1, μ(Cu Kα) = 1.252, 51487 reflections measured, 12856 unique (R_{int} = 0.0680) which were used in all calculations. The final wR_2 was 0.1642 (all data) and R_1 was 0.0598 (I≥2 σ(I)).

Structure

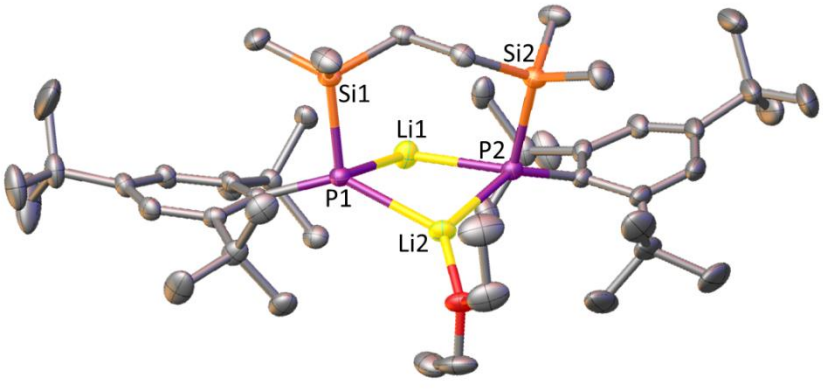

H atoms are omitted. Thermal ellipsoids are set 50% probability.

5.5.13 {SiP^{Tipp}}K$_2$(THF)$_4$ (4.13-THF)

Experimental

Single colourless block crystals of **4.13-THF** recrystallised from THF by slow evaporation. A suitable crystal with dimensions 0.39 × 0.29 × 0.18 mm^3 was selected and mounted on a MITIGEN holder in Paratone oil. on a Bruker D8 Venture diffractometer. The crystal was kept at a steady T = 100.0 K during data collection. The structure was solved with the ShelXT 2018/2 (Sheldrick, 2018) solution program using dual methods and by using Olex2 (Dolomanov et al., 2009) as the graphical interface. The model was refined with ShelXL 2018/3 (Sheldrick, 2015) using full matrix least squares minimisation on F^2.

Crystal Data

$C_{52}H_{94}K_2O_4P_2Si_2$, M_r = 979.59, triclinic, P-1 (No. 2), a = 9.3998(11) Å, b = 10.4372(13) Å, c = 15.0095(18) Å, α = 80.569(3)°, β = 89.609(4)°, γ = 80.015(3)°, V = 1430.3(3) Å^3, T = 100.0 K, Z = 1, Z' = 0.5, μ(MoKα) = 0.303, 25313 reflections measured, 7657 unique (R_{int} = 0.0318) which were used in all calculations. The final wR_2 was 0.0871 (all data) and R_1 was 0.0349 (I≥2 σ(I)).

Structure

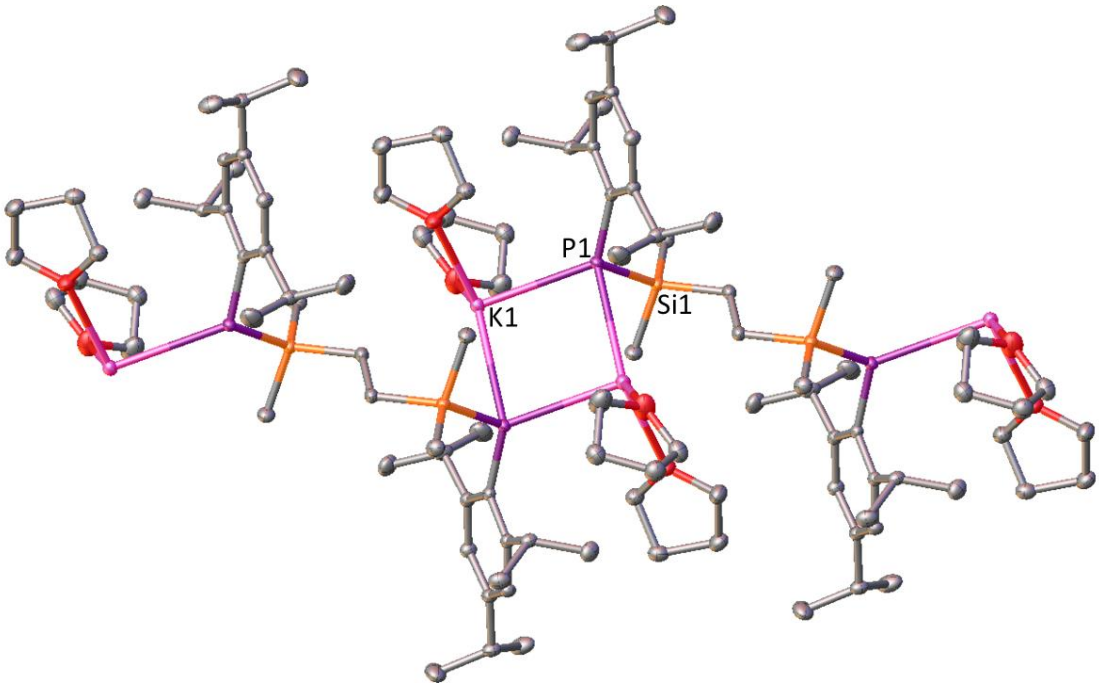

A section of the solid-state structure of **4.13-THF**. H atoms are omitted. Thermal ellipsoids are set 50% probability.

5.5.14 Full Crystallographic data for All Crystal Structures

Compound	**2.21**	**2.22**	**2.35**
Formula	$C_{46}H_{45.5}Li_{0.5}NP_2$	$C_{46}H_{48}AlNP_2$	$C_{110}H_{114}Al_2N_4P_4$
$D_{calc.}$/ g cm^{-3}	1.154	1.217	1.201
μ/mm^{-1}	0.143	0.169	0.152
Formula Weight	677.74	703.77	1669.89
Colour	colourless	colourless	translucent light colourless
Shape	block	block	block-shaped
Size/mm^3	0.13×0.10×0.08	0.32×0.29×0.15	0.53×0.34×0.27
T/K	120.0	120.0	120.0
Crystal System	triclinic	monoclinic	monoclinic
Space Group	P-1	$P2_1/c$	$P2_1/n$
a/Å	12.8944(7)	23.7789(14)	13.7243(9)
b/Å	13.2672(9)	8.2780(5)	16.5767(10)
c/Å	13.8915(7)	20.3929(11)	20.9538(13)
α/°	112.533(5)	90	90
β/°	114.314(5)	106.889(2)	104.389(7)
γ/°	91.748(5)	90	90
V/Å^3	1949.7(2)	3841.0(4)	4617.5(5)
Z	2	4	2
Z'	1	1	0.5
Wavelength/Å	0.71073	0.71073	0.71073
Radiation type	MoK_α	MoK_α	Mo K_α
Θ_{min}/°	3.411	2.322	3.222
Θ_{max}/°	25.350	29.149	25.350
Measured Refl.	21191	113817	31298
Independent Refl.	7116	10337	21838
Reflections with I > 2(I)	5015	8478	13881
R_{int}	0.0686	0.0490	0.1306
Parameters	457	465	551
Restraints	0	0	18
Largest Peak	0.481	0.469	0.540
Deepest Hole	-0.288	-0.347	-0.364
GooF	1.085	1.053	0.939
wR_2 (all data)	0.1487	0.1146	0.1253
wR_2	0.1337	0.1045	0.1175
R_1 (all data)	0.1187	0.0534	0.0930
R_1	0.0774	0.0407	0.0581

Compound	**2.38**	**2.45**	**3.18**
Formula	$C_{46}H_{47}NP_2Pd$	$C_{53}H_{54}AlBr_2NP_2$	$C_{19}H_{27}AlBr_2N_2$
$D_{calc.}$/ g cm^{-3}	1.346	1.391	1.522
μ/mm^{-1}	4.902	1.907	3.996
Formula Weight	782.18	953.71	470.22
Colour	colourless	colourless	colourless
Shape	prism-shaped	block	block
Size/mm^3	0.14×0.07×0.05	0.47×0.30×0.26	0.37×0.28×0.15
T/K	120.0	100.0	120.0
Crystal System	triclinic	triclinic	monoclinic
Space Group	P-1	P-1	$P2_1/c$
a/Å	12.6359(4)	9.9572(15)	8.1702(3)
b/Å	13.0530(3)	12.528(3)	17.6393(5)
c/Å	13.9318(5)	19.156(4)	14.3444(5)
α/°	112.057(3)	89.898(6)	90
β/°	112.870(3)	81.416(6)	96.818(3)
γ/°	90.507(2)	74.714(6)	90
V/Å^3	1929.76(12)	2277.3(7)	2052.65(12)
Z	2	2	4
Z'	1	1	1
Wavelength/Å	1.54184	0.71073	0.71073
Radiation type	Cu K$_\alpha$	MoK$_\alpha$	MoK$_\alpha$
Θ_{min}/°	3.715	2.247	3.412
Θ_{max}/°	75.992	36.413	29.675
Measured Refl.	31587	239893	18827
Independent Refl.	7955	22118	4998
Reflections with I > 2(I)	7320	19258	4093
R_{int}	0.0648	0.0609	0.0396
Parameters	460	749	222
Restraints	0	0	0
Largest Peak	1.219	0.594	0.697
Deepest Hole	-2.073	-0.617	-0.642
GooF	1.046	1.021	1.066
wR_2 (all data)	0.1281	0.0696	0.0805
wR_2	0.1243	0.0663	0.0742
R_1 (all data)	0.0514	0.0332	0.0546
R_1	0.0474	0.0257	0.0385

Compound	**3.19**	**3.20**	**4.5**
Formula	$C_{46}H_{58}Br_2Mg_2N_4$	$C_{40}H_{54}Al_2Br_2N_2O_2$	$C_{42}H_{76}P_2Si_2$
$D_{calc.}$/ g cm^{-3}	1.301	1.355	1.071
μ/mm^{-1}	1.877	3.292	0.182
Formula Weight	875.40	808.63	699.14
Colour	colourless	colourless	colourless
Shape	plate	block	plate-shaped
Size/mm^3	0.26×0.16×0.05	0.16×0.13×0.07	0.34×0.19×0.06
T/K	120.0	120.00(10)	120.01(10)
Crystal System	triclinic	monoclinic	monoclinic
Space Group	P-1	$P2_1/c$	$P2_1/c$
a/Å	8.5459(3)	12.59270(10)	14.4936(4)
b/Å	10.4384(4)	8.28970(10)	10.7623(3)
c/Å	13.5803(5)	19.8508(2)	27.8072(9)
α/°	69.090(3)	90	90
β/°	83.757(3)	106.9610(10)	91.189(3)
γ/°	81.578(3)	90	90
V/Å^3	1117.36(7)	1982.08(4)	4336.6(2)
Z	1	2	4
Z'	0.5	0.5	1
Wavelength/Å	0.71073	1.54184	0.71073
Radiation type	MoK_α	Cu K_α	Mo K_α
Θ_{min}/°	3.218	4.658	3.390
Θ_{max}/°	29.704	76.065	29.763
Measured Refl.	24855	21283	50393
Independent Refl.	5680	4126	10745
Reflections with I > 2(I)	5001	3974	8160
R_{int}	0.0344	0.0607	0.0528
Parameters	252	220	723
Restraints	0	0	3
Largest Peak	0.448	0.639	0.423
Deepest Hole	-0.434	-1.088	-0.286
GooF	1.085	1.082	1.056
wR_2 (all data)	0.0813	0.1090	0.1109
wR_2	0.0783	0.1071	0.1002
R_1 (all data)	0.0453	0.0423	0.0788
R_1	0.0363	0.0413	0.0522

Compound	**4.7**	**4.9**	**4.16a**
Formula	$C_{40}H_{76}Al_2Cl_2P_2Si_2$	$C_{42}H_{82}Al_2P_2Si_2$	$C_{60}H_{100}Li_2OP_2Si_2$
$D_{calc.}$/ g cm^{-3}	1.112	1.038	1.034
μ/mm^{-1}	0.315	0.200	1.252
Formula Weight	799.98	759.15	969.39
Colour	colourless	colourless	colourless
Shape	block	block	plate-shaped
Size/mm^3	0.50×0.43×0.38	0.37×0.21×0.15	0.18×0.06×0.04
T/K	100.0	100.0(2)	120.01(10)
Crystal System	triclinic	triclinic	triclinic
Space Group	*P*-1	*P*-1	*P*-1
a/Å	9.6003(8)	9.6084(3)	10.7047(3)
b/Å	10.3467(8)	10.3966(3)	16.7340(6)
c/Å	14.1226(12)	14.0690(5)	18.7341(7)
α/°	70.483(3)	70.397(3)	108.791(3)
β/°	79.523(3)	79.599(2)	91.685(2)
γ/°	64.775(3)	66.801(3)	100.297(2)
V/Å^3	1194.85(17)	1215.01(8)	3112.19(19)
Z	1	1	2
Z'	0.5	0.5	1
Wavelength/Å	0.71073	0.71073	1.54184
Radiation type	MoK_α	Mo K_α	Cu K_α
Θ_{min}/°	2.272	3.358	4.216
Θ_{max}/°	37.785	30.937	76.168
Measured Refl.	122016	38787	51487
Independent Refl.	12494	7136	12856
Reflections with I > 2(I)	11085	6292	10743
R_{int}	0.0299	0.0301	0.0680
Parameters	234	232	760
Restraints	0	0	264
Largest Peak	1.732	0.443	0.573
Deepest Hole	-0.634	-0.290	-0.577
GooF	1.055	1.061	1.054
wR_2 (all data)	0.1432	0.0950	0.1642
wR_2	0.1380	0.0913	0.1540
R_1 (all data)	0.0496	0.0441	0.0703
R_1	0.0436	0.0368	0.0598

Compound	**4.13-(THF)**
Formula	$C_{52}H_{94}K_2O_4P_2Si_2$
$D_{calc.}$/ g cm^{-3}	1.137
μ/mm^{-1}	0.303
Formula Weight	979.59
Colour	colourless
Shape	block
Size/mm^3	0.39×0.29×0.18
T/K	100.0
Crystal System	triclinic
Space Group	P-1
a/Å	9.3998(11)
b/Å	10.4372(13)
c/Å	15.0095(18)
α/°	80.569(3)
β/°	89.609(4)
γ/°	80.015(3)
V/Å^3	1430.3(3)
Z	1
Z'	0.5
Wavelength/Å	0.71073
Radiation type	MoK_α
Θ_{min}/°	2.200
Θ_{max}/°	30.475
Measured Refl.	25313
Independent Refl.	7657
Reflections with I > 2(I)	6344
R_{int}	0.0318
Parameters	468
Restraints	0
Largest Peak	0.386
Deepest Hole	-0.246
GooF	1.033
wR_2 (all data)	0.0871
wR_2	0.0799
R_1 (all data)	0.0469
R_1	0.0349

5.6 Supporting Figures

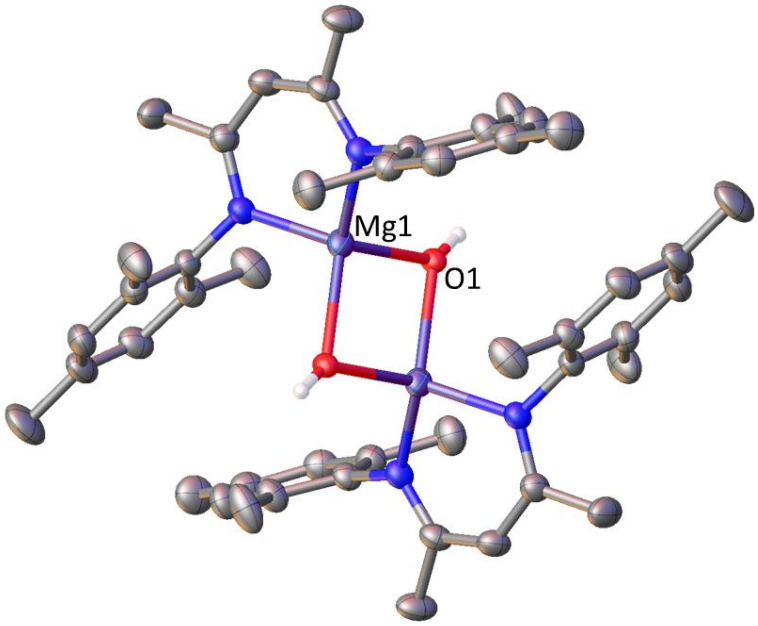

SF1 The solid-state structure of [(^{Mes}NacNac)MgOH]$_2$ (**2.45**). All H atoms, except OH, are omitted. Thermal ellipsoids set to 50% probability.

5.7 References

(1) Fulmer, G. R.; Miller, A. J. M.; Sherden, N. H.; Gottlieb, H. E.; Nudelman, A.; Stoltz, B. M.; Bercaw, J. E.; Goldberg, K. I., *Organometallics*, **2010**, *29*, 2176–2179.

(2) Klein, T.; Kickelbick, G., *Dalton Trans.*, **2020**, *49*, 9820–9834.

(3) Grüger, N.; Rodríguez, L.-I.; Wadepohl, H.; Gade, L. H., *Inorg. Chem.*, **2013**, *52*, 2050–2059.

(4) Timmer, K.; Thewissen, D. H. M. W.; Marsman, J. W., *Rec. Trav. Chim. Pays-Bas*, **1988**, *107*, 248–255.

(5) Higuchi, J.; Kuriyama, S.; Eizawa, A.; Arashiba, K.; Nakajima, K.; Nishibayashi, Y., *Dalton Trans.*, **2018**, *47*, 1117 – 1121.

(6) Grushin, V. V.; Bensimon, C.; Alper, H., *Inorg. Chem.* **1994**, *33*, 4804–4806.

(7) Hicks, J.; Juckel, M.; Paparo, A.; Dange, D.; Jones, C., *Organometallics*, **2018**, *37*, 4810–4813.

(8) Yamamoto, Y.; Chen, X.; Kojima, S.; Ohdoi, K.; Kitano, M.; Doi, Y.; Akiba, K., *J. Am. Chem. Soc.*, **1995**, *117*, 3922–3932.

(9) van den Winkel, Y.; Bastiaans, H. M. M.; Bickelhaupt, F., *J. Organomet. Chem.*, **1991**, *405*, 183–194.

(10) Bresien, J.; Schulz, A.; Villinger, A., *Dalton Trans.*, **2015**, *45*, 498–501.